UNIVERSITY OF SOUTHAMPTON

FACULTY OF ENGINEERING, SCIENCE & MATHEMATICS

INSTITUTE OF SOUND AND VIBRATION RESEARCH

UNCERTAINTY PROPAGATION IN STRUCTURAL DYNAMICS WITH SPECIAL REFERENCE TO COMPONENT MODAL MODELS

By

Esther Hills

Thesis for the degree of Doctor of Philosophy

April 2006

UNIVERSITY OF SOUTHAMPTON

ABSTRACT

FACULTY OF ENGINEERING, SCIENCE & MATHEMATICS

INSTITUTE OF SOUND AND VIBRATION RESEARCH

Doctor of Philosophy

UNCERTAINTY PROPAGATION IN STRUCTURAL DYNAMICS WITH SPECIAL REFERENCE TO COMPONENT MODAL MODELS

By

Esther Hills

This thesis investigates methods for studying how uncertainty propagates within built-up structures, from their physical parameters to their global modal behaviour. In particular it examines the use of Component Mode Synthesis (CMS) along with reduced data sets to approximate the statistics of the variable response.

Variability is introduced into the physical properties of a structure to represent inconsistencies arising from mass production of batches of nominally identical systems. Expressions are generated to relate the statistics of this variability to the statistics of the component eigenvalues and eigenvectors. These are combined to approximate the effect of physical property uncertainty on the uncoupled mass and stiffness matrices of a fixed interface CMS model. A perturbational approach is then used to generate expressions relating the statistics of the component modal behaviour, to the global eigenvalues and eigenvectors. In particular the variance of the global eigenvalues is shown to depend on the variance and covariance of the substructure local eigenvalues and the global modal eigenvectors of the unperturbed structure. From this the spread of the response of the global eigenvalues can be estimated from a single eigensolution of the baseline system, and the statistics of the substructure eigenvalues. In practice, this enables the uncertainty to be quantified at the component modal level, rather than at the physical property level; the former being more convenient to measure. A numerical example based on a 3-dimensional frame structure consisting of two sub-components is considered.

In addition to the study of techniques to propagate uncertainty within built-up structures, the typical level of variability found in manufactured structures is investigated. Results for the statistical analysis of an extensive automotive vehicle study are presented

To Graeme and in loving memory of Cassie

Table of Contents

List of Figures

List of Tables

Declaration of Authorship

I, Esther Hills, declare that this thesis entitled 'Uncertainty propagation in structural dynamics with special reference to component modal models' and the work presented in it are my own.

I confirm that:

- this work was done wholly or mainly while in candidature for a research degree at this University;
- where any part of this thesis has previously been submitted for a degree or any other qualification at this University or any other institution, this has been clearly stated;
- where I have consulted the published work of others, this is always clearly attributed;
- where I have quoted from the work of others, the source is always given. With the exception of such quotations, this thesis is entirely my own work;
- I have acknowledged all main sources of help;
- where the thesis is based on work done by myself jointly with others, I have made clear exactly what was done by others and what I have contributed myself;
- none of this work has been published before submission;

Signed: ……..

Date:……

Acknowledgements

I would like to thank my supervisors Brian Mace and Neil Ferguson for all their help and encouragement in my research and for the many hours spent proof reading this thesis.

I would like to acknowledge Jaguar Cars Ltd for their financial support, along with the Engineering and Physical Sciences Research Council (EPSRC). I would also like to thank Ford Cars Ltd for providing vehicle variability data, in particular Thomas Ahlersmeyer and Nigel Taylor for their help.

I'd like to thank my father for his help with proof reading and all of my family for always being there. Special thanks must go to Graeme, without whose support and encouragement this thesis would never have been started let alone finished, and whose patience apparently knows no bounds.

This thesis is dedicated in loving memory of Cassie.

List of Symbols

A	Cross-sectional area (m^2)
c	Viscous damping constant (Ns/m) or c speed of sound (m/s)
$E[x]$	Expected value of x
E	Young's Modulus (N/m^2)
F	Force (N)
f_j	j'th natural frequency (Hz)
$\mathbf{I}$	Identity matrix
I_x	Polar moment of area about x axis (m^4)
J	Jacobian matrix
k, K	Stiffness (N/m)
l	Length (m)
ln	Natural logarithm
m, M	Mass (kg)
$p(x)$	Probability density function of x
$\mathbb{R}$	Set of all real numbers
T	Temperature in (°C), or kinetic energy (J)
V	Potential energy (J)
x	Displacement (m)
y	Modal degrees of freedom
ε	A small random number
ζ	Viscous damping ratio
$\boldsymbol{\kappa}$	Uncoupled component stiffness matrix
λ, Λ	Eigenvalue (Hz^2)
μ	Mean
$\boldsymbol{\mu}$	Uncoupled component mass matrix
ν	Poisson's ratio
ρ	Density (kg/m^3)
σ	Standard deviation
σ^2	Variance
σ_{xy}	Covariance between x and y
$\boldsymbol{\upsilon}_{ic}$	Coupling constraint modes (m)

$\boldsymbol{\varphi}, \boldsymbol{\Phi}, \boldsymbol{\Psi}$	Eigenvector (m, unless in modal degrees of freedom in component mode synthesis formation then dimensionless)
ω	Frequency (Hz)
ω_n	Natural frequency (Hz)

1. Introduction

This thesis concerns the development of vibration modelling methods which explicitly take product variability and data uncertainty into account. The specific case considered is that of built-up structures comprising assembled components. Methods are investigated and developed for studying how uncertainty propagates within built-up structures, from their physical parameters to their global modal behaviour. In particular it examines the use of Component Mode Synthesis (CMS) along with reduced data sets to approximate the statistics of the response.

In the manufacturing process the properties of mass-produced items vary from one sample to the next. Uncertainty and variability in the properties of a structure, such as its mass or dimensions, arise from a number of causes. There will be some uncertainty in the material properties such as density and elastic modulus and from manufacturing processes such as joint properties, dimensional tolerances and boundary conditions. The properties of the structure will also vary according to environmental conditions such as temperature. There may be uncertainty in specifying the exact values of the properties to use in a numerical model. These variations produce differences in the noise and vibration behaviour of structures, and these differences become larger at higher frequencies. Thus it is not only the 'baseline' response that is of interest, but also estimates of the statistics and spread of the response for batches of structures.

In order to estimate the response statistics of collections of mass-produced structures, traditional approaches tend to consider the propagation of uncertainty directly from the physical properties to the global modes of the structure. Typically, an analysis will use a Finite Element (FE) model to obtain the modal properties. If some uncertainty exists in the physical properties of the structure, then a common route would be to use Monte Carlo (MC) simulations to allow the properties to vary pseudo-randomly and the analysis to be repeated many times. However, this process is expensive and time consuming as a full eigensolution must be found for each cycle of the MC analysis. In addition the quantification of the uncertainty in the physical parameters is complex and usually impractical.

The computational cost of a dynamic analysis may be reduced somewhat through the use of substructuring techniques such as CMS. This involves dividing a structure into a substructures or components, performing a separate analysis of each component and assembling these results into a global modal model. The component models are usually constructed using a truncated set of component modes, thus giving a reduced order global model. The component modes are

often obtained from an FE analysis but they may also be obtained experimentally. CMS methods are often employed in the analysis of extremely large FE models where for convenience the model is divided into components.

When there is uncertainty in the system properties one would like to predict the statistics of the response. One approach to this is the Local Mode Perturbational (LMP) method which combines a CMS approach with perturbational approximations. CMS is used to divide the structure into substructures and uncertainty is introduced directly into the component eigenvalues. These component eigenvalue variations are assumed to be small and an eigensolution approximation, using a perturbation, is used to estimate the global eigenvalues and eigenvectors. The LMP method will be used in this thesis as a basis for further examining the propagation of uncertainty in complex structures.

1.1 Overview of thesis

The thesis is split into three main parts. The first of these consists of chapters 2 and 3 and concerns measured variability data from manufactured parts. The second part consists of chapters 4 and 5 and considers existing analysis methods for examining the propagation of variability in structures. The final part of the thesis, which includes chapters 6 to 9, presents the Component Mode Synthesis method, which is used in conjunction with eigensolution approximations to study how variability propagates within a structure. Each of the chapters is summarised briefly below.

In order to understand the typical measured levels of variability found in manufactured structures, a literature review is presented in chapter 2. Published data concerning variability in manufactured structures is briefly reviewed. This is followed by a more detailed examination of the results for two specific cases for which the raw data is available. Two of the main drawbacks of the variability studies are the relatively small sample sizes and test condition variability.

In chapter 3, previously unpublished measured variability results are presented for an extensive automotive vehicle study. The measurements were recorded by the manufacturer as part of a NVH (Noise, Vibration and Harshness) monitoring programme, which selected a cross-section of production vehicles from two product lines prior to despatch. The work presented here is a detailed statistical analysis of the data, examining the level of variability in the results, fitting curves to the distribution and investigating the goodness-of-fit obtained. The vehicle test programme consisted of three types of measurements: airborne cabin noise attenuation, roller

induced road noise and interior measured engine noise. In addition the environmental conditions were monitored and the effect of these is investigated. From chapters 2 and 3 a general understanding is gained for the typical levels of normalised standard deviation of variability along with some comments on the probability distributions.

In chapter 4 several techniques for studying uncertainty propagation and statistical concepts are introduced, many of which are used in subsequent chapters. In the first section eigensolution approximations are discussed. The first of these uses the unperturbed system eigenvectors as assumed modeshapes and extends the Rayleigh quotient to all modes. Following this the interpolated mode method is presented. Both of these methods could be considered to be physical approximations to the eigensolution. Following this, perturbational approximations to the eigensolution are considered. The mean centred perturbation expansion method is presented along with an 'optimal' point method. Both of these perturbation methods may be considered to be mathematical approximations to the eigensolution. In the second section of this chapter some analytical techniques are presented for use in subsequent chapters. These techniques can be used, in conjunction with eigensolution approximations, to obtain various statistical properties of a system with random properties. The first of these is the generation of moments method, in which the moments of the response of a system can be related to the moments of the input variables. The second technique is the change of variable method, in which the probability density function (PDF) of the output of a linear system is related to the PDF of the inputs. A general matrix notation is also defined for use in subsequent chapters. The final section in this chapter reviews several Monte Carlo methods for obtaining numerical solutions to complex problems such as eigenvalue equations. Two methods are discussed in detail, these are stratified sampling and Latin Hypercube sampling. Both of these approaches aim to reduce the number of trial runs required to obtain a good approximation to the output distribution, whilst ensuring all areas of the input distributions are covered. In chapter 5 a two-degree of freedom system is used to evaluate some of the techniques presented in chapter 4. Variability is introduced into the physical properties of the system to represent inconsistencies arising from mass production of batches of nominally identical systems. This is then related to the resultant statistics of the response. The benefits and drawbacks of the applied methods are discussed and the difficulties of extending the methods to large structures are considered. The perturbation approach is shown to provide a possible route for propagating uncertainty in a structure, from the physical properties to the global modal properties. However, one of the main drawbacks of this method is the rapidly increasing complexity of the calculations when applied to a system with more than a few degrees of freedom.

In chapter 6 the Component Mode Synthesis method of subdividing a structure into substructures is introduced. A procedure to combine CMS techniques along with traditional approximations is presented. This extends the existing CMS methods, to propagate the variability statistics from the physical properties to the component modal and global modal properties. The process is outlined and potential areas for data reduction are highlighted. In the following sections of chapter 6 the background theory of CMS is briefly introduced for use in later chapters. The procedure for investigating the propagation of uncertainty from the physical properties of components to the response of built-up structures is examined in two stages. The first of these in chapter 7 concerns the propagation of uncertainty from the component physical properties to the component modal properties. Existing work using the LMP method has introduced arbitrary levels of variability into the component eigenvalues. Here expressions are generated to relate the statistics of the variability in the component mass and stiffness matrices to the statistics of the component eigenvalues and eigenvectors. The chapter is organised into three main sections. In the first, mathematical expressions relating the variability in the physical properties to variability in the modal properties are determined. In addition, the effect of uncertainty in the physical properties on the uncoupled mass and stiffness matrices of a fixed interface CMS model are estimated. In the next section these expressions are reviewed and discussed in the context of the potential areas for data reduction listed in chapter 6. Finally, a numerical example is presented and, through the use of a Monte Carlo simulation, each potential area for data reduction is evaluated.

In chapter 8 the second part of the procedure outlined in chapter 6 is presented. This concerns the propagation of statistics from the local modal level to the global modal properties. Mathematical expressions relating the statistics of the variability in the local modal properties to the statistics of the variability in the global modal properties are determined. In particular the variance of the global eigenvalues is shown to depend on the variance and covariance of the substructure local eigenvalues and the global modal eigenvectors of the unperturbed structure. From this the spread of the response of the global eigenvalues can be estimated from a single eigensolution of the baseline system, and the statistics of the substructure eigenvalues. In practice, this enables the uncertainty to be quantified at the component modal level, rather than the physical property level, the former being more convenient to measure. A method for obtaining the distribution of the global perturbed eigenvalues is presented, along with a discussion of possible applications of central limit theorems. If the distribution of the substructure local eigenvalues is assumed to be Gaussian, then it is shown that the distribution of the global perturbed eigenvalues will also be Gaussian, with expressions for the mean and variance generated. Approximations for the perturbed global eigenvectors are generated using a first order perturbation and this is used to obtain a first order approximation for the structure's

FRF. A simple case of two coupled rods is presented, and expressions for the statistics of the global eigenvalues, in terms of the statistics of the local eigenvalues, are developed. A numerical example is considered and a combination of correlated and uncorrelated uncertainty introduced into the local eigenvalues of each rod. The results are compared to those obtained from a Monte Carlo simulation.

In chapter 9 a more complex numerical example is considered based on a 3-dimensional frame structure characteristic of a vehicle chassis frame, consisting of two sub-components. Some variability is introduced into both the physical properties and the local modal properties of the structure, and the results from a full Monte Carlo analysis are compared to those from a reduced component modal model.

Finally some concluding remarks are presented along with recommendations for further research.

These are the novel elements in this thesis:

- Presentation of an extensive vehicle variability analysis.
- Generation of expressions to relate the statistics of physical parameter uncertainty to the statistics of the free and fixed interface local modes.
- Assembly of these to obtain the fixed interface CMS matrices in terms of the physical parameter uncertainties.
- Establishing the relationship between the free/fixed interface component variance and proposed use of the free interface variance in a fixed interface CMS method.
- Extension of the LMP method to obtain estimates for the statistics of the global eigenvalues and eigenvectors, for any general perturbations, correlated or uncorrelated, in the local eigenvalues of a structure.

Section I: Measured variability data from manufactured parts

2. Uncertainty and variability in components and built-up structures

In order to model the vibration response of structures with uncertain properties, some knowledge is required as to the nature and statistics of the variability typical of manufactured components. The statistical distribution of both the system physical properties and the system response and their relationship are of interest. With prior knowledge of the statistical distribution of the variability in a system, relatively few samples from the set are required to provide a good estimate of the moments of the distribution such as mean and variance. Currently very little published data is available on the measured statistical distribution of variability within manufactured components or the relationship between the uncertainties in the physical properties and the statistics of the measured response. Two particular pieces of information are of specific interest, the typical levels of the variance in both the physical properties and the response, and whether its distribution is Gaussian or close to Gaussian. These two factors influence the applicability of various methods for propagating uncertainty in structural systems.

This chapter briefly reviews available published data concerning variability in manufactured structures. Two specific case studies are then chosen for further investigation and statistical analysis: these are the variability in the mass and natural frequencies of a single complex component (a vehicle alloy wheel rim) and the variability in structure-borne and airborne response of a complex built-up structure (an automotive vehicle).

2.1 Literature review

Although it is likely that many manufacturers monitor and record variability information for their components, access to such data is limited. Very few studies have been published examining the response variability and, of those published, the relationship to physical property variability is in general not investigated. Typically the sample set size of the published variability data is too small to estimate the population distribution with any confidence. However, the normalised standard deviation (σ/μ) can be used to compare the relative magnitude of variability across different studies.

The available results fall into three main categories, firstly those examining the variability in measured response, secondly those investigating both the measured response and the corresponding FE numerical results' variability, and lastly studies just examining numerical

results produced by FE modelling variability. Below is a short summary of the relevant findings from each paper reviewed.

Brown and Gear [2.1] reported on a study in which they conducted tests on a set of twenty Fisher & Paykel fridges. The variability in the response of the first four modes of the compressor mounting was investigated using an impact hammer as the excitation. The average normalised standard deviation of the natural frequencies was found to be 0.04. The average normalised standard deviation of the response magnitude was 0.71. The impact hammer provided insufficient excitation to excite the primary mode of the compressor mounting. As an alternative, they attempted to use the vibration from the compressor motor as an excitation source. However, this proved to be a very variable signal and unable to provide a repeatable source excitation.

A second study also conducted by Brown and Gear investigated a set of 79 nominally identical vehicle alloy wheel rims; this case study is discussed in section 2.2 below. In summary, the study examined the variability of the first four natural modes of the wheel rims and its mass. The variability in the modes was found to be very small with the normalised standard deviations of the first four modes ranging from 0.002 to 0.005. This is not unexpected as the wheel rims consist of a single part with no joints and the manufacturing process, which involves alloy casting followed by a machined finish, is typically well controlled. Due to the large sample size of the study, it statistically provides a good set for which to further examine the distribution of the modal properties. The mass was also recorded and its normalised standard deviation was 0.007. Brown and Gear investigated the possibility of a correlation between the variability in the mass and variability in the modal properties but none was found.

Zehn and Saitov [2.2] conducted an interesting study into the variability in the thickness of a composite plate. This formed part of a study on weighting-matrix generation for parameter estimation methods used in FE model updating algorithms. They reviewed a statistical approach to generating weighting matrices that are spatially correlated for shells and plates, to update FE models iteratively to fit measured data. The spatially varying thickness of a composite plate was measured and found to have a Gaussian distribution; the observed normalised standard deviation was 0.01. A method was then examined for producing a random spatially correlated Gaussian distributed thickness weighting function for model updating. The first eight natural frequencies of the plate were measured and compared with predicted values from four FE models each using different plate thickness assumptions. The first FE model assumed a constant plate thickness; the other FE models used various different methods of spatially correlated thicknesses. The normalised standard deviation observed between the different modelling

techniques and the measured results ranged from 0.06 at the first natural frequency, increasing to 0.02 by the fourth.

The variability due to environmental changes on a large structure was reported by Cornwell et al [2.3] who investigated the modal properties of a single span concrete bridge. They conducted an investigation of how the modal properties of the bridge were affected by environmental effects, so as to discriminate these changes from those expected during damage detection monitoring. The variability of the natural frequencies of the bridge with temperature was monitored during two 24-hour periods; the first in August 1996 and the second in July 1997. The modal frequencies were found to vary by up to 6% during each test period, and the variation was found to be correlated to the temperature differentials across the deck of the bridge. The normalised standard deviation of the fundamental natural frequency was approximately 0.01 over the first testing period and 0.02 over the second.

Lardeur, Lacouture and Blain [2.4] investigated spot welding modelling techniques and the performance of FE models for the prediction of the vibration response of automotive structures. One of the cases considered was an academic structure of two plates joined by three spot welds. In order to best evaluate the performance of a selection of spot weld models, the variability in the measured modal properties of three nominally identical sets of welded plates was measured. The first six modes of the plates were noted, although some experimental issues were encountered with the measurement of the fifth mode. The normalised standard deviation between the three structures ranged from 0.01 to 0.03.

Balmès [2.5] reported one of the few studies to examine both measured response variability and variability in the FE modelling. A round robin exercise was conducted to investigate variability in test and modelled frequency response behaviour of a single structure. A simplified aircraft structure was used for the study and twelve separate laboratories measured the first eight modes of the structure. Each laboratory also produced an FE model to predict the modal properties. The normalised standard deviation of the measured modes was found to vary between 0.01 and 0.03; the normalised standard deviation obtained from the FE analysis ranged from 0.004 to 0.02. The agreement between the measured results and those obtained from the FE analysis was considered to be typical, with on average 5% error between the measured and predicted results. However, this difference was generally greater than the variability observed within them.

A similar round robin study reported by Ewins and Imregun [2.6] who investigated the capabilities and reliability of FE modelling methods. This study investigated only FE model variability and did not include measured response variability. A test structure was designed,

built and modal tested. Identical information including detailed drawings, master coordinate grid points and measured spring stiffnesses was supplied to twenty different organisations for FE modelling. Twelve submitted results for the modal properties, spring compression/extension and rotation. The normalised standard deviation of the modal predictions varied from 0.02 to 0.2, the spring compression/extension from 0.11 to 0.2, and the spring rotation normalised standard deviation was 0.38.

A further FE benchmark study was reported by Maguire [2.7]. A test structure was constructed and modal tested by Lloyd's Register, twelve companies were then invited to construct FE models of the structure based on technical drawings and material specification. Ten companies submitted full results for the first seven modes of the structure for comparison. Measured test data was then made available to the participants in order to update the FE models and submit a second set of revised modal predictions. The normalised standard deviation of the first set of modal predictions ranged from 0.04 to 0.09. The second set of correlated and updated model predictions was less variable and the normalised standard deviation ranged from 0.01 to 0.04.

The typical levels of normalised standard deviation of the response found in these studies were up to 0.03. Within the physical parameters it was found to be up to 0.01. These levels would suggest that the variability between nominally identical manufactured components is relatively low, which may have specific implications on the requirement to include higher order terms in any series expansion methods for uncertainty propagation. Interestingly the variability between different FE models of the same structure, performed by different companies, was greater at up to 0.2.

2.2 Variability in a single complex component: An alloy wheel rim

The statistical distribution of the response of a single complex manufactured component, an alloy wheel, is investigated. The original test work was conducted and reported by Brown and Gear [2.1]. The first four natural frequencies (f_1, f_2, f_3, f_4) and the mass were recorded for a set of 79 nominally identical alloy wheel rims. Figure 2-1 shows the distribution of the results. For comparison equivalent sample numbers from various probability distributions with the same mean and standard deviation as the normalised data set are also shown.

A chi-squared (χ^2) test [2.8] was conducted to test the goodness-of-fit of a selection of standard probability distributions to the data sets. Of particular interest is the goodness-of-fit to

Gaussian or close to Gaussian distributions. All of the non-Gaussian distributions selected to be trialled can under certain combinations of their parameters, become close to Gaussian in form. Further information on each of the distributions can be found in [2.9]. The maximum likelihood method was used to estimate the parameters for each of the distributions [2.10]. A summary of the subsequent χ^2 results can be found in Table 2-1. The χ^2 test is a null hypothesis test and a probability of below 95% represents a 95% confidence that the sample set cannot be rejected as having come from the distribution being tested against, see [2.10] for further information. The χ^2 test is conducted on classified (binned) data and outlying bins are summed to ensure at least five counts in each; this reduces the skewing effect of out-lying results.

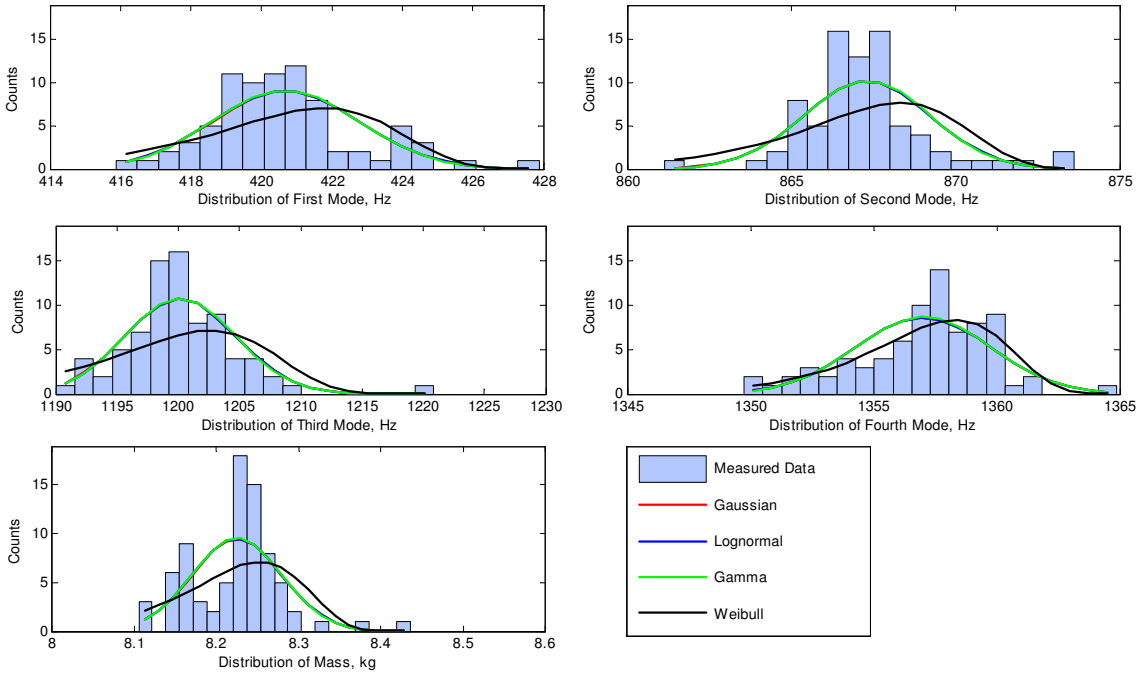

Figure 2-1 Alloy wheel rims, frequency distribution of the first four natural frequencies and the total mass with equivalent sample numbers from various standard probability distributions.

	f_1	f_2	f_3	f_4	Mass
Gaussian	0.751	0.985	0.650	0.937	0.999
Lognormal	0.740	0.984	0.645	0.938	0.999
Gamma	0.741	0.983	0.635	0.938	0.999
Weibull	1.000	1.000	1.000	0.623	1.000

Table 2-1 Summary of χ^2 probability results for goodness-of-fit tests of alloy wheel data to various distributions.

A χ^2 probability of less than 95% represents a 95% confidence that the alloy wheel response cannot be rejected as having come from the distribution being tested against, in Table 2-1 these

values are highlighted. From examination of Table 2-1, one cannot reject the hypothesis that the first, third and fourth modal frequencies fit to a Gaussian distribution. Conversely it can be seen from Figure 2-1 that the distribution for the second natural frequency and the mass have a high number of samples close to the mean with a low uneven spread, and a Gaussian distribution can be rejected as a likely fit. In general, a lognormal distribution closely approximates a Gaussian distribution for data sets where the $\sigma/\mu << 1$. This condition is approached for all of the alloy wheel data sets and the first, third and fourth modal frequencies fit either distribution. Both distributions rejected as a fit for the second modal frequency and the mass. A Gamma distribution also approaches a Gaussian distribution as the ratio σ/μ becomes increasingly small. This condition is also satisfied for the alloy wheel results and the Gamma distribution can also be rejected for the second mode and the mass. As can be seen in Figure 2-1 there is no difference between a gamma, lognormal and Gaussian distribution. It can be seen from the results in Table 2-1 that a Weibull distribution can be rejected as a good fit to all of the data sets except the fourth mode. The data sets were also tested against a Rayleigh probability distribution; the results are not included in Table 2-1 as they were all rejected above the 95% probability confidence level as not having come from this distribution.

In conclusion, a Gaussian distribution was found to be a good fit to the distribution for three of the first four natural frequencies of an alloy wheel. Due to the relative sizes of the mean and variance in the distribution of the data, a Gamma distribution approaches a Gaussian distribution and hence also fits well. A lognormal distribution fits two of the natural frequencies.

The levels of normalised standard deviation, as discussed in section 2.1, ranged from 0.002 to 0.005 for the first four modes, and 0.007 for the mass.

Brown and Gear [2.1] investigated the cross correlation between the natural frequencies and the wheel rim mass, but no correlation was found. They did not examine the possible correlation between inverse square root of the mass and the natural frequencies, but investigation of this did not yield any correlation. They also examined the cross correlations between the natural frequencies and found some correlation between the first and second mode. It was surmised that this could be due to the mode shapes for both modes being similar, but this did not appear to be valid for the third and fourth mode which, although similar in shape, did not display any significant cross correlation.

2.3 Variability in built-up structures: An automotive vehicle

Bernhard and Kompella [2.11]-[2.13] investigated the variability in the structure-borne and airborne frequency response functions (FRFs), for two different car models, namely the Isuzu Rodeo, of which 98 nominally identical vehicles were measured, and the Isuzu Pickup of which there were 57. The original test results were made available by the authors for further study. Kompella and Bernhard [2.13] reported some statistical analysis of the data; the present study extends their work with a statistical analysis of the response distribution for the two vehicle sets, and looks for any variation in the response distribution with frequency.

A brief summary of the test procedure will be given here but for further details see [2.11]-[2.13]. An identical test procedure was used for both vehicle sets. Structure-borne FRFs were measured from the front left wheel hub to interior microphones at the driver's and front passenger's ear locations; an impact hammer was used to provide the excitation. Airborne FRFs were measured from a reference exterior microphone located outside the vehicle at the front left wheel position to interior microphones at the same positions as before; a loudspeaker generating band-limited random noise, situated near to the exterior microphone was used as the acoustic source. The frequency ranges of the resultant structure-borne FRFs were 30-500Hz and 125Hz-1kHz for the airborne functions. The tests were conducted outside at the Subaru-Isuzu Automotive Inc. test track in Lafayette, Indiana. The test programme was conducted over a four-day period, with each individual test lasting approximately eight minutes.

In order to monitor the measurement process variability, a reference vehicle of each type was tested repeatedly throughout the test schedule. These results provide an indication of the measurement procedure variability in comparison to the population variability. Figure 2-2 and Figure 2-3 show the maximum envelope, minimum envelope and mean values for each FRF set, together with one example result from the reference vehicles.

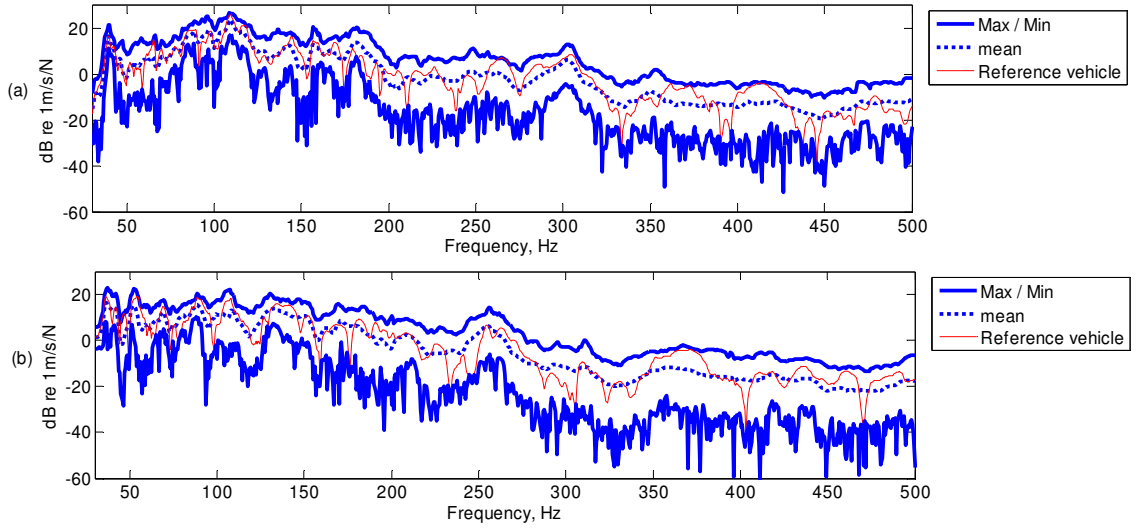

Figure 2-2 Structure-borne FRFs: (a) 57 Isuzu pickup vehicles; (b) 98 Izusu Rodeo vehicles.

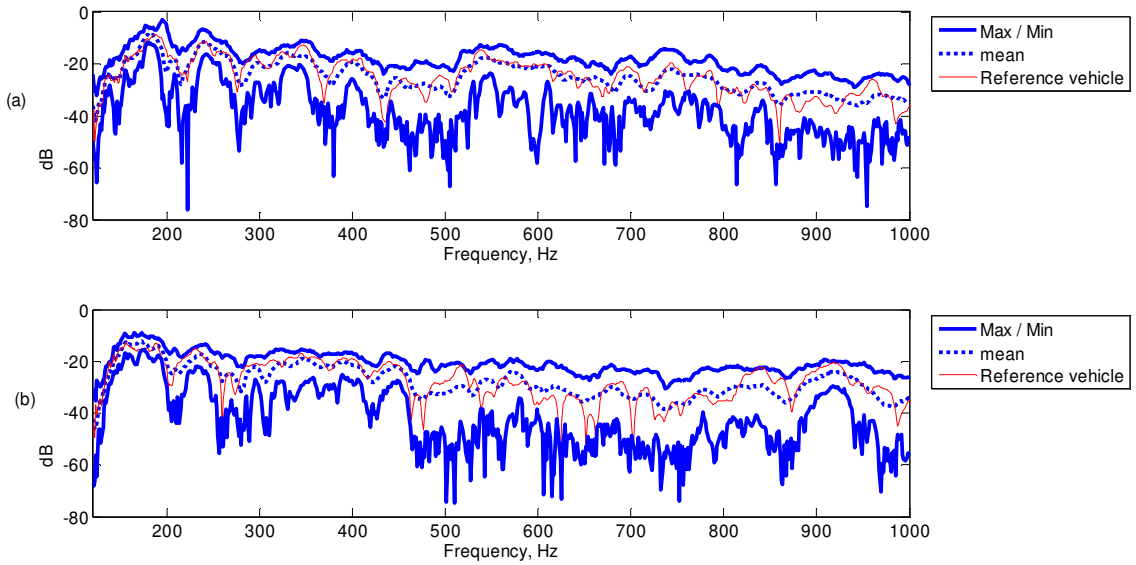

Figure 2-3 Airborne FRFs: (a) 57 Isuzu pickup vehicles; (b) 98 Izusu Rodeo vehicles.

The average range of the airborne FRFs from the maximum envelope to the minimum envelope is 21.8dB (Pick-up vehicle set) and 23.3dB (Rodeo vehicle set); the range for the structure-borne FRFs is 23.4dB (Pick-up) and 26.5dB (Rodeo). The variability increases with increasing frequency.

The temperature and humidity inside the vehicles were monitored for each test. As the vehicles were tested outside, there were significant temperature fluctuations due to the weather. The maximum and minimum recorded temperatures inside the vehicles were 47.1°C and 20.1°C. The standard deviations of the temperature and humidity reported in [2.12] have been

normalised and are listed in Table 2-2. The level of variation in the temperatures during the test, although large, is in the order of the variability reported in modal measurements and predictions discussed earlier in this chapter.

The approximate effect of temperature on the speed of sound is given by [2.16]

$$c \cong 332 + 0.6T \tag{2.1}$$

where T is the temperature in °C; at 47°C the speed of sound in dry air is approximately 360 m/s, at 20°C it is 344 m/s. The maximum and minimum relative humidity recorded inside the test vehicles were 77.5% and 18.7% respectively. The normalised standard deviations are listed in Table 2-2. Although the level of variation in the relative humidity is much larger than that seen in the temperatures, the effect on the speed of sound in air is less marked. The effect of humidity on the speed of sound in air is presented graphically in [2.17]. The speed of sound in air at 20°C and 77.5% relative humidity is approximately 344.3 m/s, at 18.7% relative humidity it is 343.6 m/s. The relative humidity can have a large effect on the absorption coefficient of the air at much higher frequencies; [2.15] includes empirical data indicating the effect of humidity levels on the absorption coefficient of air at audio frequencies. However, at mid-range audio frequencies such as 1.5kHz the effect is small and the difference in the absorption coefficient due to a relative humidity range of 18.7 - 77.5% is 0.01 - 0.005dB/m. For comparison the effect at high frequencies such as 10kHz the difference is 0.08 - 0.275dB/m.

Vehicle Set	Temperature Variation, σ/μ	Relative Humidity Variation, σ/μ
98 Rodeos	0.18	0.33
12 reference Rodeo's	0.16	0.34
57 Pickup trucks	0.17	0.30
7 reference Pickup truck's	0.20	0.35

Table 2-2 Temperature and humidity variations for Isuzu Rodeo and Pickup truck test results.

The detailed temperature and humidity data for each FRF test was not available and hence no correlation between their variability and the FRF variability could be investigated. However, it can be concluded that the temperature effect is likely to be more significant in the frequency range of the FRFs than the humidity changes, and that the variation in the temperatures is comparable in terms of normalised standard deviation to levels typically seen in modal prediction and measurement. The temperature variations will particularly affect the structure-borne FRF due to stiffness changes in rubber mountings and bushes.

The above results were displayed on a decibel scale for ease of viewing. However, the subsequent analysis of the response distribution is conducted on the linear results. In subsequent chapters the relationship between variability in the physical properties and variability in the modal properties is examined in detail. The distribution of the linear results is examined here for comparison to general variability propagation techniques used later.

Figure 2-4 to Figure 2-7 show the population mean, standard deviation and normalised standard deviation, as a function of frequency, together with those of the reference vehicle. In each case the reference vehicle mean is approximately equal to that of the population indicating that the reference vehicle is a typical sample from the population.

It can be seen that the population standard deviation (σ_p) is in general twice that of the reference vehicle (σ_r). This indicates that the variation in the sample population is predominately due to vehicle variability and not measurement variability. Table 2-3 lists the frequency averaged magnitude differences between the standard deviation for each FRF set.

FRF	$(\sigma_p) / (\sigma_r)$
Airborne FRF, rodeo 98 vehicles	2.24
Airborne FRF, pick-up 57 vehicles	2.14
Structure-borne, rodeo 98 vehicles	2.18
Structure-borne, pick-up 57 vehicles	2.86

Table 2-3 Frequency averaged magnitude difference between standard deviations for the population Isuzu Rodeo and Pickup truck test results compared to the reference vehicles.

It is also worth noting in Figure 2-4(c)-Figure 2-7(c) that there is a trend towards increased normalised standard deviation at higher frequencies, indicating that the variability increases with increasing frequency.

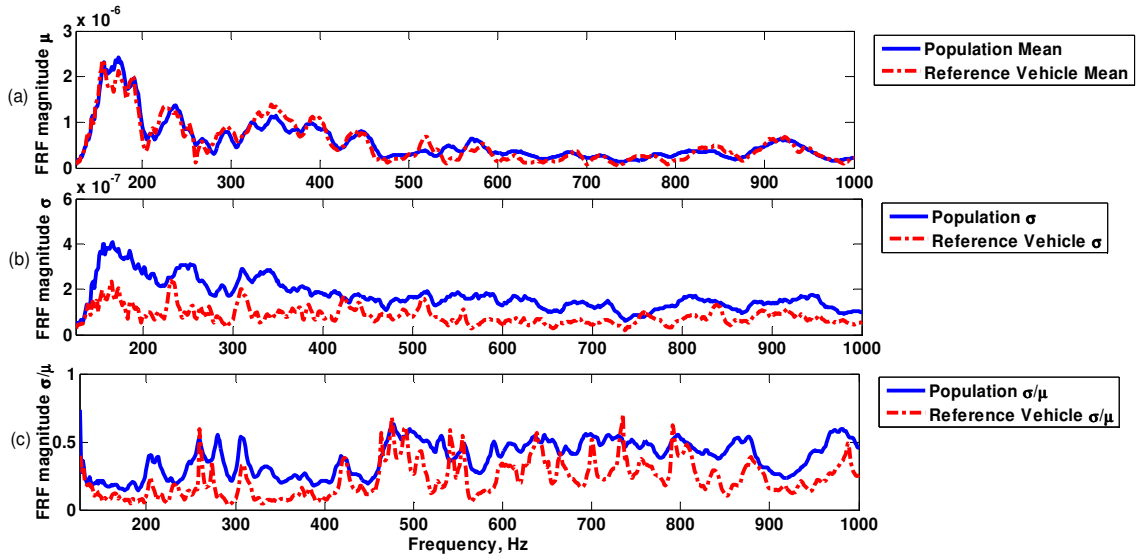

Figure 2-4 Rodeo airborne FRFs: (a) mean vs. frequency; (b) standard deviation vs. frequency; (c) normalised standard deviation.

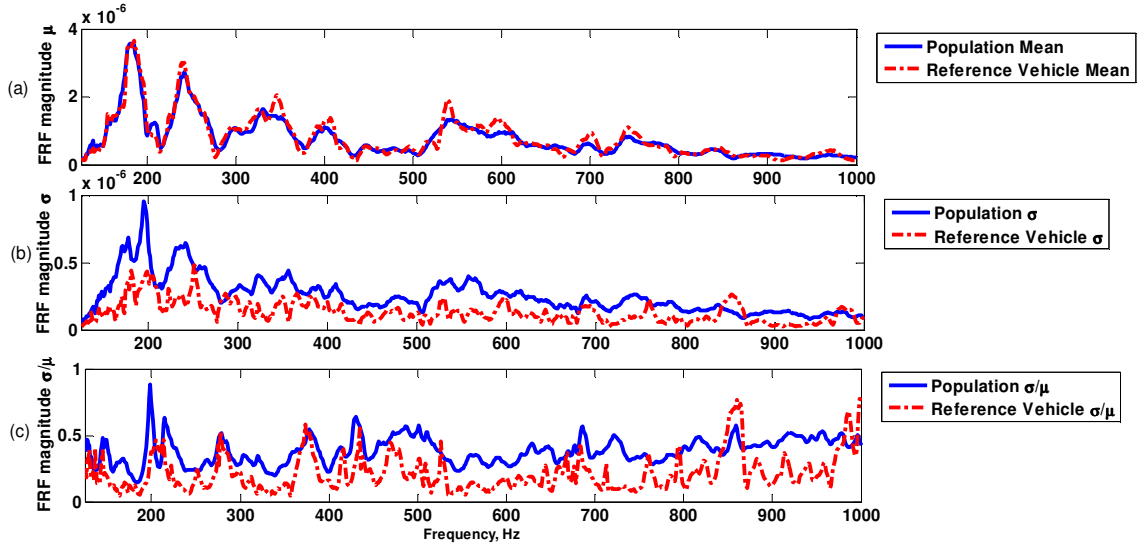

Figure 2-5 Pick-up airborne FRFs: (a) mean vs. frequency; (b) standard deviation vs. frequency; (c) normalised standard deviation.

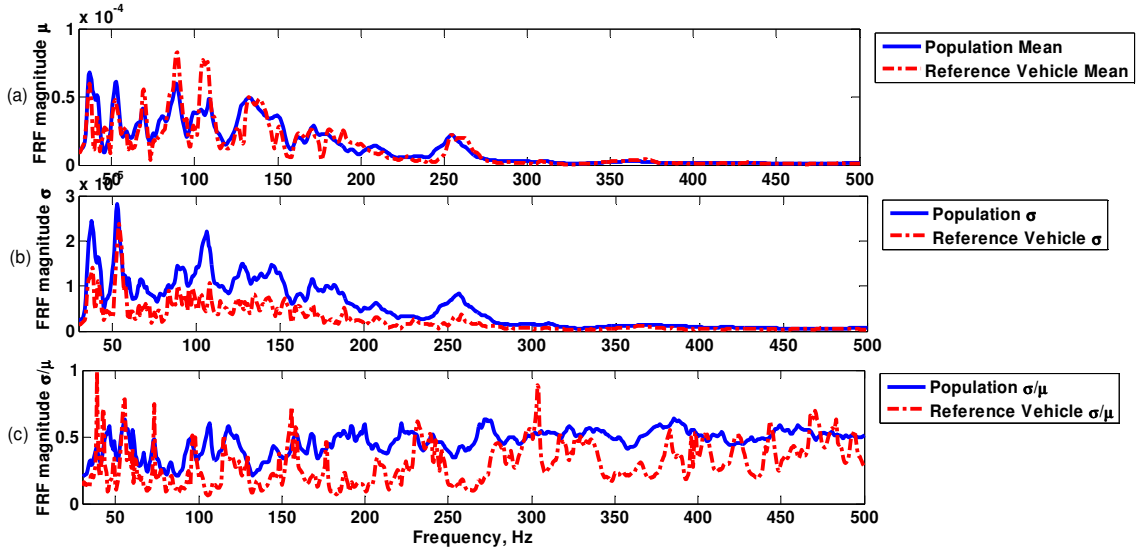

Figure 2-6 Rodeo structure-borne FRFs: (a) mean vs. frequency; (b) standard deviation vs. frequency; (c) normalised standard deviation.

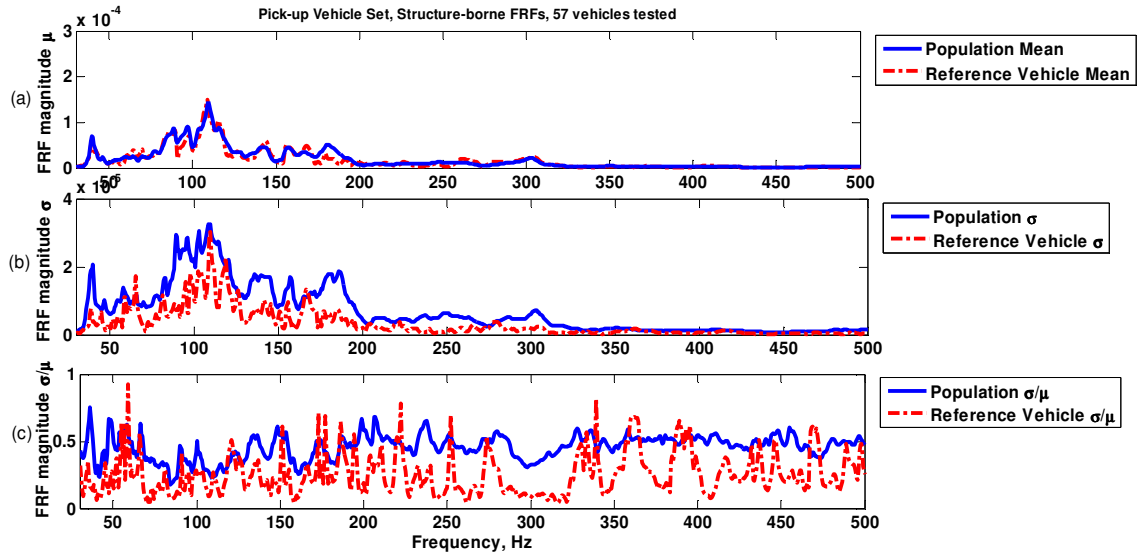

Figure 2-7 Pick-up structure-borne FRFs: (a) mean vs. frequency; (b) standard deviation vs. frequency; (c) normalised standard deviation.

Several areas have been investigated as part of the further analysis of the results. The base statistics of the response distributions (mean, standard deviation, skew and kurtosis) have been examined to investigate trends relating to frequency or the mean level of the response. Band averaging of the data was explored to highlight underlying trends. A χ^2 test was carried out on the response distributions to test the goodness-of-fit to various standard probability distributions. The more interesting results will be discussed here.

The maximum, minimum and mean values for the linear structure-borne FRFs for the Rodeo vehicle set, together with one example result from the reference vehicles, are shown in Figure 2-8 (a). The distributions of the response at two example frequency lines are also shown; 52.5Hz, Figure 2-8 (b), which corresponds to the second peak, and 450Hz, Figure 2-8 (c), which is a typical example at high frequencies. Table 2-4 contains a summary of the χ^2 results for the goodness-of-fit to a Gaussian distribution. The results are presented as the percentage of frequency lines for which the χ^2 probability is below 95%, which is considered to be a good fit. Also listed are the χ^2 results for the goodness-of-fit to a Gaussian distribution of a dummy data set containing pseudo-random numbers from a Gaussian distribution. This was used to indicate the typical results that could be expected from a random Gaussian data set of similar size to the sample data sets.

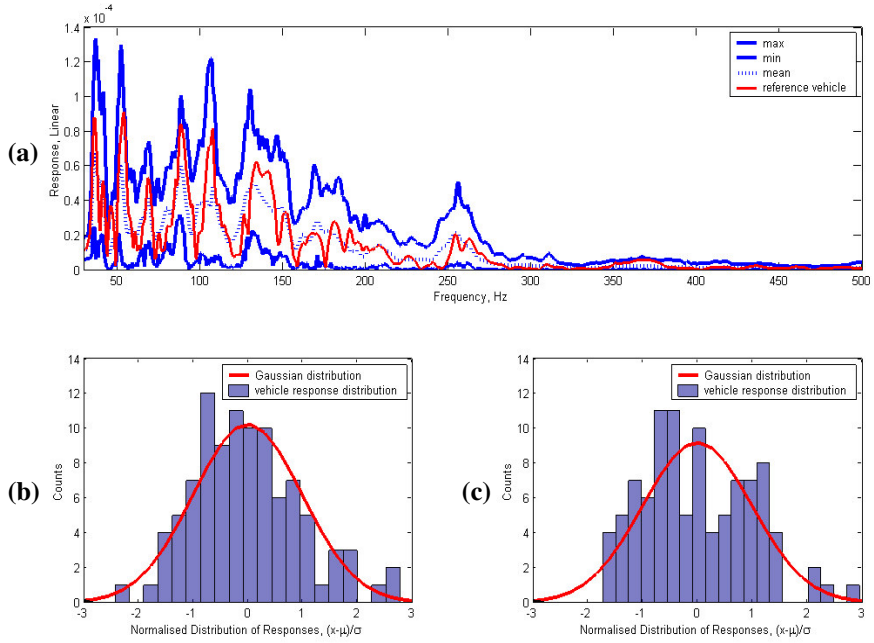

Figure 2-8 (a) Rodeo structure-borne FRFs with (b) distribution at 52.5Hz and (c) distribution at 450Hz.

In general a Gaussian distribution was found to be a good fit to the linear response data over most of the frequency range, with 76% to 85% of the frequency lines being a good fit. However, a detailed analysis of the low versus high frequency ranges displayed some differences in the χ^2 probabilities for the rodeo vehicle set. For the structure-borne FRF the low frequency range was considered to be 30-300Hz, high frequency as 300-500Hz. For the

airborne FRF the low frequency range was considered to be 125-500Hz, high frequency as 500-1000Hz. These ranges were chosen based on the levels of the mean linear responses. Approximately 8% more of the frequency lines at low frequencies were found to be a good fit to a Gaussian distribution in both the airborne and structure-borne FRF's for the rodeo vehicles. The mechanisms involved in the structure and airborne noise transmission in the vehicles will differ from low to high frequencies. At low frequencies the transmission is likely to be dominated by mass effects, whereas at higher frequencies damping will have an increased effect on the structure-borne transmission, while leakage and absorption will have an increased effect on the airborne noise. The differences in the distributions of the variability with frequency may indicate a difference in the distribution due to different mechanisms.

Goodness of Fit to Gaussian Distribution	Test Details	% 'Good Fit'	Comments
Pick-up structure-borne FRF set	57 vehicles 30-500Hz	82%	- Doesn't display low/high frequency differences
Pick-up airborne FRF set	57 vehicles 125-1000Hz	85%	- Doesn't display low/high frequency differences
'Dummy' generated data set, Gaussian distributed	57 vehicles 30-500Hz	92%	N/A
Rodeo structure-borne FRF set	98 vehicles 30-500Hz	76%	- Low/high frequency difference - Fit better at low frequency ~8%
Rodeo airborne FRF set	98 vehicles 125-1000Hz	84%	- Low/high frequency difference - Fit better at low frequency ~8%
'Dummy' generated data set, Gaussian distributed	98 vehicles 30-500Hz	94%	N/A

Table 2-4 χ^2 goodness-of-fit to a Gaussian distribution.

For comparison Table 2-5 contains the χ^2 results for the goodness-of-fit to a lognormal distribution. It can be seen that the lognormal distribution is a slightly better fit to the data than a Gaussian distribution, with 85-89% of the frequency lines being a good fit.

A lognormal distribution approaches a Gaussian distribution as $\sigma/\mu << 1$; from Figure 2-4 to Figure 2-7 it can be seen that $\sigma/\mu < 1$ and hence a lognormal distribution will start to approach a Gaussian. However, a lognormal distribution was found to be a good fit to more of the frequency lines for each FRF set of results, than a Gaussian distribution.

Goodness of Fit to Lognormal Distribution	Test Details	% 'Good Fit'	Comments
Pick-up structure-borne FRF set	57 vehicles 30-500Hz	87%	- Fit better at high frequencies ~2%
Pick-up airborne FRF set	57 vehicles 125-1000Hz	88%	- No low/high frequency differences
'Dummy' generated data set, Gaussian distributed	57 vehicles 30-500Hz	91%	N/A
Rodeo structure-borne FRF set	98 vehicles 30-500Hz	85%	- Fit better at low frequencies ~4%
Rodeo airborne FRF set	98 vehicles 125-1000Hz	89%	- No low/high frequency differences
'Dummy' generated data set, Gaussian distributed	98 vehicles 30-500Hz	92%	N/A

Table 2-5 χ^2 goodness-of-fit to a lognormal distribution.

The distribution of the linear response data was also compared to Gamma and Rayleigh distributions. A Gamma distribution approaches a Gaussian distribution as the ratio σ/μ becomes increasingly small. This is certainly true in this case and there is little difference between the two distributions with respect to goodness-of-fit. A Rayleigh distribution generally was found to be a good fit to the Pickup FRFs, but a poor fit to the Rodeo FRFs. All of the results from the χ^2 tests are summarised in Table 2-6 as the number of frequency lines with a χ^2 probability of below 95%.

Goodness of Fit to Gaussian Distribution	Test Details	Lognormal	Gaussian	Gamma	Rayleigh
Pick-up structure-borne FRF set	57 vehicles 30-500Hz	87%	82%	90%	73%
Rodeo structure-borne FRF set	98 vehicles 30-500Hz	85%	76%	85%	71%
'Dummy' structure-borne data set, Gaussian distributed	57 vehicles 30-500Hz	91%	92%	92%	0%
Pick-up airborne FRF set	57 vehicles 125-1000Hz	88%	85%	84%	43%
Rodeo airborne FRF set	98 vehicles 125-1000Hz	89%	84%	87%	49%
'Dummy' airborne data set, Gaussian distributed	57 vehicles 125-1000Hz	92%	92%	91%	0%

Table 2-6 Percentage of frequency lines with a χ^2 below 95%.

In a complex built-up structure with many degrees of freedom, such as an automotive vehicle, then the distribution of the response may be influenced by the central limit theorem [2.8]. The central limit theorem describes the case where independent random samples are taken from a population with an arbitrary distribution and have the same mean and variance. As the number of samples increases, the sum of the samples tends towards a Gaussian distribution. This may be the type of effect being seen in complex built up structures, where the probability distributions of the components may be a random distribution. However, the effect on the built-up structure may be that the distribution of the response tends towards a Gaussian distribution. For the central limit theorem to apply, the distributions of the response from the majority of the different components in the structure would need to have the same arbitrary PDF.

However, if the effect of the central limit theorem was acting, then it would also suggest that as the modal overlap increased at higher frequencies, the response distribution would tend more towards a Gaussian distribution. This was not found to be the case for this set of data. It is also worth noting that although a lognormal distribution approaches the form of a Gaussian distribution as $\sigma/\mu << 1$, a lognormal distribution was still found to be a good fit to more of the frequency lines for each FRF set than a Gaussian distribution.

It is worth discussing briefly the nature of uncertainty and variability in the context of these vehicle data sets. If the intention of collecting the data is to reveal more clearly how variability in the manufacturing process relates to variability in the noise paths in the vehicle, then the results are only partially satisfactory. The environmental conditions are not well enough controlled to minimise their influence on the results. Arguably the most significant uncertainty in a built-up structure involving rubber components is the stiffness of these joints, which in turn is highly temperature dependent. In order to minimise the environmental effects not only should the tests be carried out in a controlled environment, but also the vehicles should be temperature-soaked in this environment for several hours to allow the rubber components to settle. However, if the aim of the test data is to improve the customer experience of noise levels in the vehicle that are related to variability in the manufacturing process, then arguably the test results deliver this aim. The customer experience will include variability within the operating conditions and the environmental conditions. In either case it is still important to minimise the effect of test procedure variability, as this interferes with understanding and determination of the variability in both manufacturing tolerances and the customer experience.

2.4 Conclusions

There is very little published variability data available in order to draw conclusions on the typical levels of variability and its distribution, seen in manufactured components and structures. The literature review conducted here found the typical levels of normalised standard deviation in the response of components/structures, to be up to 0.03. Lower levels were found in single components such as the alloy wheel rim, and higher levels in built-up structures. This level of variability is relatively low and this would suggest that modelling techniques that include uncertainty by use of series expansion techniques, such as perturbation methods, may reasonably be able to ignore higher order terms. If this is the case, it constitutes a significant advantage for these methods, in terms of complexity and hence cost.

In general the distributions of the measured responses were found to be close to Gaussian in form. From analysis of the alloy wheel study conducted by Brown and Gear, the results from three of the first four modes were a good fit to both a Gaussian and Lognormal distribution. This was due to the low normalised standard deviation of the data and hence a Lognormal distribution approached a Gaussian one. The vehicles study found that a Gaussian distribution was also a good fit to between 76-85% of the frequency lines. A Gamma distribution was a good fit to slightly more of the frequency lines with 84-90% having a χ^2 fit of 95% or less. A Gamma distribution also approaches a Gaussian distribution as the ratio σ/μ becomes increasingly small and levels of $\sigma/\mu < 1$ were typical. The assumption of a Gaussian distribution for the variability has several advantages in terms of propagating variability; this will be considered in later chapters.

One of the disadvantages of the available published data on variability in structures, is the small sample size of the studies. Very little production monitoring results are available to understand further the effect of manufacturing uncertainties on response. The next chapter presents previously unpublished variability data from an automotive vehicle study, including engine noise, airborne body transfer functions and roller induced road noise. The number of vehicle samples in the study is particularly large and the controlled manner of the data collection makes it an ideal data set for variability investigations.

3. Variability in the acoustic response of two automotive vehicle models

All of the measured data used in this chapter has kindly been provided by the Ford Motor company.

In chapter two, published variability studies were reviewed and in particular two case studies were discussed in detail. The main drawbacks of the available variability results were the relatively small sample size of the studies, and the variability in test conditions contributing to the results. In this chapter, previously unpublished variability results will be presented for an extensive vehicle study. The results were collected as part of a NVH (Noise, Vibration and Harshness) programme to monitor production vehicles as part of an end-of-line testing programme. The project selected a cross-section of production vehicles prior to despatch from two product lines. Results were used to monitor production quality and to examine the effect of specific NVH components either introduced or removed from the vehicle specification. The original test work was used to compare the results between one vehicle and another, or against a target level. The work presented here is a detailed statistical analysis of the data, examining the level of variability in the results, curve-fitting to their distribution and chi-squared $\left(\chi^2\right)$ tests to examine the goodness-of-fit obtained. In general the statistical analysis or curve fitting is carried out on the linear data for direct comparison to results in chapter 2 and also for application to general propagation techniques used in later chapters. Therefore unless otherwise stated any statistical results can be assumed to be from analysis of the linear data. In some cases the results are more convenient to display on a decibel scale and this may be used to present results. The goodness of fit of a Gaussian distribution to linear results equates to the goodness of fit of a Lognormal curve to the same results in decibel form. In an engineering environment an A-weighting is often used to represent the 'human' subjective perception of noise levels. As the A-weighting is a decibel correction it would affect the distribution of the results and hence all of the results discussed here are un-weighted.

In section 3.1 the background of the data set as a whole will be explained, and this will help to present the context in which the variability arose. The vehicle test programme consisted of three sets of measurements: airborne cabin noise, roller induced road noise and interior measured engine noise. These data sets will be considered separately and are discussed in sections 3.2 to 3.4, in section 3.5 the environmental conditions of the test work will be analysed, then in section 3.6 some general comments and conclusions of the study will be discussed.

3.1 Background

The vehicle data was collected between November 2002 and July 2004, and comprises results from tests on two car models. For reasons of confidentiality these will be referred to as set 'A' and set 'B'. Set 'A' is from model A, a small hatchback with both a 3-door and 5-door derivative; the total number of vehicles tested in this set is 814. Set 'B' is from model B, a mid-sized family 5-door car; the number of vehicles in this set is 316. Both sets include results from a variety of vehicle specifications including diesel and petrol engines, manual and automatic gearboxes, different interior trim levels and different wheels and tyres. For each vehicle a comprehensive record of its specification was recorded, Table 3-1 summarises the most relevant specification items that are likely to affect interior noise. A full list is given in Appendix B. All the test work was carried out in a semi-anechoic test chamber as shown in Figure 3-1.

Hand of drive - LHD or RHD
Engine - size and type
Fuel - diesel or petrol
Tyres - manfacturer, type, size
Vehicle model year
Wheel rim - size and material
Sunroof
Transmission - manual or automatic
Version - trim level
Vin - vehicle indetification number

Table 3-1 Specification details recorded for vehicle study.

Figure 3-1 Semi-anechoic vehicle test chamber.

The environmental conditions were monitored and the temperature and the humidity recorded for each test. The effect of the environmental conditions will be discussed in section 3.5.

All of the results were analysed in groups according to body type, the numbers of vehicles of each type are shown in Table 3-2. The engine noise measurements were also sub-divided into fuel type, see section 3.4 for details.

Vehicle	Number Tested
model A 3-door	411
model A 5-door	403
model B	316

Table 3-2 Number of vehicles of each body style.

The variability in the results includes any changes to the build specification of the vehicles over the period of data collection, i.e. November 2002 and July 2004. No specific details of any such changes are available.

3.2 Cabin airborne interior noise

Sets of external sound source speakers were used in conjunction with microphones inside the cabin to estimate the general airborne noise attenuation of the vehicles. Each test was performed in the semi-anechoic chamber with six sets of source speakers at locations around the exterior of the vehicle. The speakers were connected to a noise generator producing spectrally shaped random noise. The speaker locations were selected to focus specifically on areas near to high-level noise sources on the vehicle. Two sets were placed by the front and rear tyres for estimating the attenuation of the body to airborne road noise. A third set was placed underneath the engine to examine the transparency of the body to engine noise. A fourth speaker set was located near the rear floor pan to examine transmission loss from the exhaust orifice. Two further sets were located near the front and rear of the vehicle, to examine acoustic transparency to general airborne noise. The function of each loudspeaker group was checked at the beginning of each shift by measuring the acoustic output of the loudspeaker groups. The receiver microphones inside the vehicle were positioned at the four occupant outer ear locations. Each set of exterior speakers was activated separately and the interior levels at each microphone recorded. All the results were stored as 1/3-octave spectra over a frequency range of 50Hz to 10kHz. Figure 3-2 shows the interior microphones attached to a frame to ensure repeatability of the interior noise measurement locations.

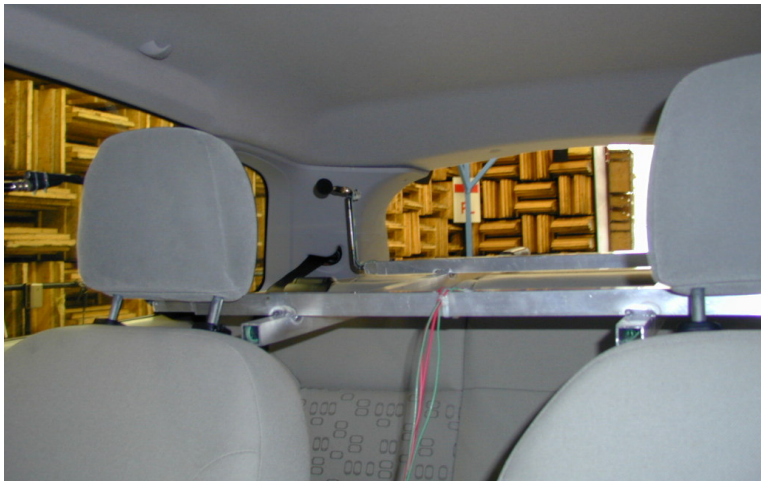

Figure 3-2 Interior microphones at the four outer ear positions.

Examples of the variability within the airborne noise measurements from each of the three body types are shown in Figure 3-3 to Figure 3-5; for ease of presentation the results are shown on a decibel scale. The results are displayed as Noise Reduction (NR) values which are defined as

$$\text{NR}\ [\text{dB}] = \text{excitation level [dB]} - \text{response level [dB]} \qquad (3.1)$$

Also shown are the maximum/minimum envelopes for the decibel results and the average in each 1/3-octave band.

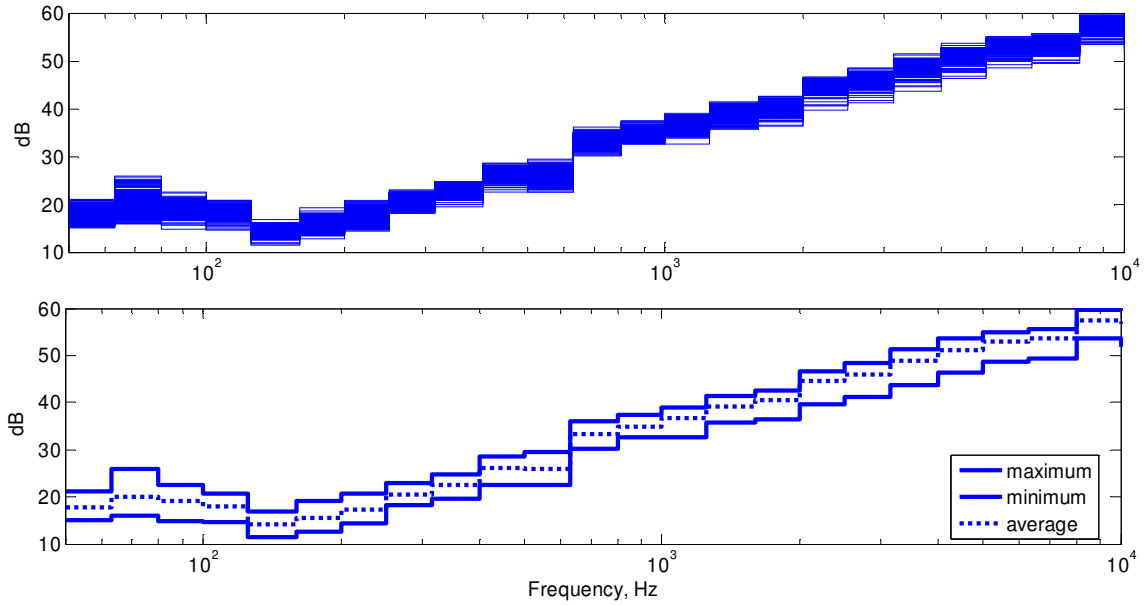

Figure 3-3 Typical Noise Reduction (higher is better): data set A 3-door, interior microphone number 3, exterior speaker set 5.

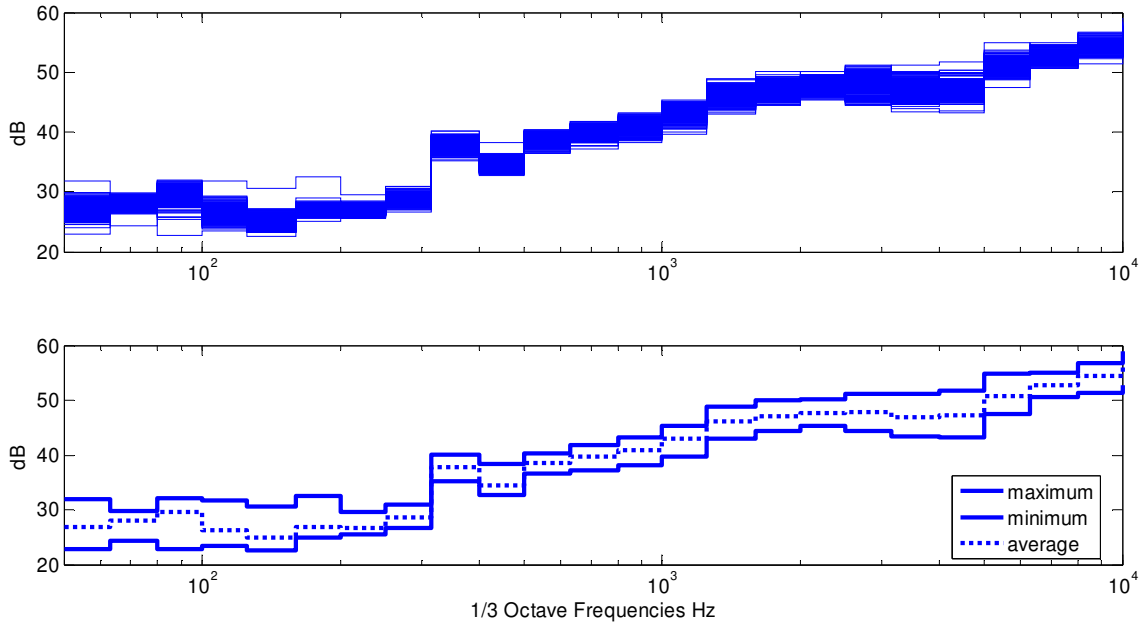

Figure 3-4 Typical Noise Reduction (higher is better): data set A 5-door, interior microphone number 1, exterior speaker set 1.

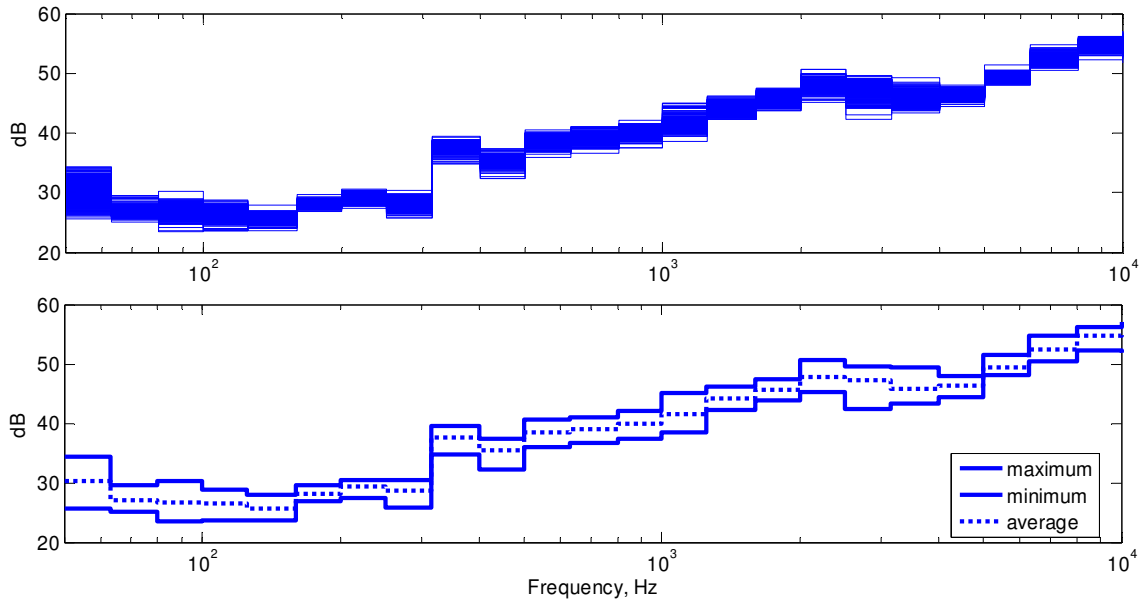

Figure 3-5 Typical Noise Reduction (higher is better): data set B, interior microphone number 2, exterior speaker set 1.

The calculated 1/3-octave NR levels show a spread of results for each body style as shown in Figure 3-3 to Figure 3-5. It is potentially of interest to discover whether the outlying results, the maximum/minimum in each 1/3-octave band, are in general from particularly good/poor vehicles. If so these vehicles may be exceptional cases which may disproportionably affect any subsequent statistical analysis. In order to investigate whether this is the case the vehicles are

'ranked' in each 1/3-octave band in order of level. The vehicles are awarded a rank value for that frequency band, one being the lowest and N being the highest, where N is the number of vehicles in that test set. These ranks numbers are then averaged with respect to frequency for each vehicle, resulting in a value associated with each vehicle representing its 'level' in the population. The distribution of the rank values for subsets of vehicle results, such as different body styles, can then be examined for extreme outlying results. An example distribution is shown in Figure 3-6.

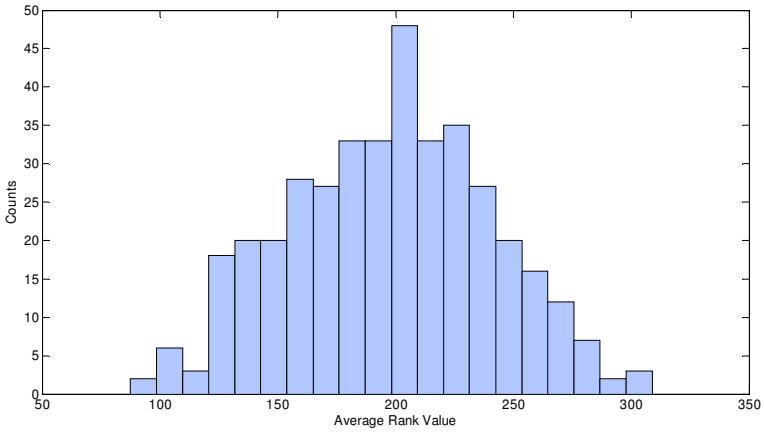

Figure 3-6 Distribution of average rank value, set A 5-door, interior microphone number 1, exterior speaker set 1.

As the vehicles were ranked from one to N, then the mean value of the average rank values is given by $(1+N)/2$. The lowest possible average rank value that would represent a vehicle result which has the lowest NR in every 1/3-octave band would be given by a value of one. The highest possible rank value that would represent a vehicle result which has the highest NR in every 1/3-octave band would be given by a value of N. As it can be seen from Figure 3-6 there are no extreme outlying rank values for the results from set A 5-door. The lowest/highest rank values seen for this vehicle set are well removed from the possible limits of one and N, indicating that there are no single vehicles which are the lowest/highest in every, or even most, 1/3-octave bands. Similar distributions were examined for the other two body styles (see examples in Figure 3-7 and Figure 3-8); again there were no significant outlying results.

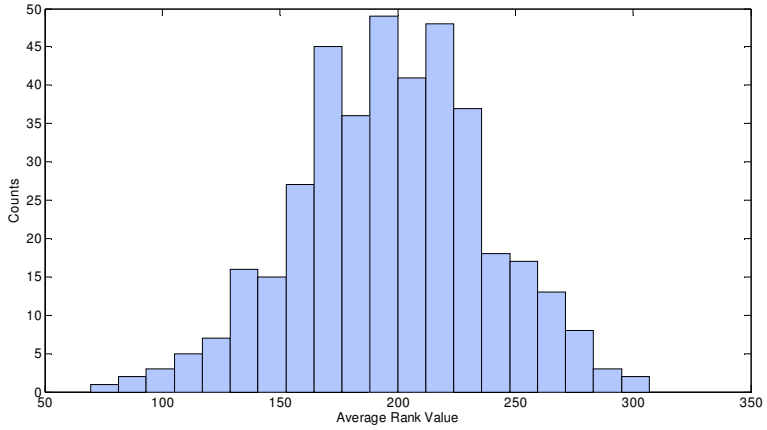

Figure 3-7 Distribution of average rank value, set A 3-door, interior microphone number 1, exterior speaker set 3.

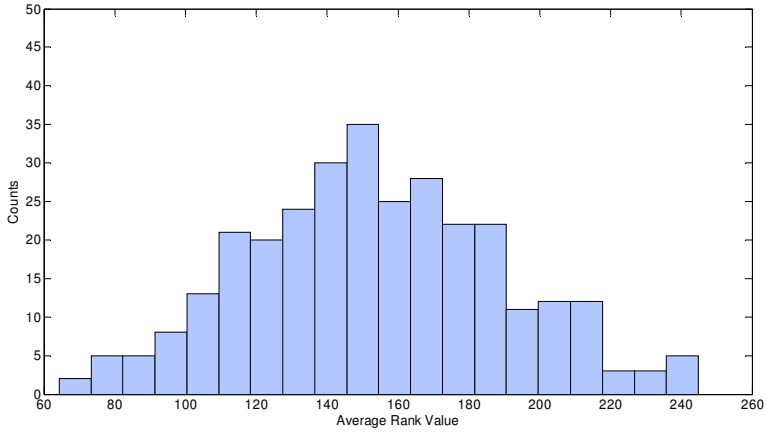

Figure 3-8 Distribution of average rank value, set B, interior microphone number 2, exterior speaker set 6.

The statistical distribution of the 1/3-octave NR levels (examples shown in Figure 3-3 to Figure 3-5) has been examined in each frequency band (24 in total), for each combination of interior microphone (4 microphones) and exterior speaker (6 speakers). Thus for each data set there were 576 sets of measurements. A χ^2 test was used to determine the goodness-of-fit of several standard distributions to each data set. The standard distributions examined were Gaussian, lognormal, gamma, Rayleigh and Weibull. There is some evidence from previous studies (see chapter 2), that the distribution of the response from nominally identical structures is Gaussian or close to Gaussian. All of the alternative distributions selected to be trialled, can under certain combinations of their parameters, become close to Gaussian in form. Further information on each of the distributions can be found in [3.1]. The maximum likelihood method was used to estimate the parameters for each of the distributions. Examples of typical results for each body type, at low, mid and high frequencies are shown in Figure 3-9 to Figure 3-17. The distributions are shown as normalised to zero mean and unit standard deviation. Each set of results are

classified or 'binned' into twenty bins of equal width; the width depending on the range of that distribution.

In order to avoid any outlying results disproportionably affecting the χ^2 result, the outlying bins are summed to ensure a minimum of four counts in each bin. The χ^2 test is a negative hypothesis test. The results are presented as the percentage of frequency bands for which the χ^2 probability is below 95%, which equates to a 95% confidence that the set of results cannot be rejected as having come from the distribution they are being tested against. The χ^2 results for the curve fitting are shown in Table 3-3. The distribution that fits the most frequency bands for each vehicle model is highlighted. Also shaded are distributions that are close to the best fit, this is chosen to be within 5% of the 'best fit' value, as these might be considered also to be good fits to the results.

	Gaussian	Lognormal	Gamma	Rayleigh	Weibull
set A 3dr	55.0%	56.6%	58.2%	0.0%	13.4%
set A 5dr	61.5%	66.3%	67.7%	0.0%	10.6%
set B	70.3%	79.9%	79.3%	0.0%	13.7%

Table 3-3 Airborne interior NR, percentage of frequency lines that have a $\chi^2 \leq 0.95$.

Three distributions could not be rejected as being a good fit to over 50% of the frequency bands for the airborne cabin NR; these were the Gaussian, lognormal and gamma distributions. Examining the results by vehicle model it can be seen that a gamma distribution was the best fit to the results from both the 3-door and 5-door results in set A, where 58.2% and 67.7% of the frequency bands respectively have a $\chi^2 \leq 0.95$. A lognormal distribution was also a good fit to these results with 56.6% and 66.3% of the results for the set A 3-door and 5-door being a good fit. A lognormal distribution was the best fit to the results from set B where 79.9% of the frequency bands have a $\chi^2 \leq 0.95$, however a gamma distribution was also a good fit with 79.3%. Neither a Rayleigh nor a Weibull distribution was a good fit to the results.

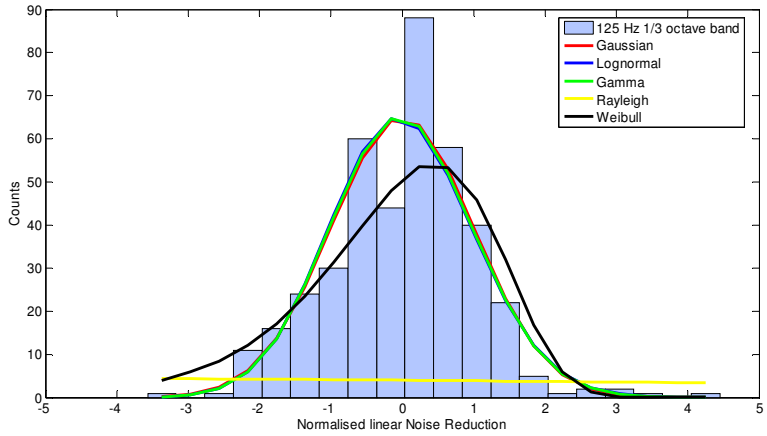

Figure 3-9 Distribution of airborne interior NR: data set A 3-door, interior microphone 2, source speaker set 1, 125Hz 1/3-octave band.

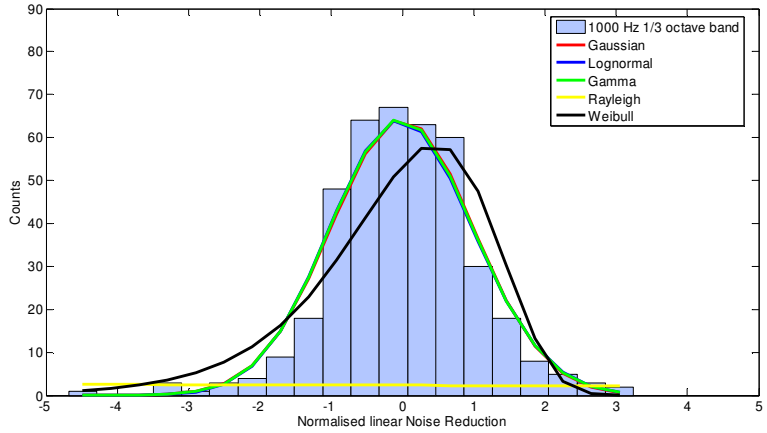

Figure 3-10 Distribution of airborne interior NR: data set A 3-door, interior microphone 2, source speaker set 1, 1kHz 1/3-octave band.

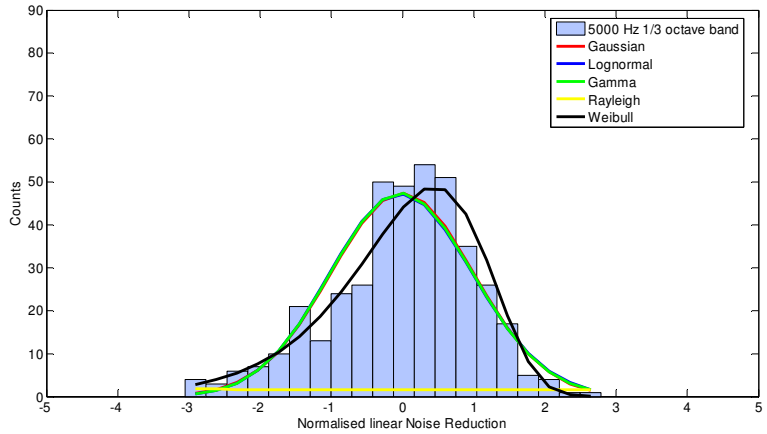

Figure 3-11 Distribution of airborne interior NR: data set A 3-door, interior microphone 2, source speaker set 1, 5kHz 1/3-octave band.

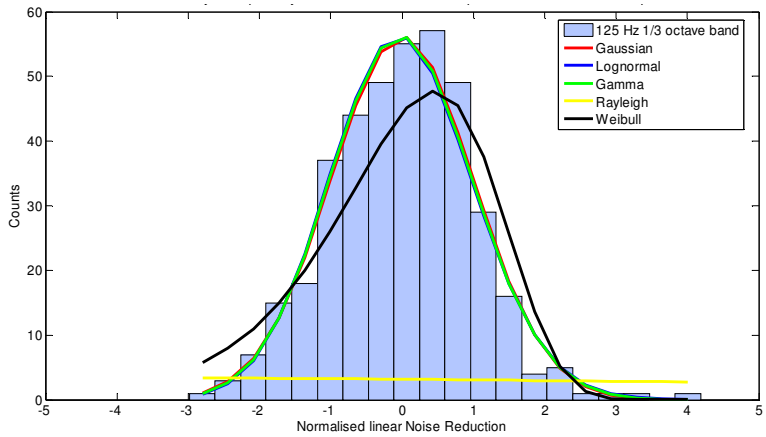

Figure 3-12 Distribution of airborne interior NR: data set A 5-door, interior microphone 2, source speaker set 1, 125Hz 1/3-octave band.

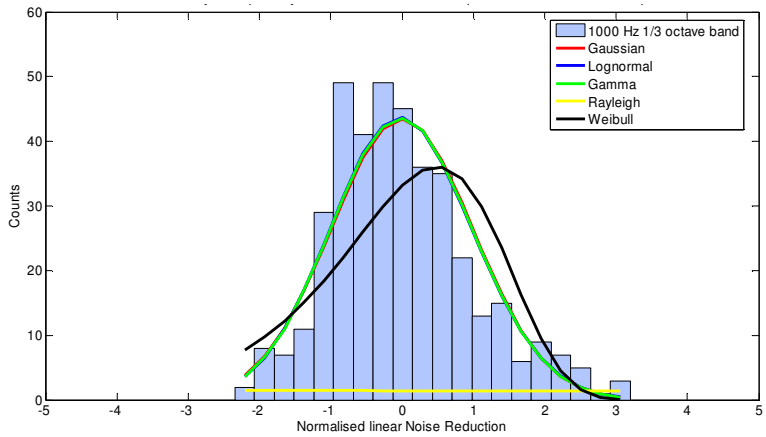

Figure 3-13 Distribution of airborne interior NR: data set A 5-door, interior microphone 2, source speaker set 1, 1kHz 1/3-octave band.

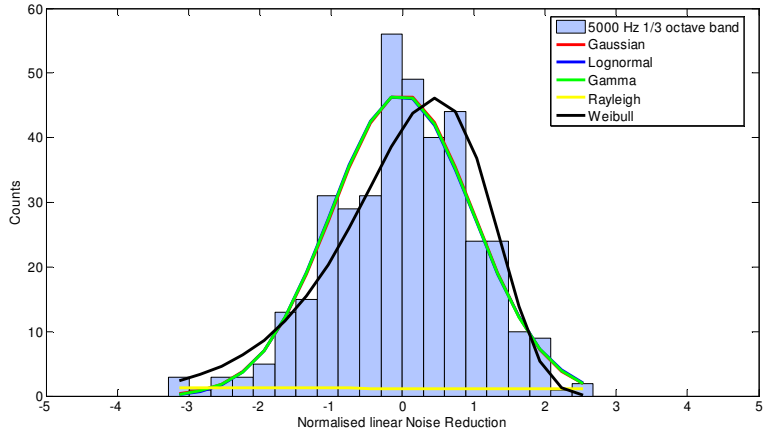

Figure 3-14 Distribution of airborne interior NR: data set A 5-door, interior microphone 2, source speaker set 1, 5kHz 1/3-octave band.

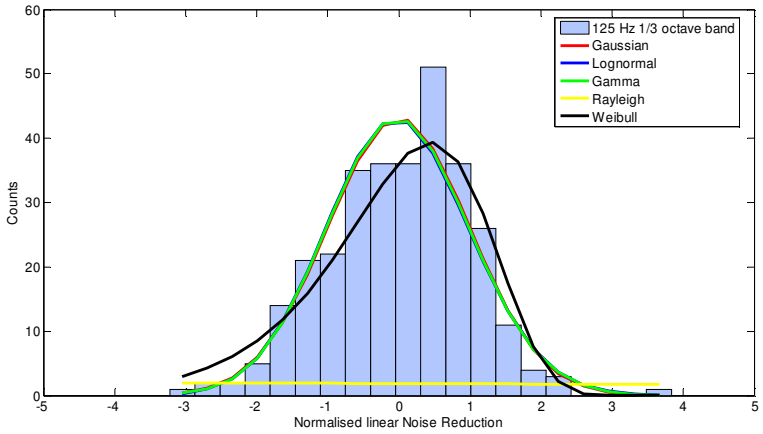

Figure 3-15 Distribution of airborne interior NR: data set B, interior microphone 2, source speaker set 1, 125Hz 1/3-octave band.

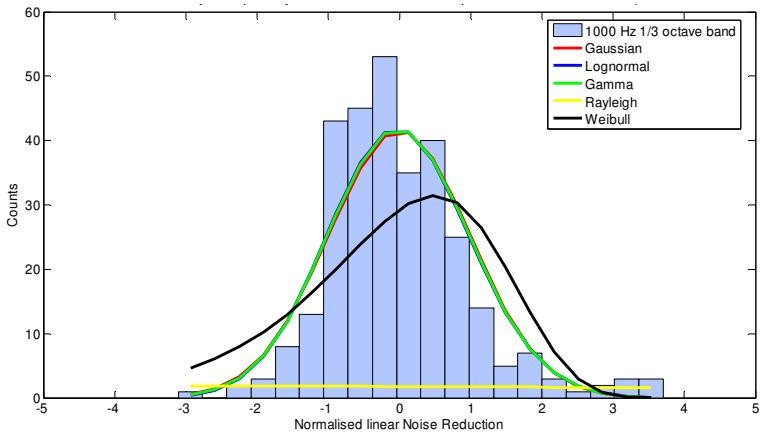

Figure 3-16 Distribution of airborne interior NR: data set B, interior microphone 2, source speaker set 1, 1kHz 1/3-octave band.

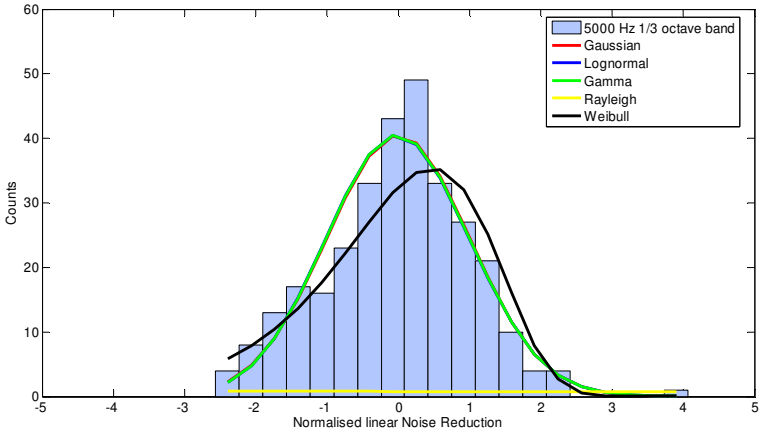

Figure 3-17 Distribution of airborne interior NR: data set B, interior microphone 2, source speaker set 1, 5kHz 1/3-octave band.

Further investigations were carried out to examine the results with respect to frequency. For this purpose the low frequencies are defined as 50Hz to 1kHz, and high frequencies as 1kHz to

10kHz. Again the results are presented as the percentage of the frequency bands, at either low or high frequency, for which $\chi^2 \leq 0.95$. The results are shown in Table 3-4 and Table 3-5.

At lower frequencies the distribution of the levels can be seen to be a good fit to a lognormal distribution, where between 67.0% and 74.7% of the frequency bands cannot be rejected as having come from a lognormal distribution. At higher frequencies a Gaussian distribution is the best fit to the results from set A (58.3% to 68.8%), but for set B, a gamma distribution fits slightly more of the frequency bands (88.3%), although a Gaussian distribution also fits a large percentage (85.8%).

	Gaussian	Lognormal	Gamma	Rayleigh	Weibull
set A 3dr	52.7%	67.0%	66.1%	0.0%	5.7%
set A 5dr	56.3%	74.7%	72.3%	0.0%	9.5%
set B	59.2%	74.7%	72.9%	0.0%	14.3%

Table 3-4 Airborne interior NR, percentage of frequency lines below 1kHz that have $\chi^2 \leq 0.95$.

	Gaussian	Lognormal	Gamma	Rayleigh	Weibull
set A 3dr	58.3%	42.1%	47.1%	0.0%	24.2%
set A 5dr	68.8%	54.6%	61.3%	0.0%	12.1%
set B	85.8%	87.1%	88.3%	0.0%	12.9%

Table 3-5 Airborne interior NR, percentage of frequency lines above 1kHz that have $\chi^2 \leq 0.95$.

One hypothesis for the differences between the statistical distributions of the NR levels at low frequencies to that at high frequencies is that it may be due to sealing of the vehicles. At lower frequencies below 1kHz it may be controlled by the transmission loss of the vehicle body, whereas at higher frequencies it is more likely to be affected by leakage and sealing of small holes in the body. If this is the case the different mechanisms may have different distributions.

It is also worth examining the normalised standard deviation of the results. Figure 3-18 shows the average of the 24 data sets (6 external source speakers to 4 internal receiver microphones) with respect to frequency for each data set. The levels of normalised standard deviation are generally high in comparison to those in published variability data sets, (as discussed in chapter 2), where a typical level of 0.01 is seen. This is not unexpected as the data sets A 3-door, A 5-door and set B, still contain a range of different vehicle model specifications including trim levels. Whereas the published variability data from manufactured components discussed in chapter 2 reviews the variability within groups of nominally identical components. However,

the levels of normalised standard deviation are lower than those in the airborne transfer functions from the Isuzu vehicle sets of identical vehicles discussed in chapter 2.3, where the levels generally range between 0.2 and 0.6. This is probably due to improved test facilities and hence a reduction in the environmental variability particularly temperature, for which the Isuzu vehicle sets had a normalised standard deviation of 0.17-0.18 compared to 0.11 for models A and B.

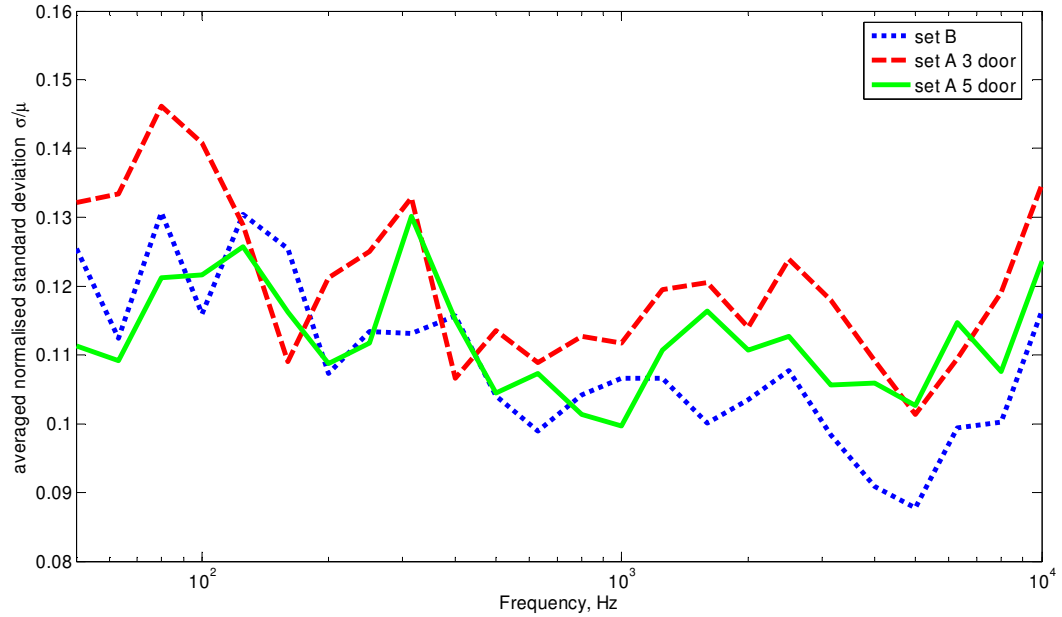

Figure 3-18 Normalised standard deviation of the airborne interior NR.

The distribution of the overall cabin NR was also examined. The overall levels are calculated over the frequency range 200Hz-10kHz as the very low frequencies dominate the level and these tend to be more affected by background noise issues (due to low excitation levels from the speakers at these frequencies). The overall NR level is given by

$$\text{overall NR}\ [\text{dB}] = -10\log\left(\frac{\sum_{n} 10^{\frac{-\text{NR}_n}{10}}}{n}\right) \tag{3.2}$$

where n is the number of 1/3-octave bands (200Hz-10kHz is 18 bands) and NR_n is the Noise Reduction level in decibels for the n'th 1/3-octave band. This calculation assumes the source spectrum to be flat. Table 3-6 shows the percentage of the data sets (24 in total) for which the distribution tested cannot be rejected as being a good fit. A Gaussian distribution is a good fit to

the results from each of the vehicle body styles, fitting 54-67% of the results. A lognormal and gamma distribution are also a good fit to the results for set A 5-door and set B; these distribution types approach a Gaussian as $\sigma/\mu \ll 1$ and this is certainly the case for these results. Examples of the distributions of the overall NR are shown in Figure 3-19 to Figure 3-21.

	Gaussian	Lognormal	Gamma	Rayleigh	Weibull
set A 3dr	54.2%	37.5%	37.5%	0.0%	16.7%
set A 5dr	66.7%	66.7%	66.7%	0.0%	16.7%
set B	58.3%	62.5%	62.5%	0.0%	16.7%

Table 3-6 Airborne interior NR, percentage of overall level of FRFs that have $\chi^2 \leq 0.95$.

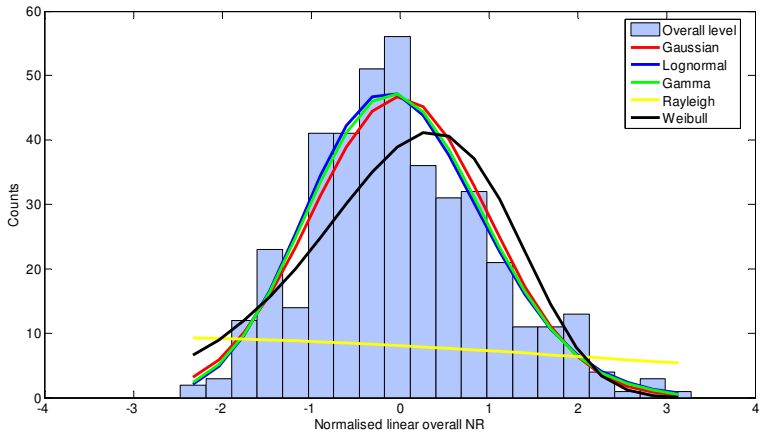

Figure 3-19 Distribution of the overall airborne interior NR: data set A 3-door, interior microphone 1, source speaker set 5.

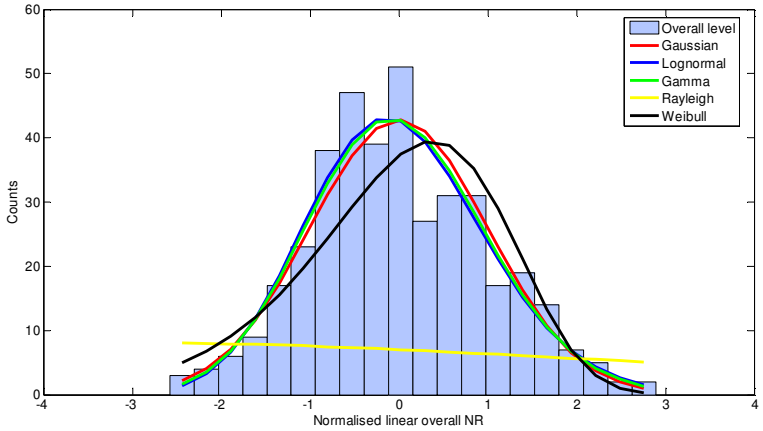

Figure 3-20 Distribution of the overall airborne interior NR: data set A 5-door, interior microphone 1, source speaker set 5.

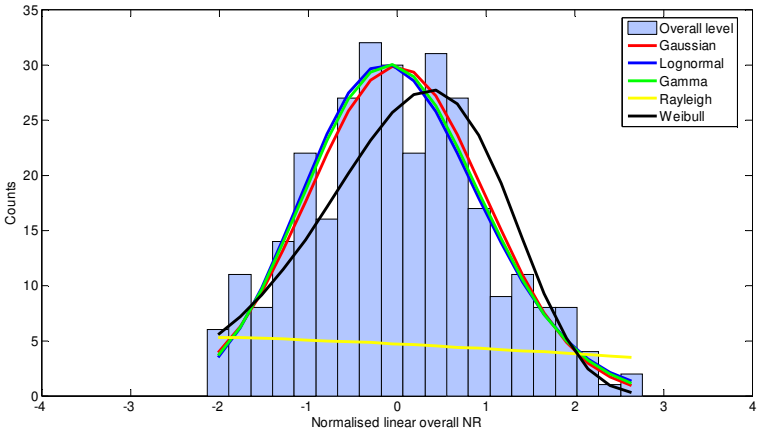

Figure 3-21 Distribution of the overall airborne interior NR: data set B, interior microphone 1, source speaker set 5.

Conclusions

Three distributions could not be rejected as being a good fit to over 50% of the frequency bands for the airborne cabin NR; these were the Gaussian, lognormal and gamma distributions. The gamma distribution was the best fit to the results from both the 3-door and 5-door set A and a lognormal distribution was the best fit to the set B results.

A frequency breakdown concluded that at lower frequencies the distribution was well described by a lognormal distribution. At higher frequencies the results were best described by a Gaussian distribution, although a gamma distribution fitted marginally more results for set B.

Examination of the distribution of the overall levels suggests a Gaussian distribution to be the most representative of the spread of results.

3.3 Roller induced road noise

For the road noise measurements the vehicle was installed on a dynamometer roller test rig, see Figure 3-22. The roller surface has two test surfaces, a smooth surface and a 'rough' surface consisting of a random pattern of 'projections' to simulate a coarse impact input into the tyre (Patent DE 102004002506 A1 04.08.2005). Figure 3-23 shows a vehicle installed on the road noise rollers. The tests were conducted on the 'rough' surface at 50kph (30mph) steady state; 1/3-octave interior noise measurements were collected from 20Hz to 10kHz. The microphone test frame as used for the airborne cabin measurements was used to ensure repeatable

positioning of the interior microphones at the front and rear occupant outer ear positions. Examples of the variability within the road noise measurements from each of the three body types are shown in Figure 3-24 to Figure 3-26; for ease of presentation the results are shown on a decibel scale. Also shown are the maximum/minimum envelopes for the decibel results and the average in each 1/3-octave band.

Each axle of the vehicle was tested separately, thus with 4 interior microphones and 28 third-octave frequency bands, there are 224 sets of results for each of the vehicle tests. The results are analysed in groups according to body type, the numbers of vehicles of each type are shown in Table 3-2.

Figure 3-22 Vehicle road noise dynamometer with patented surface.

Figure 3-23 A test vehicle installed on the road noise rollers with patented surface.

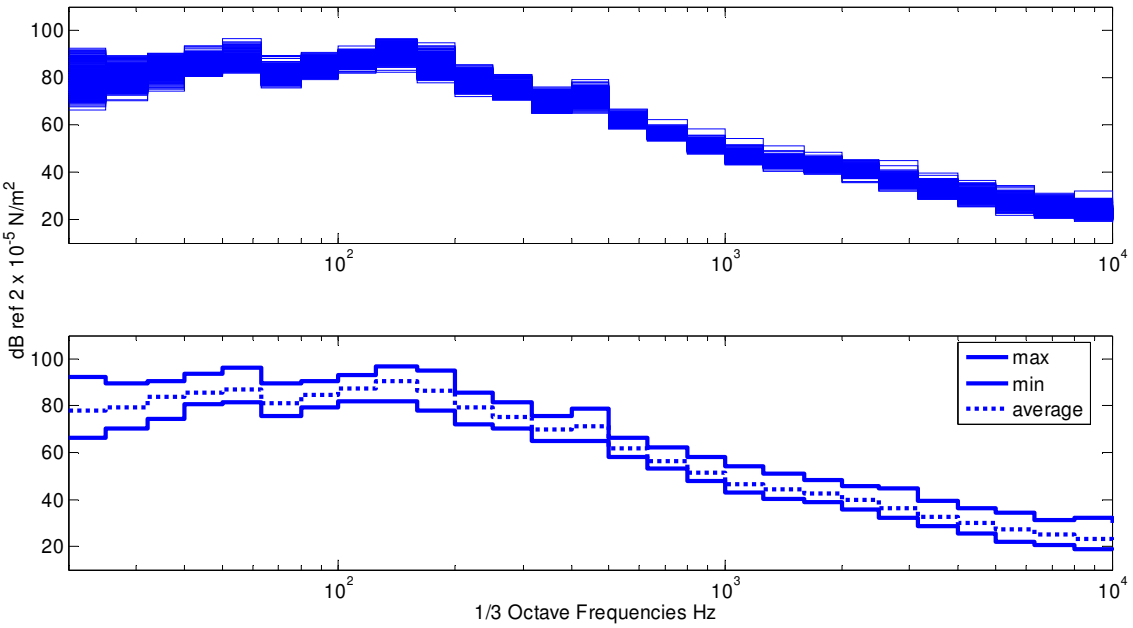

Figure 3-24 Road noise example: set A 3-door interior microphone number 2, front axle, 'rough' surface, 407 vehicles.

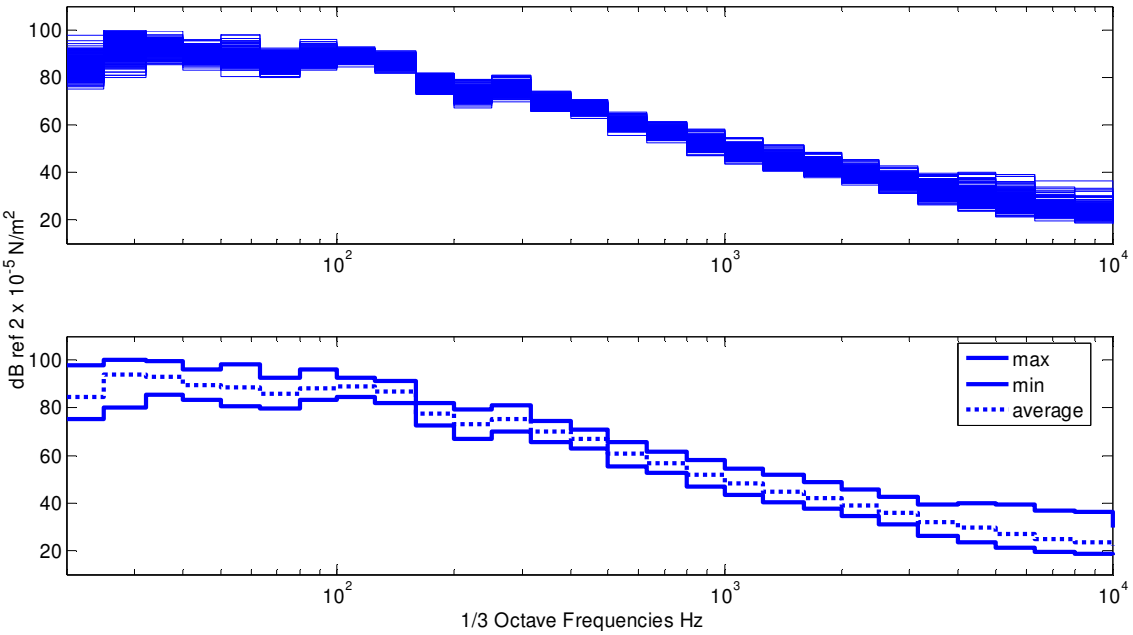

Figure 3-25 Road noise example: set A 5-door interior microphone number 2, rear axle, 'rough' surface, 393 vehicles.

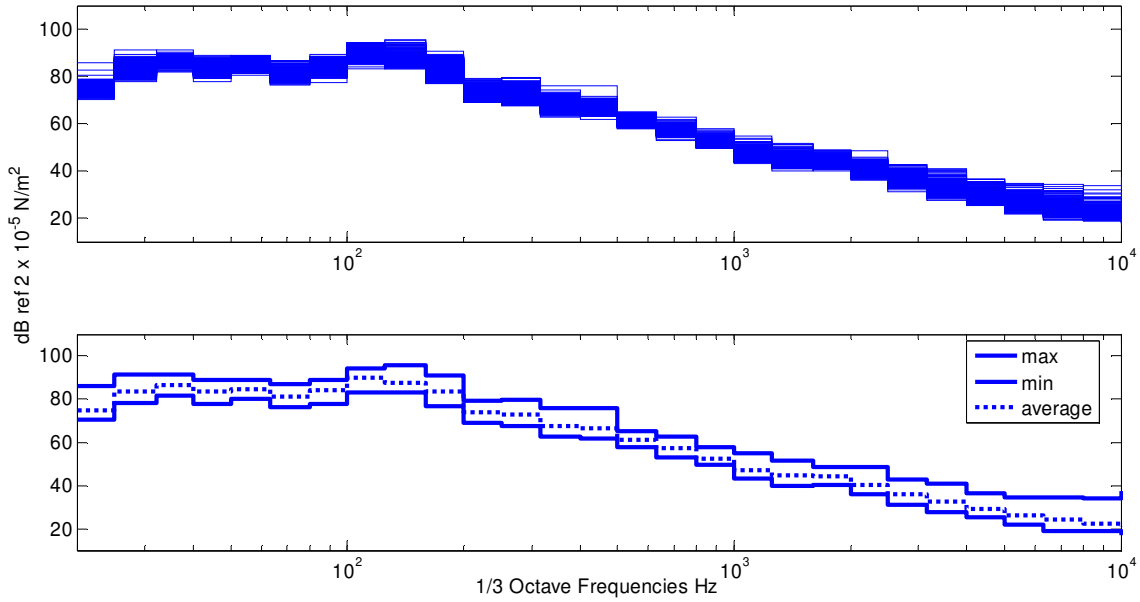

Figure 3-26 Road noise example: set B interior microphone number 1, front axle, 'rough' surface, 306 vehicles.

Using a similar method to that described in the airborne noise section, the results can be ranked to check for any extreme outlying results within the populations. The vehicles were ranked from one to N and so the mean value of the average rank values is given by $(1+N)/2$. The lowest possible average rank value that would represent a vehicle result which was the quietest in every 1/3-octave band would be given by a value of one. The highest possible rank value that would represent a vehicle result which was the loudest in every 1/3-octave band would be given by a value of N. A typical distribution of the average rank values for set A 5-door is shown in Figure 3-27. It can be seen for this example, that there is a group of three vehicles at the lower end of the average rank values which are generally quieter than the rest of the population and a group of four vehicles at the higher end of the average rank values for which the levels are generally higher than the rest of the population. However, none of these vehicles are close to the limits for the average rank values and hence are not significant outlying results in the population. Similar distributions can be found for the results from set A 3-door and set B.

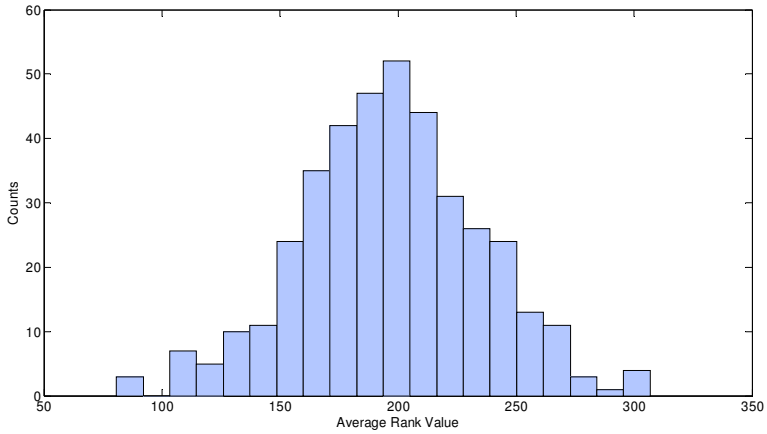

Figure 3-27 Distribution of average rank value, set A 5-door, interior microphone number 1, front axle.

The subsequent statistical analysis is conducted on the linear data. Examples of the typical distributions of 1/3-octave levels for each body type, at low, mid and high frequencies are shown in Figure 3-28 to Figure 3-36. The distributions are shown as normalised to zero mean and unit standard deviation. The results for each body type are shown on the same scales for comparison. Each set of results are classified or 'binned' into twenty bins of equal width; the width depending on the range of that distribution. The examples shown are typical of the results for most frequencies for all the data sets. However, one particular frequency band at 315Hz is slightly different and will be discussed later.

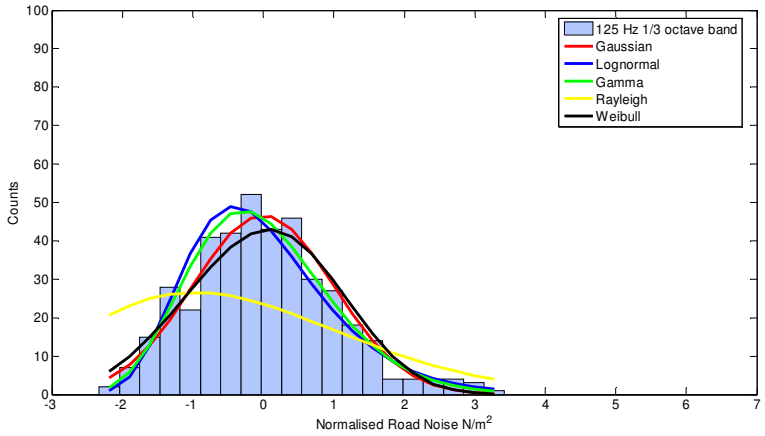

Figure 3-28 Example of the road noise distribution at 125Hz, data set A 3-door, interior microphone 2, front axle.

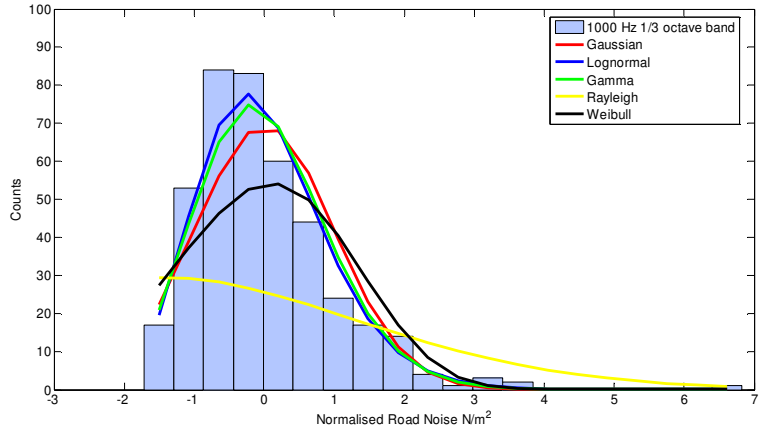

Figure 3-29 Example of the road noise distribution at 1kHz, data set A 3-door, interior microphone 2, front axle.

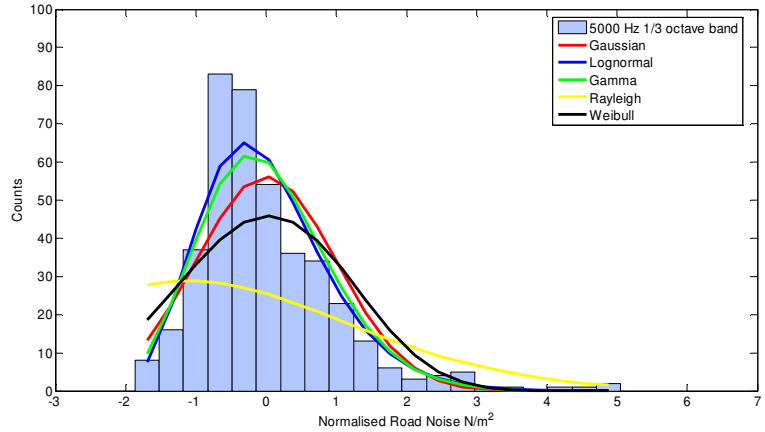

Figure 3-30 Example of the road noise distribution at 5kHz, data set A 3-door, interior microphone 2, front axle.

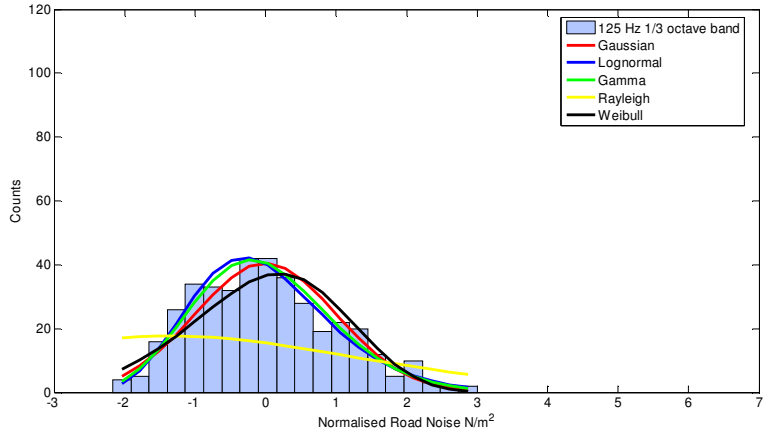

Figure 3-31 Example of the road noise distribution at 125Hz, data set A 5-door, interior microphone 3, rear axle.

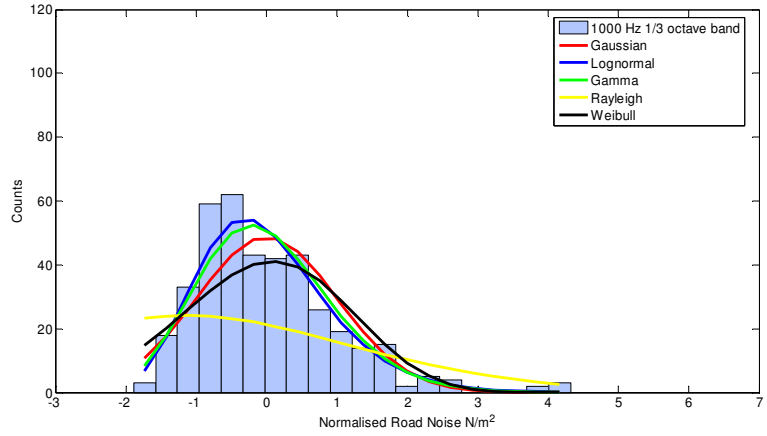

Figure 3-32 Example of the road noise distribution at 1kHz, data set A 5-door, interior microphone 3, rear axle.

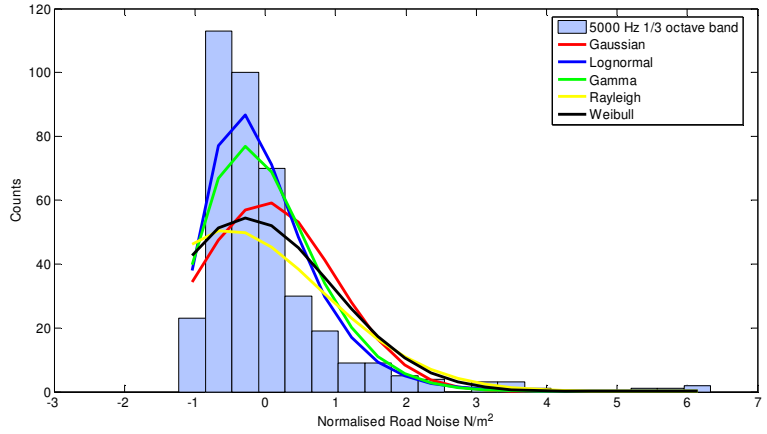

Figure 3-33 Example of the road noise distribution at 5kHz, data set A 5-door, interior microphone 3, rear axle.

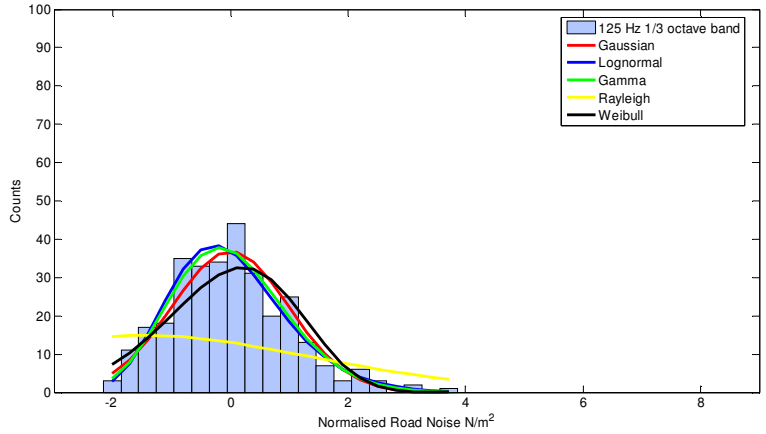

Figure 3-34 Example of the road noise distribution at 125Hz, data set B, interior microphone 1, front axle.

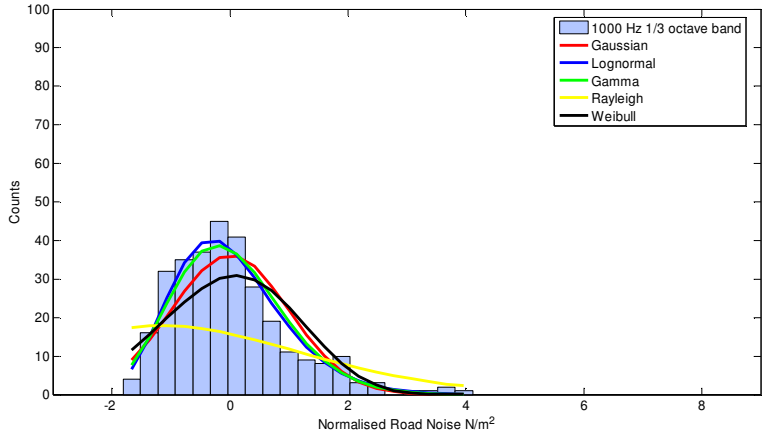

Figure 3-35 Example of the road noise distribution at 1kHz, data set B, interior microphone 1, front axle.

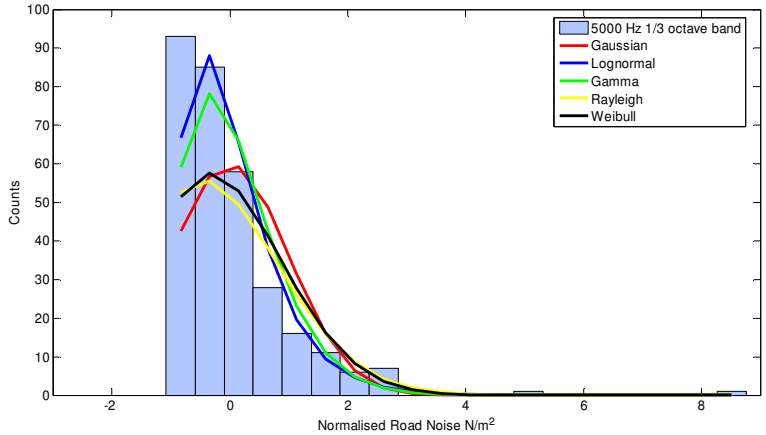

Figure 3-36 Example of the road noise distribution at 5kHz, data set B, interior microphone 1, front axle.

A χ^2 test was applied to evaluate the goodness-of-fit of several distributions. The percentages of the data sets that cannot be rejected as having come from each distribution are shown in Table 3-7. As before the distribution that fits the most frequency bands for each vehicle model is highlighted. Also shaded are distributions that are close to the best fit, this is chosen to be within 5% of the 'best fit' value, as these might be considered to also be good fits to the results. A lognormal distribution was the best fit to the results from all the data sets with between 40.6% and 46.4% of the frequency bands with a $\chi^2 \leq 0.95$.

	Gaussian	Lognormal	Gamma	Rayleigh	Weibull
set A 3dr	9.8%	40.6%	27.7%	0.0%	5.8%
set A 5dr	12.1%	43.3%	34.4%	0.4%	7.6%
set B	17.4%	46.4%	41.5%	0.0%	5.8%

Table 3-7 Roller induced road noise, percentage of frequency lines that have $\chi^2 \leq 0.95$.

Within the data sets for the different vehicle body types there was a selection of different tyre sizes and wheel rim materials. In order to evaluate the variability within a set of identical tyres and rims, a χ^2 test was applied to a reduced set. Data set A 3-door was used as this was the largest data set. The data set was filtered to contain only results from vehicles with steel rims and a single tyre size (175/65-R14) from one manufacturer (111 vehicles). As before χ^2 test was applied to evaluate the goodness-of-fit of several distributions. The percentages of the data sets that cannot be rejected as having come from each distribution are shown in Table 3-8.

	Gaussian	Lognormal	Gamma	Rayleigh	Weibull
set A 3dr	35.7%	62.9%	55.4%	0.4%	23.7%

Table 3-8 Steel wheel rims, tyre size 175/65-R14, percentage of frequency lines that have $\chi^2 \leq 0.95$.

As it can be seen from the above results significantly more of the frequency lines, 63%, are a good fit to a Lognormal distribution when examining results within a set of nominally identical wheels/tyres.

At higher frequencies, above 1kHz, the interior noise measurements can be affected by squeaks and rattles in the vehicles being excited by the vibration of the rough roller input. Such intermittent noises inside the cabin are highly variable and unrepeatable. In order to understand the underlying distribution of the results without the additional variability of squeaks and rattles,

the results were analysed for a limited frequency range from 20Hz to 1kHz. The χ^2 tests are summarised in Table 3-9. These results are not sorted by tyre size or rim material, i.e. they include all wheels/tyres.

	Gaussian	Lognormal	Gamma	Rayleigh	Weibull
set A 3dr	13.2%	59.0%	45.1%	0.0%	9.0%
set A 5dr	18.1%	57.6%	45.1%	0.7%	9.7%
set B	22.2%	60.4%	52.8%	0.0%	7.6%

Table 3-9 Roller induced road noise, percentage of frequency lines 20Hz-1kHz that have $\chi^2 \leq 0.95$.

It can be seen from the results in Table 3-9 that more of the data sets have a $\chi^2 \leq 0.95$ when tested against the selected distributions. A lognormal distribution is still the best fit to the results from all the data sets, with between 57.6% and 60.4% of the data sets being a good fit to a lognormal distribution. Compared to between 40.6% and 46.4% for the frequency range 20Hz-10kHz.

The effect of both limiting the frequency range and only examining nominally identical wheels/tyres can be combined. In Table 3-10 the results from the χ^2 tests for a limited frequency range using results from data set A 3-door filtered to only contain results from vehicles with steel rims and a single tyre size (175/65-R14) from one manufacturer, are summarised.

	Gaussian	Lognormal	Gamma	Rayleigh	Weibull
set A 3dr	50.0%	77.8%	71.5%	0.7%	35.4%

Table 3-10 Steel wheel rims, tyre size 175/65-R14, 111 vehicles, percentage of frequency lines 20Hz-1kHz that have $\chi^2 \leq 0.95$.

It can be seen that when the frequency range is limited to 20Hz-1kHz and the wheels/tyres are limited to be nominally identical, the number of frequency lines that are a good fit to a Lognormal distribution increases significantly from 40.6% in Table 3-7 to 77.8% shown above. The effect of limiting the frequency range when examining nominally identical tyres improved the number of frequency lines that were a good fit to a Lognormal distribution from 62.9% in Table 3-8, to 77.8% above.

The distribution of the overall levels road noise was also examined. Table 3-11 shows the percentage of the overall road noise data sets (8 in total) for which the distribution tested cannot be rejected as being a good fit. The overall level is calculated as that from 50Hz to 1kHz. Data set A 3-door results are a good fit to a Gaussian, lognormal or gamma distribution. The results from data set A 5-door are a good fit to a lognormal or gamma distributions. All the distributions tested are a poor fit to the results from set B, the best fitting is only 25% for a lognormal and gamma distributions. These results can be examined further and some typical examples from set B can be seen in Figure 3-37 and Figure 3-38. As it can be seen from the results, the distributions vary greatly in terms of skew and spread, which goes some way to explaining the poor fit of the distributions tested.

	Gaussian	Lognormal	Gamma	Rayleigh	Weibull
set A 3dr	87.5%	87.5%	87.5%	0.0%	0.0%
set A 5dr	37.5%	62.5%	62.5%	0.0%	12.5%
set B	12.5%	25.0%	25.0%	0.0%	12.5%

Table 3-11 Road noise, percentage of overall level of FRFs that have $\chi^2 \leq 0.95$.

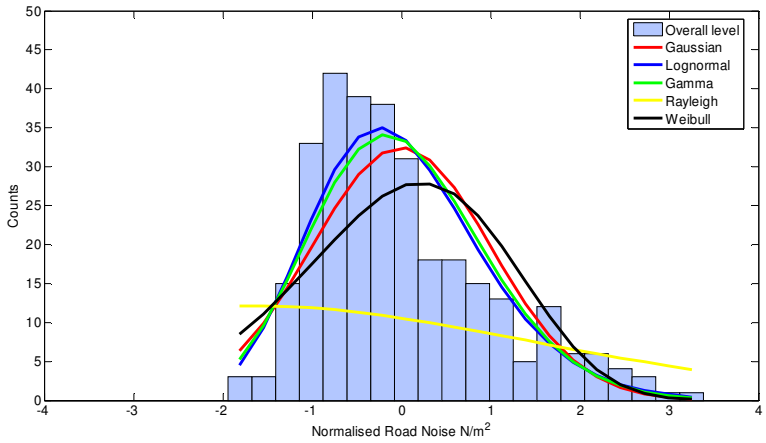

Figure 3-37 Distribution of the overall interior road noise: data set B, interior microphone 1, front axle.

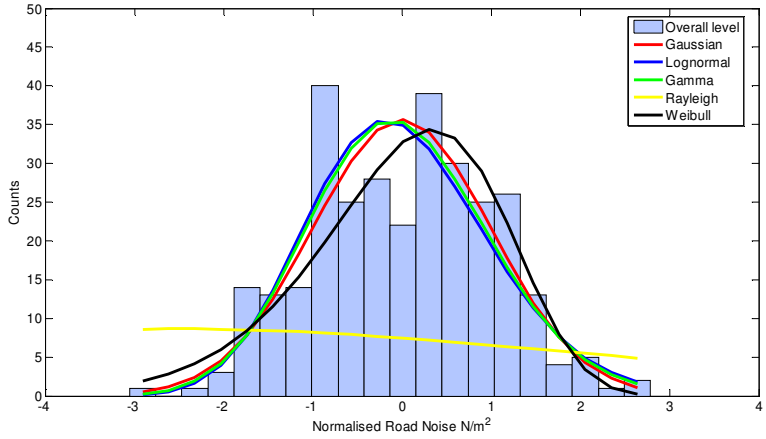

Figure 3-38 Distribution of the overall interior road noise: data set B, interior microphone 1, rear axle.

As already discussed, the distributions of the road noise data sets are typically represented by the examples in Figure 3-28 to Figure 3-36, except for the 315Hz band. The distribution for this band in data set A appears to be bi-modal, as can be seen in Figure 3-39 and Figure 3-40. Data set B does not display a bi-modal feature at this frequency see Figure 3-41. Information supplied by Ford suggests that this effect is due to the wheel rim material and this can be confirmed by analysing the results according to rim material type.

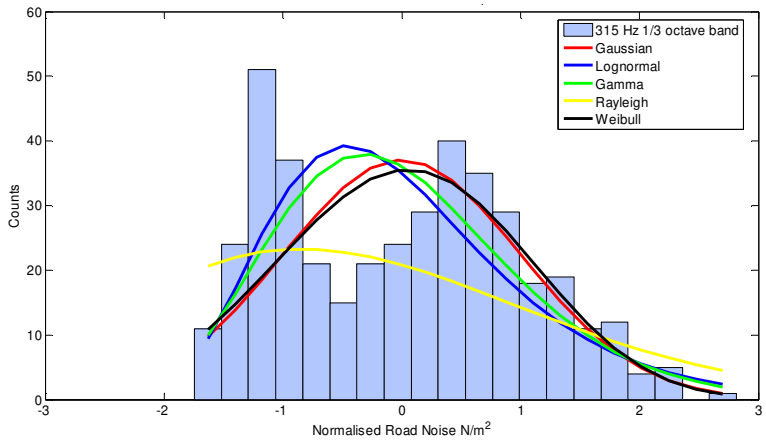

Figure 3-39 Road noise distribution, data set A 3-door, 315Hz band, interior microphone 1, front axle.

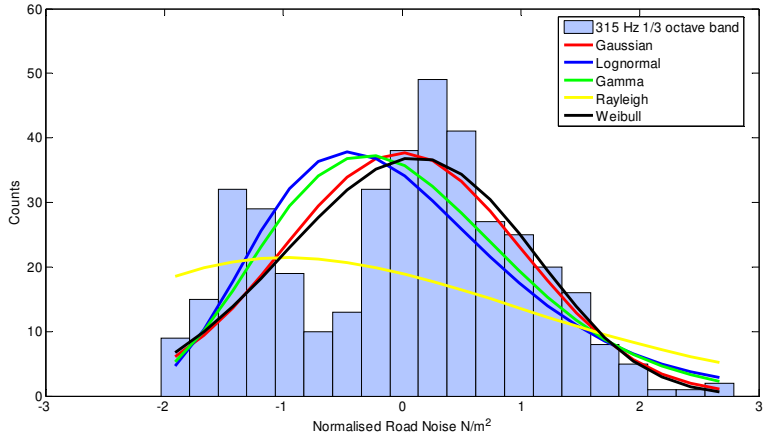

Figure 3-40 Road noise distribution, data set A 5-door, 315Hz band, interior microphone 1, front axle.

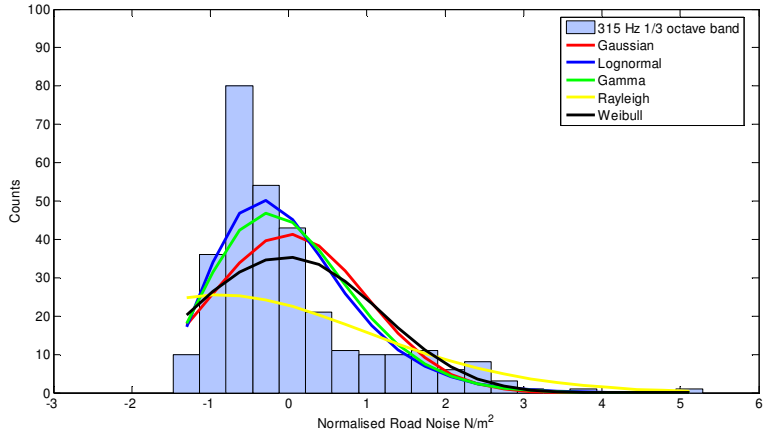

Figure 3-41 Road noise distribution, data set B, 315Hz band, interior microphone 1, front axle.

Figure 3-42 shows the distribution for the 315Hz band from vehicle set A 3-door, with only vehicles with steel wheel rims included (263 vehicles in total). For comparison Figure 3-43 shows the distribution for the vehicles from set A 3-door with alloy wheel rims included (144 vehicles in total). Analyses of the results from set A 5-door show the same behaviour, but have not been presented here.

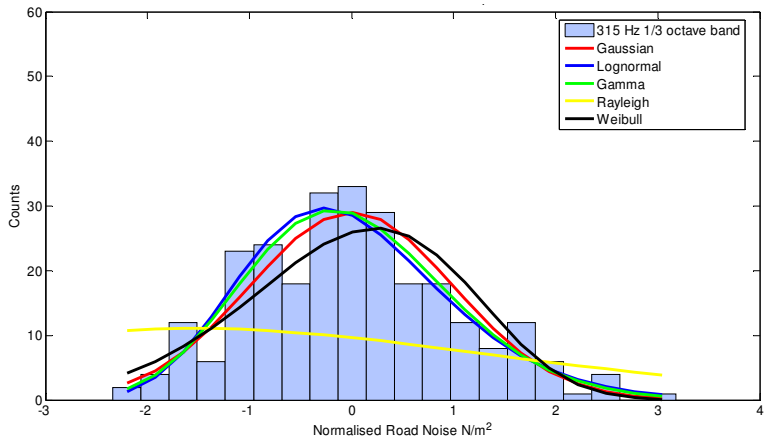

Figure 3-42 Road noise distribution, data set A 3-door, steel wheel rims only, 315Hz band, interior microphone 1, front axle, 263 vehicles.

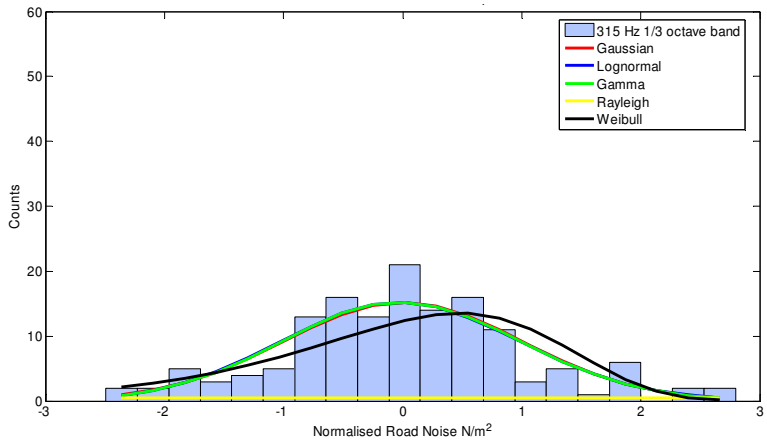

Figure 3-43 Road noise distribution, data set A 3-door, alloy wheel rims only, 315Hz band, interior microphone 1, front axle, 144 vehicles.

As it can be seen from the above figures, the bi-modal feature of the 315Hz is due to wheel rim material differences. This frequency band would normally contain the tyre cavity frequency for tyres of this size. The tyre cavity frequency is the resonance frequency of the air cavity formed inside the tyre/rim. It is likely that in the tyre acoustic cavity is being excited, which in turn is exciting the modes in the wheel rim. As the mass of the wheel rim changes with steel or alloy wheel, different modes may be excited thus causing the bi-modal spread of results seen at this frequency.

The normalised standard deviation was also examined; see Figure 3-44, which shows the average of the 8 road noise data sets (4 internal microphones, front and rear axle) with respect to frequency for each model body type.

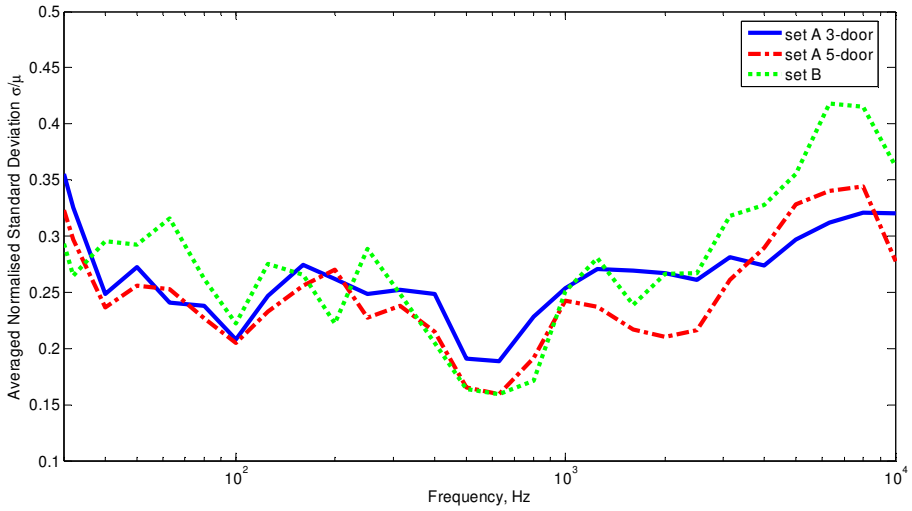

Figure 3-44 Normalised standard deviation of the road noise.

The level of variability within the road noise data is quite high with the averaged normalised standard deviation ranging from 0.16 to 0.47. As already mentioned, the vehicles were fitted with a selection of tyres and the tread pattern and size of these is likely to have a significant effect on the road noise, which will increase the expected levels of standard deviation in each data set. The level of variability below 1kHz can be seen to generally be lower than that above 1kHz which again suggests that there may be some very variable high frequency noises in the vehicles such as squeaks and rattles contributing to the results. The levels of normalised standard deviation within a set of nominally identical wheels and tyres can be investigated. The data set was filtered to only contain results from vehicles with steel rims and a single tyre size (175/65-R14) from one manufacturer (111 vehicles). Figure 3-45 shows a comparison of the averaged normalised standard deviation for this group of nominally identical wheels/tyres to the full set of results for that vehicle body. As can be seen from these results the levels of variability are lower for the set of nominally identical wheels/tyres in the frequency range 40Hz-600Hz. In this range the level is typically 0.2. This would suggest that at very low and very high frequencies, the variability in the road noise is not due to tyre/wheel differences. At high frequencies it has been suggested that this is due to squeaks and rattles in the vehicles. There is no obvious cause suggested for the variability at very low frequencies. The room acoustics will cause standing waves in the test chamber at these frequencies but provided the vehicles are located in the same position within the chamber these should be repeatable.

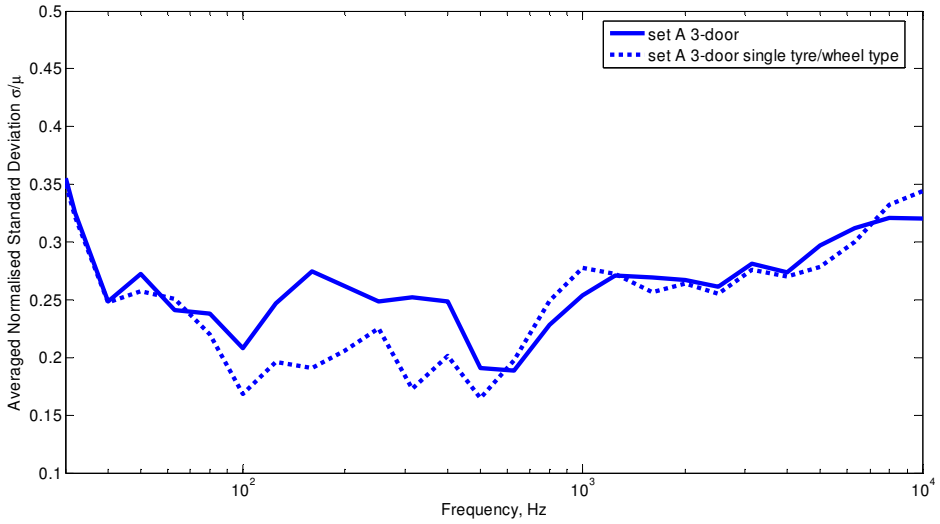

Figure 3-45 Normalised standard deviation, single tyre/wheel type.

Conclusions

The main frequency range of interest for the road noise is 20Hz to 1kHz. The distribution of the linear road noise frequency bands can be well described by a lognormal distribution. The overall level of road noise can be well described by either a lognormal or a gamma distribution. Data set A displays a bi-modal feature in the 315Hz band, which is due to wheel rim material differences. The typical levels of normalised standard deviation are 0.275. If the results are sorted by wheel/tyre type then the levels of normalised standard deviation are lower between 40Hz-600Hz, typically 0.2.

3.4 Engine noise

The engine noise measurements were also conducted in the semi-anechoic test chamber. The vehicles were installed onto the smooth dynamometer rollers to minimise tyre noise. The tests consisted of a 2nd gear wide-open-throttle (WOT) condition. Interior noise measurements were taken at the four outer ear locations as in the previous test work. At each 50rpm increment 1/3-octave spectra were recorded from 1000rpm to 5950rpm for the petrol engines and 4000rpm for the diesels. Examples of the typical variability within the engine noise levels for each body type and fuel type are shown in Figure 3-46 to Figure 3-51. All the examples are at 2000rpm engine speed for comparison. For ease of viewing the results are shown on a decibel scale with maximum, minimum and average decibel levels, although the curve fitting was conducted on the linear data. The results have been grouped according to body type and fuel.

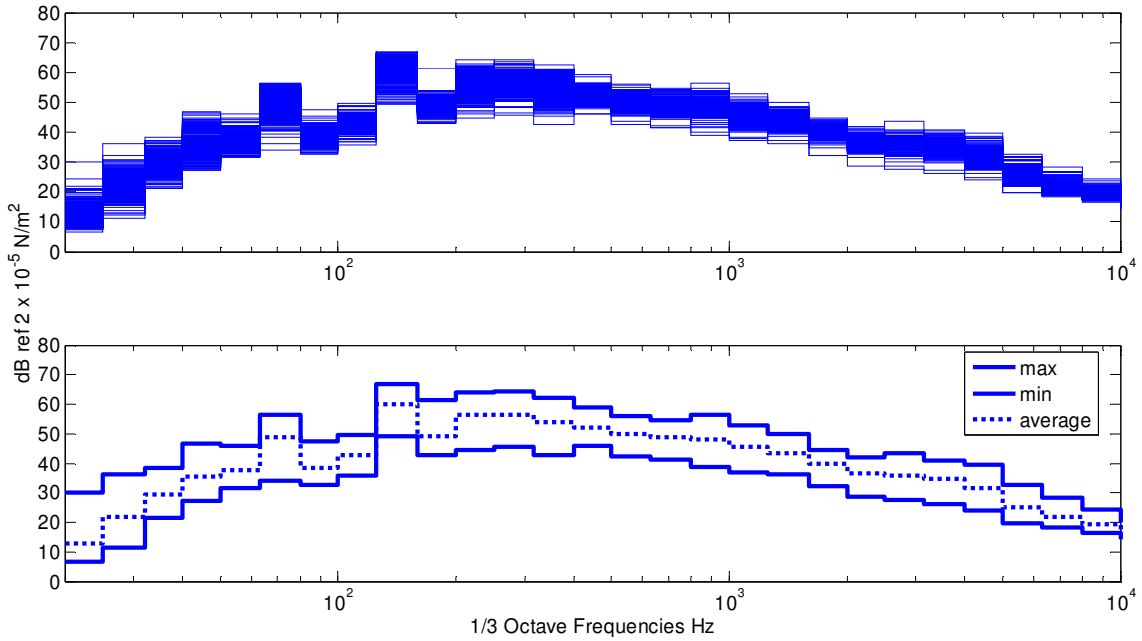

Figure 3-46 Engine noise 2nd gear WOT: data set A 3-door petrol, interior microphone 1, 2000rpm.

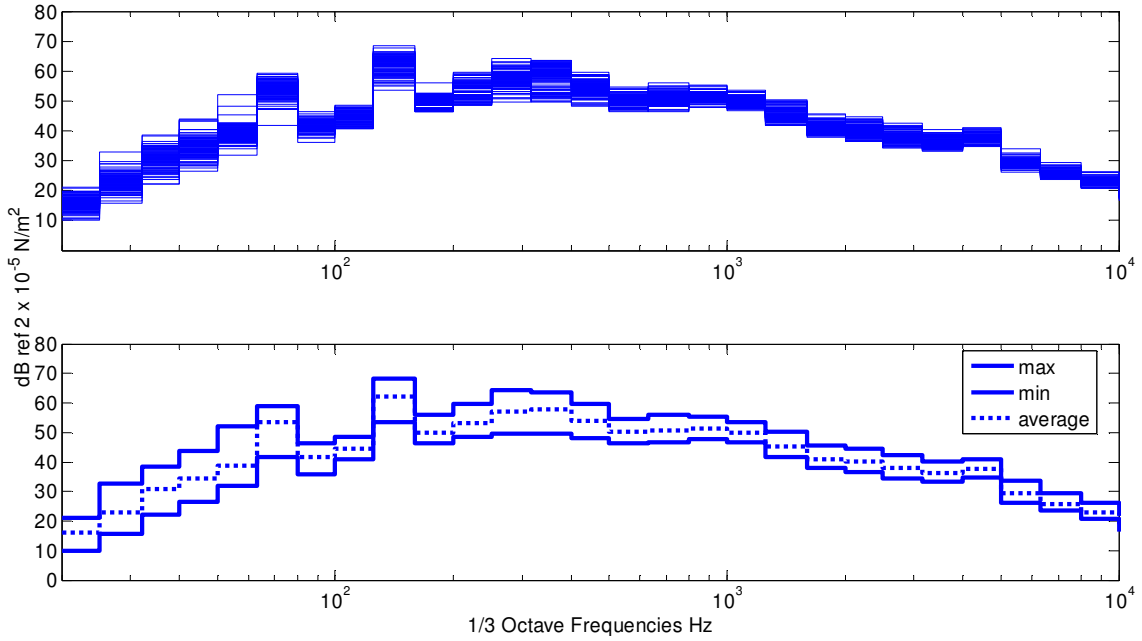

Figure 3-47 Engine noise 2nd gear WOT: data set A 3-door diesel, interior microphone 1, 2000rpm.

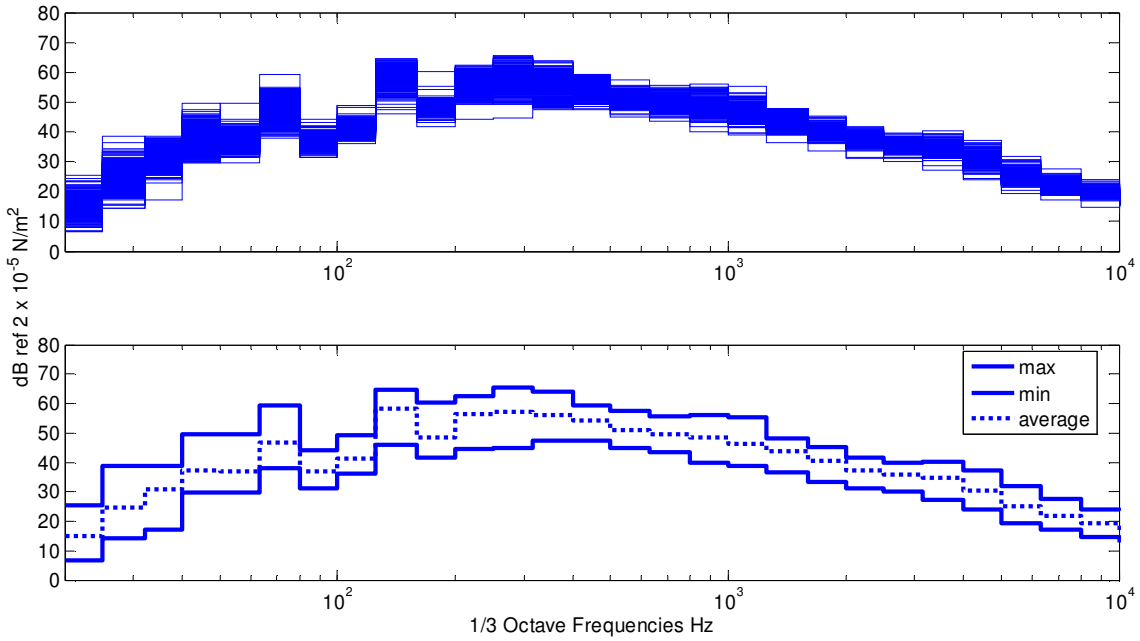

Figure 3-48 Engine noise 2nd gear WOT: data set A 5-door petrol, interior microphone 1, 2000rpm.

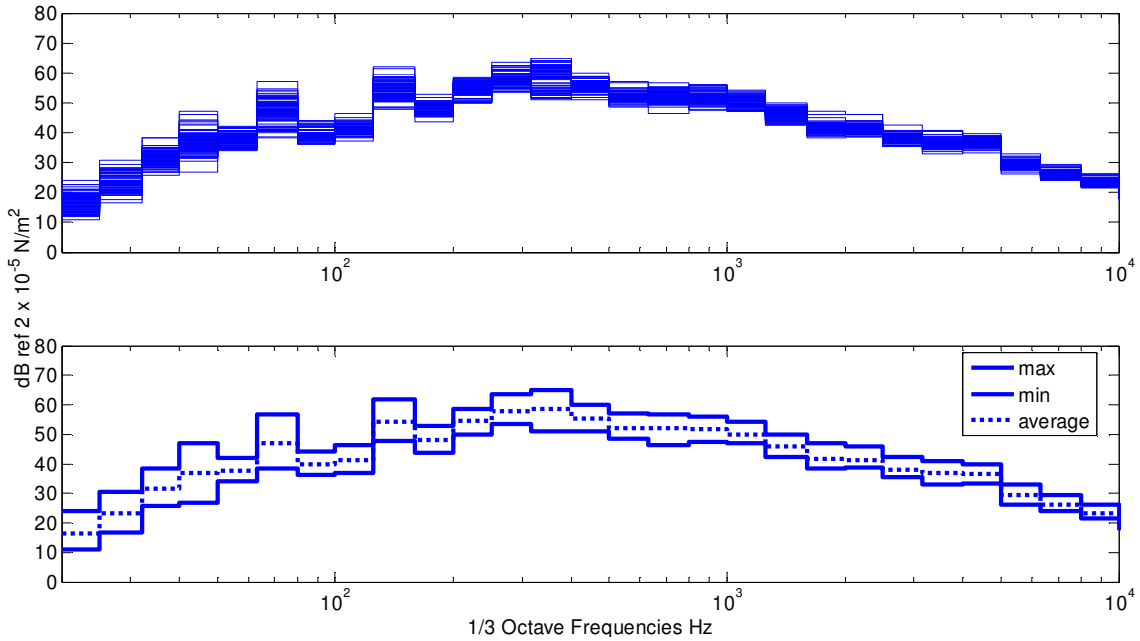

Figure 3-49 Engine noise 2nd gear WOT: data set A 5-door diesel, interior microphone 1, 2000rpm.

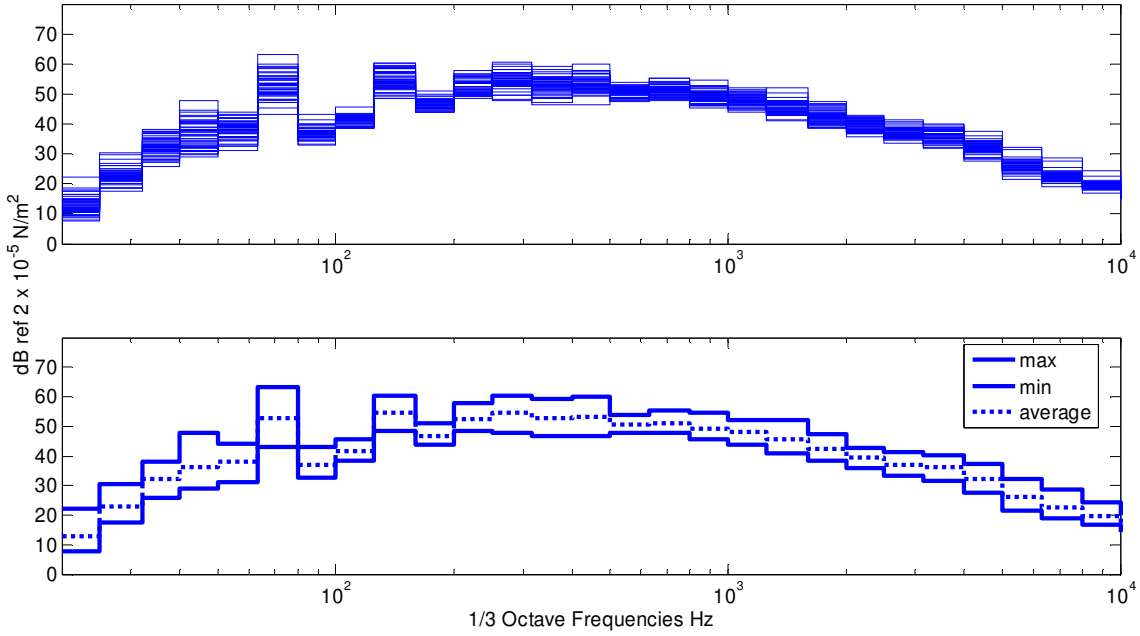

Figure 3-50 Engine noise 2nd gear WOT: data set B petrol, interior microphone 1, 2000rpm.

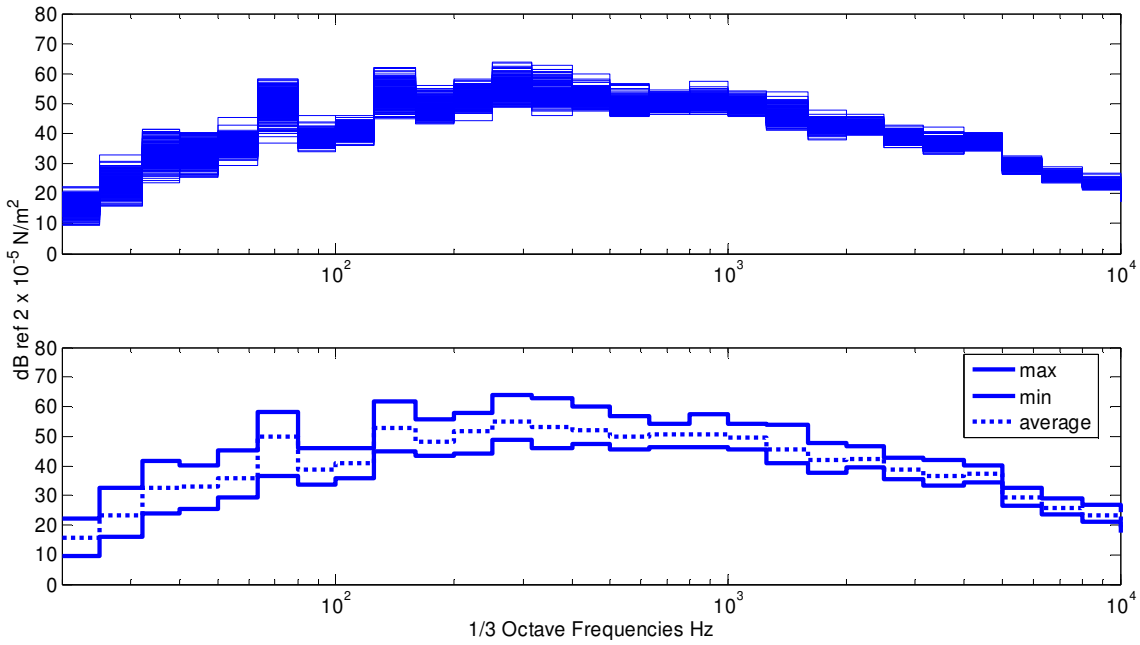

Figure 3-51 Engine noise 2nd gear WOT: data set B diesel, interior microphone 1, 2000rpm.

Using a similar method to that described earlier, the results were ranked to check for any extreme outlying results within the populations. The ranking exercise is a useful indication of whether particularly quiet or noisy vehicles exist in the population, i.e. vehicles which are the lowest/highest in each, or most, 1/3-octave bands. The distributions of the average rank values

were similar to those results from the airborne and road noise ranking exercises, and so for brevity will not be presented here; there were no significant outlying results.

Not all the vehicles used for the airborne cabin noise measurements and the road noise, were also tested for engine noise. Table 3-12 shows a breakdown of the numbers of vehicles in each group for the engine noise. A χ^2 test has been applied to test the goodness of fit to various standard distributions. The distribution of the variability is examined at each 1/3-octave frequency band, for each rpm increment, at each microphone (11200 distributions for the petrol data sets, 6832 distributions for the diesel data sets).

Body style	Petrol	Diesel
Model A 3-door	307	100
Model A 5-door	312	81
Model B	45	261

Table 3-12 The number of vehicles tested for 2nd gear WOT engine noise.

The results from the statistical analysis of the linear data are summarised in Table 3-13. A lognormal distribution provides the best fit to most of the frequency and rpm bands, and cannot be rejected as being a good fit for between 66.8% and 85.6% of the data sets. A Gaussian distribution fits significantly less data sets. Typical examples of the distribution of the engine noise are shown in Figure 3-52 to Figure 3-57; the examples are all at 2000rpm and 1kHz for comparison. Due to the large variation in the number of results in each set according to body type and fuel type, the distributions are not plotted in the same scales.

	Gaussian	Lognormal	Gamma	Rayleigh	Weibull
set A 3dr petrol	15.7%	66.8%	52.1%	1.8%	7.7%
set A 5dr petrol	31.8%	75.6%	67.8%	2.7%	14.9%
set B petrol	68.9%	85.6%	83.4%	18.0%	68.3%
set A 3dr diesel	59.6%	80.2%	77.8%	7.4%	45.7%
set A 5dr diesel	63.3%	80.4%	78.3%	6.7%	46.6%
set B diesel	31.7%	70.2%	62.5%	2.0%	13.8%

Table 3-13 Engine noise 2nd gear full load, percentage of frequency lines that have $\chi^2 \leq 0.95$.

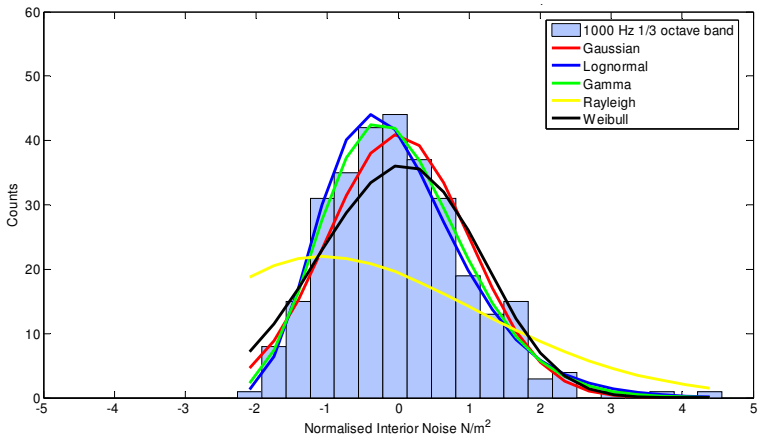

Figure 3-52 Engine noise distribution, data set A 3-door petrol, 2000rpm, 1kHz, interior microphone 1.

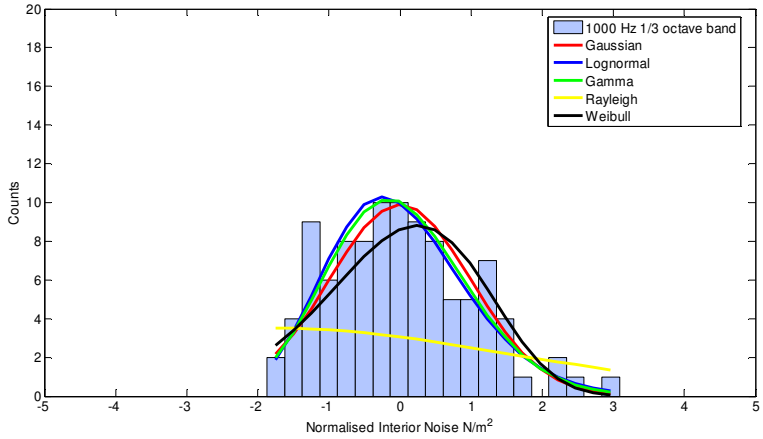

Figure 3-53 Engine noise distribution, data set A 3-door diesel, 2000rpm, 1kHz, interior microphone 1.

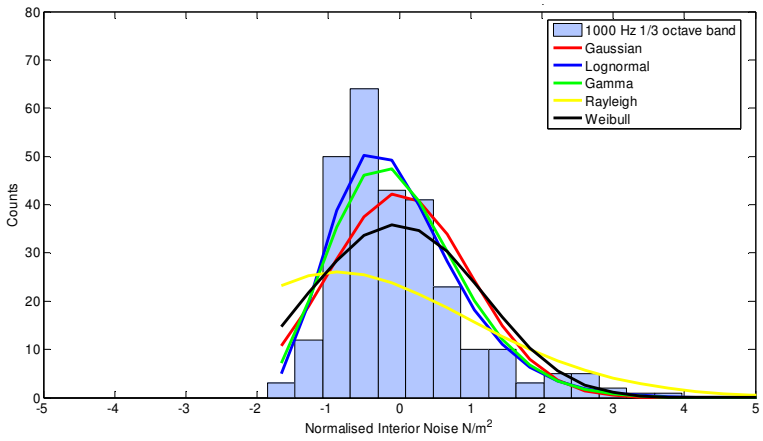

Figure 3-54 Engine noise distribution, data set A 5-door petrol, 2000rpm, 1kHz, interior microphone 1.

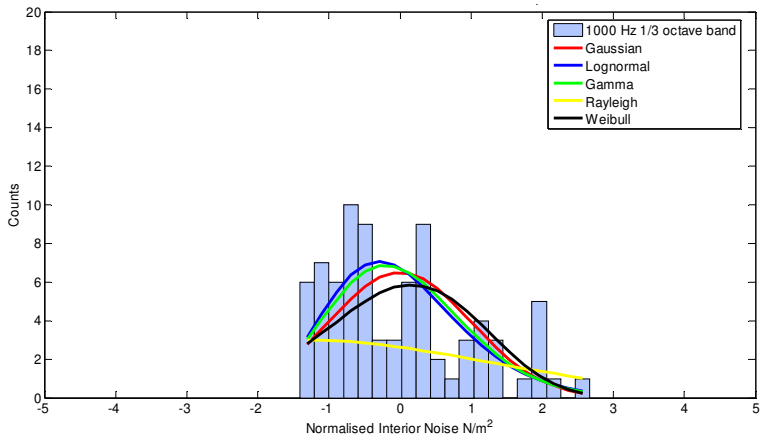

Figure 3-55 Engine noise distribution, data set A 5-door diesel, 2000rpm, 1kHz, interior microphone 1.

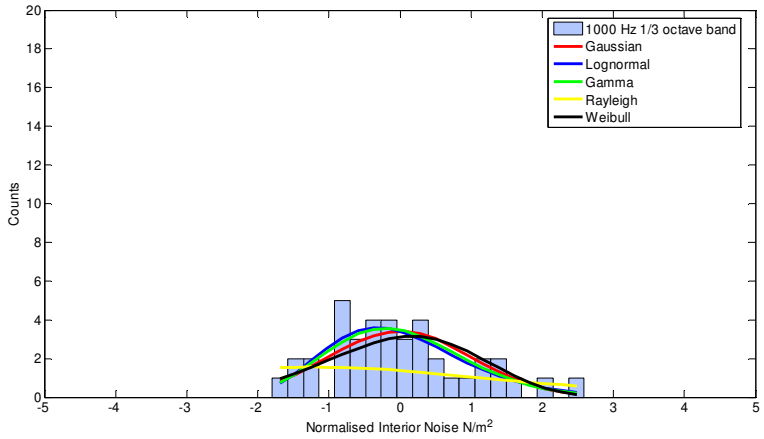

Figure 3-56 Engine noise distribution, data set B petrol, 2000rpm, 1kHz, interior microphone 1.

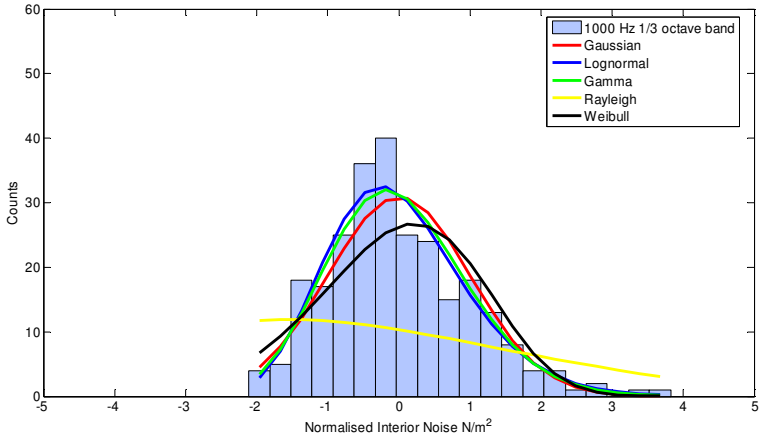

Figure 3-57 Engine noise distribution, data set B diesel, 2000rpm, 1kHz, interior microphone 1.

Although the vehicles are tested on the smooth rollers, the 315Hz band still displays some bi-modal features and all the distributions tested are a poor fit to the results in this band. The results of a frequency breakdown to examine any low/high frequency differences are listed in

Table 3-14 and Table 3-15; there were no general frequency trends and data sets in both frequency ranges were well described by a lognormal distribution.

	Gaussian	Lognormal	Gamma	Rayleigh	Weibull
set A 3dr petrol	13.4%	73.7%	57.4%	2.7%	11.6%
set A 5dr petrol	22.2%	76.2%	67.0%	4.2%	18.5%
set B petrol	63.3%	85.4%	82.8%	27.3%	67.2%
set A 3dr diesel	57.1%	80.0%	78.8%	11.5%	54.5%
set A 5dr diesel	64.4%	81.9%	81.1%	10.5%	60.6%
set B diesel	19.3%	67.8%	58.3%	3.1%	15.1%

Table 3-14 Engine noise 2nd gear full load, percentage of frequency lines 20Hz to 1kHz that have $\chi^2 \leq 0.95$.

	Gaussian	Lognormal	Gamma	Rayleigh	Weibull
vehicle set A 3dr petrol	19.8%	54.4%	42.4%	0.0%	0.8%
vehicle set A 5dr petrol	48.9%	74.6%	69.2%	0.0%	8.5%
vehicle set B petrol	79.1%	85.9%	84.4%	1.1%	70.5%
vehicle set A 3dr diesel	64.2%	80.6%	75.9%	0.0%	29.9%
vehicle set A 5dr diesel	61.1%	77.7%	73.3%	0.0%	21.3%
vehicle set B diesel	54.1%	74.7%	70.1%	0.0%	11.7%

Table 3-15 Engine noise 2nd gear full load, percentage of frequency lines 1kHz to 10 kHz that have $\chi^2 \leq 0.95$.

The overall engine noise levels were also examined; typical results can be seen in Figure 3-58 to Figure 3-63. As before the results are plotted in decibels for ease of viewing along with decibel maximum, minimum and average levels, although the curve fitting analysis is performed on the linear data. Also shown are the A-weighted results as these are more representative of the customer experience of the interior noise, although there was no curve fitting analysis conducted on these.

The results from the χ^2 curve fitting to the linear overall levels are shown in Table 3-16. The results summarise the percentage of the measurements for which the distribution tested cannot

be rejected as being a good fit. From the results it can be seen that both the lognormal and gamma distributions are good fit to the results. All of the vehicles tested had 4-cylinder engines, although there was a range of petrol, diesel and different engine sizes. The full load engine noise in a 4-cylinder engine is dominated by the second engine order (2EO) and the fourth (4EO). During the tests both the 2EO and the 4EO were recorded separately and the distribution of these specific orders has been examined.

	Gaussian	Lognormal	Gamma	Rayleigh	Weibull
set A 3dr petrol	39.0%	79.5%	74.5%	0.0%	17.3%
set A 5dr petrol	53.0%	83.8%	80.3%	0.5%	22.5%
set B petrol	82.5%	90.5%	91.0%	4.3%	71.8%
set A 3dr diesel	70.1%	84.0%	79.9%	4.9%	65.6%
set A 5dr diesel	79.1%	80.3%	83.2%	0.4%	66.0%
set B diesel	37.7%	73.0%	67.2%	0.0%	23.0%

Table 3-16 Engine noise 2nd gear full load, percentage of overall levels at each rpm step that have $\chi^2 \leq 0.95$.

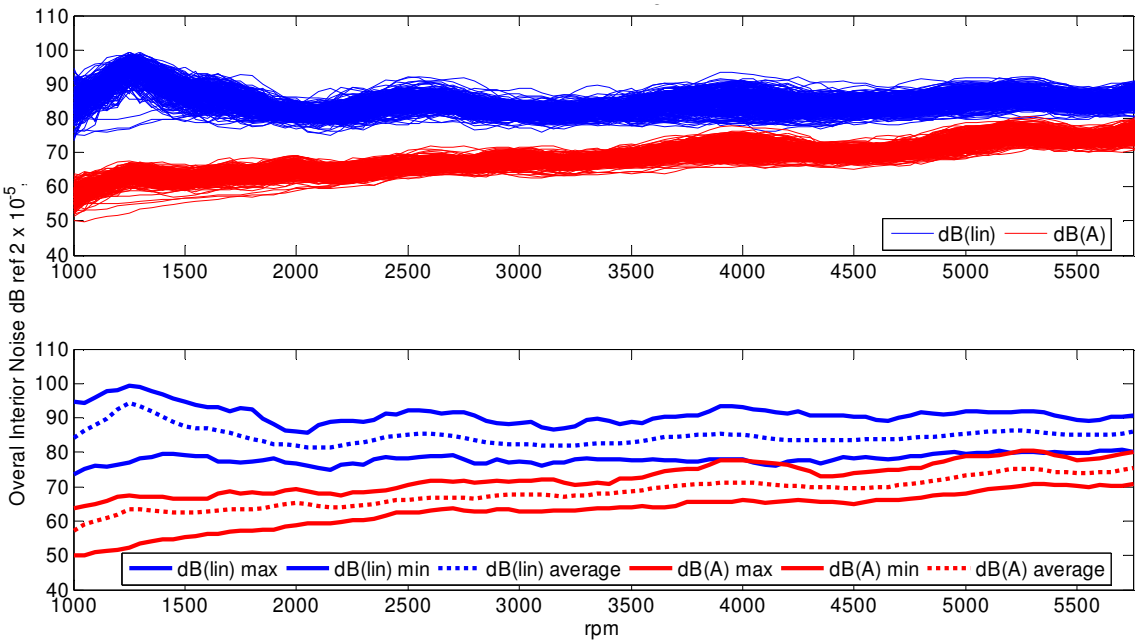

Figure 3-58 Engine noise overall level, 2nd gear full load, data set A 3-door, petrol, interior microphone 1.

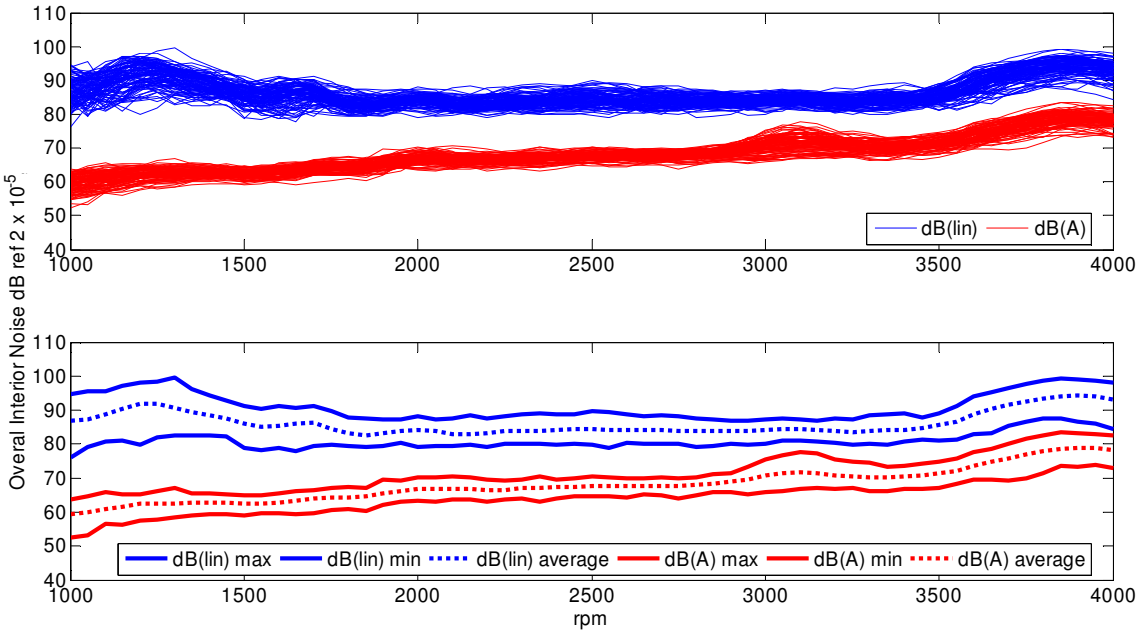

Figure 3-59 Engine noise overall level, 2nd gear full load, data set A 3-door, diesel, interior microphone 1.

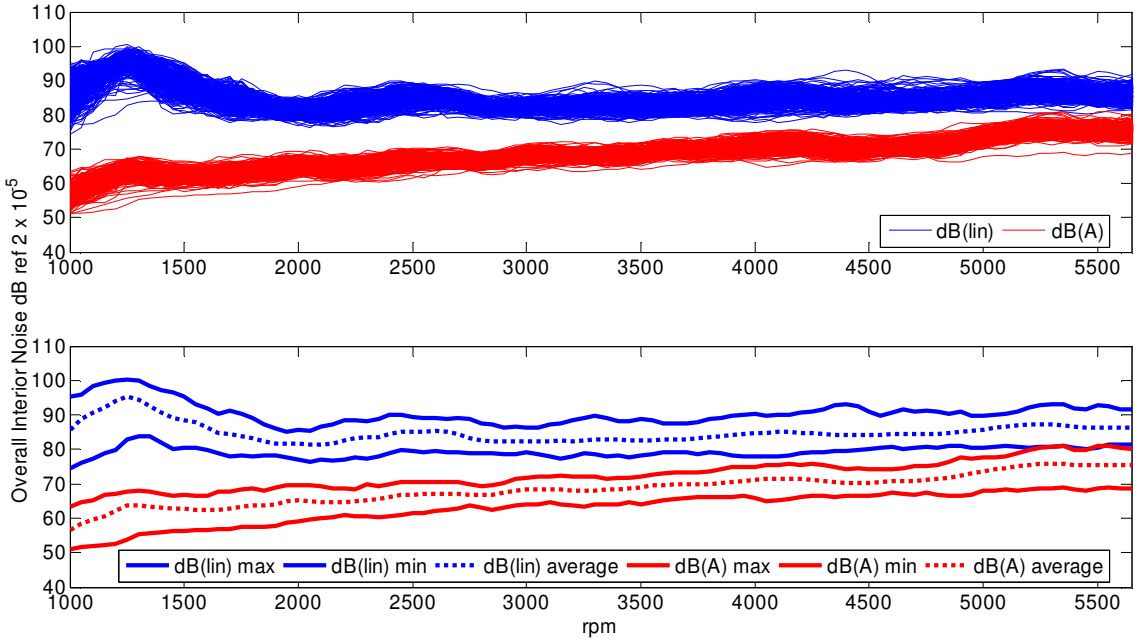

Figure 3-60 Engine noise overall level, 2nd gear full load, data set A 5-door, petrol, interior microphone 1.

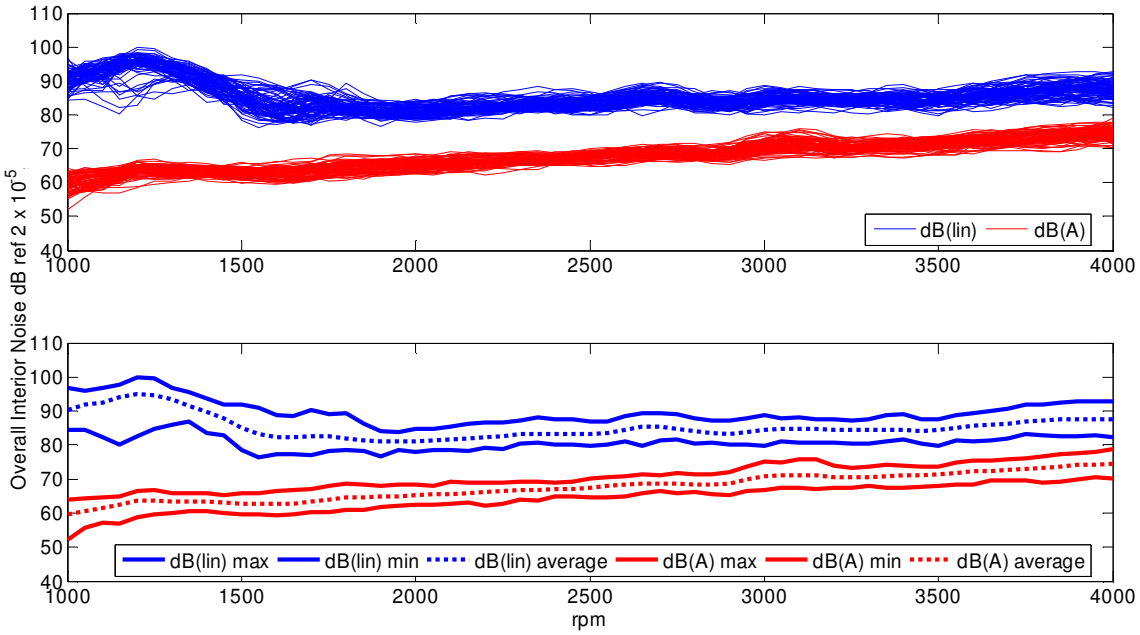

Figure 3-61 Engine noise overall level, 2nd gear full load, data set A 5-door, diesel, interior microphone 1.

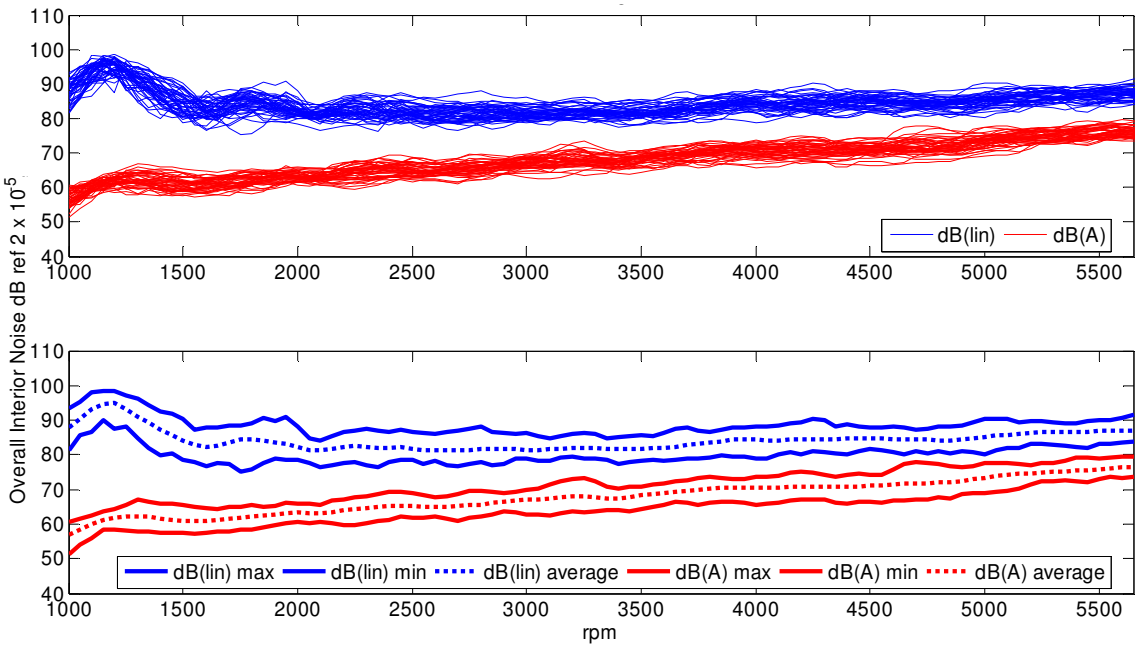

Figure 3-62 Engine noise overall level, 2nd gear full load, data set B, petrol, interior microphone 1.

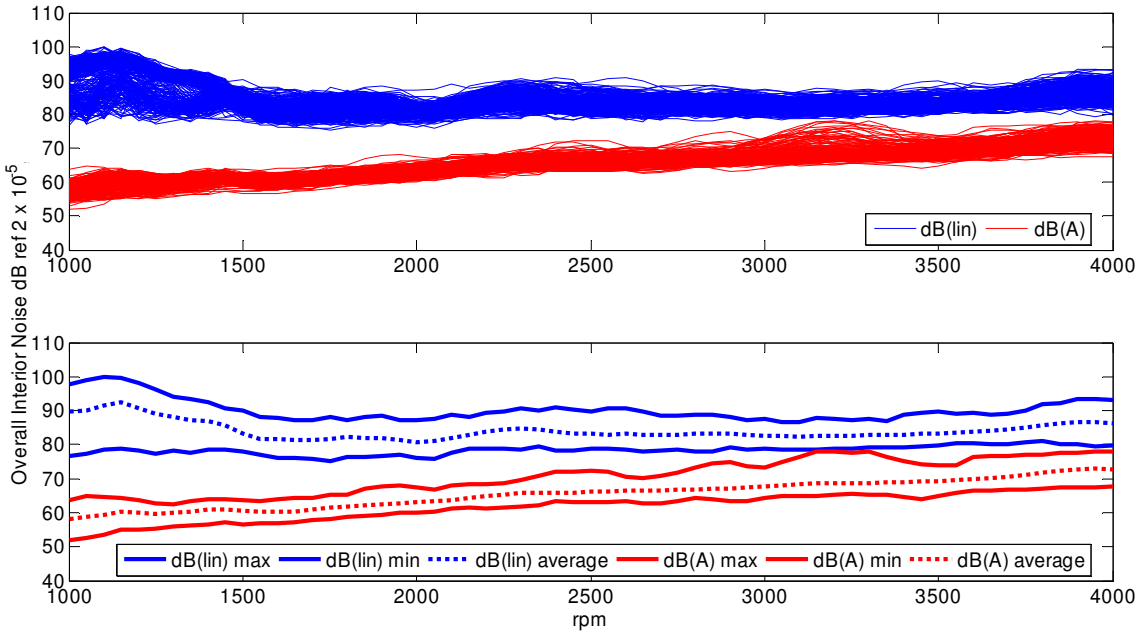

Figure 3-63 Engine noise overall level, 2nd gear full load, data set B, diesel, interior microphone 1.

Table 3-17 lists the results for the χ^2 testing of the 2EO and Table 3-18 for the 4EO. A gamma distribution provides a fit to the most 2EO data sets, and this is consistent for all the vehicle model body types and fuel types. A lognormal distribution fits the most 4EO data sets; again this is the case for all the vehicle model body types and fuel. The division of the results for the overall levels perhaps becomes clearer as it is likely that cases where the 4EO is a relatively high contributor to the overall level, the best fit may tend to change from gamma towards lognormal.

	Gaussian	Lognormal	Gamma	Rayleigh	Weibull
set A 3dr petrol	28.3%	52.5%	67.3%	7.3%	45.8%
set A 5dr petrol	36.3%	56.3%	68.8%	8.0%	51.0%
set B petrol	73.3%	84.0%	85.0%	50.8%	80.3%
set A 3dr diesel	63.1%	73.0%	78.7%	33.6%	78.3%
set A 5dr diesel	74.6%	75.8%	82.4%	18.4%	78.3%
set B diesel	40.2%	50.0%	66.8%	14.8%	62.7%

Table 3-17 Engine noise 2nd gear full load, percentage of 2nd engine order at each rpm step that has $\chi^2 \leq 0.95$.

	Gaussian	Lognormal	Gamma	Rayleigh	Weibull
set A 3dr petrol	11.8%	63.5%	45.0%	0.0%	8.8%
set A 5dr petrol	23.5%	69.8%	59.8%	0.0%	18.8%
set B petrol	56.8%	78.8%	77.0%	19.8%	61.5%
set A 3dr diesel	70.5%	86.5%	84.4%	2.5%	55.3%
set A 5dr diesel	74.6%	91.8%	88.5%	0.0%	62.3%
set B diesel	26.2%	77.9%	66.8%	2.0%	13.5%

Table 3-18 Engine noise 2nd gear full load, percentage of 4th engine order at each rpm step that has $\chi^2 \leq 0.95$.

Conclusions

A lognormal distribution provides the best fit to the majority of the engine noise results, with it being a good fit to approximately 67% to 85% of the data sets. There are no low/high frequency differences. The overall engine noise could be described by a lognormal or gamma distribution. A gamma distribution is the best fit to the second engine order noise, whereas the fourth engine order is best described by a lognormal distribution. The 315Hz 1/3-octave band displays some bi-modal behaviour as seen in the road noise tests and is most likely due to wheel rim material differences affecting the tyre cavity frequency.

3.5 Effect of environmental conditions

The environmental conditions were monitored and the temperature and the humidity recorded for each test. Whilst the test chamber was a more stable environment than the outdoor testing of vehicles discussed in chapter 2, the variability in the temperature and humidity was still relatively high. The distributions of the recorded conditions for the whole data set are shown in Figure 3-64 and Figure 3-68.

As each vehicle was being installed in the chamber and the microphones positioned inside it, the vehicle will have started to acclimatise to the ambient conditions in the chamber. If the test work was being conducted in winter, then the vehicles were given an additional 20 minutes in the chamber, with the vehicle doors and tailgate open, to warm-up. Prior to the road noise tests

the vehicles were run on the rough surface to excite the suspension system and bring it up to an operating temperature. Similarly for the powertrain noise testing, the engines were cycled through several WOT/over-runs to warm-up the vehicle.

Although both variations in temperature and humidity will have an effect on the behaviour of the vehicles, as care was taken in their pre-conditioning it is reasonable to assume that the environmental conditions inside the chamber are representative of the conditions of the vehicles during the test.

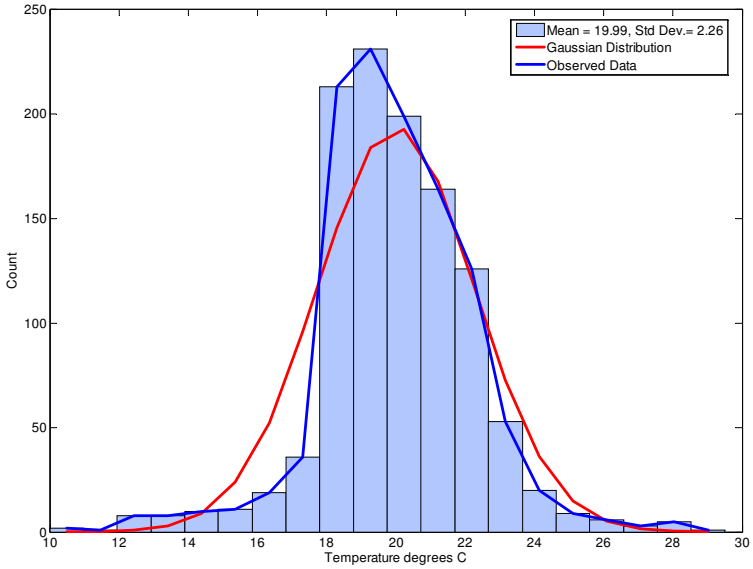

Figure 3-64 Vehicle study temperature distribution, 1130 vehicles.

The minimum and maximum recorded temperatures were 10°C and 29.5°C; the normalised standard deviation of the temperature variation was 0.11. For comparison the normalised standard deviation of the temperature variation in the Isuzu vehicles sets discussed in chapter 2 was 0.17-0.18. There are two main possible effects of the temperature on the measurements, the first of these is the effect on the speed of sound and the second is the effect on the stiffness of structural components particularly rubber ones such as suspension bushes or engine mounts. The approximate effect of temperature on the speed of sound for the range of temperatures encountered during the testing would be 338m/s (10°C) to 349.7m/s (29.5°C), see equation (2.1) from chapter 2. These levels of variation in temperature are comparable in terms of normalised standard deviation, to levels typically seen in modal response prediction and measurement. To examine the possible effect of temperature on the results, the averaged normalised standard deviation of the airborne frequency response results has been examined for a limited temperature range of 19-20°C. This range was chosen from the distribution of temperatures shown in Figure 3-64 as the mode of the results. The number of vehicles tested at 19-20°C form

a subset of the results from the main population; Table 3-19 shows the number of vehicles of each type that were tested at a temperature of 19-20°C.

Vehicle	Number Tested	
	petrol	diesel
model A 3-door	120	36
model A 5-door	67	14
model B	19	74

Table 3-19 Number of vehicles tested at a chamber temperature of 19-20°C.

The results for the airborne NR tests are shown in Figure 3-65 which shows a comparison of the average normalised standard deviation of the results for the whole population, compared to that for only vehicles tested at 19-20°C.

The effect of temperature on the structural transmission paths such as the engine and suspension mounts cannot be estimated without knowledge of the material properties and the operating temperatures. However, the results from the road noise and engine noise tests will include any variability from both airborne and structure borne noise. In a similar manner to the airborne NR tests, a comparison can be made for the road noise and engine noise tests, of vehicles tested at 19-20°C verses the whole population. These results are shown in Figure 3-66 and Figure 3-67. In addition the same pre-test procedure was used to warm-up the vehicles prior to testing, which will reduce the variability of the structural transmission path temperatures.

As it can be seen for all the tests, there is little difference in the averaged normalised standard deviation for temperature limited results when compared to the full set of results, for all the tests. This is significant as it demonstrates that for this study the variability in the chamber air temperature, which is considered to be representative of the vehicle ambient temperature, does not noticeably contribute towards the variability in the measured response.

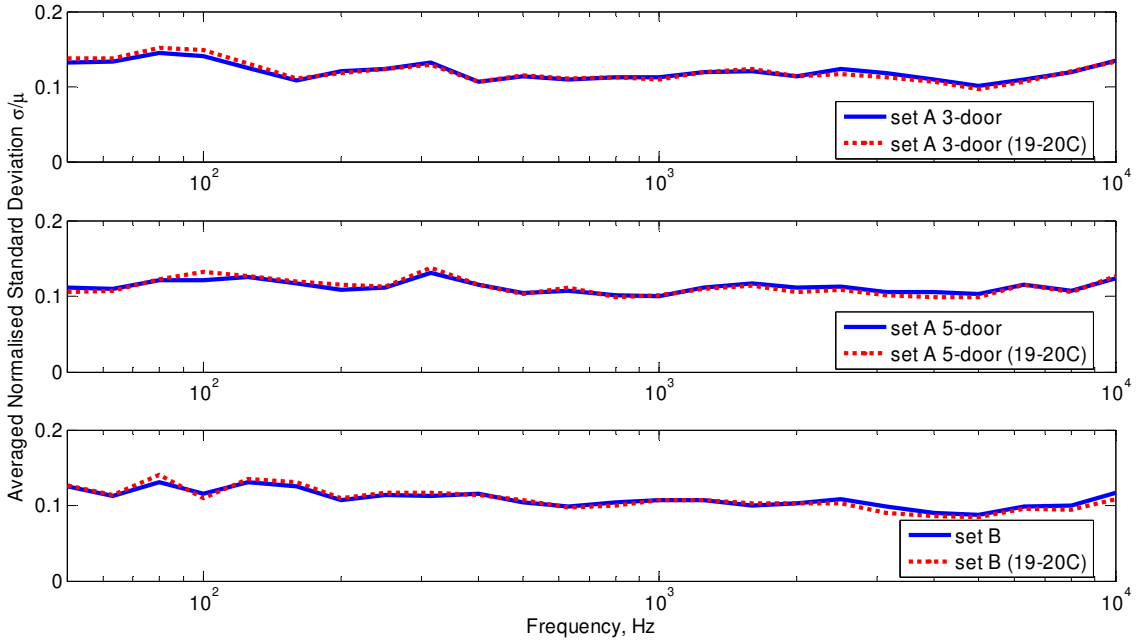

Figure 3-65 Averaged normalised standard deviation of the airborne noise, results filtered by temperature.

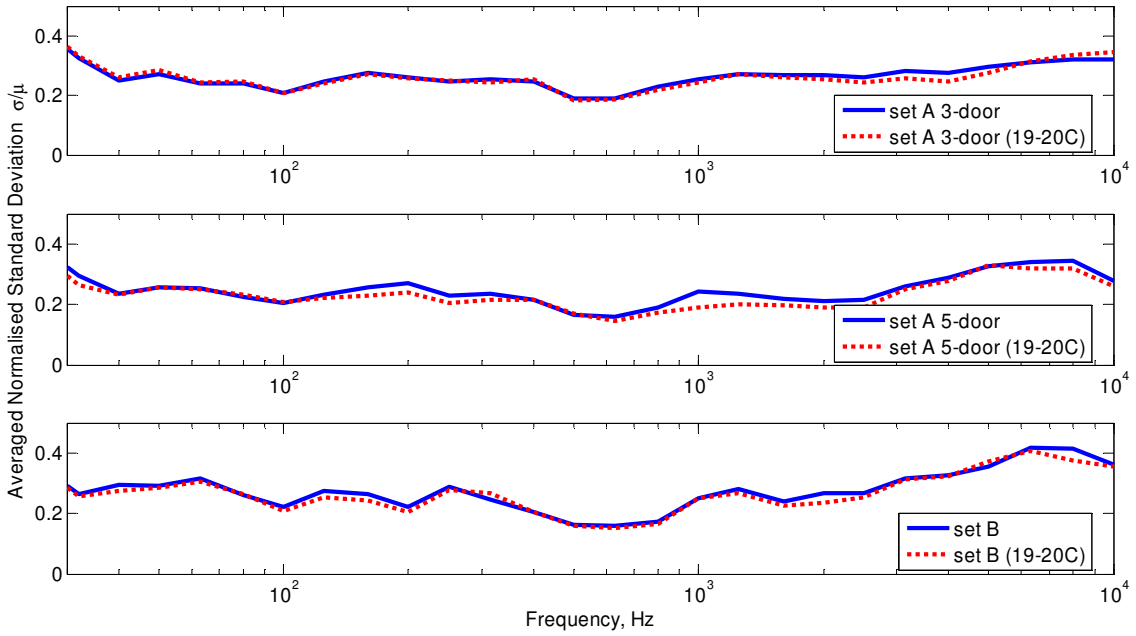

Figure 3-66 Averaged normalised standard deviation of the road noise, results filtered by temperature.

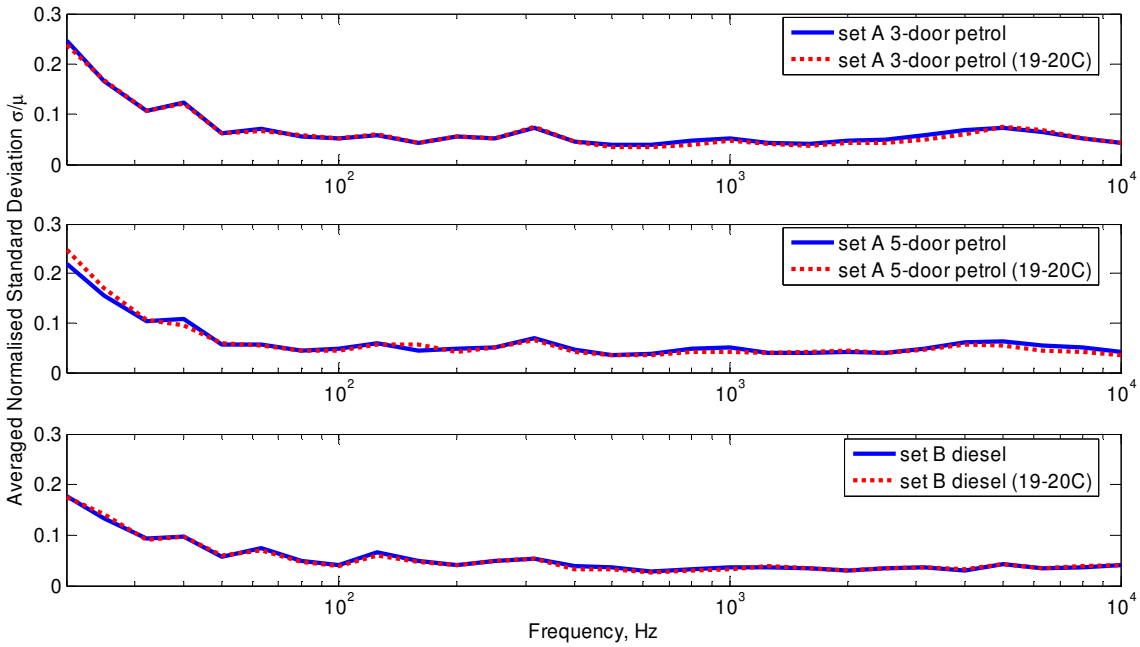

Figure 3-67 Averaged normalised standard deviation of the engine noise, results filtered by temperature.

The minimum and maximum recorded relative humidity was 27% and 91%; the normalised standard deviation of the humidity variation is 0.37. For comparison the normalised standard deviation of the humidity variation in the Isuzu vehicles sets discussed in chapter 2 was 0.3-0.33. The effect of humidity on the speed of sound in air is presented graphically in [2.14]. The speed of sound in air at 20°C and 27% relative humidity is approximately 343.7 m/s, and at 91% relative humidity 344.5 m/s. The relative humidity can have an effect on the absorption coefficient of the air at high frequencies [2.15]. For example, at 10kHz the absorption coefficient is approximately 0.075dB/m at 27% humidity, increasing to 0.25dB/m at 91% humidity. However, this effect is quite small and is unlikely to have any significant effect on the results compared to the other sources of variability in the measurements.

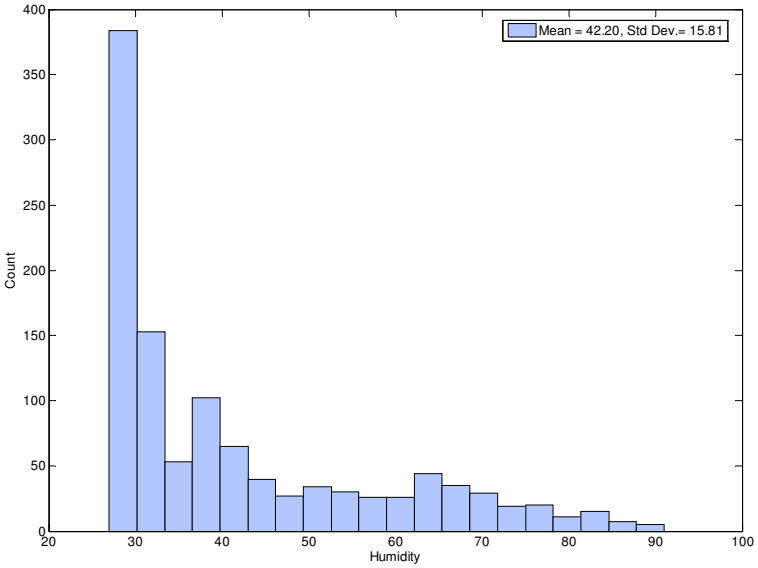

Figure 3-68 Vehicle study humidity distribution, 1130 vehicles.

3.6 Conclusions

In this chapter the results from the statistical analysis of an extensive and previously unpublished vehicle variability study, have been presented and discussed. The data analysed is from three types of vehicle test conditions: airborne cabin noise, roller induced road noise measurements and interior measured engine noise. In general the statistical analysis was conducted on the linear data.

The airborne cabin noise measurements used external speakers as noise sources and gave an indication of the cabin attenuation. A Gaussian distribution was in general a good fit to the distributions of the results. Three distributions could not be rejected as being a good fit to over 50% of the frequency bands; these were the Gaussian, lognormal and gamma distributions. A lognormal and a gamma distribution were in some cases a better fit to the results than a Gaussian, however the actual statistical parameters of these distributions were such that they approached Gaussian in form. The gamma distribution fitted the most data sets for model A and a lognormal for model B. A frequency breakdown of the results concluded that at lower frequencies the distributions of results were well described by a lognormal distribution. At higher frequencies the results were mixed, with a Gaussian distribution being the best fit to data set A results and a gamma distribution being the best fit to those from data set B. It is hypothesised that the differences in distributions may be due to different transmission mechanisms. At higher frequencies the airborne cabin noise is likely to be highly dependent on vehicle sealing. Whereas at lower frequencies the transmission loss of the cabin will be more

dependent on its mass. The distribution of the overall levels was best described by a Gaussian distribution. The typical levels of normalised standard deviation for the airborne cabin noise were between 0.09 and 0.145. These levels are lower than those seen in the vehicle test discussed in chapter 2.

The roller induced road noise tests were conducted on a test rig with simulated coarse road input. The vehicles were tested with the production treaded tyres fitted. A lognormal distribution was found to be a good description of the spread of results for the road noise frequency bands. The overall levels were equally well described by either a lognormal or a gamma distribution. Data set A results displayed a bi-modal feature in the 315Hz band which is typically associated with tyre cavity frequencies. This bi-modal distribution was shown to be due to wheel rim material differences. Typical levels of normalised standard deviation for the road noise were found to range between 0.16 and 0.47. For a reduced population containing nominally identical wheel rims and tyres this was shown to reduce to approximately 0.2. At higher frequencies, above 600Hz, there was no noticeable reduction in the levels of normalised standard deviation for the reduced population. This suggests the variability in the road noise above 600Hz is not due to wheel and tyre differences.

The engine noise tests consisted of a 2^{nd} gear WOT; the test was conducted on a dynamometer test rig on smooth rollers. A lognormal distribution provides the best fit to the majority of the engine noise results and there were no differences found between the fit at low or high frequencies. All of the vehicles tested had 4-cylinder engines, although there was an assortment of engine sizes and a mixture of petrol and diesel fuel types. The distributions of the two most dominant engine orders, second and fourth, were investigated. A gamma distribution was the best fit to the second engine order noise, whereas the fourth engine order was best described by a lognormal distribution. The combination of these results is seen in the overall engine noise levels which were equally well described by a lognormal or gamma distribution.

The air temperature and humidity within the test chamber were recorded for each test. The temperature ranged from 10°C to 29.5°C, with a normalised standard deviation of 0.11. This is lower than that seen in the outdoor vehicle testing presented in chapter 2. The normalised standard deviation was examined for a reduced population of vehicles only tested between 19-20°C. For each type of test, i.e. airborne cabin noise, road noise and engine noise, there was no difference in the levels of normalised standard deviation between the limited temperature set and the population as a whole. This result is very significant as it provides evidence that the variation in the ambient temperature did not contribute to the variability in the measured response.

The data presented here forms an extensive variability study and contributes greatly to the available information on typical variability found between nominally identical manufactured structures. Two of the key issues in progressing the techniques to include variability in the modelling of structures, are knowledge of the typical levels of variability found in real structures, and the distribution of such variability. There are certain advantages in being able to reasonably assume that either the levels of variability are low or that they are close to Gaussian distributed. The results from the vehicle data sets presented here would suggest that the typical levels of averaged normalised standard deviation range from 0.09 to 0.32. However, the higher levels were seen in the road noise results where the different wheel rim materials have contributed to the variations. A more realistic range based on the variability of nominally identical wheels and tyres is 0.09 to 0.2. The frequency distributions of the linear results were in general best described by a lognormal distribution, and therefore the decibel results will be best described by a Gaussian distribution.

Section II: Analysis methods for the propagation of variability in structures

In the previous section of this thesis the measured variability data from manufactured parts was examined. A literature survey of published variability data was presented along with new results from an extensive vehicle study. The aim of this work was to establish the typical levels and distribution of variability in components and structures, in order to enable an informed choice of suitable methods for modelling the propagation of this variability and the choice of input data. The work concluded that the typical level of normalised standard deviation in the response of components was up to 0.03. For complex built-up structures the normalised standard deviation was in the region of 0.09 to 0.2. In general the frequency distributions of the linear results were in general best described by a lognormal distribution, and therefore the decibel results best described by a Gaussian distribution.

In the following section, existing analysis methods for examining the propagation of variability in structures are reviewed. The methods are presented in chapter 4, and in chapter 5 a simple two-degree of freedom is used to further understand their application. Following this suitability of the various the methods are considered in conjunction with the findings from the measured data.

4. Methods for uncertainty propagation in structural dynamics

In this chapter various statistical concepts and techniques for studying uncertainty propagation will be introduced. These techniques will be used in the following chapters to investigate the propagation of uncertainty from the component physical properties, to the component modal properties and the global modal properties and subsequently to variability in the structural response.

To begin with various methods to approximate the eigensolution will be discussed. The first of these uses the unperturbed system eigenvectors as assumed modeshapes and extends the Rayleigh quotient to all modes. The second approximation considered is the interpolated mode method. This develops the concept of using eigenvectors as a basis for estimating eigenvalues by interpolation between previously calculated eigenvectors. An approximate eigenvalue is then obtained from the Rayleigh quotient. Both of these methods could be considered to be physical approximations to the eigensolution.

The next types of approximation considered are perturbation methods. The first of these is a mean centred perturbation expansion of the eigenvalues. This method is commonly used in random eigenvalue problems and works well when the uncertainties are small, with a Gaussian, or close to Gaussian, distribution. The second perturbation approach considers the expansion of the eigenvalues about an 'optimal' point, which is selected such that the first moment or mean of each eigenvalue is estimated most accurately. Both of these perturbation methods could be considered to be mathematical approximations to the eigensolution.

In the second section in this chapter some analytical techniques are presented which can be used, in conjunction with eigensolution approximations, to obtain various statistical properties of the response of a system with random properties. The first of these is the generation of moments method, in which the moments of the response of a system can be related to the moments of the input variables. These input variables can be physical dimensions, material properties, etc. This can be used to obtain expressions for the mean and variance of the system response in terms of the mean and variance of the system variables. The second technique is the change of variable method, where the probability density function (PDF) of the output of a linear system is related to the PDFs of the inputs. This method can be used, for example, to obtain expressions for the PDF of the natural frequencies of a system. The last technique is a matrix notation which can be used to present the moments of a linear function in terms of the moments of the input, in particular the mean and variance.

The final section in this chapter presents several Monte Carlo methods for obtaining numerical solutions to complex problems such as eigenvalue equations. Two methods discussed in detail are stratified sampling and Latin Hypercube sampling. Both of these approaches aim to reduce the number of trial runs required to obtain a good approximation to the output distribution, whilst ensuring all areas of the input distributions are covered.

4.1 Eigensolution approximations

In order to propagate statistics from the physical properties to the modal properties of a structure, some form of eigensolution approximation is generally required to obtain a linear relationship between the two. In the following section several such approximations are presented and discussed.

If the equation of motion of a system is given by

$$\mathbf{M}\ddot{\mathbf{x}} + \mathbf{K}\mathbf{x} = \mathbf{0} \tag{4.1}$$

Then the eigenfrequencies $\boldsymbol{\lambda}$ and eigenvectors $\boldsymbol{\varphi}$ are given by

$$\left(\mathbf{K} - \boldsymbol{\lambda}\mathbf{M}\right)\boldsymbol{\varphi} = \mathbf{0} \tag{4.2}$$

The physical degrees of freedom x, are related to the modal degrees of freedom y, thus

$$\mathbf{x} = \boldsymbol{\varphi}\mathbf{y} \tag{4.3}$$

Substituting equation (4.3) into (4.1), and pre-multiplying by $\boldsymbol{\varphi}^{\mathbf{T}}$ the equation of motion can be expressed in terms of the modal coordinates

$$\boldsymbol{\varphi}^{\mathbf{T}}\mathbf{M}\boldsymbol{\varphi}\ddot{\mathbf{y}} + \boldsymbol{\varphi}^{\mathbf{T}}\mathbf{K}\boldsymbol{\varphi}\mathbf{y} = \mathbf{0} \tag{4.4}$$

The mass and stiffness matrices are now un-coupled and contain no off diagonal elements. If the eigenvectors are mass normalised then

$$\begin{aligned} \boldsymbol{\varphi}^{\mathbf{T}}\mathbf{M}\boldsymbol{\varphi} &= \mathbf{M}_{\mathbf{j}} \\ \boldsymbol{\varphi}^{\mathbf{T}}\mathbf{K}\boldsymbol{\varphi} &= \mathbf{K}_{\mathbf{j}} \end{aligned} \tag{4.5}$$

where

$$\begin{aligned} \mathbf{M}_{\mathbf{j}} &= \mathbf{I} \\ \mathbf{K}_{\mathbf{j}} &= diag\left(\lambda_j\right) \end{aligned} \tag{4.6}$$

For the general formulation of the eigenvalue problem see [4.1].

4.1.1 Baseline modeshapes as assumed shape functions

An approximation for the eigenfrequencies can be obtained if the eigenvectors of a baseline system are used as assumed modeshapes for the perturbed or uncertain system, and the Rayleigh quotient [4.1] is calculated for all modes.

Suppose that the mass and stiffness of the system are perturbed such that

$$\begin{aligned} \mathbf{M} &= \bar{\mathbf{M}} + \Delta\mathbf{M} = \bar{\mathbf{M}} \bullet \left(\mathbf{1} + \boldsymbol{\varepsilon}_m\right) \\ \mathbf{K} &= \bar{\mathbf{K}} + \Delta\mathbf{K} = \bar{\mathbf{K}} \bullet \left(\mathbf{1} + \boldsymbol{\varepsilon}_k\right) \end{aligned} \tag{4.7}$$

where $\Delta\mathbf{M} = \bar{\mathbf{M}} \bullet \boldsymbol{\varepsilon}_m$ and $\Delta\mathbf{K} = \bar{\mathbf{K}} \bullet \boldsymbol{\varepsilon}_k$ and the dot product $(\bullet)$ is defined as the Hadamard or element-wise multiplication. If the nominal and perturbed mass and stiffness matrices are known, then the perturbation matrices $\boldsymbol{\varepsilon}_m$ and $\boldsymbol{\varepsilon}_k$ are such that

$$\begin{aligned} \bar{\mathbf{K}} \bullet \boldsymbol{\varepsilon}_k &= \left(\mathbf{K} - \bar{\mathbf{K}}\right) \\ \bar{\mathbf{M}} \bullet \boldsymbol{\varepsilon}_m &= \left(\mathbf{M} - \bar{\mathbf{M}}\right) \end{aligned} \tag{4.8}$$

It should be noted that the elements of $\boldsymbol{\varepsilon}_m$ and $\boldsymbol{\varepsilon}_k$ must be symmetric and hence are correlated. The eigenfrequencies of the perturbed system can be then approximated as

$$\lambda_j \cong \frac{\bar{\lambda}_j + \bar{\boldsymbol{\varphi}}_j{}^T \Delta\mathbf{K}\ \bar{\boldsymbol{\varphi}}_j}{1 + \bar{\boldsymbol{\varphi}}_j{}^T \Delta\mathbf{M}\ \bar{\boldsymbol{\varphi}}_j} = \frac{\bar{\lambda}_j + \bar{\boldsymbol{\varphi}}_j{}^T \left(\bar{\mathbf{K}} \bullet \boldsymbol{\varepsilon}_k\right)\ \bar{\boldsymbol{\varphi}}_j}{1 + \bar{\boldsymbol{\varphi}}_j{}^T \left(\bar{\mathbf{M}} \bullet \boldsymbol{\varepsilon}_m\right)\ \bar{\boldsymbol{\varphi}}_j} \tag{4.9}$$

where λ_j is the *j*'th eigenvalue of the perturbed system, $\bar{\lambda}_j$ is the *j*'th eigenvalue of the baseline system and $\bar{\boldsymbol{\varphi}}_j$ is the *j*'th mass normalised eigenvector of the baseline system. The term $\bar{\boldsymbol{\varphi}}_j^T \Delta\mathbf{M}\, \bar{\boldsymbol{\varphi}}_j$ is the change in the modal mass, and $\bar{\boldsymbol{\varphi}}_j^T \Delta\mathbf{K}\, \bar{\boldsymbol{\varphi}}_j$ the change in the modal stiffness.

This method uses the baseline system eigenvectors as trial solutions (assumed modeshapes) for the perturbed system and presumes the modeshapes to be equal to those of the baseline system. Essentially this is the same as projecting the changes in mass and stiffness on the baseline modes and then ignoring cross-modal coupling terms. This method is limited to small variations in the physical properties and becomes more inaccurate at higher frequencies as the eigenvectors become more sensitive to variations in the physical properties. It is also limited to well separated natural frequencies.

4.1.2 Interpolated mode method

The interpolated mode method, developed by Bhaskar [4.2], is a method in which estimates of eigenvalues are made by interpolation between previously calculated values. These are 'exact' values for some known parameter values. These calculated eigenvalues provide an interval within which the eigenvalue for a different set of parameters will fall. Earlier work [4.3] used a weighted average based on the closeness of the parameter values to either end of the interval, whilst the later work [4.2] examines averaging the eigenvectors themselves.

Consider an interval $p_0 \le p \le p_f$ in which p is some parameter that describes the system. The eigensolution at either end of the interval are given by exact calculation

$$\mathbf{K_0}\boldsymbol{\varphi}_{\mathbf{j\_0}} = \lambda_{j\_0}\mathbf{M_0}\boldsymbol{\varphi}_{\mathbf{j\_0}} \qquad \text{and} \qquad \mathbf{K_f}\boldsymbol{\varphi}_{\mathbf{j\_f}} = \lambda_{j\_f}\mathbf{M_f}\boldsymbol{\varphi}_{\mathbf{j\_f}} \tag{4.10}$$

A non-dimensional parameter t is defined as

$$t = \frac{p - p_0}{p_f - p_0} \tag{4.11}$$

such that $0 \le t \le 1$. The weighting factors t and $(1-t)$ are used to interpolate the mode shapes obtained from $\boldsymbol{\varphi}_{\mathbf{j\_0}}$ and $\boldsymbol{\varphi}_{\mathbf{j\_f}}$, thus for the *j*'th mode (the *j* subscript has been dropped)

$$\boldsymbol{\varphi}_{\mathbf{j}} = (1-t)\left(\boldsymbol{\varphi}_{\mathbf{j\_0}}\right) + (t)\left(\boldsymbol{\varphi}_{\mathbf{j\_f}}\right) \tag{4.12}$$

The interpolated mode is used as an approximation for the exact modeshape and the approximate eigenvalue is calculated from the Rayleigh quotient

$$\lambda_j \cong \frac{\boldsymbol{\varphi}_{\mathbf{j}}{}^{\mathbf{T}}\mathbf{K}\boldsymbol{\varphi}_{\mathbf{j}}}{\boldsymbol{\varphi}_{\mathbf{j}}{}^{\mathbf{T}}\mathbf{M}\boldsymbol{\varphi}_{\mathbf{j}}} \tag{4.13}$$

This method can be used for gross parameter variations and is not restricted to small variations. However, the interpolation will be more accurate for parameter values near the ends of the interval with the largest errors being close to the centre of the interval. Whilst the eigenvectors are linearly interpolated, the eigenvalues are not and the non-linear dependence of the coefficient matrices $\mathbf{K}$ and $\mathbf{M}$ on the parameter p is incorporated into the Rayleigh quotient.

The method can be extended to multi-dimensional parameter spaces. For example consider the variations in the eigenvalues with respect to two parameters p_1 and p_2 which vary in the parameter space as $0 \le p_1 \le a$ and $0 \le p_2 \le b$. The non-dimensional parameters t_1 and t_2 are defined as

$$t_1 = \frac{p_1}{a} \quad \text{and} \quad t_2 = \frac{p_2}{b} \tag{4.14}$$

where $0 \le t_1 \le 1$ and $0 \le t_2 \le 1$. The interpolated eigenvector is then calculated as

$$\boldsymbol{\varphi}_{\mathbf{j}}(p_1, p_2) \cong (1-t_1)(1-t_2)\boldsymbol{\varphi}_{\mathbf{j\_00}} + t_1(1-t_2)\boldsymbol{\varphi}_{\mathbf{j\_a0}} + (1-t_1)t_2\boldsymbol{\varphi}_{\mathbf{j\_0b}} + t_1t_2\boldsymbol{\varphi}_{\mathbf{j\_ab}} \tag{4.15}$$

where $\boldsymbol{\varphi}_{\mathbf{j\_rs}} = \boldsymbol{\varphi}_{\mathbf{j}}(p_1 = r, p_2 = s)$. The four eigenvectors at corners of the interval rectangle $[0,a]\times[0,b]$ need to be calculated exactly.

The interpolated mode method has one specific drawback; it does not lead directly to an approximate expression for the eigenvalues of the perturbed system in terms of the eigenvalues of the baseline system. It requires an expression of the interval of the variability rather than its PDF. For this reason the interpolated mode method is perhaps more suited to possibilistic analysis.

A way to overcome this disadvantage might be to allow each variable input parameter (with a known PDF) to vary over the fixed interval of $\pm 3\sigma$. If the variability were, Gaussian distributed, this interval would be expected to contain 99.7% of the variability samples. The interpolated mode analysis would then conducted on the N-dimensional parameter space represented by these intervals (where N is the number of variable input parameters).

There are two major disadvantages with this proposal. The first is that the eigenvectors are most accurately estimated near the ends of the intervals and therefore the least accurately estimated region is that in which the variability terms are near their mean value, which is the area that would be expected to be most critical. Secondly, if the system has N degrees of freedom and hence an N–dimensional interval space, it will be necessary to calculate 2^N eigenvectors exactly, so if N is large the computation may become lengthy.

4.1.3 Perturbation methods

Perturbation methods use a Taylor series expansion to approximate the eigensolution. There are two main types of perturbations, those which are centred about the mean value of the baseline or unperturbed system eigenvalues, and those which are centred about some other optimal point. For both expansions, the eigensolution for the perturbed system is approximated by a series summation of terms of increasing power of the random input variables. These power terms become increasingly complex to calculate, but if the random input variables are assumed to be small (as the variability between nominally identical structures is small), then the higher terms also become increasingly small. Often only the first or second order terms of the series are retained and these are the terms considered here.

The perturbation methods can also be used to approximate the perturbed eigenvectors of the structure. A first order approximation of these will be discussed in the context of the mean centred perturbation approach.

In the following sections, the perturbation method will be applied to the case of an undamped structure with random mass and stiffness properties. The mass and stiffness matrices are assumed to possess some known statistical properties which can be described in terms of smooth, continuous, at least twice differentiable functions of a random vector $\mathbf{x}$ (twice in order to be able to form a second order perturbation). The mean value of $\mathbf{x}$ is $\boldsymbol{\mu}$ where $\boldsymbol{\mu} \in \mathbb{R}$; thus the baseline or unperturbed mass and stiffness matrices are given by

$$\mathbf{M}(\boldsymbol{\mu}) = \bar{\mathbf{M}}, \quad \text{and} \quad \mathbf{K}(\boldsymbol{\mu}) = \bar{\mathbf{K}} \tag{4.16}$$

The baseline eigenvalues $\left(\lambda_j(\boldsymbol{\mu}) = \bar{\lambda}_j\right)$ are obtained from $\bar{\mathbf{K}}\bar{\boldsymbol{\varphi}}_j = \bar{\lambda}_j \bar{\mathbf{M}}\bar{\boldsymbol{\varphi}}_j$. The eigenvalues of the perturbed system are given by

$$\mathbf{K}(\mathbf{x})\boldsymbol{\varphi}_j = \lambda_j(\mathbf{x})\mathbf{M}(\mathbf{x})\boldsymbol{\varphi}_j \tag{4.17}$$

and due to the assumptions regarding the mass and stiffness matrices, the eigenvalues are smooth and at least twice differentiable functions of $\mathbf{x}$.

4.1.3.1 Mean centred perturbation method

The mean centred perturbation approach expands the perturbed system eigenvalues, $\lambda_j(\mathbf{x})$, about their mean $\boldsymbol{\mu}$ baseline value. The expansion up to including the second order term is given by [4.4]

$$\lambda_j(\mathbf{x}) \cong \lambda_j(\boldsymbol{\mu}) + \underbrace{\left(\frac{\partial \lambda_j(\mathbf{x})}{\partial \mathbf{x}}\right)^T\Bigg|_{\mathbf{x}=\boldsymbol{\mu}} (\mathbf{x}-\boldsymbol{\mu})}_{\text{first order term}} + \underbrace{\frac{1}{2}(\mathbf{x}-\boldsymbol{\mu})^T \mathbf{D}_{\lambda_j}(\boldsymbol{\mu})\Big|_{\mathbf{x}=\boldsymbol{\mu}} (\mathbf{x}-\boldsymbol{\mu})}_{\text{second order term}} \tag{4.18}$$

where $\left.\frac{\partial \lambda_j(\mathbf{x})}{\partial \mathbf{x}}\right|_{\mathbf{x}=\boldsymbol{\mu}}$ is the gradient vector of the perturbed eigenvalues, $\lambda_j(\mathbf{x})$, and $\mathbf{D}_{\lambda_j}(\boldsymbol{\mu})\Big|_{\mathbf{x}=\boldsymbol{\mu}}$ is the Hessian matrix of them given by $\left\{\mathbf{D}_{\lambda_j}(\boldsymbol{\mu})\right\}_{kl} = \left.\frac{\partial^2 \lambda_j(\mathbf{x})}{\partial x_k \partial x_l}\right|_{\mathbf{x}=\boldsymbol{\mu}}$. The baseline eigenvalues $\lambda_j(\boldsymbol{\mu})$ are from the unperturbed system when $\mathbf{x} = \boldsymbol{\mu}$.

First order eigenvalues

If the variations in $\mathbf{x}$ are small then the second order term is often ignored and the first order approximation is given by [4.5]

$$\lambda_j(\mathbf{x}) \cong \lambda_j(\boldsymbol{\mu}) + \left(\frac{\partial \lambda_j(\mathbf{x})}{\partial \mathbf{x}}\right)^T \Bigg|_{\mathbf{x}=\boldsymbol{\mu}} (\mathbf{x}) \tag{4.19}$$

From equation (4.17)

$$\left[\mathbf{K}(\mathbf{x}) - \lambda_j(\mathbf{x})\mathbf{M}(\mathbf{x})\right]\boldsymbol{\varphi}_j(\mathbf{x}) = 0 \tag{4.20}$$

Pre-multiplying by $\boldsymbol{\varphi}_j(\mathbf{x})^T$

$$\boldsymbol{\varphi}_j(\mathbf{x})^T\left[\mathbf{K}(\mathbf{x}) - \lambda_j(\mathbf{x})\mathbf{M}(\mathbf{x})\right]\boldsymbol{\varphi}_j(\mathbf{x}) = 0 \tag{4.21}$$

Differentiating equation (4.21) with respect to the *k*'th value of $\mathbf{x}$, x_k gives

$$\begin{aligned}&\frac{\partial \boldsymbol{\varphi}_j(\mathbf{x})^T}{\partial x_k}\left[\mathbf{K}(\mathbf{x}) - \lambda_j(\mathbf{x})\mathbf{M}(\mathbf{x})\right]\boldsymbol{\varphi}_j(\mathbf{x}) + \boldsymbol{\varphi}_j(\mathbf{x})^T\left[\frac{\partial\left(\mathbf{K}(\mathbf{x}) - \lambda_j(\mathbf{x})\mathbf{M}(\mathbf{x})\right)}{\partial x_k}\right]\boldsymbol{\varphi}_j(\mathbf{x}) \\ &+\boldsymbol{\varphi}_j(\mathbf{x})^T\left[\mathbf{K}(\mathbf{x}) - \lambda_j(\mathbf{x})\mathbf{M}(\mathbf{x})\right]\frac{\partial \boldsymbol{\varphi}_j(\mathbf{x})}{\partial x_k} = 0\end{aligned} \tag{4.22}$$

The first and the third term of equation (4.22) are zero by virtue of equation (4.20) and because $\left[\mathbf{K}(\mathbf{x}) - \lambda_j(\mathbf{x})\mathbf{M}(\mathbf{x})\right]$ is a symmetric matrix, therefore

$$\boldsymbol{\varphi}_j(\mathbf{x})^T\left[\frac{\partial\left(\mathbf{K}(\mathbf{x}) - \lambda_j(\mathbf{x})\mathbf{M}(\mathbf{x})\right)}{\partial x_k}\right]\boldsymbol{\varphi}_j(\mathbf{x}) = 0 \tag{4.23}$$

The derivative of $\left[\mathbf{K}(\mathbf{x}) - \lambda_j(\mathbf{x})\mathbf{M}(\mathbf{x})\right]$ is

$$\frac{\partial\left(\mathbf{K}(\mathbf{x}) - \lambda_j(\mathbf{x})\mathbf{M}(\mathbf{x})\right)}{\partial x_k} = \left[\frac{\partial \mathbf{K}(\mathbf{x})}{\partial x_k} - \lambda_j(\mathbf{x})\frac{\partial \mathbf{M}(\mathbf{x})}{\partial x_k} - \frac{\partial \lambda_j(\mathbf{x})}{\partial x_k}\mathbf{M}(\mathbf{x})\right] \tag{4.24}$$

If the eigenvectors are mass normalised such that $\boldsymbol{\varphi}_j(\mathbf{x})^T \mathbf{M}(\mathbf{x})\boldsymbol{\varphi}_j(\mathbf{x}) = 1$, then, combining equations (4.23) and (4.24)

$$\frac{\partial \lambda_j(\mathbf{x})}{\partial x_k} = \boldsymbol{\varphi}_j(\mathbf{x})^T \left[\frac{\partial \mathbf{K}(\mathbf{x})}{\partial x_k} - \lambda_j(\mathbf{x}) \frac{\partial \mathbf{M}(\mathbf{x})}{\partial x_k} \right] \boldsymbol{\varphi}_j(\mathbf{x}) \tag{4.25}$$

or

$$\frac{\partial \lambda_j(\mathbf{x})}{\partial x_k} = \boldsymbol{\varphi}_j(\mathbf{x})^T \mathbf{G}_j(\mathbf{x}) \boldsymbol{\varphi}_j(\mathbf{x}) \tag{4.26}$$

where

$$\mathbf{G}_j(\mathbf{x}) = \left[\frac{\partial \mathbf{K}(\mathbf{x})}{\partial x_k} - \lambda_j(\mathbf{x}) \frac{\partial \mathbf{M}(\mathbf{x})}{\partial x_k} \right] \tag{4.27}$$

Forming this into the vector equivalent and using the derivative of a matrix w.r.t. a vector (see Appendix A), equation (4.26) is of the form

$$\frac{\partial \lambda_j(\mathbf{x})}{\partial \mathbf{x}} = \begin{bmatrix} \boldsymbol{\varphi}_j(\mathbf{x})^T \left[\frac{\partial \mathbf{K}(\mathbf{x})}{\partial x_1} - \lambda_j(\mathbf{x}) \frac{\partial \mathbf{M}(\mathbf{x})}{\partial x_1} \right] \boldsymbol{\varphi}_j(\mathbf{x}) \\ \boldsymbol{\varphi}_j(\mathbf{x})^T \left[\frac{\partial \mathbf{K}(\mathbf{x})}{\partial x_2} - \lambda_j(\mathbf{x}) \frac{\partial \mathbf{M}(\mathbf{x})}{\partial x_2} \right] \boldsymbol{\varphi}_j(\mathbf{x}) \\ \vdots \\ \boldsymbol{\varphi}_j(\mathbf{x})^T \left[\frac{\partial \mathbf{K}(\mathbf{x})}{\partial x_k} - \lambda_j(\mathbf{x}) \frac{\partial \mathbf{M}(\mathbf{x})}{\partial x_k} \right] \boldsymbol{\varphi}_j(\mathbf{x}) \end{bmatrix} \tag{4.28}$$

Therefore from equation (4.19), the first order mean centred perturbation of the eigenvalues is given by

$$\lambda_j(\mathbf{x}) \cong \lambda_j(\boldsymbol{\mu}) + \boldsymbol{\varphi}_j(\boldsymbol{\mu})^T \left(\sum_k \left(\frac{\partial \mathbf{K}(\mathbf{x})}{\partial x_k} - \lambda_j(\boldsymbol{\mu}) \frac{\partial \mathbf{M}(\mathbf{x})}{\partial x_k} \right) x_k \right) \boldsymbol{\varphi}_j(\boldsymbol{\mu}) \tag{4.29}$$

This provides a linear relationship between the eigenvalues and the random input variables. If the random variables in $\mathbf{x}$ are Gaussian distributed, then the eigenvalues will also be Gaussian distributed, and a closed-form expression for their joint PDF can be obtained [4.6]-[4.11]. The

example here has not considered damping; a study by Adhikari [4.12] and [4.13] has considered a first order perturbation for non-proportionally damped systems. Adhikari showed that if the variations are small such that a first order perturbation can be applied, the complex eigenvalues and eigenvectors can be obtained. A simple numerical example was used to compare the results to those obtained from Monte Carlo simulations and the method was shown to work well even for high levels of damping.

Second order eigenvalues

A second-order perturbation can be obtained if the Hessian matrix in equation (4.18) is retained. Plaut and Huseyin [4.14] have shown that if the eigenvalues are distinct then the Hessian matrix of $\lambda_j(\mathbf{x})$ is given by

$$\left\{\mathbf{D}_{\lambda_j}(\boldsymbol{\mu})\right\}_{kl} = \left.\frac{\partial^2 \lambda_j(\mathbf{x})}{\partial x_k \partial x_l}\right|_{\mathbf{x}=\boldsymbol{\mu}} \tag{4.30}$$

where

$$\frac{\partial^2 \lambda_j(\mathbf{x})}{\partial x_k \partial x_l} = \boldsymbol{\varphi}_j(\mathbf{x})^T \left[\frac{\partial^2 \mathbf{K}(\mathbf{x})}{\partial x_k \partial x_l} - \lambda_j(\mathbf{x}) \frac{\partial \mathbf{M}^2(\mathbf{x})}{\partial x_k \partial x_l}\right] \boldsymbol{\varphi}_j(\mathbf{x}) - \left(\boldsymbol{\varphi}_j(\mathbf{x})^T \frac{\partial \mathbf{M}(\mathbf{x})}{\partial x_k} \boldsymbol{\varphi}_j(\mathbf{x})\right)\left(\boldsymbol{\varphi}_j(\mathbf{x})^T \mathbf{G}_{jl(\mathbf{x})} \boldsymbol{\varphi}_j(\mathbf{x})\right)$$
$$- \left(\boldsymbol{\varphi}_j(\mathbf{x})^T \frac{\partial \mathbf{M}(\mathbf{x})}{\partial x_l} \boldsymbol{\varphi}_j(\mathbf{x})\right)\left(\boldsymbol{\varphi}_j(\mathbf{x})^T \mathbf{G}_{jk(\mathbf{x})} \boldsymbol{\varphi}_j(\mathbf{x})\right) + 2\sum_{\substack{r=1 \\ r \neq j}}^{N} \frac{\left(\boldsymbol{\varphi}_j(\mathbf{x})^T \mathbf{G}_{jk(\mathbf{x})} \boldsymbol{\varphi}_j(\mathbf{x})\right)\left(\boldsymbol{\varphi}_j(\mathbf{x})^T \mathbf{G}_{jl(\mathbf{x})} \boldsymbol{\varphi}_j(\mathbf{x})\right)}{\lambda_j(\mathbf{x}) - \lambda_r(\mathbf{x})} \tag{4.31}$$

As can be seen from this term, the second order expansion can rapidly become complicated and hence expensive to calculate. If the basic random variables in $\mathbf{x}$ are Gaussian distributed, the perturbed eigenvalues are given by a quadratic form in $\mathbf{x}$, [4.15] and [4.16]. In chapter 5 the first and second order, mean centred perturbations will be applied to a simple example of a two degree of freedom system for further discussion.

First order eigenvectors

Fox and Kapoor [4.5] present two methods for the first order perturbation of the eigenvectors. The first of these only requires knowledge of the *j*'th unperturbed eigenvector, but is prone to numerical problems. The second method calculates the perturbed eigenvector as a linear combination of the unperturbed eigenvectors, such that

$$\frac{\partial \boldsymbol{\varphi}_j(\mathbf{x})}{\partial x_k} \cong \sum_{p=1}^{n} a_{jkp} \boldsymbol{\varphi}_p(\boldsymbol{\mu}) \tag{4.32}$$

where the index p gives all the global modes. From differentiating the eigenvector in equation (4.20), we obtain

$$\left[\mathbf{K}(\mathbf{x}) - \lambda_j(\mathbf{x})\mathbf{M}(\mathbf{x})\right] \frac{\partial \boldsymbol{\varphi}_j(\mathbf{x})}{\partial x_k} = -\frac{\partial\left(\mathbf{K}(\mathbf{x}) - \lambda_j(\mathbf{x})\mathbf{M}(\mathbf{x})\right)}{\partial x_k} \boldsymbol{\varphi}_j(\mathbf{x}) \tag{4.33}$$

Substituting equation (4.32) into (4.33) gives

$$\left[\mathbf{K}(\mathbf{x}) - \lambda_j(\mathbf{x})\mathbf{M}(\mathbf{x})\right] \sum_{p=1}^{n} a_{jkp} \boldsymbol{\varphi}_p(\boldsymbol{\mu}) = -\frac{\partial\left(\mathbf{K}(\mathbf{x}) - \lambda_j(\mathbf{x})\mathbf{M}(\mathbf{x})\right)}{\partial x_k} \boldsymbol{\varphi}_j(\mathbf{x}) \tag{4.34}$$

and pre-multiplying both sides of equation (4.34) by $\boldsymbol{\varphi}_p(x)^T$, $\mathrm{p} \neq j$

$$\sum_{p=1}^{n} a_{jkp} \boldsymbol{\varphi}_p(x)^T \left[\mathbf{K}(\mathbf{x}) - \lambda_j(\mathbf{x})\mathbf{M}(\mathbf{x})\right] \boldsymbol{\varphi}_p(\boldsymbol{\mu}) = -\boldsymbol{\varphi}_p(x)^T \frac{\partial\left(\mathbf{K}(\mathbf{x}) - \lambda_j(\mathbf{x})\mathbf{M}(\mathbf{x})\right)}{\partial x_k} \boldsymbol{\varphi}_j(\mathbf{x}) \tag{4.35}$$

From this we obtain

$$a_{jkp} = \frac{\boldsymbol{\varphi}_p(\mathbf{x})^T \left[\frac{\partial \mathbf{K}(\mathbf{x})}{\partial x_k} - \lambda_j(\mathbf{x}) \frac{\partial \mathbf{M}(\mathbf{x})}{\partial x_k}\right] \boldsymbol{\varphi}_j(\mathbf{x})}{\lambda_j - \lambda_p}, \qquad \mathrm{p} \neq j \tag{4.36}$$

In order to obtain the result for $p = j$, the expression for the mass normalised eigenvectors $\boldsymbol{\varphi}_j(\mathbf{x})^T \mathbf{M}(\mathbf{x}) \boldsymbol{\varphi}_j(\mathbf{x}) = 1$ is differentiated to obtain the equation

$$2\boldsymbol{\varphi}_j(\mathbf{x})^T \mathbf{M}(\mathbf{x}) \frac{\partial \boldsymbol{\varphi}_j(\mathbf{x})}{\partial x_k} = -\boldsymbol{\varphi}_j(\mathbf{x})^T \frac{\partial \mathbf{M}(\mathbf{x})}{\partial x_k} \boldsymbol{\varphi}_j(\mathbf{x}) \tag{4.37}$$

Equation (4.32) is substituted into the above to obtain

$$a_{jkj} = -\frac{1}{2}\boldsymbol{\varphi}_j(\mathbf{x})^T \frac{\partial \mathbf{M}(\mathbf{x})}{\partial x_k}\boldsymbol{\varphi}_j(\mathbf{x}) \tag{4.38}$$

Combining these the perturbed eigenvectors are approximated by

$$\boldsymbol{\varphi}_j(\mathbf{x}) \cong \boldsymbol{\varphi}_j(\boldsymbol{\mu}) + \sum_k \left(\begin{array}{l} -\frac{1}{2}\boldsymbol{\varphi}_j(\mathbf{x})^T \frac{\partial \mathbf{M}(\mathbf{x})}{\partial x_k}\boldsymbol{\varphi}_j(\mathbf{x})\boldsymbol{\varphi}_j(\boldsymbol{\mu})x_k \\ +\sum_{\substack{p=1 \\ p\neq j}}^{n} \frac{\boldsymbol{\varphi}_p(\mathbf{x})^T\left[\frac{\partial \mathbf{K}(\mathbf{x})}{\partial x_k} - \lambda_j(\mathbf{x})\frac{\partial \mathbf{M}(\mathbf{x})}{\partial x_k}\right]\boldsymbol{\varphi}_j(\mathbf{x})}{\lambda_j - \lambda_p}\boldsymbol{\varphi}_p(\boldsymbol{\mu})x_k \end{array} \right) \tag{4.39}$$

where x_k is the k'th term of variability vector $\mathbf{x}$.

The summation in equation (4.32) is sometimes constrained to a subset of the global modes to reduce the computational expense. Estimating the perturbed eigenvectors enables a more accurate estimation of the FRF of the perturbed structure.

4.1.3.2 Optimal point perturbation method

An optimised perturbation method has been proposed by Adhikari and Langley [4.17] in which the expansion of the perturbed eigenvalues $\lambda_j(\mathbf{x})$ is centred about a point $\boldsymbol{\alpha}$ in the $\mathbf{x}$-space. The aim is to choose the point $\boldsymbol{\alpha}$ such that the expansion is optimised in some sense.

From equation (4.18) the expansion up to and including the second order term is given by

$$\lambda_j(\mathbf{x}) \cong \lambda_j(\boldsymbol{\alpha}) + \underbrace{\left(\frac{\partial \lambda_j(\mathbf{x})}{\partial \mathbf{x}}\right)^T\Bigg|_{\mathbf{x}=\boldsymbol{\alpha}}(\mathbf{x}-\boldsymbol{\alpha})}_{\text{first order term}} + \underbrace{\frac{1}{2}(\mathbf{x}-\boldsymbol{\alpha})^T \mathbf{D}_{\lambda_j}(\boldsymbol{\alpha})\big|_{\mathbf{x}=\boldsymbol{\alpha}}(\mathbf{x}-\boldsymbol{\alpha})}_{\text{second order term}} \tag{4.40}$$

In order to choose the optimal point $\boldsymbol{\alpha}$ it is helpful to consider the form of the PDFs of the random variables. Adhikari and Friswell [4.4] considered the case where the basic random variables were described by the joint probability density function $p_{\mathbf{x}}(\mathbf{x})$,

$$p_{\mathbf{x}}(\mathbf{x}) = e^{-L(\mathbf{x})} \tag{4.41}$$

where $-L(\mathbf{x})$ is the log-likelihood function. If $\mathbf{x}$ is an *m*-dimensional multivariate Gaussian random vector with a mean $\boldsymbol{\mu} \in \mathbb{R}^m$ and covariance $\boldsymbol{\sigma} \in \mathbb{R}^{mxm}$ then [4.4]

$$L(\mathbf{x}) = \frac{m}{2}\ln(2\pi) + \frac{1}{2}\ln\|\boldsymbol{\sigma}\| + \frac{1}{2}(\mathbf{x}-\boldsymbol{\mu})^T \boldsymbol{\sigma}^{-1}(\mathbf{x}-\boldsymbol{\mu}) \tag{4.42}$$

The optimal point $\boldsymbol{\alpha}$ was then selected such that the first moment of each eigenvalue was accurately calculated. Using equation (4.41) the mean of $\lambda_j(\mathbf{x})$ can be expressed as

$$\bar{\lambda}_j = E\left[\lambda_j(\mathbf{x})\right] = \int \lambda_j(\mathbf{x})\, p_{\mathbf{x}}(\mathbf{x}) d\mathbf{x} = \int \lambda_j(\mathbf{x}) e^{-L(\mathbf{x})} d\mathbf{x} = \int e^{-h_j(\mathbf{x})} d\mathbf{x} \tag{4.43}$$

where $h_j(\mathbf{x}) = L(\mathbf{x}) - \ln\lambda_j(\mathbf{x})$. There are still several difficulties associated with determining the exact value of $\bar{\lambda}_j$, but a Taylor expansion may be used about a point where $h_j(\mathbf{x})$ has a minimum. This point represents the region where there is the maximum contribution to the integral in equation (4.43) and thus the error in evaluating the integral is minimised.
The optimal point can be obtained from

$$\frac{\partial h_j(\mathbf{x})}{\partial x_k} = 0 \tag{4.44}$$

or

$$\frac{\partial L(\mathbf{x})}{\partial x_k} = \frac{1}{\lambda_j(\mathbf{x})}\frac{\partial \lambda_j(\mathbf{x})}{\partial x_k}, \quad \forall k \tag{4.45}$$

Hence, for all k at $\mathbf{x} = \boldsymbol{\alpha}$

$$\frac{\partial \lambda_j(\boldsymbol{\alpha})}{\partial x_k} = \lambda_j(\boldsymbol{\alpha})\frac{\partial L(\boldsymbol{\alpha})}{\partial x_k} \tag{4.46}$$

Adhikari and Friswell conclude that this implies that at the optimal point the gradient vectors of the eigenvalues and the log-likelihood function are parallel. Numerical solutions are required to the non-linear set of equations in (4.46) and $\boldsymbol{\alpha} = \boldsymbol{\mu}$ can be used as a starting point.

When considering the application of the optimal point method to structures with uncertain properties, the benefits of optimising the expansion point may be minimal. As the response of the structures is often considered to vary about the baseline or unperturbed response, this would suggest that the mean value of the baseline eigenvalues is already a suitable point to expand around. Furthermore, from the investigations of data sets from real components and structures discussed in chapters 2 and 3, the distributions are often found to be Gaussian or near Gaussian in form, hence, the distribution $p_{\mathbf{x}}(\mathbf{x})$ is centred around the mean.

4.2 Analytical propagation of statistics

Once an approximation for the eigensolution has been obtained, it can be used to propagate various statistics of the physical properties (mass and stiffness matrices), to the statistics of the modal properties. In this section two methods are discussed for analysing how various statistics may be propagated through a linear system. The output or response parameter statistics are then estimated analytically.

4.2.1 Generation of moments

The moments of a system's response can be related to the moments of the system inputs, this method is sometimes referred to as the 'Generation of Moments' method [4.18]. Suppose the output y is given by a function of the input parameter x as

$$y = f(x) \tag{4.47}$$

where $f(x) = \sum_{n=0}^{\infty} a_n x^n$, for example

$$y = \frac{1}{(1 - c_1 x)^n} \tag{4.48}$$

where c_1 and n are constants. The power series expansion converges if $|c_1 x| < 1$. The mean of y can be written as

$$E[y] = E\left[\sum_{n=0}^{\infty} a_n x^n\right] = \sum_{n=0}^{\infty} a_n E\left[x^n\right] \tag{4.49}$$

For example, for the case considered in equation (4.48), $a_n = c_1^n$ and the mean and variance become

$$E[y] = \mu_y = \sum_{r=0}^{\infty} \binom{n+r-1}{r} c_1^r E[x^r] \tag{4.50}$$

$$\sigma_y^2 = E[y^2] - \mu_y^2 \tag{4.51}$$

where $\binom{n+r-1}{r} = \frac{(n+r-1)!}{r!(n-1)!}$. It can be shown that

$$E[y^2] = \sum_{r=0}^{\infty} \binom{2n+r-1}{r} c_1^r E[x^r] \tag{4.52}$$

These power series expansions can be used to express the first and second (and higher) moments of the system response in terms of the variability in the physical properties.

4.2.2 Change of variable method

The change of variable method can be used to obtain the PDF of an output variable y if the PDF of the input variable x is known [4.19]. For example, suppose the system is described by

$$y = f(x) \tag{4.53}$$

where the probability density function of x is given by $p(x)$. The PDF for y is given by

$$p(y) = \frac{np(x)}{|f'(x)|} \tag{4.54}$$

where it is assumed that y is an n-valued function of x. If the functional relationship between the two random variables x and y is assumed to be single valued and one-to-one, then this becomes

$$p(y) = \frac{p(x)}{|f'(x)|} \tag{4.55}$$

This technique can be used in conjunction with eigensolution approximations to examine the natural frequencies of a system.

An extension of the change of variable method [4.19] allows the joint probability density function for two single-valued continuous random variables with continuous partial derivatives to be defined. For example, if $y_1 = y_1(x_1, x_2)$, $y_2 = y_2(x_1, x_2)$, and x_1 and x_2 are the inputs then the joint probability density function of the output is

$$p(y_1, y_2) = \frac{p(x_1, x_2)}{\mathbf{J}} \tag{4.56}$$

where J is the Jacobian is given by

$$\mathbf{J} = \begin{vmatrix} \frac{\partial y_1}{\partial x_1} & \frac{\partial y_1}{\partial x_2} \\ \frac{\partial y_2}{\partial x_1} & \frac{\partial y_2}{\partial x_2} \end{vmatrix} \tag{4.57}$$

In the case where a single output variable is related to two uncertain input parameters, a dummy output variable is introduced in order to evaluate the Jacobian in (4.57). The resultant joint probability density function can be reduced to a single PDF by integration over the dummy variable.

The general multivariate expression for the change of variable method $\mathbf{y}_n = y_n(\mathbf{x}_n)$ is given by

$$p(\mathbf{y}) = \frac{p(\mathbf{x})}{\mathbf{J}} \tag{4.58}$$

where

$$p(y_1, y_2, ..., y_n) = \frac{p(x_1, x_2, .., x_n)}{\begin{vmatrix} \frac{\partial y_1}{\partial x_1} & \frac{\partial y_1}{\partial x_2} & \cdots & \frac{\partial y_1}{\partial x_n} \\ \frac{\partial y_2}{\partial x_1} & \frac{\partial y_2}{\partial x_2} & \cdots & \frac{\partial y_2}{\partial x_n} \\ \cdots & \cdots & \cdots & \cdots \\ \frac{\partial y_n}{\partial x_1} & \frac{\partial y_n}{\partial x_2} & \cdots & \frac{\partial y_n}{\partial x_n} \end{vmatrix}} \tag{4.59}$$

This more general expression is used in chapter 5, in conjunction with two eigensolution approximations, to examine the multi-input, multi-output relationship of an undamped two degree of freedom system, with variable mass and stiffness.

4.2.3 Matrix notation of moments

A matrix notation can be a useful method of presenting the moments of a linear function in terms of the moments of the input, in particular the mean and variance. In general if a function of output variables $\mathbf{y}$ is given by

$$\mathbf{y} = \mathbf{A}\mathbf{x} \tag{4.60}$$

where $\mathbf{x}$ is a vector of input variables and $\mathbf{A}$ is a matrix of constants relating the two. Then the mean value of $\mathbf{y}$ is given by

$$E[\mathbf{y}] = \mathbf{A}E[\mathbf{x}] \tag{4.61}$$

If the mean value of $\mathbf{x}$ is zero then the mean value of $\mathbf{y}$ is zero, $E[\mathbf{x}] = 0 \;\; \therefore E[\mathbf{y}] = 0$, and for this case the variance of $\mathbf{y}$ is given by

$$\begin{aligned} E\left[\mathbf{y}\mathbf{y}^{\mathbf{T}}\right] &= \mathbf{A}E\left[\mathbf{x}\mathbf{x}^{\mathbf{T}}\right]\mathbf{A}^{\mathbf{T}} \\ \operatorname{var}(\mathbf{y}) &= \mathbf{A}\operatorname{var}(\mathbf{x})\mathbf{A}^{\mathbf{T}} \end{aligned} \tag{4.62}$$

where $\operatorname{var}(\mathbf{x})$ and $\operatorname{var}(\mathbf{y})$ are the variance/covariance matrices of $\mathbf{x}$ and $\mathbf{y}$. These variance/covariance matrices have a special form with the variance of the inputs/outputs on the leading diagonal and covariance's between terms on the off-diagonals, thus

$$\operatorname{var}(\mathbf{x}) = \begin{bmatrix} E\left[x_1^{\,2}\right] & E[x_2x_1] & \cdots & E[x_nx_1] \\ E[x_1x_2] & E\left[x_2^{\,2}\right] & \cdots & E[x_nx_2] \\ \vdots & \vdots & \ddots & \vdots \\ E[x_1x_n] & E[x_2x_n] & \cdots & E\left[x_n^{\,2}\right] \end{bmatrix} \tag{4.63}$$

where $x_1, x_2, \cdots, x_n$ are the function inputs. As it can be seen above these matrices are symmetrical, being reflected in the diagonal.

This format arranging the input and outputs of a linear function will be used later to simplify the application of perturbation estimations to the propagation of statistics from both physical uncertainties and local modal uncertainties.

4.3 Monte Carlo methods

Monte Carlo (MC) methods are used to obtain numerical solutions to complicated problems for which an analytical solution cannot be easily found. They are a family of techniques in which an estimate of the PDF or distribution of an output quantity is found by running repeated simulations with input values being pseudo-randomly selected. They can be used in structural dynamics to generate an approximate PDF of the modal properties. Various MC methods use different techniques for selecting the values of the pseudo-random input values, the most simple of these being unconstrained random generation of input values from the PDF of the input quantity. A significant advantage of the MC method is that no assumptions are made about the system except for the PDFs of the input parameters and these can be of any form. The main drawback of the method is the large number of trials required to obtain a good approximation to the output PDF.

This motivates the development of constrained MC methods which are methods by which accurate estimates of the output statistics are found using a relatively small number of trials, by selecting the input data in a non-random manner. Two types of constrained MC methods are discussed below.

4.3.1 Stratified sampling

The stratified sampling method aims to reduce the number of trial runs required to obtain a good approximation of the output distribution, whilst ensuring all areas of the input distributions are covered. This is done by dividing the input parameter distributions into partitions. Random samples are then generated from each partition of the sample space, thus ensuring an even distribution of samples. This method ensures some samples will be generated in the tails of the input distribution, which may otherwise be unlikely. One of the simplest forms of stratified

sampling is that where the input parameter domain is divided into partitions of equal probability. However, other methods of division may be more suitable if for example a particular region of the input domain is of interest.

As an illustration, consider $Y = f(\mathbf{x})$ where $\mathbf{x}$ taken from the domain Ω such that $\mathbf{x} \in \Omega \in \mathbb{R}^n$. The inexact input quantities are $\mathbf{x} = \{x_1, x_2, ..., x_n\}$. The method for stratified sampling is as follows [4.19]:

- Divide the domain, Ω of the input parameter into N partitions given by $\{S_i, i = 1, 2, ..., N\}$ such that no two partitions overlap and the union of all the partitions equals the whole domain Ω;
- Take random sample sets of m_i values from each region S_i according to the joint PDF. of the input quantities, such that $\{\mathbf{x}^{ij}, j = 1, 2, ..., m_i\}$;
- Run the model with each set of parameters to produce a set of results y_{ij}.

If $N = 1$, then only one partition covering the whole sample domain is selected and the method is the same as unconstrained sampling. The output quantity Y is considered to be a scalar in the above, although this is not necessary for the method.

If the probability of a sample having come from a particular partition is given by $P(\mathbf{x} \in S_i) = p_i$ and the total number of sample sets of data is $M = m_1 + m_2 + ... + m_N$, then it can be shown that the unbiased estimator for the distribution function $P(Y \le y)$ is given by [4.19]

$$\bar{P}(y) = \sum_{i=1}^{N} \frac{p_i}{m_i} \sum_{j=1}^{m_i} g(y, y_{ij})$$
$$g(y, y_{ij}) = \begin{cases} 1, & y - y_{ij} \ge 0 \\ 0, & y - y_{ij} < 0 \end{cases} \tag{4.64}$$

The unbiased estimators for the mean and variance are given by

$$\bar{y} = \sum_{i=1}^{N} \frac{p_i}{m_i} \sum_{j=1}^{m_i} y_{ij}$$
$$s^2 = \sum_{i=1}^{N} \frac{p_i}{m_i} \sum_{j=1}^{m_i} \left(y_{ij} - \bar{y} \right)^2 \tag{4.65}$$

If m_i and p_i are chosen such that $m_i = p_i M$ then the sampling is referred to as proportional sampling. A popular method divides the input parameter domain into partitions of equal probability such that $p_i = 1/N$, $i = 1, 2, ..., N$.

4.3.2 Latin hypercube sampling

Standard Latin Hypercube (LH) sampling [4.21] was first proposed by McKay *et al.* [4.20] as a method for further reducing the required number of realisations in a stratified MC simulation. If m denotes the number of realisations and K the number of random variables, then a m x K matrix $\mathbf{P}$ is created in which each column contains a random permutation of $1, 2, ..., m$. A second m x K matrix $\mathbf{R}$ is created containing independent random numbers generated from the uniform $(0,1)$ distribution. The basic sampling matrix $\mathbf{S}$ is then defined as

$$\mathbf{S} = \frac{1}{m}(\mathbf{P} - \mathbf{R}) \tag{4.66}$$

Each element of $\mathbf{S}$, s_{ij} is then mapped onto its target distribution

$$\mathbf{x}_{ij} = F_{x_j}^{-1}\left(s_{ij}\right) \tag{4.67}$$

where $F_{x_j}^{-1}$ is the inverse of the target cumulative distribution function for variable j. The vector $\mathbf{x}_i = \left[x_{i1} \quad x_{i2} \quad .... \quad x_{ik} \right]$ now contains the input data for one computation.

For example [4.21], if a system has two random variables, $K = 2$, and $m = 5$ trials or realisations, then $\mathbf{P}$ and $\mathbf{R}$ could be given by

$$\mathbf{P} = \begin{bmatrix} 1 & 2 \\ 2 & 4 \\ 3 & 3 \\ 4 & 1 \\ 5 & 5 \end{bmatrix}, \qquad \mathbf{R} = \begin{bmatrix} 0.60 & 0.83 \\ 0.42 & 0.11 \\ 0.69 & 0.51 \\ 0.32 & 0.58 \\ 0.83 & 0.32 \end{bmatrix} \tag{4.68}$$

Using equation (4.66), $\mathbf{S}$ is given by

$$\mathbf{S} = \begin{bmatrix} 0.08 & 0.23 \\ 0.32 & 0.78 \\ 0.46 & 0.50 \\ 0.74 & 0.08 \\ 0.83 & 0.94 \end{bmatrix} \tag{4.69}$$

Figure 4-1 shows the resultant sample space.

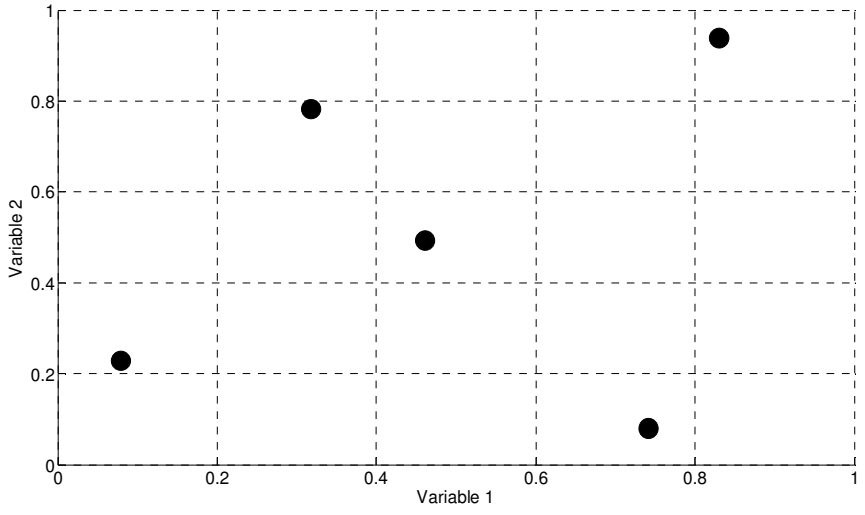

Figure 4-1 Example LH sample space.

There is a risk that some spurious correlation may appear in the generated sample space, however this may be reduced by modifying the matrix $\mathbf{P}$ by means of dividing by $m+1$, mapping it to a Gaussian distribution with zero mean and unit standard deviation, and applying a Cholesky decomposition [4.22].

4.4 Conclusions

In order to propagate statistics from the physical properties to the modal properties of a structure, some form of eigensolution approximation is generally used to obtain a simplified relationship between the two. Various techniques can then be applied to obtain the moments or PDF of the modal properties in terms of the moments or PDF of the physical properties.

Several eigensolution approximations have been presented here and each of them has their merits and drawbacks for application to uncertain structures. The first group of these make use of the eigenvectors of the baseline system. The simplest method uses the eigenvectors of the unperturbed structure as assumed modeshapes for the perturbed structure. Whilst this is the quickest and easiest method to implement, it is also one of the least accurate. The second method to use the eigenvectors of the unperturbed system is the interpolated mode method. This has some benefits over the previous method, although the number of sets of exact eigenvectors required increases rapidly with the number of variable parameters. However, the main disadvantage of this method to the propagation of statistics, is that it is an interval based method, and as such is perhaps more suited to a possibilistic approach where no statistical information is available.

The second group of approximations are the perturbation methods, which use Taylor series expansions to approximate the eigensolution. The mean centred approach is more suitable for distributions which are Gaussian or close to Gaussian, and providing the uncertainty in the structure is small, a first order perturbation may provide satisfactory accuracy. For large structures calculation of the second order terms could be prohibitive. Estimates can also be made for the perturbed system eigenvectors, allowing for a more representative estimate of the FRF than those using the unperturbed system eigenvectors. For distributions that are not closely Gaussian in form, an optimal point perturbation will probably provide a more accurate method, although some care would be required in deciding the criteria on which to optimise the expansion point.

An alternative approach to the analytical eigensolution approximations is offered by Monte Carlo simulations. These have the advantage of being able to accommodate large structures with no assumptions being required about the system apart from the PDFs of the input parameters. They provide a numerical solution, estimating the PDF of the system response. The downside to their generality is the large number of trials required to obtain a good estimate of the response. Several constrained techniques have been developed which impose some selection criteria on

the pseudo-random input parameters. Two methods discussed were stratified sampling and Latin Hypercube sampling, both of which provide a good reduction in the number of trials required. However, the MC approach will still be limited by computational expense for large structures.

From chapters 2 and 3, it was concluded that there was some evidence for assuming the levels of variability to be small and Gaussian or close to Gaussian distributed. Based on this the mean centred perturbation methods would seem to be suitable for propagating variability in uncertain structures. In the subsequent chapter the example of a two degree of freedom system is used to examine further a selection of the methods presented here.

5. The propagation of uncertainty in simple systems

In this chapter the propagation of uncertainty in simple systems is studied by applying some of the techniques presented in chapter 4. Variability is introduced into the physical properties of a basic system to represent the potential inconsistencies arising from mass production of batches of nominally identical systems. The aim is to relate the statistics of the variable physical parameters to the statistics of the modal properties. Also of interest are the distributions of the modal properties and their relationship to parameter variability.

The single degree of freedom system has been considered by Hills et al. see [5.1] and [5.2]. Here the example of a two degree of freedom system is considered. Variability is introduced into the physical properties of the system and the statistics of these are related to the resultant statistics of the variable response. It is assumed that the statistics of the system property variation are known. However, the analysis methods used impose no limitations on the type of this distribution.

Firstly, the baseline system is introduced and nomenclature defined. Then the properties of the perturbed or variable system are defined. The first approximation applied to the system is the use of baseline modeshapes as assumed shape functions. Next a first order perturbational expansion is used to estimate the system eigenvalues and the relationship between the statistics of these and the statistics of the physical properties examined. The first order approximation is then extended to include the system eigenvectors. A further second order term is calculated for the eigenvalues and a more accurate relationship between the statistics of these and the physical parameter statistics generated. Lastly the interpolated mode method is considered with reference to the two degree of freedom system.

Finally, the benefits and drawbacks of the applied methods are discussed. The difficulties of extending the methods to large structures and the problems associated with increasing model complexity are considered.

5.1 The baseline system

Consider the example of an undamped two-degree of freedom system as shown in Figure 5-1.

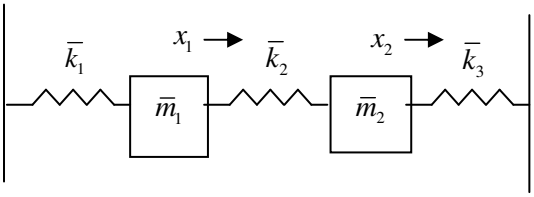

Figure 5-1 Two-degree of freedom system.

The equation of motion for the baseline un-perturbed system is given by

$$\bar{\mathbf{M}}\ddot{\mathbf{x}} + \bar{\mathbf{K}}\mathbf{x} = \mathbf{0} \tag{5.1}$$

where

$$\begin{aligned} \bar{\mathbf{M}} &= \begin{bmatrix} \bar{m}_1 & 0 \\ 0 & \bar{m}_2 \end{bmatrix} \\ \bar{\mathbf{K}} &= \begin{bmatrix} \bar{k}_1 + \bar{k}_2 & -\bar{k}_2 \\ -\bar{k}_2 & \bar{k}_2 + \bar{k}_3 \end{bmatrix} \\ \mathbf{x} &= \begin{bmatrix} x_1 \\ x_2 \end{bmatrix} \end{aligned} \tag{5.2}$$

In general an over-bar will be used to represent baseline or unperturbed values.

The eigenfrequencies $\bar{\boldsymbol{\lambda}}$ and eigenvectors $\bar{\boldsymbol{\varphi}}$ are given by

$$\left(\bar{\mathbf{K}} - \bar{\boldsymbol{\lambda}}\bar{\mathbf{M}}\right)\bar{\boldsymbol{\varphi}} = \mathbf{0} \tag{5.3}$$

where

$$\begin{aligned} \bar{\boldsymbol{\lambda}} &= \begin{bmatrix} \bar{\lambda}_1 & 0 \\ 0 & \bar{\lambda}_2 \end{bmatrix} \\ \bar{\boldsymbol{\varphi}} &= \begin{bmatrix} \bar{\phi}_{1,1} & \bar{\phi}_{2,1} \\ \bar{\phi}_{1,2} & \bar{\phi}_{2,2} \end{bmatrix} \end{aligned} \tag{5.4}$$

The eigenvector suffixes represent the mode number and the degree of freedom respectively. The physical degrees of freedom x, are related to the modal degrees of freedom y, thus

$$\mathbf{x} = \bar{\boldsymbol{\varphi}}\mathbf{y} \tag{5.5}$$

where $\mathbf{y} = \begin{bmatrix} y_1 & y_2 \end{bmatrix}^T$. Substituting equation (4.3) into (4.1), and pre-multiplying by $\bar{\boldsymbol{\varphi}}^{\mathbf{T}}$ the equation of motion can be expressed in terms of the modal coordinates

$$\bar{\boldsymbol{\varphi}}^{\mathbf{T}}\bar{\mathbf{M}}\bar{\boldsymbol{\varphi}}\ddot{\mathbf{y}} + \bar{\boldsymbol{\varphi}}^{\mathbf{T}}\bar{\mathbf{K}}\bar{\boldsymbol{\varphi}}\mathbf{y} = \mathbf{0} \tag{5.6}$$

The mass and stiffness matrices are now un-coupled and contain no off diagonal elements. Assuming the eigenvectors are mass normalised then

$$\begin{aligned} \bar{\boldsymbol{\varphi}}^{\mathbf{T}}\bar{\mathbf{M}}\bar{\boldsymbol{\varphi}} &= \bar{\mathbf{M}}_{\mathbf{j}} \\ \bar{\boldsymbol{\varphi}}^{\mathbf{T}}\bar{\mathbf{K}}\bar{\boldsymbol{\varphi}} &= \bar{\mathbf{K}}_{\mathbf{j}} \end{aligned} \tag{5.7}$$

where

$$\begin{aligned} \bar{\mathbf{M}}_{\mathbf{j}} &= \begin{bmatrix} 1 & 0 \\ 0 & 1 \end{bmatrix} \\ \bar{\mathbf{K}}_{\mathbf{j}} &= \begin{bmatrix} \bar{\lambda}_1 & 0 \\ 0 & \bar{\lambda}_2 \end{bmatrix} \end{aligned} \tag{5.8}$$

5.2 The perturbed system

Let all the physical properties vary such that

$$\begin{aligned} k_i &= \bar{k}_i\left(1+\varepsilon_i\right),\ i = 1,2,3 \\ m_i &= \bar{m}_i\left(1+\varepsilon_{i+3}\right),\ i = 1,2 \end{aligned} \tag{5.9}$$

where ε_i are small random variables with zero mean. At this stage no assumptions are made on the distributions of ε_i. The perturbed mass and stiffness matrices are functions of ε and given by

$$\begin{aligned} \mathbf{K} &= \mathbf{K}(\boldsymbol{\varepsilon}) = \begin{bmatrix} \bar{k}_1\left(1+\varepsilon_1\right)+\bar{k}_2\left(1+\varepsilon_2\right) & -\bar{k}_2\left(1+\varepsilon_2\right) \\ -\bar{k}_2\left(1+\varepsilon_2\right) & \bar{k}_2\left(1+\varepsilon_2\right)+\bar{k}_3\left(1+\varepsilon_3\right) \end{bmatrix} \\ \mathbf{M} &= \mathbf{M}(\boldsymbol{\varepsilon}) = \begin{bmatrix} \bar{m}_1\left(1+\varepsilon_4\right) & 0 \\ 0 & \bar{m}_2\left(1+\varepsilon_5\right) \end{bmatrix} \end{aligned} \tag{5.10}$$

This can also be written as

$$\begin{aligned}\mathbf{K} &= \bar{\mathbf{K}} + \Delta\bar{\mathbf{K}} \\ \mathbf{M} &= \bar{\mathbf{M}} + \Delta\bar{\mathbf{M}}\end{aligned} \tag{5.11}$$

where $\Delta\bar{\mathbf{K}}$ and $\Delta\bar{\mathbf{M}}$ are given by

$$\begin{aligned}\Delta\bar{\mathbf{K}} &= \bar{\mathbf{K}} \bullet \boldsymbol{\varepsilon}_k = \begin{bmatrix} \bar{k}_1\varepsilon_1 + \bar{k}_2\varepsilon_2 & -\bar{k}_2\varepsilon_2 \\ -\bar{k}_2\varepsilon_2 & \bar{k}_2\varepsilon_2 + \bar{k}_3\varepsilon_3 \end{bmatrix} \\ \Delta\bar{\mathbf{M}} &= \bar{\mathbf{M}} \bullet \boldsymbol{\varepsilon}_m = \begin{bmatrix} \bar{m}_1\varepsilon_4 & 0 \\ 0 & \bar{m}_2\varepsilon_5 \end{bmatrix}\end{aligned} \tag{5.12}$$

The dot product is defined as the Hadamard element-wise multiplication. The full solution of eigenfrequencies and eigenvectors is given by

$$\left(\mathbf{K} - \boldsymbol{\lambda}\mathbf{M}\right)\boldsymbol{\varphi} = \mathbf{0} \tag{5.13}$$

where the perturbed eigenvalues $\boldsymbol{\lambda}$ and eigenvectors $\boldsymbol{\varphi}$ are given by

$$\begin{aligned}\boldsymbol{\lambda} &= \begin{bmatrix} \lambda_1 & 0 \\ 0 & \lambda_2 \end{bmatrix} \\ \boldsymbol{\varphi} &= \begin{bmatrix} \phi_{1,1} & \phi_{2,1} \\ \phi_{1,2} & \phi_{2,2} \end{bmatrix}\end{aligned} \tag{5.14}$$

5.3 Baseline modeshapes as assumed shape functions

An approximation for the eigenfrequencies can be obtained if the eigenvectors of the baseline system are used as assumed modeshapes for the perturbed system, and the Rayleigh quotient is extended to all modes. From chapter 4, the eigenfrequencies of the perturbed system can be approximated as

$$\lambda_j \cong \frac{\bar{\lambda}_j + \bar{\boldsymbol{\varphi}}_j{}^T \Delta\bar{\mathbf{K}}\bar{\boldsymbol{\varphi}}_j}{1 + \bar{\boldsymbol{\varphi}}_j{}^T \Delta\bar{\mathbf{M}}\bar{\boldsymbol{\varphi}}_j} \tag{5.15}$$

where λ_j is the *j*'th eigenvalue of the perturbed system, $\bar{\lambda}_j$ is the *j*'th eigenvalue of the baseline system and $\bar{\boldsymbol{\varphi}}_j$ is the *j*'th mass normalised eigenvector of the baseline system.

Equation (5.15) can be expanded to give

$$\lambda_j \cong \frac{\bar{\lambda}_j + \bar{\phi}_{j,1}{}^2 \bar{k}_1 \varepsilon_1 + \bar{k}_2 \left(\bar{\phi}_{j,1} - \bar{\phi}_{j,2}\right)^2 \varepsilon_2 + \bar{\phi}_{j,2}{}^2 \bar{k}_3 \varepsilon_3}{1 + \bar{\phi}_{j,1}{}^2 m_1 \varepsilon_4 + \bar{\phi}_{j,2}{}^2 m_2 \varepsilon_5} \tag{5.16}$$

An interesting test to apply to this approximation is to examine the estimated perturbed natural frequency under the condition where all the variability terms are equal and hence $\varepsilon_1 = \varepsilon_2 = \varepsilon_3 = \varepsilon_4 = \varepsilon_5 = \varepsilon$. Applying this condition to the approximate system eigenvalues in equation (5.16) it can be shown that $\lambda_j = \bar{\lambda}_j$. This confirms that if all the masses and stiffness are perturbed by an equal amount, then by definition the natural frequencies of the system will remain unchanged.

Using the expectation method (see Appendix A), the expected or mean value of the eigenvalues of the perturbed system are given by

$$\mu_{\lambda_j} = E\left[\lambda_j\right] \cong E\left[\frac{\bar{\lambda}_j + \bar{\boldsymbol{\varphi}}_j{}^T \Delta\bar{\mathbf{K}} \bar{\boldsymbol{\varphi}}_j}{1 + \bar{\boldsymbol{\varphi}}_j{}^T \Delta\bar{\mathbf{M}} \bar{\boldsymbol{\varphi}}_j}\right] \tag{5.17}$$

In order to progress this expression further the right-hand side can be re-arranged to the form $E\left[\frac{A}{B}\right] = E\left[A\frac{1}{B}\right]$, and if the system mass and stiffness are assumed to be independent then equation (5.17) becomes

$$\mu_{\lambda_j} \cong E\left[\bar{\lambda}_j + \bar{\boldsymbol{\varphi}}_j{}^T \Delta\bar{\mathbf{K}} \bar{\boldsymbol{\varphi}}_j\right] E\left[\frac{1}{1 + \bar{\boldsymbol{\varphi}}_j{}^T \Delta\bar{\mathbf{M}} \bar{\boldsymbol{\varphi}}_j}\right] \tag{5.18}$$

The quotient part of equation (5.18) can now expanded using a power series expansion such that

$$E\left[\frac{1}{1 + \bar{\boldsymbol{\varphi}}_j{}^T \Delta\bar{\mathbf{M}} \bar{\boldsymbol{\varphi}}_j}\right] \cong E\left[1 - \bar{\boldsymbol{\varphi}}_j{}^T \Delta\bar{\mathbf{M}} \bar{\boldsymbol{\varphi}}_j + \left(\bar{\boldsymbol{\varphi}}_j{}^T \Delta\bar{\mathbf{M}} \bar{\boldsymbol{\varphi}}_j\right)^2 \ldots\right] \tag{5.19}$$

In order for the expansion to converge then $\left|\bar{\boldsymbol{\varphi}}_j{}^T \Delta\bar{\mathbf{M}}\bar{\boldsymbol{\varphi}}_j\right| < 1$. As the variabilities ε_i were assumed to be small then the higher terms of the expansion will become progressively smaller and may reasonably be ignored. Using equation (5.19) and substituting $\Delta\bar{\mathbf{K}}$ and $\Delta\bar{\mathbf{M}}$ in equation (5.18) gives

$$\mu_{\lambda_j} \cong \left(\bar{\lambda}_j + \bar{\boldsymbol{\varphi}}_j{}^T E\left[\Delta\bar{\mathbf{K}}\right]\bar{\boldsymbol{\varphi}}_j\right)\left(1 - \bar{\boldsymbol{\varphi}}_j{}^T E\left[\Delta\bar{\mathbf{M}}\right]\bar{\boldsymbol{\varphi}}_j + E\left[\left(\bar{\boldsymbol{\varphi}}_j{}^T \Delta\bar{\mathbf{M}}\bar{\boldsymbol{\varphi}}_j\right)^2\right]\right) \tag{5.20}$$

As the variabilities were assumed to have zero mean such that $E\left[\Delta\bar{\mathbf{K}}\right] = E\left[\Delta\bar{\mathbf{M}}\right] = \mathbf{0}$, therefore

$$\mu_{\lambda_j} \cong \bar{\lambda}_j\left(1 + E\left[\left(\bar{\boldsymbol{\varphi}}_j{}^T \Delta\bar{\mathbf{M}}\bar{\boldsymbol{\varphi}}_j\right)^2\right]\right) \tag{5.21}$$

This can be expanded and shown to give

$$\mu_{\lambda_j} \cong \bar{\lambda}_j\left(1 + \left(\bar{\boldsymbol{\varphi}}_j{}^2\right)^T \operatorname{var}\left(\Delta\bar{\mathbf{M}}\right)\bar{\boldsymbol{\varphi}}_j{}^2\right) \tag{5.22}$$

where $\operatorname{var}\left(\Delta\bar{\mathbf{M}}\right)$ is the variance/covariance matrix of $\Delta\bar{\mathbf{M}}$, defined as

$$\operatorname{var}\left(\Delta\bar{\mathbf{M}}\right) \equiv \operatorname{var}\left(\bar{\mathbf{M}}\bullet\boldsymbol{\varepsilon}_m\right) = \begin{bmatrix} m_1{}^2\sigma_{\varepsilon_4}^2 & m_1 m_2 \sigma_{\varepsilon_4\varepsilon_5} \\ m_1 m_2 \sigma_{\varepsilon_4\varepsilon_5} & m_2{}^2\sigma_{\varepsilon_5}^2 \end{bmatrix} \tag{5.23}$$

and $\bar{\boldsymbol{\varphi}}_j{}^2$ represents the Hadamard element-wise square of the eigenvector such that, $\bar{\boldsymbol{\varphi}}_j{}^2 = \begin{bmatrix} \phi_{j,1}{}^2 & \phi_{j,2}{}^2 \end{bmatrix}^T$. The relationship in Equation (5.22) directly relates the mean of the system eigenvalues to the variance and covariance of the mass variability terms.

It can be noted that the variance/covariance matrix $\operatorname{var}\left(\Delta\bar{\mathbf{M}}\right)$ contains variance terms on the leading diagonal and covariance terms on the off-diagonals. If the variability in the masses is independent then the covariance terms are zero $\sigma_{\varepsilon_4\varepsilon_5} = 0$.

From equation (5.22) it can be noted that the mean of the system eigenvalues is independent of the mean of the variability, this is because the variability was assumed to have zero mean. In addition, the mean of the system eigenvalues is independent of the variability in the stiffness.

This effect is introduced by the assumption that the stiffness and mass terms were independent, which in practice is not usually the case.

This approximation for the system eigenfrequencies based on using the eigenvectors of the baseline system as assumed modeshapes, provides a very coarse estimation. This method can be extended to obtain the expected variance of the perturbed eigenvalues, and using the change of variable method to obtain a PDF of the eigenvalues assuming a given PDF of the mass and stiffness. However, this shall be left as an exercise since more refined approximations are available and these will be investigated in the following sections.

5.4 Eigenvalue estimation: first order perturbation

Applying the general expression for a mean centred first order perturbation as presented in chapter 4, the perturbed system eigenvalues for the example of a two d.o.f are given by

$$\lambda_j \cong \bar{\lambda}_j + \left(\frac{\partial \lambda_j(\boldsymbol{\varepsilon})}{\partial \boldsymbol{\varepsilon}} \right)^T \Bigg|_{\boldsymbol{\varepsilon}=\boldsymbol{\mu}_\varepsilon} \boldsymbol{\varepsilon} \tag{5.24}$$

where

$$\left. \frac{\partial \lambda_j(\boldsymbol{\varepsilon})}{\partial \boldsymbol{\varepsilon}} \right|_{\boldsymbol{\varepsilon}=\boldsymbol{\mu}_\varepsilon} = \begin{bmatrix} \bar{\boldsymbol{\varphi}}_j{}^T \left[\dfrac{\partial \mathbf{K}}{\partial \varepsilon_1} - \bar{\lambda}_j \dfrac{\partial \mathbf{M}}{\partial \varepsilon_1} \right] \bar{\boldsymbol{\varphi}}_j \\ \bar{\boldsymbol{\varphi}}_j{}^T \left[\dfrac{\partial \mathbf{K}}{\partial \varepsilon_2} - \lambda_j \dfrac{\partial \mathbf{M}}{\partial \varepsilon_2} \right] \bar{\boldsymbol{\varphi}}_j \\ \vdots \\ \bar{\boldsymbol{\varphi}}_j{}^T \left[\dfrac{\partial \mathbf{K}}{\partial \varepsilon_i} - \lambda_j \dfrac{\partial \mathbf{M}}{\partial \varepsilon_i} \right] \bar{\boldsymbol{\varphi}}_j \end{bmatrix} \tag{5.25}$$

and where $\boldsymbol{\varepsilon}_i$ is the i'th element of the variability vector $\boldsymbol{\varepsilon}$ which is given by $\boldsymbol{\varepsilon} = \begin{bmatrix} \varepsilon_1 & \varepsilon_2 & \varepsilon_3 & \varepsilon_4 & \varepsilon_5 \end{bmatrix}^T$ and $\boldsymbol{\mu}_\varepsilon$ is the vector of mean values of $\boldsymbol{\varepsilon}$. The partial derivatives in equation (5.24) are given by (all other partial derivatives result in null matrices)

$$\begin{aligned} &\frac{\partial \mathbf{K}}{\partial \varepsilon_1} = \begin{bmatrix} \bar{k}_1 & 0 \\ 0 & 0 \end{bmatrix}, \frac{\partial \mathbf{K}}{\partial \varepsilon_2} = \begin{bmatrix} \bar{k}_2 & -\bar{k}_2 \\ -\bar{k}_2 & \bar{k}_2 \end{bmatrix}, \frac{\partial \mathbf{K}}{\partial \varepsilon_3} = \begin{bmatrix} 0 & 0 \\ 0 & \bar{k}_3 \end{bmatrix} \\ &\frac{\partial \mathbf{M}}{\partial \varepsilon_4} = \begin{bmatrix} \bar{m}_1 & 0 \\ 0 & 0 \end{bmatrix}, \frac{\partial \mathbf{M}}{\partial \varepsilon_5} = \begin{bmatrix} 0 & 0 \\ 0 & \bar{m}_2 \end{bmatrix} \end{aligned} \tag{5.26}$$

Substituting and evaluating the elements in equation (5.24), the eigenvalues of the system can be shown to be given by

$$\lambda_j \cong \bar{\lambda}_j + \begin{bmatrix} \bar{\phi}_{j,1}{}^2 \bar{k}_1 \\ \left(\bar{\phi}_{j,1} - \bar{\phi}_{j,2}\right)^2 \bar{k}_2 \\ \bar{\phi}_{j,2}{}^2 \bar{k}_3 \\ -\bar{\phi}_{j,1}{}^2 \bar{\lambda}_j \bar{m}_1 \\ -\bar{\phi}_{j,2}{}^2 \bar{\lambda}_j \bar{m}_2 \end{bmatrix}^T \begin{Bmatrix} \varepsilon_1 \\ \varepsilon_2 \\ \varepsilon_3 \\ \varepsilon_4 \\ \varepsilon_5 \end{Bmatrix} \tag{5.27}$$

This can be simplified to

$$\lambda_j \cong \bar{\lambda}_j + \mathbf{A}_j{}^T \boldsymbol{\varepsilon} \tag{5.28}$$

where

$$\mathbf{A}_j = \left.\frac{\partial \lambda_j(\boldsymbol{\varepsilon})}{\partial \boldsymbol{\varepsilon}}\right|_{\boldsymbol{\varepsilon}=\boldsymbol{\mu}_\varepsilon} = \begin{bmatrix} \bar{\phi}_{j,1}{}^2 \bar{k}_1 \\ \left(\bar{\phi}_{j,1} - \bar{\phi}_{j,2}\right)^2 \bar{k}_2 \\ \bar{\phi}_{j,2}{}^2 \bar{k}_3 \\ -\bar{\phi}_{j,1}{}^2 \bar{\lambda}_j \bar{m}_1 \\ -\bar{\phi}_{j,2}{}^2 \bar{\lambda}_j \bar{m}_2 \end{bmatrix} \tag{5.29}$$

and $\mathbf{A}_j$ is a vector of dimension n where n is the number of variability terms in $\boldsymbol{\varepsilon}$. As the eigenvectors were assumed to be mass normalised the terms in $\mathbf{A}_j$ relate to the modal stiffness and modal mass in the system. For example $\left(\bar{\phi}_{j,1}{}^2 \bar{k}_1\right)$ is the modal stiffness of the spring element $\bar{k}_1$ and $\left(\bar{\phi}_{j,1}{}^2 \bar{m}_1\right)$ is the modal mass of $\bar{m}_1$.

Using expectation, the mean or expected value of the eigenvalues is given by

$$\mu_{\lambda_j} \cong \bar{\lambda}_j + \mathbf{A}_j{}^T \boldsymbol{\mu}_{\boldsymbol{\varepsilon}} \tag{5.30}$$

If the variability is assumed to have zero mean such that $\boldsymbol{\mu}_{\boldsymbol{\varepsilon}} = \mathbf{0}$ then equation (5.30) simply reduces to $\mu_{\lambda_j} \cong \bar{\lambda}_j$.

Using the first order approximation in equation (5.28) an expression can be obtained for the variance of the perturbed eigenvalues. If the change in the perturbed eigenvalues is given by $\delta_{\lambda_j} = \left(\lambda_j - \overline{\lambda}_j\right)$, then from equation (5.28)

$$\delta_{\lambda_j} \cong \mathbf{A}_j{}^T \boldsymbol{\varepsilon} \tag{5.31}$$

If the variabilities are assumed to have zero mean $\boldsymbol{\mu}_{\boldsymbol{\varepsilon}} = \mathbf{0}$, then it can be shown that

$$\text{var}\left(\delta_{\lambda_j}\right) \cong \mathbf{A}_j{}^T \, \text{var}\left(\boldsymbol{\varepsilon}\right) \mathbf{A}_j \tag{5.32}$$

where $\text{var}\left(\boldsymbol{\varepsilon}\right)$ is the variance/covariance matrix of the variability terms given by

$$\text{var}\left(\boldsymbol{\varepsilon}\right) = \begin{bmatrix} \sigma_{\varepsilon_1}^2 & \sigma_{\varepsilon_1\varepsilon_2} & \sigma_{\varepsilon_1\varepsilon_3} & \sigma_{\varepsilon_1\varepsilon_4} & \sigma_{\varepsilon_1\varepsilon_5} \\ \sigma_{\varepsilon_1\varepsilon_2} & \sigma_{\varepsilon_2}^2 & \sigma_{\varepsilon_2\varepsilon_3} & \sigma_{\varepsilon_2\varepsilon_4} & \sigma_{\varepsilon_2\varepsilon_5} \\ \sigma_{\varepsilon_1\varepsilon_3} & \sigma_{\varepsilon_2\varepsilon_3} & \sigma_{\varepsilon_3}^2 & \sigma_{\varepsilon_3\varepsilon_4} & \sigma_{\varepsilon_3\varepsilon_5} \\ \sigma_{\varepsilon_1\varepsilon_4} & \sigma_{\varepsilon_2\varepsilon_4} & \sigma_{\varepsilon_3\varepsilon_4} & \sigma_{\varepsilon_4}^2 & \sigma_{\varepsilon_4\varepsilon_5} \\ \sigma_{\varepsilon_1\varepsilon_5} & \sigma_{\varepsilon_2\varepsilon_5} & \sigma_{\varepsilon_3\varepsilon_5} & \sigma_{\varepsilon_4\varepsilon_5} & \sigma_{\varepsilon_5}^2 \end{bmatrix} \tag{5.33}$$

and $\text{var}\left(\delta_{\lambda_j}\right)$ is the variance of the change in the perturbed eigenvalues. This directly relates the variance of the system eigenvalues to the variance and covariance of the variability in the stiffnesses and masses. If the variability terms are independent then the covariance terms disappear, then expanding equation (5.32) the variance of the system eigenvalues is given by

$$\text{var}\left(\delta_{\lambda_j}\right) \cong \left(\overline{\phi}_{j,1}{}^2 \overline{k}_1\right)^2 \sigma_{\varepsilon_1}^2 + \left(\left(\overline{\phi}_{j,1} - \overline{\phi}_{j,2}\right)^2 \overline{k}_2\right)^2 \sigma_{\varepsilon_2}^2 + \left(\overline{\phi}_{j,2}{}^2 \overline{k}_3\right)^2 \sigma_{\varepsilon_3}^2 + \left(\overline{\phi}_{j,1}{}^2 \overline{\lambda}_j \overline{m}_1\right)^2 \sigma_{\varepsilon_4}^2 + \left(\overline{\phi}_{j,2}{}^2 \overline{\lambda}_j \overline{m}_2\right)^2 \sigma_{\varepsilon_5}^2 \tag{5.34}$$

where each term could be considered to be the modal variance of a physical element.

5.4.1 Distribution of the eigenvalues

The change of variable technique discussed in chapter 4 can be used in conjunction with the first order approximation, to propagate the PDF of the mass and stiffness and obtain an estimate of

the PDF of the eigenvalues of the system. However, even for the simple two degree of freedom system, five separate variables have been defined which will lead to a lengthy transformation. Therefore, two possible reduced scenarios are now considered, the first with a single variable system property and the second with two independent variable system properties.

Scenario One: Single uncertain system property

Assume that $\varepsilon_2 = \varepsilon_3 = \varepsilon_4 = \varepsilon_5 = 0$ so that the only variability in the system is due to ε_1 and the mass and stiffness matrices are given by

$$\mathbf{K} = \begin{bmatrix} \bar{k}_1(1+\varepsilon_1) + \bar{k}_2 & -\bar{k}_2 \\ -\bar{k}_2 & \bar{k}_2 + \bar{k}_3 \end{bmatrix}$$
$$\mathbf{M} = \bar{\mathbf{M}} = \begin{bmatrix} \bar{m}_1 & 0 \\ 0 & \bar{m}_2 \end{bmatrix} \tag{5.35}$$

From equation (5.28) the system eigenvalues are given by

$$\lambda_j \cong \bar{\lambda}_j + \mathbf{A}_j{}^T \boldsymbol{\varepsilon} \tag{5.36}$$

where $\boldsymbol{\varepsilon} = \begin{bmatrix} \varepsilon_1 & 0 & 0 & 0 & 0 \end{bmatrix}^T$, thus

$$\lambda_j \cong \bar{\lambda}_j + \bar{\phi}_{j,1}{}^2 \bar{k}_1 \varepsilon_1 \tag{5.37}$$

From chapter 4, if a function is given by $y = f(x)$, then the PDF of y is given be

$$p(y) = \frac{np(x)}{\left| f'(x) \right|} \tag{5.38}$$

where $p(x)$ is the PDF of x and each value of y corresponds to n values of x. As the expression in (5.37) is single valued and one-to-one, $n = 1$ and hence combining this with equation (5.38) gives

$$p(\lambda_j) \cong \frac{p(\varepsilon_1)}{\left|\frac{d\left(\overline{\lambda}_j + \overline{\phi}_{j,1}{}^2 \overline{k}_1 \varepsilon_1\right)}{d\varepsilon_1}\right|} = \frac{p(\varepsilon_1)}{\left|\overline{\phi}_{j,1}{}^2 \overline{k}_1\right|} \tag{5.39}$$

This directly relates the PDF of the system eigenvalues to the PDF of the variable stiffness term ε_1. The expression $\left|\overline{\phi}_{j,1}{}^2 \overline{k}_1\right|$ represents the magnitude of the modal stiffness associated with spring $\overline{k}_1$. In order to evaluate equation (5.39) for a specified variability PDF the expression for the variability ε_1 in terms of the system eigenvalues must be substituted back into equation (5.39). For example, if ε_1 was Gaussian distributed with zero mean and variance $\sigma_{\varepsilon_1}{}^2$, then from equation (5.39) and substituting back in $\varepsilon_1 \cong \frac{\lambda_j - \overline{\lambda}_j}{\overline{\phi}_{j,1}{}^2 \overline{k}_1}$, the PDF of the system eigenvalues is given by

$$p(\lambda_j) \cong \frac{e^{-\frac{\left(\lambda_j - \overline{\lambda}_j\right)^2}{2\sigma_{\varepsilon_1}{}^2 \overline{\phi}_{j,1}{}^4 \overline{k}_1{}^2}}}{\sigma_{\varepsilon_1}\sqrt{2\pi}\left|\overline{\phi}_{j,1}{}^2 \overline{k}_1\right|} \tag{5.40}$$

The system eigenvalues are Gaussian distributed about a mean value of $\overline{\lambda}_j$ and variance $\sigma_{\varepsilon_1}\left|\overline{\phi}_{j,1}{}^2 \overline{k}_1\right|$. However, there is no limitation on the form of the PDF for the variable ε_1. For example consider if ε_1 was Rayleigh distributed and given by

$$p(\varepsilon_1) = \frac{\varepsilon_1}{s_{\varepsilon_1}{}^2} e^{\frac{-\varepsilon_1{}^2}{2s_{\varepsilon_1}{}^2}} \tag{5.41}$$

with a mean of $\mu_{\varepsilon_1} = s_{\varepsilon_1}\sqrt{\frac{\pi}{2}}$ and variance of $\sigma_{\varepsilon_1}^2 = \frac{4-\pi}{2} s_{\varepsilon_1}{}^2$. The PDF of the system eigenvalues is then given by

$$p(\lambda_j) \cong \frac{\left(\lambda_j - \overline{\lambda}_j\right) e^{\frac{-\left(\lambda_j - \overline{\lambda}_j\right)^2}{2s_{\varepsilon_1}{}^2 \overline{\phi}_{j,1}{}^4 \overline{k}_1{}^2}}}{s_{\varepsilon_1}{}^2 \overline{\phi}_{j,1}{}^4 \overline{k}_1{}^2} \tag{5.42}$$

This has the form of a Rayleigh distribution where $s_{\lambda_j} = s\bar{\phi}_{j,1}{}^2\bar{k}_1$ and is centred around a point $\bar{\lambda}_j$.

Scenario Two: Two uncertain system properties

Consider the scenario where $\varepsilon_2 = \varepsilon_4 = \varepsilon_5 = 0$ such that $\boldsymbol{\varepsilon} = \begin{bmatrix} \varepsilon_1 & 0 & \varepsilon_3 & 0 & 0 \end{bmatrix}^T$ and hence the perturbed stiffness matrix is given by

$$\mathbf{K} = \begin{bmatrix} \bar{k}_1(1+\varepsilon_1) + \bar{k}_2 & -\bar{k}_2 \\ -\bar{k}_2 & \bar{k}_2 + \bar{k}_3(1+\varepsilon_3) \end{bmatrix} \tag{5.43}$$

Using equation (5.28) and expanding, the system eigenvalues are given by

$$\lambda_j \cong \bar{\lambda}_j + \bar{\phi}_{j,1}{}^2\bar{k}_1\varepsilon_1 + \bar{\phi}_{j,2}{}^2\bar{k}_3\varepsilon_3 \tag{5.44}$$

The change of variable technique for two single-valued continuous random variables with continuous partial derivatives is given by (see chapter 4)

$$p(y_1, y_2) = \frac{p(x_1, x_2)}{\begin{vmatrix} \frac{\partial y_1}{\partial x_1} & \frac{\partial y_1}{\partial x_2} \\ \frac{\partial y_2}{\partial x_1} & \frac{\partial y_2}{\partial x_2} \end{vmatrix}} \tag{5.45}$$

where $y_1 = y_1(x_1, x_2), \quad y_2 = y_2(x_1, x_2)$. Combining equations (5.44) and (5.45), and defining an additional variable u such that $u = \varepsilon_3$, gives

$$p(\lambda_j, u) = \frac{p(\varepsilon_1, \varepsilon_3)}{\begin{vmatrix} \frac{\partial \lambda_j}{\partial \varepsilon_1} & \frac{\partial \lambda_j}{\partial \varepsilon_3} \\ \frac{\partial u}{\partial \varepsilon_1} & \frac{\partial u}{\partial \varepsilon_3} \end{vmatrix}} \cong \frac{p(\varepsilon_1, \varepsilon_3)}{\begin{vmatrix} \bar{\phi}_{j,1}{}^2\bar{k}_1 & \bar{\phi}_{j,2}{}^2\bar{k}_3 \\ 0 & 1 \end{vmatrix}} = \frac{p(\varepsilon_1, \varepsilon_3)}{\bar{\phi}_{j,1}{}^2\bar{k}_1} \tag{5.46}$$

Assuming that ε_1 and ε_3 are independent, the distribution $p(\lambda_j)$ can be obtained by integrating along u thus

$$p(\lambda_j) \cong \int_{-\infty}^{\infty} \frac{p(\varepsilon_1)\, p(\varepsilon_3)}{\bar{\phi}_{j,1}{}^2 \bar{k}_1} d\varepsilon_3 \tag{5.47}$$

This directly relates the PDF of the system eigenvalues to the PDFs of the variables ε_1 and ε_3. Upon first inspection it appears from equation (5.47) that the modal stiffness of the second spring $\bar{k}_3$ does not affect the PDF of the system eigenvalues. However, the modal stiffness term for this spring will be re-introduced into the expression by the substitution of the expression for ε_1 in terms of the system eigenvalues and ε_3 (from equation (5.44)) which is required before the integral can be evaluated.

Again there are no restrictions to the PDFs of the input variables, the simplest example being Gaussian distributed variables with zero mean, then the system eigenvalues are also Gaussian distributed and given by

$$p(\lambda_j) \cong \frac{e^{-\frac{(\lambda_j - \bar{\lambda}_j)^2}{2\left(\bar{\phi}_{j,1}{}^4 \bar{k}_1{}^2 \sigma_{\varepsilon_1}{}^2 + \bar{\phi}_{j,2}{}^4 \bar{k}_3{}^2 \sigma_{\varepsilon_3}{}^2\right)}}}{\sqrt{\bar{\phi}_{j,1}{}^4 \bar{k}_1{}^2 \sigma_{\varepsilon_1}{}^2 + \bar{\phi}_{j,2}{}^4 \bar{k}_3{}^2 \sigma_{\varepsilon_3}{}^2}\sqrt{2\pi}} \tag{5.48}$$

where the mean is given by $\bar{\lambda}_j$ and the variance $\sigma_{\lambda_j}^2 = \bar{\phi}_{j,1}{}^4 \bar{k}_1{}^2 \sigma_{\varepsilon_1}{}^2 + \bar{\phi}_{j,2}{}^4 \bar{k}_3{}^2 \sigma_{\varepsilon_3}{}^2$.

5.5 Eigenvector estimation: first order perturbation

From chapter 4 the first order mean centred perturbation of the eigenvectors is given by

$$\boldsymbol{\varphi}_j \cong \bar{\boldsymbol{\varphi}}_j + \sum_i \left(-\frac{1}{2} \bar{\boldsymbol{\varphi}}_j{}^T \frac{\partial \mathbf{M}}{\partial \varepsilon_i} \bar{\boldsymbol{\varphi}}_j \bar{\boldsymbol{\varphi}}_j \varepsilon_i + \sum_{\substack{p=1 \\ p \neq j}}^{n} \frac{\bar{\boldsymbol{\varphi}}_p{}^T \left[\dfrac{\partial \mathbf{K}}{\partial \varepsilon_i} - \bar{\lambda}_j \dfrac{\partial \mathbf{M}}{\partial \varepsilon_i} \right] \bar{\boldsymbol{\varphi}}_j}{\bar{\lambda}_j - \bar{\lambda}_p} \bar{\boldsymbol{\varphi}}_p \varepsilon_i \right) \tag{5.49}$$

where the index p gives all the global modes and ε_i is the i'th term of variability vector $\boldsymbol{\varepsilon}$. Applying this general expression to the example of a two d.o.f. the *j*'th eigenvector is approximated as

$$\boldsymbol{\varphi}_j \cong \bar{\boldsymbol{\varphi}}_j - \frac{1}{2}\mathbf{B}_j{}^T \boldsymbol{\varepsilon}\bar{\boldsymbol{\varphi}}_j + \sum_{\substack{p=1 \\ p\neq j}}^{n} \frac{1}{\bar{\lambda}_j - \bar{\lambda}_p}\mathbf{A}_{jp}{}^T \boldsymbol{\varepsilon}\bar{\boldsymbol{\varphi}}_p \tag{5.50}$$

where the vector of variabilities $\boldsymbol{\varepsilon}$ is given by $\boldsymbol{\varepsilon} = \begin{bmatrix}\varepsilon_1 & \varepsilon_2 & \varepsilon_3 & \varepsilon_4 & \varepsilon_5\end{bmatrix}^T$ and the constants $\mathbf{B}_j$ and $\mathbf{A}_{jp}$ are given by

$$\mathbf{B}_j = \begin{bmatrix} \bar{\boldsymbol{\varphi}}_j{}^T \dfrac{\partial \mathbf{M}}{\partial \varepsilon_1}\bar{\boldsymbol{\varphi}}_j \\ \bar{\boldsymbol{\varphi}}_j{}^T \dfrac{\partial \mathbf{M}}{\partial \varepsilon_2}\bar{\boldsymbol{\varphi}}_j \\ \bar{\boldsymbol{\varphi}}_j{}^T \dfrac{\partial \mathbf{M}}{\partial \varepsilon_3}\bar{\boldsymbol{\varphi}}_j \\ \bar{\boldsymbol{\varphi}}_j{}^T \dfrac{\partial \mathbf{M}}{\partial \varepsilon_4}\bar{\boldsymbol{\varphi}}_j \\ \bar{\boldsymbol{\varphi}}_j{}^T \dfrac{\partial \mathbf{M}}{\partial \varepsilon_5}\bar{\boldsymbol{\varphi}}_j \end{bmatrix} = \begin{bmatrix} 0 \\ 0 \\ 0 \\ \bar{\phi}_{j,1}{}^2 \bar{m}_1 \\ \bar{\phi}_{j,2}{}^2 \bar{m}_2 \end{bmatrix} \tag{5.51}$$

$$\mathbf{A}_{jp} = \begin{bmatrix} \bar{\boldsymbol{\varphi}}_p{}^T \left[\dfrac{\partial \mathbf{K}}{\partial \varepsilon_1} - \bar{\lambda}_j \dfrac{\partial \mathbf{M}}{\partial \varepsilon_1}\right]\bar{\boldsymbol{\varphi}}_j \\ \bar{\boldsymbol{\varphi}}_p{}^T \left[\dfrac{\partial \mathbf{K}}{\partial \varepsilon_2} - \bar{\lambda}_j \dfrac{\partial \mathbf{M}}{\partial \varepsilon_2}\right]\bar{\boldsymbol{\varphi}}_j \\ \bar{\boldsymbol{\varphi}}_p{}^T \left[\dfrac{\partial \mathbf{K}}{\partial \varepsilon_3} - \bar{\lambda}_j \dfrac{\partial \mathbf{M}}{\partial \varepsilon_3}\right]\bar{\boldsymbol{\varphi}}_j \\ \bar{\boldsymbol{\varphi}}_p{}^T \left[\dfrac{\partial \mathbf{K}}{\partial \varepsilon_4} - \bar{\lambda}_j \dfrac{\partial \mathbf{M}}{\partial \varepsilon_4}\right]\bar{\boldsymbol{\varphi}}_j \\ \bar{\boldsymbol{\varphi}}_p{}^T \left[\dfrac{\partial \mathbf{K}}{\partial \varepsilon_5} - \bar{\lambda}_j \dfrac{\partial \mathbf{M}}{\partial \varepsilon_5}\right]\bar{\boldsymbol{\varphi}}_j \end{bmatrix} = \begin{bmatrix} \bar{\phi}_{p,1}\bar{\phi}_{j,1}\bar{k}_1 \\ \left(\bar{\phi}_{p,1} - \bar{\phi}_{p,2}\right)\left(\bar{\phi}_{j,1} - \bar{\phi}_{j,2}\right)\bar{k}_2 \\ \bar{\phi}_{p,2}\bar{\phi}_{j,2}\bar{k}_3 \\ -\bar{\phi}_{p,1}\bar{\phi}_{j,1}\bar{\lambda}_j\bar{m}_1 \\ -\bar{\phi}_{p,2}\bar{\phi}_{j,2}\bar{\lambda}_j\bar{m}_2 \end{bmatrix} \tag{5.52}$$

Using expectation, the mean or expected value of the eigenvectors is given by

$$\mu_{\boldsymbol{\varphi}_j} \cong \bar{\boldsymbol{\varphi}}_j - \frac{1}{2}\mathbf{B}_j{}^T \boldsymbol{\mu}_{\boldsymbol{\varepsilon}}\bar{\boldsymbol{\varphi}}_j + \sum_{\substack{p=1 \\ p\neq j}}^{n} \frac{1}{\bar{\lambda}_j - \bar{\lambda}_p}\mathbf{A}_{jp}{}^T \boldsymbol{\mu}_{\boldsymbol{\varepsilon}}\bar{\boldsymbol{\varphi}}_p \tag{5.53}$$

If the variability is assumed to have zero mean such that $\boldsymbol{\mu}_{\boldsymbol{\varepsilon}} = \mathbf{0}$ then equation (5.53) simply reduces to $\mu_{\boldsymbol{\varphi}_j} \cong \overline{\boldsymbol{\varphi}}_j$.

5.6 Eigenvalue estimation: second order perturbation

The equation for a mean centred second order perturbation approximation of the eigensolution is given by (from chapter 4)

$$\lambda_j \cong \overline{\lambda}_j + \underbrace{\left(\frac{\partial \lambda_j}{\partial \boldsymbol{\varepsilon}}\right)^T\Bigg|_{\boldsymbol{\varepsilon}=\boldsymbol{\mu}_\varepsilon}}_{\text{first order term}} \boldsymbol{\varepsilon} + \underbrace{\frac{1}{2}(\boldsymbol{\varepsilon})^T \mathbf{D}_{\lambda_j}\Big|_{\boldsymbol{\varepsilon}=\boldsymbol{\mu}_\varepsilon} \boldsymbol{\varepsilon}}_{\text{second order term}} \tag{5.54}$$

where

$$\left\{\mathbf{D}_{\lambda_j}\right\}_{il} = \left.\frac{\partial^2 \lambda_j}{\partial \varepsilon_i \partial \varepsilon_l}\right|_{\boldsymbol{\varepsilon}=\boldsymbol{\mu}_\varepsilon} \tag{5.55}$$

$$\begin{aligned}\frac{\partial^2 \lambda_j}{\partial \varepsilon_i \partial \varepsilon_l} &= \overline{\boldsymbol{\varphi}}_j{}^T \left[\frac{\partial^2 \mathbf{K}}{\partial \varepsilon_i \partial \varepsilon_l} - \overline{\lambda}_j \frac{\partial^2 \mathbf{M}}{\partial \varepsilon_i \partial \varepsilon_l}\right] \overline{\boldsymbol{\varphi}}_j - \left(\overline{\boldsymbol{\varphi}}_j{}^T \frac{\partial \mathbf{M}}{\partial \varepsilon_i} \overline{\boldsymbol{\varphi}}_j\right)\left(\overline{\boldsymbol{\varphi}}_j{}^T G_{lj} \overline{\boldsymbol{\varphi}}_j\right) \\ &- \left(\overline{\boldsymbol{\varphi}}_j{}^T \frac{\partial \mathbf{M}}{\partial \varepsilon_l} \overline{\boldsymbol{\varphi}}_j\right)\left(\overline{\boldsymbol{\varphi}}_j{}^T G_{ij} \overline{\boldsymbol{\varphi}}_j\right) + 2\sum_{\substack{r=1 \\ r \neq j}}^{N} \frac{\left(\overline{\boldsymbol{\varphi}}_j{}^T G_{ij} \overline{\boldsymbol{\varphi}}_j\right)\left(\overline{\boldsymbol{\varphi}}_j{}^T G_{lj} \overline{\boldsymbol{\varphi}}_j\right)}{\lambda_j - \lambda_r}\end{aligned} \tag{5.56}$$

The baseline mass and stiffness matrices are as given for the first order expansion, therefore as before the vector of random variables and the first order partial derivatives are given by

$$\boldsymbol{\varepsilon} = \begin{bmatrix}\varepsilon_1 & \varepsilon_2 & \varepsilon_3 & \varepsilon_4 & \varepsilon_5\end{bmatrix}^T \tag{5.57}$$

$$\frac{\partial \mathbf{K}}{\partial \varepsilon_1} = \begin{bmatrix}\overline{k}_1 & 0 \\ 0 & 0\end{bmatrix},\ \frac{\partial \mathbf{K}}{\partial \varepsilon_2} = \begin{bmatrix}\overline{k}_2 & -\overline{k}_2 \\ -\overline{k}_2 & \overline{k}_2\end{bmatrix},\ \frac{\partial \mathbf{K}}{\partial \varepsilon_3} = \begin{bmatrix}0 & 0 \\ 0 & \overline{k}_3\end{bmatrix},\ \frac{\partial \mathbf{M}}{\partial \varepsilon_4} = \begin{bmatrix}\overline{m}_1 & 0 \\ 0 & 0\end{bmatrix},\ \frac{\partial \mathbf{M}}{\partial \varepsilon_5} = \begin{bmatrix}0 & 0 \\ 0 & \overline{m}_2\end{bmatrix} \tag{5.58}$$

All other first order partial derivatives are null matrices. The second order partial derivatives of the uncertain mass and stiffness matrices are null matrices,

$$\frac{\partial^2 \mathbf{K}}{\partial \varepsilon_i \partial \varepsilon_l} = \mathbf{0}, \qquad \frac{\partial^2 \mathbf{M}}{\partial \varepsilon_i \partial \varepsilon_l} = \mathbf{0} \tag{5.59}$$

Therefore equation (5.56) becomes

$$\frac{\partial^2 \lambda_j}{\partial \varepsilon_i \partial \varepsilon_l} = 2\sum_{\substack{r=1 \\ r\neq j}}^{N} \frac{\left(\bar{\boldsymbol{\varphi}}_j{}^T G_{ij} \bar{\boldsymbol{\varphi}}_j\right)\left(\bar{\boldsymbol{\varphi}}_j{}^T G_{lj} \bar{\boldsymbol{\varphi}}_j\right)}{\lambda_j - \lambda_r} - \left(\bar{\boldsymbol{\varphi}}_j{}^T \frac{\partial \mathbf{M}}{\partial \varepsilon_i} \bar{\boldsymbol{\varphi}}_j\right)\left(\bar{\boldsymbol{\varphi}}_j{}^T G_{lj} \bar{\boldsymbol{\varphi}}_j\right) - \left(\bar{\boldsymbol{\varphi}}_j{}^T \frac{\partial \mathbf{M}}{\partial \varepsilon_l} \bar{\boldsymbol{\varphi}}_j\right)\left(\bar{\boldsymbol{\varphi}}_j{}^T G_{ij} \bar{\boldsymbol{\varphi}}_j\right)$$

(5.60)

This can be converted into matrix format such that the second order term as a whole is given by

$$\frac{1}{2}(\boldsymbol{\varepsilon})^T \left[2\sum_{\substack{r=1 \\ r\neq j}}^{2} \frac{\mathbf{A}_j \mathbf{A}_j{}^T}{\bar{\lambda}_j - \bar{\lambda}_r} - \mathbf{B}_j \mathbf{A}_j{}^T - \mathbf{A}_j \mathbf{B}_j{}^T \right] \boldsymbol{\varepsilon} \tag{5.61}$$

where $\mathbf{A}_j$ is as given in equation (5.29), and $\mathbf{B}_j$ in equation (5.51), such that

$$\mathbf{A}_j \mathbf{B}_j{}^T = \begin{bmatrix} 0 & 0 & 0 & \bar{\phi}_{j,1}{}^4 \bar{m}_1 \bar{k}_1 & \bar{\phi}_{j,1}{}^2 \bar{\phi}_{j,2}{}^2 \bar{k}_1 \bar{m}_2 \\ 0 & 0 & 0 & \bar{\phi}_{j,1}{}^2 \left(\bar{\phi}_{j,1} - \bar{\phi}_{j,2}\right)^2 \bar{k}_2 \bar{m}_1 & \bar{\phi}_{j,2}{}^2 \left(\bar{\phi}_{j,1} - \bar{\phi}_{j,2}\right)^2 \bar{k}_2 \bar{m}_2 \\ 0 & 0 & 0 & \bar{\phi}_{j,1}{}^2 \bar{\phi}_{j,2}{}^2 \bar{k}_3 \bar{m}_1 & \bar{\phi}_{j,2}{}^4 \bar{k}_3 \bar{m}_2 \\ 0 & 0 & 0 & -\bar{\phi}_{j,1}{}^4 \bar{m}_1{}^2 \bar{\lambda}_j & -\bar{\phi}_{j,1}{}^2 \bar{\phi}_{j,2}{}^2 \bar{m}_1 \bar{m}_2 \bar{\lambda}_j \\ 0 & 0 & 0 & -\bar{\lambda}_j \bar{\phi}_{j,1}{}^2 \bar{m}_1 \bar{\phi}_{j,2}{}^2 \bar{m}_2 & -\bar{\lambda}_j \bar{\phi}_{j,2}{}^4 \bar{m}_2{}^2 \end{bmatrix} \tag{5.62}$$

The mean centred second order perturbation approximation of the eigensolution for a two d.o.f. system from equation (5.54) becomes

$$\lambda_j \cong \bar{\lambda}_j + \mathbf{A}_j{}^T \boldsymbol{\varepsilon} + \frac{1}{2}(\boldsymbol{\varepsilon})^T \left[2\sum_{\substack{r=1 \\ r\neq j}}^{2} \frac{\mathbf{A}_j \mathbf{A}_j{}^T}{\bar{\lambda}_j - \bar{\lambda}_r} - \mathbf{B}_j \mathbf{A}_j{}^T - \mathbf{A}_j \mathbf{B}_j{}^T \right] \boldsymbol{\varepsilon} \tag{5.63}$$

It can be shown that if $\varepsilon_1 = \varepsilon_2 = \varepsilon_3 = \varepsilon_4 = \varepsilon_5 = \varepsilon$ such that all the masses and stiffness are perturbed by an equal amount and the eigenvectors are mass normalised, then the natural frequencies of the system remain unchanged $\lambda_j \cong \bar{\lambda}_j$.

If the variability in the system is assumed to have zero mean such that $\boldsymbol{\mu}_{\boldsymbol{\varepsilon}} = \mathbf{0}$, then the mean or expected value of the eigenvalues is given by

$$\mu_{\lambda_j} \cong \bar{\lambda}_j + (\mathbf{1})^T \left(\left[\sum_{\substack{r=1 \\ r \neq j}}^{2} \frac{\mathbf{A}_j \mathbf{A}_j^T}{\bar{\lambda}_j - \bar{\lambda}_r} - \mathbf{B}_j \mathbf{A}_j^T - \mathbf{A}_j \mathbf{B}_j^T \right] \bullet \mathrm{var}(\boldsymbol{\varepsilon}) \right) \mathbf{1} \tag{5.64}$$

where $\mathrm{var}(\boldsymbol{\varepsilon})$ is given in equation (5.33) and $\mathbf{1}$ is a unit vector of size equal to that of $\boldsymbol{\varepsilon}$ such that $\mathbf{1} = [1 \;\; 1 \;\; 1 \;\; 1 \;\; 1]^T$. Note the dot product $(\bullet)$ in equation (5.64) which is defined as the Hadamard or element-wise multiplication. Equation (5.64) directly relates the mean value of the system eigenvalues to the statistics (variance and covariance) of the random variables ε_i. It consists of terms representing the modal mass/stiffness of the elements, the variance of the variability in the elements, the covariance of the variability between elements and finally the modal spacing of the system eigenvalues.

If the random variables are independent such that the covariance's are zero, then the off-diagonal terms in $\mathrm{var}(\boldsymbol{\varepsilon})$ are zero and the mean of the system eigenvalues depends on the unperturbed system eigenvalues and the variance of the random variables.

The variance of the system eigenvalues can be calculated from equation (5.63); this will not be done here as the resultant expression will be somewhat lengthy. However, a reduced expression for the variance is shown below, based on the assumptions that the random variables have zero mean and are independent. If the change in the perturbed eigenvalues is given by $\delta_{\lambda_j} = \left(\lambda_j - \bar{\lambda}_j \right)$, then from equation (5.63)

$$\delta_{\lambda_j} \cong \mathbf{A}_j^T \boldsymbol{\varepsilon} + \frac{1}{2} \boldsymbol{\varepsilon}^T \left[2 \sum_{\substack{r=1 \\ r \neq j}}^{2} \frac{\mathbf{A}_j \mathbf{A}_j^T}{\bar{\lambda}_j - \bar{\lambda}_r} - \mathbf{B}_j \mathbf{A}_j^T - \mathbf{A}_j \mathbf{B}_j^T \right] \boldsymbol{\varepsilon} \tag{5.65}$$

For brevity let

$$\mathbf{C}_j = \sum_{\substack{r=1 \\ r \neq j}}^{2} \frac{\mathbf{A}_j \mathbf{A}_j^T}{\bar{\lambda}_j - \bar{\lambda}_r} - \mathbf{B}_j \mathbf{A}_j^T - \mathbf{A}_j \mathbf{B}_j^T \tag{5.66}$$

Therefore

$$\delta_{\lambda_j} \cong \mathbf{A}_j{}^T \boldsymbol{\varepsilon} + \boldsymbol{\varepsilon}^T \mathbf{C}_j \boldsymbol{\varepsilon} \tag{5.67}$$

The variance of the change in the perturbed eigenvalues is given by

$$\mathrm{var}\left(\delta_{\lambda_j}\right) \cong E\left[\left(\mathbf{A}_j{}^T \boldsymbol{\varepsilon} + \boldsymbol{\varepsilon}^T \mathbf{C}_j \boldsymbol{\varepsilon}\right)\left(\mathbf{A}_j{}^T \boldsymbol{\varepsilon} + \boldsymbol{\varepsilon}^T \mathbf{C}_j \boldsymbol{\varepsilon}\right)^T\right] \tag{5.68}$$

If the variabilities are assumed to be independent such that the covariance's are zero then this can be rearranged as

$$\mathrm{var}\left(\delta_{\lambda_j}\right) \cong \mathbf{A}_j{}^T \,\mathrm{var}(\boldsymbol{\varepsilon})\,\mathbf{A}_j + 2E\left[\boldsymbol{\varepsilon}^T \mathbf{C}_j \boldsymbol{\varepsilon}\boldsymbol{\varepsilon}^T \mathbf{A}_j\right] + E\left[\boldsymbol{\varepsilon}^T \mathbf{C}_j{}^T \boldsymbol{\varepsilon}\boldsymbol{\varepsilon}^T \mathbf{C}_j \boldsymbol{\varepsilon}\right] \tag{5.69}$$

where the term $E\left[\boldsymbol{\varepsilon}^T \mathbf{C}_j \boldsymbol{\varepsilon}\boldsymbol{\varepsilon}^T \mathbf{A}_j\right]$ is the skew of the variabilites and $E\left[\boldsymbol{\varepsilon}^T \mathbf{C}_j{}^T \boldsymbol{\varepsilon}\boldsymbol{\varepsilon}^T \mathbf{C}_j \boldsymbol{\varepsilon}\right]$ is the kurtosis. If the PDF of the random variables is known and of a standard form, then equation (5.69) can easily be evaluated.

5.6.1 Distribution of the eigenvalues

In a similar manner to the first order perturbation, the change of variable technique can be used to propagate the PDF of the mass and stiffness, to obtain an estimate of the PDF of the eigenvalues of the system. Again, a reduced scenario are will be considered, in this case as the expressions quickly become quite lengthy a single uncertain system property will be considered.

Assuming $\varepsilon_2 = \varepsilon_3 = \varepsilon_4 = \varepsilon_5 = 0$ and that the only variability in the system is due to ε_1, the mass and stiffness matrices are as given in equation (5.35).

From equation (5.63) and expanding, the system eigenvalues are given by

$$\lambda_j \cong \bar{\lambda}_j + \bar{\phi}_{j,1}{}^2 \bar{k}_1 \varepsilon_1 + \varepsilon_1{}^2 \bar{\phi}_{j,1}{}^4 \bar{k}_1{}^2 \sum_{\substack{r=1 \\ r \neq j}}^{2} \frac{1}{\bar{\lambda}_j - \bar{\lambda}_r} \tag{5.70}$$

The change of variable technique for a single variable is given by

$$p(y) = \frac{np(x)}{\left|f'(x)\right|} \tag{5.71}$$

where each value of y corresponds to n values of x. As the expression in (5.70) is not single valued and one-to-one, then $n = 2$ and hence combining equations (5.70) and (5.71) gives

$$p(\lambda_j) \cong \frac{2p(\varepsilon_1)}{\left|\bar{\phi}_{j,1}{}^2 \bar{k}_1 + 2\varepsilon_1 \bar{\phi}_{j,1}{}^4 \bar{k}_1{}^2 \sum_{\substack{r=1 \\ r \neq j}}^{2} \frac{1}{\bar{\lambda}_j - \bar{\lambda}_r}\right|} \tag{5.72}$$

This directly relates the PDF of the system eigenvalues to the PDF of the uncertain stiffness term ε_1 and includes terms representing the modal stiffness of the spring k_1 and the modal spacing. For example, if ε_1 was Gaussian distributed with zero mean and variance $\sigma_{\varepsilon_1}{}^2$, then from equation (5.72)

$$p(\lambda_j) \cong \frac{2e^{-\frac{\varepsilon_{\varepsilon_1}{}^2}{2\sigma_{\varepsilon_1}{}^2}}}{\sigma_{\varepsilon_1}\sqrt{2\pi}\left|\bar{\phi}_{j,1}{}^2 \bar{k}_1 + 2\varepsilon_1 \bar{\phi}_{j,1}{}^4 \bar{k}_1{}^2 \sum_{\substack{r=1 \\ r \neq j}}^{2} \frac{1}{\bar{\lambda}_j - \bar{\lambda}_r}\right|} \tag{5.73}$$

However, an expression for ε_1 is required for substitution into equation (5.73), this can be obtained from the quadratic equation formed by equation (5.70) namely

$$\varepsilon_1{}^2 \bar{\phi}_{j,1}{}^4 \bar{k}_1{}^2 \left(\sum_{\substack{r=1 \\ r \neq j}}^{2} \frac{1}{\bar{\lambda}_j - \bar{\lambda}_r} \right) + \bar{\phi}_{j,1}{}^2 \bar{k}_1 \varepsilon_1 + \bar{\lambda}_j - \lambda_j \cong 0 \tag{5.74}$$

Using the standard format for a solution to a quadratic equation and substituting, the expression for the PDFs of the system eigenvalues are given by

$$p(\lambda_j) \cong \frac{2e^{\dfrac{\left(-1\pm\sqrt{\left(1-4\left(\sum_{\substack{r=1\\ r\neq j}}^{2}\frac{\bar{\lambda}_j-\lambda_j}{\bar{\lambda}_j-\bar{\lambda}_r}\right)\right)}\right)^2}{8\sigma_{\varepsilon_1}{}^2\bar{\phi}_{j,1}{}^4\bar{k}_1{}^2\left(\sum_{\substack{r=1\\ r\neq j}}^{2}\frac{1}{\bar{\lambda}_j-\bar{\lambda}_r}\right)^2}}}{\sigma_{\varepsilon_1}\sqrt{2\pi}\bar{\phi}_{j,1}{}^2\bar{k}_1\sqrt{\left(1-4\left(\sum_{\substack{r=1\\ r\neq j}}^{2}\frac{\bar{\lambda}_j-\lambda_j}{\bar{\lambda}_j-\bar{\lambda}_r}\right)\right)}} \tag{5.75}$$

A similar method to this can be used for more complicated scenarios with multiple variable system properties, however the expressions rapidly become lengthy and difficult to manipulate.

5.7 Interpolated mode method

The interpolated mode method as discussed in chapter 4 approximates the eigenvalue of a perturbed system from interpolation between previously calculated eigenvectors. It can be applied to a two d.o.f. system; consider a simplified version of the two d.o.f. system where there is only variability in one stiffness element k_1 such that the mass and stiffness matrices are given by

$$\begin{aligned}\mathbf{K} &= \begin{bmatrix} \bar{k}_1(1+\varepsilon_1)+\bar{k}_2 & -\bar{k}_2 \\ -\bar{k}_2 & \bar{k}_2+\bar{k}_3 \end{bmatrix} \\ \mathbf{M} &= \begin{bmatrix} \bar{m}_1 & 0 \\ 0 & \bar{m}_2 \end{bmatrix}\end{aligned} \tag{5.76}$$

An interval needs to be defined over which ε_1 will vary, for example assume that as the variability is small, that ε_1 varies between $-0.1 \le \varepsilon_1 \le 0.1$ and therefore k_1 varies by 10%. The stiffness matrices at either end of the interval are given by

$$\begin{aligned}\mathbf{K}_0 &= \begin{bmatrix} 0.9\bar{k}_1+\bar{k}_2 & -\bar{k}_2 \\ -\bar{k}_2 & \bar{k}_2+\bar{k}_3 \end{bmatrix} \\ \mathbf{K}_f &= \begin{bmatrix} 1.1\bar{k}_1+\bar{k}_2 & -\bar{k}_2 \\ -\bar{k}_2 & \bar{k}_2+\bar{k}_3 \end{bmatrix}\end{aligned} \tag{5.77}$$

The eigen solutions at either end of the interval are therefore given by the exact calculations

$$\mathbf{K}_0\boldsymbol{\varphi}_{\mathbf{j\_0}} = \lambda_{j\_0}\mathbf{M}\boldsymbol{\varphi}_{\mathbf{j\_0}} \qquad \text{and} \qquad \mathbf{K}_f\boldsymbol{\varphi}_{\mathbf{j\_f}} = \lambda_{j\_f}\mathbf{M}_{\mathbf{f}}\boldsymbol{\varphi}_{\mathbf{j\_f}} \tag{5.78}$$

A non-dimensional parameter t is defined as

$$t = \frac{\varepsilon_1 + 0.1}{0.2} \tag{5.79}$$

such that $0 \le t \le 1$. The weighting factors t and $(1-t)$ are used to interpolate the mode shapes obtained from $\boldsymbol{\varphi}_{\mathbf{j\_0}}$ and $\boldsymbol{\varphi}_{\mathbf{j\_f}}$, thus for the *j*'th mode

$$\boldsymbol{\varphi}_j = (1-t)\left(\boldsymbol{\varphi}_{\mathbf{j\_0}}\right) + (t)\left(\boldsymbol{\varphi}_{\mathbf{j\_f}}\right) \tag{5.80}$$

The Rayleigh quotient is then used in conjunction with the interpolated mode as an assumed modeshape to approximate the eigenvalue solution

$$\lambda_j = \frac{\boldsymbol{\varphi}_j{}^T\left(\bar{\mathbf{K}} + \Delta\bar{\mathbf{K}}\right)\boldsymbol{\varphi}_j}{\boldsymbol{\varphi}_j{}^T\left(\bar{\mathbf{M}} + \Delta\bar{\mathbf{M}}\right)\boldsymbol{\varphi}_j} \tag{5.81}$$

As discussed earlier in chapter 4, one drawback of the interpolated mode method is that is does not directly result in an approximate expression relating the perturbed system eigenvalues in terms of the baseline system eigenvalues. The method is essentially an interval analysis rather than a statistical method, and as such cannot be directly used to propagate the PDF of the variability through to the response variability. For this reason the interpolated mode method is perhaps more suited to possibilistic analysis.

It was suggested in chapter 4 that each system variable could be considered to vary over a fixed interval of $\pm 3\sigma$. Thus leading to some basic understanding of the propagation of the statistical interval of the system property variability to the response variability. If the variability was, for example, Gaussian distributed, this interval would be expected to contain 99.7% of the variability samples. The interpolated mode analysis is then conducted on the N-dimensional parameter space represented by these intervals (where N is the number of variability parameters). For example, consider the two d.o.f. system with three variable parameters such that

$$\mathbf{K} = \begin{bmatrix} \bar{k}_1(1+\varepsilon_1) + \bar{k}_2(1+\varepsilon_2) & -\bar{k}_2(1+\varepsilon_2) \\ -\bar{k}_2(1+\varepsilon_2) & \bar{k}_2(1+\varepsilon_2) + \bar{k}_3 \end{bmatrix}$$
$$\mathbf{M} = \begin{bmatrix} \bar{m}_1(1+\varepsilon_4) & 0 \\ 0 & \bar{m}_2 \end{bmatrix} \tag{5.82}$$

The variability parameter intervals are given by

$$L_i \le \varepsilon_i \le H_i \tag{5.83}$$

where the lower limit of each variable L_i is equivalent to -3σ and the higher limit of each variable H_i is equivalent to $+3\sigma$. The non-dimensional parameters t_i are defined as

$$t_i = \frac{\varepsilon_i - L_i}{H_i - L_i} \tag{5.84}$$

The interpolated eigenvector can then calculated as

$$\boldsymbol{\varphi}_j(\varepsilon_1,\varepsilon_2,\varepsilon_3) = (1-t_1)(1-t_2)(1-t_3)\boldsymbol{\varphi}_{j\_LLL} + t_1(1-t_2)(1-t_3)\boldsymbol{\varphi}_{j\_HLL} + (1-t_1)t_2(1-t_3)\boldsymbol{\varphi}_{j\_LHL}$$
$$+(1-t_1)(1-t_2)t_3\boldsymbol{\varphi}_{j\_LLH} + t_1t_2(1-t_3)\boldsymbol{\varphi}_{j\_HHL} + (1-t_1)t_2t_3\boldsymbol{\varphi}_{j\_LHH} + t_1(1-t_2)t_3\boldsymbol{\varphi}_{j\_HLH} + t_1t_2t_3\boldsymbol{\varphi}_{j\_HHH} \tag{5.85}$$

where $\boldsymbol{\varphi}_{j\_rst} = \boldsymbol{\varphi}_j(\varepsilon_1 = r, \varepsilon_2 = s, \varepsilon_3 = t)$. The eight eigenvectors at corners of the interval cube $[L_1,H_1]\times[L_2,H_2]\times[L_3,H_3]$ need to be calculated exactly. The interpolated eigenvector can then used with the Rayleigh quotient to calculate the eigenvalue solution approximately.

There are two major disadvantages with this technique. The eigenvectors are most accurately estimated near the ends of the intervals and therefore the least accurately estimated region is that in which the variability terms are near their mean value, which is the area that would be expected to be most critical. In addition, the application of the method to large N degree of freedom systems requires an N-dimensional interval space to be considered, and 2^N eigenvectors to be calculated exactly.

5.8 Conclusions

In this chapter the propagation of uncertainty in simple systems was reviewed. The example of a two degree of freedom system was considered and variability introduced into its physical properties. Expressions were generated to relate the statistics of the modal properties to the statistics of the mass and stiffness of the system.

The first approximation investigated was the use of baseline modeshapes as assumed shape functions. This is essentially a physical approximation and probably the least accurate. Next a first order perturbational expansion was used to estimate the system eigenvalues and the relationship between the statistics of these and the statistics of the physical properties. This was extended to include a second order term for a more accurate result. Once the perturbation expansion has been used to approximate the system eigenvalues, relating the variance of the eigenvalues to the variance in the system mass and stiffness is relatively straightforward. In the following chapter the perturbation method will be extended to investigate the statistics of larger multi-degree of freedom systems. However, obtaining the distribution of the eigenvalues is somewhat more complex and impractical to extend to larger systems. Therefore, in the following chapter the general techniques for obtaining the eigenvalue distribution for larger systems will be discussed and some observations made on the potential application of the central limit theorem. The final eigensolution approximation applied to a two degree of freedom system was the interpolated mode method. As the method is essentially an interval analysis it is more suited to a possibilistic analysis and less useful in the propagation of statistics.

Section III: Component Mode Synthesis methods

6. Component mode synthesis

From chapter 5 it can be seen that a perturbational expansion approach provides a possible route for propagating uncertainty in a structure, from the physical properties to the global modal response. However, one of the main drawbacks of this method is the rapidly increasing complexity of the calculations when applied to a system with more than a few degrees of freedom. A possible method for overcoming this drawback is through the use of Component Mode Synthesis to subdivide a structure into smaller substructures. This has additional relevance when considering the modelling of built-up structures which consist of several smaller structures which may be manufactured independently and possess statistically independent uncertainties.

In the first section of this chapter the concept of combining component mode synthesis (CMS) techniques along with traditional approximations is presented. The procedure is outlined in general and potential areas for data reduction and model simplification are highlighted. Following this the background theory of CMS will be briefly introduced for use in later chapters. This approach is a substructuring technique for dynamic analysis of structures. It involves dividing a structure into substructures or components, performing a separate analysis of the components and assembling these results into a global modal model. The term 'component modes' refers to the use of Ritz vectors or assumed modes that are used as basis vectors for each component. Often reduced order component models are used and thus a reduced order global model assembled. Typically the component modes are obtained from an FE analysis, however they may also be obtained experimentally or analytically. CMS methods are also sometimes employed in the analysis of extremely large FE models where for convenience the model is divided into components.

The CMS method was first introduced by Hurty [6.1] who examined substructure coupling of models in a FE form. This introduced the concept of using component modes as trial functions or basis vectors. This work was extended by Craig and Bampton [6.2] who simplified the method to consider rigid body modes and redundant interface modes as constraint modes. The first part of this section will give a detailed derivation of the general CMS method, with an assumed matrix of component modes. This will include some guidelines on the possible choices of assumed component modes. Then some particular types of component modes will be discussed, and in some cases their derivation given.

Then two of the most popular CMS techniques will be introduced, free and fixed interface methods. The free interface method uses free interface normal component modes combined with residual flexibility attachment modes as assumed component modes. The fixed interface method uses fixed interface normal modes combined with displacement constraint modes as assumed component modes. Published work often considers undamped CMS models, hence the techniques will be introduced as applied to undamped systems, subsequently the inclusion of damping will be considered separately. All of the CMS techniques will be discussed as applied to discretised structures, where the structure is represented as an assembly of discrete structural elements, thereby obtaining a set of equations which are conveniently expressed in matrix algebra. All of the eigenvectors are assumed to be mass normalised unless stated otherwise.

6.1 Uncertainty propagation using a component modal method

Typically a basic mid-frequency analysis will use the physical properties of a structure to model the modal response, commonly using Finite Element Analysis (FEA). The Frequency Response Function (FRF) for the structure is then found using modal summation. If some uncertainty exists in the physical properties of the structure then a common route would be to use Monte Carlo simulations to allow the properties to vary randomly and the analysis repeated many times. This process is represented by the flowchart in Figure 6-1.

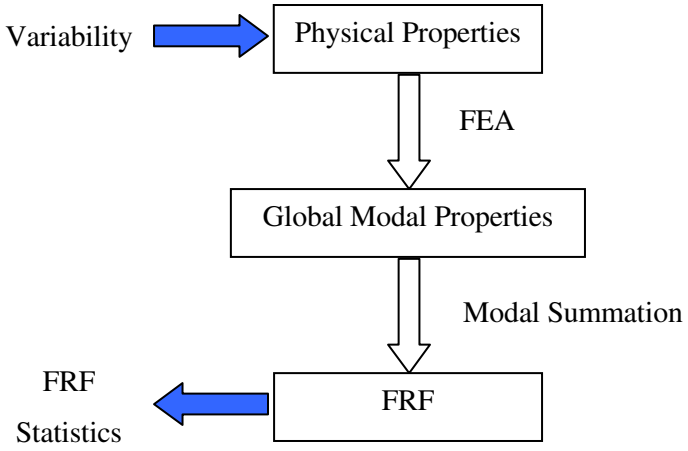

Figure 6-1 Typical Monte Carlo analysis of variability.

However, this process is expensive and time consuming as a full eigensolution must be found for each cycle of the MC analysis. Potential areas for approximation include the use of

eigensolution approximations, such as the perturbational approach used in chapter 5, and the use of a reduced or truncated set of global modes in the modal summation to obtain the FRF.

An alternative method is to use CMS to divide the structure into substructures or components which can then be analysed separately and these results assembled into a global model. A representation of this process is shown in Figure 6-2. The theory behind the CMS process and two common types of CMS analysis, fixed interface analysis and free interface analysis, are discussed in detail in section 6.2. Briefly, an eigensolution is performed on each substructure to obtain a set of component modes, which depending on the type of CMS analysis may include normal modes of free vibration, rigid-body modes, constraint modes or attachment modes. These are combined in some form (dependent on the chosen method) to create a set of assumed modes or trial vectors for the full structure.

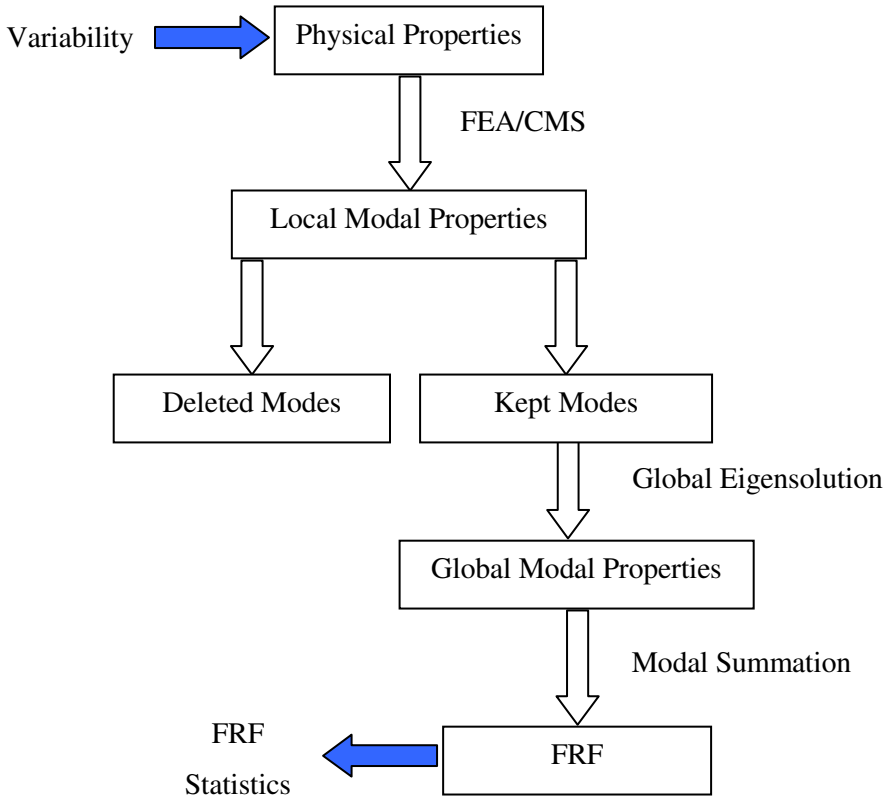

Figure 6-2 Basic CMS analysis of a structure.

If all the component modes are used then the CMS process does not offer any reduction in computational cost over a standard global FEA outlined in Figure 6-1. However, one of the main benefits of the CMS analysis is the possibility to use a reduced set of component modes, referred to as 'kept' modes, to describe the subsystem behaviour. In addition there is some benefit when modelling extremely large or complex structures in that the components may be

supplied from different manufacturers, which offers the possibility of assembling modal models from different suppliers. Typically the component modes are obtained from an FE analysis, however they may also be obtained experimentally.

Possible approximations may also be made by simplification of the physical uncertainties. For example, the joints between components will exhibit some uncertainty, which may be highly variable according to the manufacturing process. This source of uncertainty, if ignored, will approximate the behaviour of the built-up structure.

A further extension of this method is the Local Mode Perturbational method (LMP) first proposed by Mace and Shorter [6.3]. This method introduces uncertainty directly into the component eigenvalues, thereby eliminating the consideration of physical property variations. These component eigenvalue variations are assumed to be small and an eigensolution approximation is used to estimate the global eigenvalues and eigenvectors. In this case a perturbational approximation is used. A representation of this process is shown in Figure 6-3.

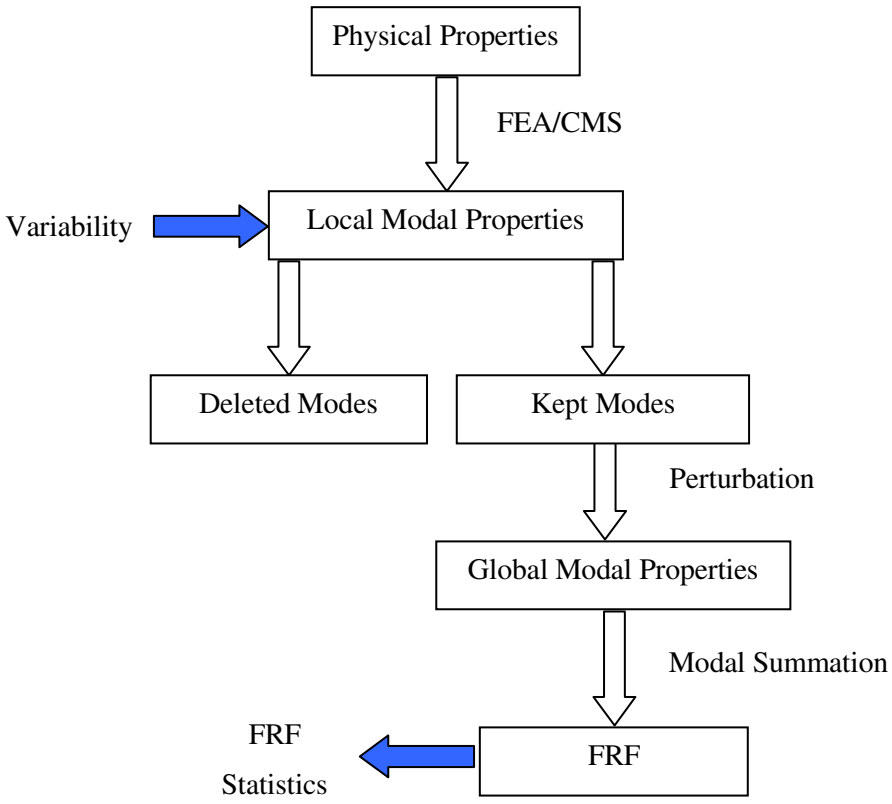

Figure 6-3 Local Mode Perturbational Method.

The method as proposed by Mace and Shorter uses a fixed interface CMS method. Three main areas of approximation are introduced. The first two of these are involved with the CMS method

(explained in detail in section 6.2) which uses local component fixed interface modeshapes and constraint modes. As the LMP method only considers variability in the component eigenvalues, the variability in the component modeshapes and constraint modes is not included. Thirdly, an eigensolution approximation is used to obtain the global modal response. The LMP method will be applied in this thesis to generate expressions for the statistics of the global modal response, in terms of the statistics of the local modal behaviour.

Two further potential areas for approximations are proposed here; the use of free interface component eigenvalues statistics in place of the fixed interface values and the disregard of covariance between components. Both of these proposals will be examined in further detail in chapter 8.

In summary the potential areas for data reduction and approximation are as follows:

1) Simplification or approximation of the physical uncertainties such as ignoring joint uncertainties
2) Truncation of the set of local modes to a reduced set of kept modes
3) Assuming constant local eigenvectors e.g. assuming fixed interface local modeshapes remain unchanging
4) Assuming constant local constraint modeshapes
5) Simplification or approximation of the component uncertainties such as ignoring covariance between components
6) Use of free interface component statistics to approximate fixed interface component statistics
7) Truncation of the set of global modes to a reduced set of kept modes
8) Use of eigen solution approximations such as perturbational expansions

These areas for approximation are summarised in Figure 6-4. The LMP method will be used in this thesis as a basis for further examining the propagation of uncertainty in complex structures. In the following two chapters the transmission of uncertainty from the physical properties to the global FRF will be divided into two stages. Chapter 7 will examine the relationship between the variations in the physical properties of a component to the resultant variations in the modal properties. Chapter 8 will examine the relationship between variations in the local modal properties and the resultant variations in the global modal properties and the FRF response.

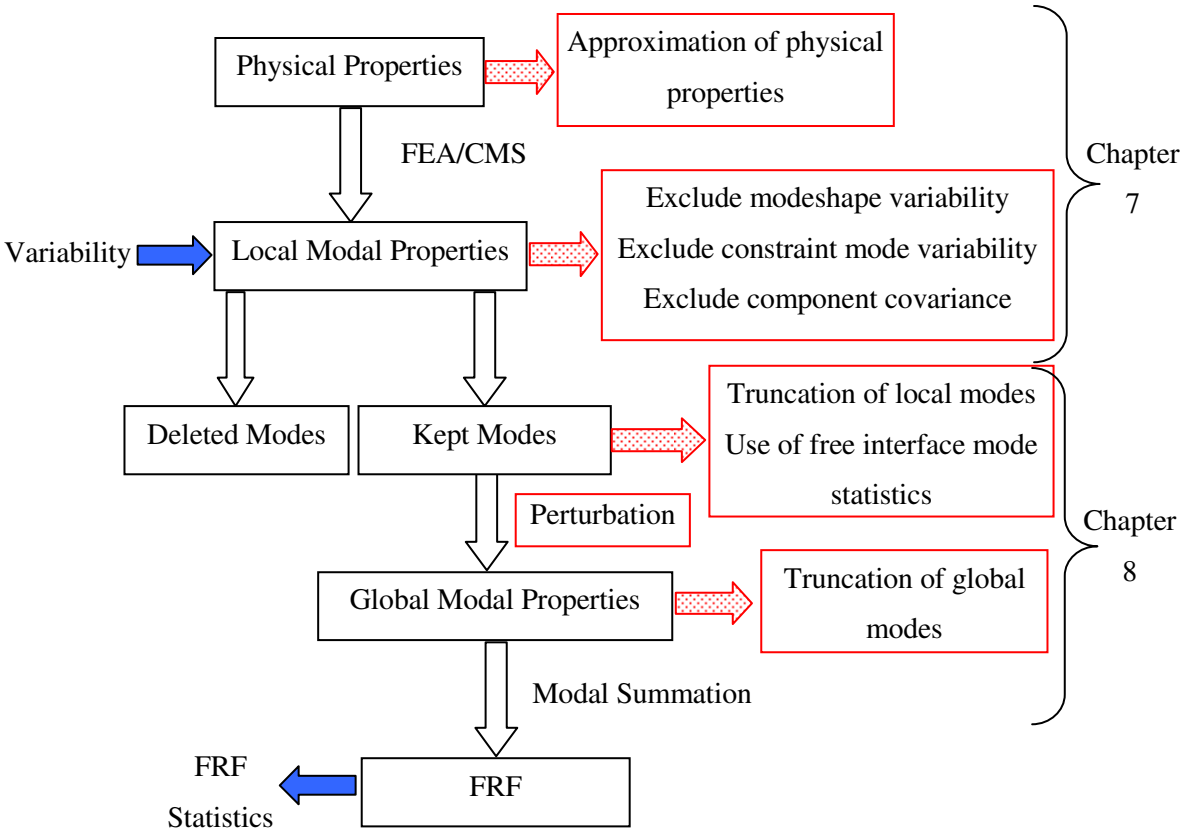

Figure 6-4 Potential areas for data reduction and approximation.

In both chapters 7 and 8, the propagation of statistics and the PDF of the response will be considered. The effect on both eigenvalues and eigenvectors will be discussed along with examples considering both correlated and uncorrelated sources of uncertainty.

6.2 The component mode synthesis method

In this section the background theory for the CMS method is presented and two popular types of CMS analysis, fixed interface and free interface methods, are discussed in detail. The CMS methods presented here are Lagrange multiplier based generalised substructure coupling procedures (4.10) from [6.4].

The undamped equation of motion for a structure is given by

$$\mathbf{M}\ddot{\mathbf{x}} + \mathbf{K}\mathbf{x} = \mathbf{F} \tag{6.1}$$

where $\mathbf{x}$ is the vector of physical d.o.f., $\mathbf{M}$ and $\mathbf{K}$ are the mass and stiffness matrices and $\mathbf{F}$ is the vector of external forces. The structure is divided into n substructures, where the mass and stiffness of the i'th subsystem are given by $\mathbf{M}^{(i)}$ and $\mathbf{K}^{(i)}$. The vector of physical d.o.f. $\mathbf{x}$ can be partitioned into the d.o.f. related to each substructure, such that

$$\mathbf{x} = \left[\left(\mathbf{x}^{(1)}\right)^T \quad \left(\mathbf{x}^{(2)}\right)^T \quad \cdots \quad \left(\mathbf{x}^{(n)}\right)^T \right]^T \tag{6.2}$$

The vectors of physical d.o.f. for each substructure can be partitioned into interior (subscript i) and coupling (subscript c) d.o.f. such that

$$\mathbf{x}^{(i)} = \begin{bmatrix} \mathbf{x}_i^{(i)} \\ \mathbf{x}_c^{(i)} \end{bmatrix} \tag{6.3}$$

The sub-matrices of the mass and stiffness $\mathbf{M}$ and $\mathbf{K}$, that relate to each subsystem are given by

$$\mathbf{M}^{(i)} = \begin{bmatrix} \mathbf{m}_{ii}^{(i)} & \mathbf{m}_{ic}^{(i)} \\ \mathbf{m}_{ci}^{(i)} & \mathbf{m}_{cc}^{(i)} \end{bmatrix} \tag{6.4}$$

$$\mathbf{K}^{(i)} = \begin{bmatrix} \mathbf{k}_{ii}^{(i)} & \mathbf{k}_{ic}^{(i)} \\ \mathbf{k}_{ci}^{(i)} & \mathbf{k}_{cc}^{(i)} \end{bmatrix} \tag{6.5}$$

These form the block diagonal matrices of $\mathbf{M}$ and $\mathbf{K}$. The force vector associated with the *i*'th substructure is given by

$$\mathbf{F}^{(i)} = \begin{bmatrix} \mathbf{f}_i^{(i)} \\ \mathbf{f}_c^{(i)} \end{bmatrix} \tag{6.6}$$

The equation of motion for each substructure is therefore

$$\mathbf{M}^{(i)}\ddot{\mathbf{x}}^{(i)} + \mathbf{K}^{(i)}\mathbf{x}^{(i)} = \mathbf{F}^{(i)} \tag{6.7}$$

Consider two coupled components (α and β) that have a common boundary or interface. It is assumed that some higher component modeshapes have been removed in order that a reduced

global solution can be found; the additional subscripts of k and d will be used later to represent 'kept' and 'deleted' modes.

The equation for motion for the undamped components may be partitioned into interior and coupling d.o.f. such that at the coupling interface the physical displacements are constrained by

$$\mathbf{x}_c^{(\alpha)} = \mathbf{x}_c^{(\beta)} \tag{6.8}$$

and the coupling forces are related by

$$\mathbf{f}_c^{(\alpha)} + \mathbf{f}_c^{(\beta)} = 0 \tag{6.9}$$

The physical d.o.f. $\mathbf{x}$ may be characterised by a set of generalised coordinates $\mathbf{p}$ by the transformation

$$\mathbf{x} = \boldsymbol{\upsilon}\mathbf{p} \tag{6.10}$$

where $\boldsymbol{\upsilon}$ is a set of pre-selected component modes and is a transformation from the physical domain to the $\mathbf{p}$ domain given by

$$\mathbf{p} \equiv \begin{bmatrix} \mathbf{p}^{(\alpha)} \\ \mathbf{p}^{(\beta)} \end{bmatrix} \tag{6.11}$$

It can be shown that the expressions for the system kinetic and potential energy, from Lagrange's equation of motion, are given by [6.4]

$$T = \frac{1}{2}\dot{\mathbf{p}}^T \boldsymbol{\mu}\dot{\mathbf{p}} = \frac{1}{2}\dot{\mathbf{p}}^{(\alpha)T}\boldsymbol{\mu}^{(\alpha)}\dot{\mathbf{p}}^{(\alpha)} + \frac{1}{2}\dot{\mathbf{p}}^{(\beta)T}\boldsymbol{\mu}^{(\beta)}\dot{\mathbf{p}}^{(\beta)} \tag{6.12}$$

$$V = \frac{1}{2}\mathbf{p}^T \boldsymbol{\kappa}\mathbf{p} = \frac{1}{2}\mathbf{p}^{(\alpha)T}\boldsymbol{\kappa}^{(\alpha)}\mathbf{p}^{(\alpha)} + \frac{1}{2}\mathbf{p}^{(\beta)T}\boldsymbol{\kappa}^{(\beta)}\mathbf{p}^{(\beta)} \tag{6.13}$$

where

$$\begin{aligned} \boldsymbol{\mu}^{(\alpha)} &= \boldsymbol{\upsilon}^{(\alpha)T}\mathbf{M}^{(\alpha)}\boldsymbol{\upsilon}^{(\alpha)} \\ \boldsymbol{\kappa}^{(\alpha)} &= \boldsymbol{\upsilon}^{(\alpha)T}\mathbf{K}^{(\alpha)}\boldsymbol{\upsilon}^{(\alpha)} \end{aligned} \tag{6.14}$$

are the transformed component mass and stiffness matrices (similarly for component β) and the global transformed mass and stiffness matrices are given by

$$\boldsymbol{\mu} \equiv \begin{bmatrix} \boldsymbol{\mu}^{(\alpha)} & \mathbf{0} \\ \mathbf{0} & \boldsymbol{\mu}^{(\beta)} \end{bmatrix}, \quad \boldsymbol{\kappa} \equiv \begin{bmatrix} \boldsymbol{\kappa}^{(\alpha)} & \mathbf{0} \\ \mathbf{0} & \boldsymbol{\kappa}^{(\beta)} \end{bmatrix} \tag{6.15}$$

The constraint equations for the system such as (6.8) and (6.9) can be expressed in terms of the generalised coordinates $\mathbf{p}$ and combined to form a constraint matrix $\mathbf{C}$ given by

$$\mathbf{C}\mathbf{p} = 0 \tag{6.16}$$

The Lagrangian for the system can be written as

$$L = T - V + \boldsymbol{\sigma}^T \mathbf{C}\mathbf{p} \tag{6.17}$$

where $\boldsymbol{\sigma}$ is a vector of Lagrange multipliers. It can be shown [6.4] that the system equation of motion is given by

$$\boldsymbol{\mu}\ddot{\mathbf{p}} + \boldsymbol{\kappa}\mathbf{p} = \mathbf{C}^T\boldsymbol{\sigma} \tag{6.18}$$

This can be solved by introducing a linear transformation, where

$$\mathbf{p} = \mathbf{S}\mathbf{q} \tag{6.19}$$

The generalised coordinates $\mathbf{p}$ can be partitioned into dependent $(\mathbf{p}_D)$ and linearly independent $(\mathbf{p}_l)$ coordinates such that equation (6.16) becomes

$$\begin{bmatrix} \mathbf{C}_{DD} & \mathbf{C}_{Dl} \end{bmatrix} \begin{bmatrix} \mathbf{p}_D \\ \mathbf{p}_l \end{bmatrix} = \mathbf{0} \tag{6.20}$$

Substituting this into equation (6.19) defines both $\mathbf{S}$ and $\mathbf{q}$

$$\mathbf{p} \equiv \begin{bmatrix} \mathbf{p}_D \\ \mathbf{p}_l \end{bmatrix} = \begin{bmatrix} -\mathbf{C}_{DD}^{-1}\mathbf{C}_{Dl} \\ \mathbf{I}_{ll} \end{bmatrix} \mathbf{p}_l \equiv \mathbf{S}\mathbf{q} \tag{6.21}$$

Substituting equation (6.19) into (6.18), and pre-multiplying by $\mathbf{S}^T$, the equation of motion for the system becomes

$$\mathbf{M}_q\ddot{\mathbf{q}} + \mathbf{K}_q\mathbf{q} = \mathbf{S}^T\mathbf{C}^T\boldsymbol{\sigma} \tag{6.22}$$

where $\mathbf{M}_q = \mathbf{S}^T\boldsymbol{\mu}\mathbf{S}$ and $\mathbf{K}_q = \mathbf{S}^T\boldsymbol{\kappa}\mathbf{S}$ represent the uncoupled mass and stiffness matrices for the structure. From equations (6.19) and (6.16) it can be seen that $\mathbf{CS} = \mathbf{0}$, thus the equation of motion for the system in uncoupled coordinates, is given by

$$\mathbf{M}_q\ddot{\mathbf{q}} + \mathbf{K}_q\mathbf{q} = \mathbf{0} \tag{6.23}$$

In forming the assumed mode matrix some decision must be made on which modes to include and if a reduced order global model is required, how many of each set of modes to keep. Noor and Peters [6.5] proposed the following selection criteria for choosing the assumed modes:

1. Linear independence and completeness
2. Low computational expense in their generation, and simplicity of automatic selection of their number
3. Good approximation properties, in the sense of solution accuracy
4. Simplicity of obtaining the system response characteristics of interest
5. If test verification of component modal models is required, then the assumed modes should be easily updateable
6. If test-based reduced order models of components are to be coupled, then the assumed modes should be amendable to test acquisition of complete and accurate component data

Decisions on the number of modes to keep in a reduced order model will depend on the size and complexity of the models and the frequency range of interest.

6.3 Component modes

The assumed mode matrix is formed from a selection of component modes. These may include normal modes of free vibration, rigid-body modes, constraint modes, attachment modes and Krylov vectors [6.11].

Normal modes are the modes of eigenvectors of a component and these are grouped according to their type. Fixed interface normal modes are those eigenvectors of a component whose interface degrees of freedom (d.o.f.) are fixed, or constrained. They are obtained from an eigensolution for a component

$$\left(\mathbf{k}_{ii}^{(i)} - \lambda_j^{(i)}\mathbf{m}_{ii}^{(i)}\right)\left(\boldsymbol{\varphi}_i\right)_j = \mathbf{0}, \;\; j = 1,2,...,n \tag{6.24}$$

Similarly, free interface normal modes are those eigenvectors of a component whose interface degrees of freedom are free or unconstrained and are given by the eigensolution to

$$\left(\mathbf{K}^{(i)} - \lambda_j^{(i)}\mathbf{M}^{(i)}\right)\left(\boldsymbol{\varphi}\right)_j = \mathbf{0}, \;\; j = 1,2,...,n \tag{6.25}$$

Loaded interface normal modes are those in which some lumped mass or stiffness elements are introduced at the interface d.o.f. Various hybrid interface normal modes, which include a combination of these types have been suggested [6.6].

A constraint mode is defined as the static deformation of a substructure when a unit displacement (or rotation) is specified at one d.o.f. of a set of constraint coordinates $\mathbf{C}$ whilst all the other coordinates of that set are constrained, and the remaining d.o.f.s have no force applied. When $\mathbf{C}$ consists of the coupling d.o.f. the constraint mode $\boldsymbol{\gamma}$ can be found from

$$\begin{bmatrix} \mathbf{k}_{ii} & \mathbf{k}_{ic} \\ \mathbf{k}_{ci} & \mathbf{k}_{cc} \end{bmatrix} \begin{bmatrix} \boldsymbol{\upsilon}_{ic} \\ \mathbf{I}_{cc} \end{bmatrix} = \begin{bmatrix} \mathbf{0}_{ic} \\ \mathbf{R}_{cc} \end{bmatrix} \tag{6.26}$$

where $\mathbf{R}_{cc}$ is a set of reaction forces. From equation (6.26) it can be seen that

$$\boldsymbol{\upsilon}_{ic} = -\left(\mathbf{k}_{ii}\right)^{-1}\mathbf{k}_{ic} \tag{6.27}$$

The set of constraint modes $\boldsymbol{\gamma}$ when $\mathbf{C}$ consists of the coupling d.o.f., is therefore given by

$$\boldsymbol{\gamma} = \begin{bmatrix} \boldsymbol{\upsilon}_{ic} \\ \mathbf{I}_{cc} \end{bmatrix} = \begin{bmatrix} -\left(\mathbf{k}_{ii}\right)^{-1}\mathbf{k}_{ic} \\ \mathbf{I}_{cc} \end{bmatrix} \tag{6.28}$$

An attachment mode is the component displacement vector to a unit static force applied at one of the component d.o.f., often selected to be an interface d.o.f. Attachment modes can be obtained from the columns of the flexibility matrix $\mathbf{G}$ which is the inverse of the stiffness matrix. The columns of the flexibility matrix are the attachment modes for a restrained component; can also be written in terms of the modes of the component as

$$\mathbf{G} = \boldsymbol{\varphi} \begin{bmatrix} diag\left(\lambda_j\right) & \mathbf{0} \\ \mathbf{0} & \ddots \end{bmatrix}^{-1} \boldsymbol{\varphi}^T \tag{6.29}$$

If some higher component modeshapes are removed in order that a reduced global solution can be found, then the part of the flexibility matrix that is associated with the deleted modes is given by

$$\mathbf{G}_d = \mathbf{G} - \boldsymbol{\varphi}_k \begin{bmatrix} diag\left(\lambda_j\right)_k & \mathbf{0} \\ \mathbf{0} & \ddots \end{bmatrix}^{-1} \boldsymbol{\varphi}_k{}^T \tag{6.30}$$

where the subscript k represents the kept modes. Residual attachment modes may be defined for forces applied at the coupling coordinates as

$$\boldsymbol{\upsilon}_d = \mathbf{G}_d \mathbf{f}_c = \left[\mathbf{G} - \boldsymbol{\varphi}_k \begin{bmatrix} diag\left(\lambda_j\right)_k & \mathbf{0} \\ \mathbf{0} & \ddots \end{bmatrix}^{-1} \boldsymbol{\varphi}_k{}^T \right] \begin{bmatrix} \mathbf{0}_{ic} \\ \mathbf{I}_{cc} \end{bmatrix} \tag{6.31}$$

where $\mathbf{F}_c$ are the coupling forces. This can be expanded and expressed in terms of the deleted modes, thus

$$\boldsymbol{\upsilon}_d = \boldsymbol{\varphi}_d \begin{bmatrix} diag\left(\lambda_j\right)_d & \mathbf{0} \\ \mathbf{0} & \ddots \end{bmatrix}^{-1} \boldsymbol{\varphi}_{cd}{}^T \tag{6.32}$$

When a component has rigid body freedom, special ‘inertia relief’ attachment modes are used where an equilibrated system of loads is applied to the component.

Two of the most common CMS methods will now be presented in detail, the free interface method and the fixed interface method.

6.4 Free interface method

The free interface method combines free interface substructure normal modes with residual attachment modes. In general the free interface method is more difficult to implement than the fixed interface method, but has some specific advantages in the test verification of FE models [6.6]. The method presented below was first proposed by Rubin [6.7]. It incorporates the effects of residual flexibility in both the component mass and stiffness matrices. An earlier method proposed by MacNeal [6.8] only considered the effects of residual flexibility on the component stiffness matrix.

Let the transformation of the displacement d.o.f. to the generalised d.o.f. for a structure be given by

$$\mathbf{x} = \boldsymbol{\upsilon}\mathbf{p} = \begin{bmatrix} \boldsymbol{\varphi}_k & \boldsymbol{\upsilon}_d \end{bmatrix} \begin{bmatrix} \mathbf{p}_k \\ \mathbf{p}_d \end{bmatrix} \tag{6.33}$$

where $\boldsymbol{\varphi}_k$ are the kept normal free interface modes, $\boldsymbol{\upsilon}_d$ are the residual attachment modes corresponding to the deleted modes which are defined in equation (6.32). Consider as before, two coupled components (α and β) that have a common boundary or interface. The d.o.f. of $\mathbf{p}$ can be ordered as in equation (6.20) into dependent and linearly independent coordinates, such that

$$\mathbf{p} = \begin{bmatrix} \mathbf{p}_d^{(\alpha)} \\ \mathbf{p}_d^{(\beta)} \\ \hdashline \mathbf{p}_k^{(\alpha)} \\ \mathbf{p}_k^{(\beta)} \end{bmatrix} \tag{6.34}$$

In order to form a free interface solution to the equation of motion for the structure from equation (6.23), the terms $\boldsymbol{\mu}$, $\boldsymbol{\kappa}$, $\mathbf{C}$ and $\mathbf{S}$ must be formed. From equation (6.14) the expression for the component $\boldsymbol{\mu}^{(i)}$ is given by

$$\boldsymbol{\mu}^{(i)} = \boldsymbol{\upsilon}^{(i)T} \mathbf{M}^{(i)} \boldsymbol{\upsilon}^{(i)} \tag{6.35}$$

Substituting $\boldsymbol{\upsilon}^{(i)}$ into this expression gives

$$\boldsymbol{\mu}^{(i)} = \begin{bmatrix} \boldsymbol{\varphi}_k^{(i)T} \\ \boldsymbol{\upsilon}_d^{(i)T} \end{bmatrix} \mathbf{M}^{(i)} \begin{bmatrix} \boldsymbol{\varphi}_k^{(i)} & \boldsymbol{\upsilon}_d^{(i)} \end{bmatrix} \tag{6.36}$$

$\boldsymbol{\mu}^{(i)}$ can be partitioned into sub-matrices arising from kept or deleted modes thus

$$\boldsymbol{\mu}^{(i)} = \begin{bmatrix} \boldsymbol{\mu}_{kk}^{(i)} & \boldsymbol{\mu}_{kd}^{(i)} \\ \boldsymbol{\mu}_{dk}^{(i)} & \boldsymbol{\mu}_{dd}^{(i)} \end{bmatrix} \tag{6.37}$$

From equation (6.36) it can be shown that

$$\begin{aligned} \boldsymbol{\mu}_{kk}^{(i)} &= \mathbf{I}_{kk}^{(i)} \\ \boldsymbol{\mu}_{kd}^{(i)} &= \boldsymbol{\mu}_{dk}^{(i)T} = \mathbf{0} \\ \boldsymbol{\mu}_{dd}^{(i)} &= \boldsymbol{\upsilon}_d^{(i)T} \mathbf{M}^{(i)} \boldsymbol{\upsilon}_d^{(i)} \end{aligned} \tag{6.38}$$

Substituting the expression for $\boldsymbol{\upsilon}_d$ from equation (6.32) into that for $\boldsymbol{\mu}_{dd}^{(i)}$ above gives

$$\boldsymbol{\mu}_{dd}^{(i)} = \boldsymbol{\varphi}_d^{(i)} \begin{bmatrix} diag\left(\lambda_j^{(i)}\right)_d & \mathbf{0} \\ \mathbf{0} & \ddots \end{bmatrix}^{-1} \begin{bmatrix} diag\left(\lambda_j^{(i)}\right)_d & \mathbf{0} \\ \mathbf{0} & \ddots \end{bmatrix}^{-1} \boldsymbol{\varphi}_{cd}^{(i)T} \tag{6.39}$$

Using a similar method expressions for $\boldsymbol{\kappa}^{(i)}$ can be shown to be given by

$$\begin{aligned} \boldsymbol{\kappa}_{kk}^{(i)} &= \begin{bmatrix} diag\left(\lambda_j^{(i)}\right)_{kk} & \mathbf{0} \\ \mathbf{0} & \ddots \end{bmatrix} \\ \boldsymbol{\kappa}_{kd}^{(i)} &= \boldsymbol{\kappa}_{dk}^{(i)T} = \mathbf{0} \\ \boldsymbol{\kappa}_{dd}^{(i)} &= \boldsymbol{\upsilon}_{cd}^{(i)} \end{aligned} \tag{6.40}$$

These expressions for component level $\boldsymbol{\mu}$ and $\boldsymbol{\kappa}$ can be used to form the global expressions from equation (6.15) (these are re-ordered to the format in equation (6.34))

$$\boldsymbol{\mu} = \begin{bmatrix} \boldsymbol{\mu}_{dd}^{(\alpha)} & \mathbf{0} & \mathbf{0} & \mathbf{0} \\ \mathbf{0} & \boldsymbol{\mu}_{dd}^{(\beta)} & \mathbf{0} & \mathbf{0} \\ \mathbf{0} & \mathbf{0} & \mathbf{I}_{kk}^{(\alpha)} & \mathbf{0} \\ \mathbf{0} & \mathbf{0} & \mathbf{0} & \mathbf{I}_{kk}^{(\beta)} \end{bmatrix} \tag{6.41}$$

$$\boldsymbol{\kappa} = \begin{bmatrix} \boldsymbol{\kappa}_{dd}^{(\alpha)} & \mathbf{0} & \mathbf{0} & \mathbf{0} \\ \mathbf{0} & \boldsymbol{\kappa}_{dd}^{(\beta)} & \mathbf{0} & \mathbf{0} \\ \mathbf{0} & \mathbf{0} & diag\left(\lambda_j^{(\alpha)}\right)_{kk} & \mathbf{0} \\ \mathbf{0} & \mathbf{0} & \mathbf{0} & diag\left(\lambda_j^{(\beta)}\right)_{kk} \end{bmatrix} \tag{6.42}$$

The constraint matrix $\mathbf{C}$ can be formed from the constraint equation. The first of these is given by equation (6.8) namely

$$\mathbf{x}_c^{(\alpha)} - \mathbf{x}_c^{(\beta)} = \mathbf{0} \tag{6.43}$$

The second constraint equation must be formed thus. The general undamped equation of motion for a component is given by (the component superscripts have been dropped for convenience)

$$\mathbf{M}\ddot{\mathbf{x}} + \mathbf{K}\mathbf{x} = \mathbf{F} \tag{6.44}$$

Using equations (6.33) and (6.14) this can be transformed to generalised coordinates as

$$\boldsymbol{\mu}_{kk}\ddot{\mathbf{p}}_k + \boldsymbol{\kappa}_{kk}\mathbf{p}_k = \boldsymbol{\varphi}_k^T\mathbf{F} \tag{6.45}$$

$$\boldsymbol{\mu}_{dd}\ddot{\mathbf{p}}_d + \boldsymbol{\kappa}_{dd}\mathbf{p}_d = \boldsymbol{\upsilon}_d^T\mathbf{F} \tag{6.46}$$

These equations are uncoupled since the modes $\boldsymbol{\varphi}_k$ are orthogonal to $\boldsymbol{\varphi}_d$, and from equation (6.32) the modes $\boldsymbol{\upsilon}_d$ are a linear combination of those in $\boldsymbol{\varphi}_d$.

The response at $\mathbf{p}_d$ will now be approximated as a pseudo-static response by ignoring the contribution from $\ddot{\mathbf{p}}_d$, such that

$$\boldsymbol{\kappa}_{dd}\mathbf{p}_d \cong \boldsymbol{\upsilon}_d^T\mathbf{F} \tag{6.47}$$

Under free vibration conditions the only forces arise from coupling forces $\mathbf{f}_c$. Combining this with $\boldsymbol{\kappa}_{dd} = \boldsymbol{\upsilon}_d{}^T\mathbf{K}\boldsymbol{\upsilon}_d$ from equation (6.14), the value of $\boldsymbol{\upsilon}_d$ from equation (6.32) and pre-multiplying the expression for $\mathbf{K}^{-1}$ in equation (6.29), equation (6.47) becomes

$$\left(\boldsymbol{\varphi}_{cd} \begin{bmatrix} diag\left(\lambda_j\right)_d & \mathbf{0} \\ \mathbf{0} & \ddots \end{bmatrix}^{-1} \boldsymbol{\varphi}_{cd}{}^{T} \right) \left(\mathbf{p}_d - \mathbf{f}_c \right) \cong \mathbf{0} \tag{6.48}$$

As the first part of this expression is non-singular then $\mathbf{p}_d \cong \mathbf{f}_c$. Since from equation (6.9) $\mathbf{f}_c^{(\alpha)} + \mathbf{f}_c^{(\beta)} = 0$, then $\mathbf{p}_d^{(\alpha)} + \mathbf{p}_d^{(\beta)} = 0$. This can be used as the second constraint equation.

Combining these constraint equations it can be shown that

$$\mathbf{C} = \begin{bmatrix} \mathbf{C}_{DD} & \mathbf{C}_{Dl} \end{bmatrix} = \left[\begin{array}{cc|cc} \boldsymbol{\upsilon}_{cd}^{(\alpha)} & -\boldsymbol{\upsilon}_{cd}^{(\beta)} & \boldsymbol{\varphi}_{ck}^{(\alpha)} & -\boldsymbol{\varphi}_{ck}^{(\beta)} \\ \mathbf{I} & \mathbf{I} & \mathbf{0} & \mathbf{0} \end{array}\right] \tag{6.49}$$

The expression for $\mathbf{S}$ is given by equation (6.21) as

$$\mathbf{S} = \begin{bmatrix} -\mathbf{C}_{DD}^{-1}\mathbf{C}_{Dl} \\ \mathbf{I}_{ll} \end{bmatrix} \tag{6.50}$$

It can be shown that $\mathbf{C}_{DD}^{-1}$ is given by

$$\mathbf{C}_{DD}^{-1} = \begin{bmatrix} \mathbf{c} & \mathbf{c}\boldsymbol{\upsilon}_{cd}^{(\beta)} \\ -\mathbf{c} & \left(\mathbf{I} - \mathbf{c}\boldsymbol{\upsilon}_{cd}^{(\beta)}\right) \end{bmatrix} \tag{6.51}$$

where $\mathbf{c} = \left[\boldsymbol{\upsilon}_{cd}^{(\alpha)} + \boldsymbol{\upsilon}_{cd}^{(\beta)} \right]^{-1}$ which from equation (6.40) can also be written as $\mathbf{c} = \left[\boldsymbol{\kappa}_{dd}^{(\alpha)} + \boldsymbol{\kappa}_{dd}^{(\beta)} \right]^{-1}$. Combining (6.49), (6.50) and (6.51) results in the transformation matrix

$$\mathbf{S} = \begin{bmatrix} -\mathbf{c}\boldsymbol{\varphi}_{ck}^{(\alpha)} & \mathbf{c}\boldsymbol{\varphi}_{ck}^{(\beta)} \\ \mathbf{c}\boldsymbol{\varphi}_{ck}^{(\alpha)} & -\mathbf{c}\boldsymbol{\varphi}_{ck}^{(\beta)} \\ \mathbf{I} & \mathbf{0} \\ \mathbf{0} & \mathbf{I} \end{bmatrix} \tag{6.52}$$

All of the terms $\boldsymbol{\mu}$, $\boldsymbol{\kappa}$ and $\mathbf{S}$, have been formed and hence a solution to the system equation of motion for the structure can be found. From equation (6.23)

$$\mathbf{M}_q \ddot{\mathbf{q}} + \mathbf{K}_q \mathbf{q} = \mathbf{0} \tag{6.53}$$

where $\mathbf{M_q} = \mathbf{S}^T \boldsymbol{\mu} \mathbf{S}$ and $\mathbf{K_q} = \mathbf{S}^T \boldsymbol{\kappa} \mathbf{S}$. Evaluating the uncoupled mass and stiffness matrices for the structure they can be seen to have special forms thus

$$\mathbf{M_q} = \begin{bmatrix} \mathbf{M_q}^{(\alpha\alpha)} & \mathbf{M_q}^{(\alpha\beta)} \\ \mathbf{M_q}^{(\beta\alpha)} & \mathbf{M_q}^{(\beta\beta)} \end{bmatrix} \tag{6.54}$$

$$\mathbf{K_q} = \begin{bmatrix} \mathbf{K_q}^{(\alpha\alpha)} & \mathbf{K_q}^{(\alpha\beta)} \\ \mathbf{K_q}^{(\beta\alpha)} & \mathbf{K_q}^{(\beta\beta)} \end{bmatrix} \tag{6.55}$$

where

$$\mathbf{K_q}^{(\alpha\alpha)} = \begin{bmatrix} diag\left(\lambda_j^{(\alpha)}\right)_k & \mathbf{0} \\ \mathbf{0} & \ddots \end{bmatrix} + \boldsymbol{\varphi}_{ck}^{(\alpha)T} \mathbf{c} \boldsymbol{\varphi}_{ck}^{(\alpha)} \tag{6.56}$$

$$\mathbf{K_q}^{(\alpha\beta)} = \left(\mathbf{K_q}^{(\alpha\beta)}\right)^T = -\boldsymbol{\varphi}_{ck}^{(\alpha)T} \mathbf{c} \boldsymbol{\varphi}_{ck}^{(\beta)} \tag{6.57}$$

$$\mathbf{K_q}^{(\beta\beta)} = \begin{bmatrix} diag\left(\lambda_j^{(\beta)}\right)_k & \mathbf{0} \\ \mathbf{0} & \ddots \end{bmatrix} + \boldsymbol{\varphi}_{ck}^{(\beta)T} \mathbf{c} \boldsymbol{\varphi}_{ck}^{(\beta)} \tag{6.58}$$

$$\mathbf{M_q}^{(\alpha a)} = \mathbf{I}_{kk}^{(\alpha)} + \boldsymbol{\varphi}_{ck}^{(\alpha)T} \mathbf{d} \boldsymbol{\varphi}_{ck}^{(\alpha)} \tag{6.59}$$

$$\mathbf{d} = \mathbf{c}^T \left[\boldsymbol{\mu}_{dd}^{(\alpha)} + \boldsymbol{\mu}_{dd}^{(\beta)} \right] \mathbf{c} \tag{6.60}$$

$$\mathbf{M_q}^{(\alpha\beta)} = \left(\mathbf{M_q}^{(\alpha\beta)}\right)^T = -\boldsymbol{\varphi}_{ck}^{(\alpha)T} \mathbf{d} \boldsymbol{\varphi}_{ck}^{(\beta)} \tag{6.61}$$

$$\mathbf{M_q}^{(\beta\beta)} = \mathbf{I}_{kk}^{(\beta)} + \boldsymbol{\varphi}_{ck}^{(\beta)T} \mathbf{d} \boldsymbol{\varphi}_{ck}^{(\beta)} \tag{6.62}$$

The global eigenvalues and vectors are found from $\left[\mathbf{K_q} - \lambda_p \mathbf{M_q}\right] \boldsymbol{\varphi}_p = 0$ where $\boldsymbol{\varphi}_p$ is the p'th global modeshape and λ_p is the p'th global eigenvalue.

The p'th global modeshape given by $\boldsymbol{\varphi}_p$, relates the component modal degrees of freedom to the global modal degrees of freedom, thus it expresses the modeshape in terms of the subsystem component modes. These modeshapes are assumed to be mass normalised and can be related to the physical global eigenvectors $\boldsymbol{\psi}_p$ by the following transformation

$$\boldsymbol{\psi}_p = \mathbf{S} \boldsymbol{\varphi}_p \tag{6.63}$$

In general the free interface method is more difficult to implement than the fixed interface method, however free interface eigenvalues are much easier to obtain experimentally than fixed interface measurements. The potential use of measured free interface component eigenvalues in a fixed interface CMS model is discussed in chapter 7.

6.5 Fixed interface method

The fixed interface method uses fixed interface normal modes as trial functions. By definition the fixed interface modes always have zero displacement at the component interfaces and so do not alone represent a complete set for the global response. The constraint modes are therefore used in conjunction with the fixed interface modes, to ensure continuity across the component junctions. Hurty [6.1] proposed an approach using fixed interface normal modes combined with rigid-body modes and redundant interface constraint modes. This was later simplified by Craig and Bampton [6.2] to combine the rigid-body modes and redundant interface constraint modes into a single set of constraint modes. This method is presented below.

From equation (6.10) the physical d.o.f. $\mathbf{x}$ may be characterised by a set of generalised coordinates $\mathbf{p}$ by the transformation

$$\mathbf{x} = \boldsymbol{\upsilon}\mathbf{p} \tag{6.64}$$

The d.o.f. for each substructure can be partitioned into interior and coupling d.o.f. as in equation (6.3)

$$\mathbf{x}^{(i)} = \begin{bmatrix} \mathbf{x}_i^{(i)} \\ \mathbf{x}_c^{(i)} \end{bmatrix} \tag{6.65}$$

The assumed mode matrix consists of 'kept' fixed interface normal modes $\boldsymbol{\varphi}_k$ and a set of coupling constraint modes $\boldsymbol{\gamma}$ (equation (6.28)). This can be partitioned into interior and coupling d.o.f. thus (the component superscript has been dropped for convenience)

$$\begin{bmatrix} \mathbf{x}_i \\ \mathbf{x}_c \end{bmatrix} = \begin{bmatrix} \boldsymbol{\varphi}_{ik} & \boldsymbol{\upsilon}_{ic} \\ \mathbf{0} & \mathbf{I}_{cc} \end{bmatrix} \begin{bmatrix} \mathbf{p}_k \\ \mathbf{p}_c \end{bmatrix} \tag{6.66}$$

and it can be seen that $\mathbf{x}_c = \mathbf{p}_c$. Also, from equation (6.27) $\boldsymbol{\upsilon}_{ic} = -\left(\mathbf{k}_{ii}\right)^{-1}\mathbf{k}_{ic}$.

From equation (6.14)

$$\begin{aligned}\boldsymbol{\mu} &= \boldsymbol{\upsilon}^T\mathbf{M}\boldsymbol{\upsilon}\\ \boldsymbol{\kappa} &= \boldsymbol{\upsilon}^T\mathbf{K}\boldsymbol{\upsilon}\end{aligned} \tag{6.67}$$

Partitioning $\boldsymbol{\mu}$ and expanding

$$\boldsymbol{\mu} = \begin{bmatrix}\boldsymbol{\mu}_{kk} & \boldsymbol{\mu}_{kc}\\ \boldsymbol{\mu}_{ck} & \boldsymbol{\mu}_{cc}\end{bmatrix} = \begin{bmatrix}\boldsymbol{\varphi}_{ik} & \mathbf{0}\\ \boldsymbol{\upsilon}_{ic} & \mathbf{I}_{cc}\end{bmatrix}\begin{bmatrix}\mathbf{m}_{ii} & \mathbf{m}_{ic}\\ \mathbf{m}_{ci} & \mathbf{m}_{cc}\end{bmatrix}\begin{bmatrix}\boldsymbol{\varphi}_{ik} & \boldsymbol{\upsilon}_{ic}\\ \mathbf{0} & \mathbf{I}_{cc}\end{bmatrix} \tag{6.68}$$

Expanding gives,

$$\boldsymbol{\mu}_{kk} = \mathbf{I}_{kk} \tag{6.69}$$

$$\boldsymbol{\mu}_{kc} = \boldsymbol{\mu}_{ck}{}^T = \boldsymbol{\varphi}_{ik}{}^T\left(\mathbf{m}_{ii}\boldsymbol{\upsilon}_{ic} + \mathbf{m}_{ic}\right) \tag{6.70}$$

$$\boldsymbol{\mu}_{cc} = \boldsymbol{\upsilon}_{ic}{}^T\left(\mathbf{m}_{ii}\boldsymbol{\upsilon}_{ic} + \mathbf{m}_{ic}\right) + \mathbf{m}_{ci}\boldsymbol{\upsilon}_{ic} + \mathbf{m}_{cc} \tag{6.71}$$

Similarly $\boldsymbol{\kappa}$ can be partitioned and expanded to give

$$\boldsymbol{\kappa}_{kk} = \begin{bmatrix}diag\left(\lambda_j\right)_k & \mathbf{0}\\ \mathbf{0} & \ddots\end{bmatrix} \tag{6.72}$$

$$\boldsymbol{\kappa}_{kc} = \boldsymbol{\kappa}_{ck}^T = \mathbf{0} \tag{6.73}$$

$$\boldsymbol{\kappa}_{cc} = \mathbf{k}_{cc} - \mathbf{k}_{ci}\left(\mathbf{k}_{ii}\right)^{-1}\mathbf{k}_{ic} \tag{6.74}$$

Consider as before, two coupled components (α and β) that have a common boundary or interface. The d.o.f. of $\mathbf{p}$ can be ordered into kept and coupling coordinates for each component, such that

$$\mathbf{p} = \begin{bmatrix}\mathbf{p}_k^{(\alpha)}\\ \mathbf{p}_c^{(\alpha)}\\ \mathbf{p}_k^{(\beta)}\\ \mathbf{p}_c^{(\beta)}\end{bmatrix} \tag{6.75}$$

Since $\mathbf{x}_c^{(\alpha)} = \mathbf{p}_c^{(\alpha)}$ and $\mathbf{x}_c^{(\beta)} = \mathbf{p}_c^{(\beta)}$, the displacement constraint condition given in (6.8) i.e. $\mathbf{x}_c^{(\alpha)} = \mathbf{x}_c^{(\beta)}$ can be written as

$$\left[\mathbf{0} \quad \mathbf{I} \quad \mathbf{0} \mid -\mathbf{I}\right] \begin{bmatrix} \mathbf{p}_k^{(\alpha)} \\ \mathbf{p}_c^{(\alpha)} \\ \mathbf{p}_k^{(\beta)} \\ \hdashline \mathbf{p}_c^{(\beta)} \end{bmatrix} = \mathbf{0} \tag{6.76}$$

From equation (6.20)

$$\left[\mathbf{C}_{DD} \quad \mathbf{C}_{Dl}\right] \begin{bmatrix} \mathbf{p}_D \\ \mathbf{p}_l \end{bmatrix} = \mathbf{0} \tag{6.77}$$

If $\mathbf{p}_c^{(\beta)}$ is assumed to be the dependent coordinate, and the order of equation (6.77) is reversed then the constraint matrix $\mathbf{C}$ can be seen to be

$$\mathbf{C} = \left[\mathbf{0} \quad \mathbf{I} \quad \mathbf{0} \mid -\mathbf{I}\right] \tag{6.78}$$

From equation (6.21), namely

$$\mathbf{p} \equiv \begin{bmatrix} \mathbf{p}_D \\ \mathbf{p}_l \end{bmatrix} = \begin{bmatrix} -\mathbf{C}_{DD}^{-1}\mathbf{C}_{Dl} \\ \mathbf{I}_{ll} \end{bmatrix} \mathbf{p}_l \equiv \mathbf{S}\mathbf{q} \tag{6.79}$$

and $\mathbf{p}_c^{(\alpha)} = \mathbf{p}_c^{(\beta)}$, $\mathbf{S}$ can be found ($\mathbf{q}$ has been ordered to separate the normal modes coordinates from the coupling coordinates)

$$\begin{bmatrix} \mathbf{p}_k^{(\alpha)} \\ \mathbf{p}_c^{(\alpha)} \\ \mathbf{p}_k^{(\beta)} \\ \mathbf{p}_c^{(\beta)} \end{bmatrix} = \begin{bmatrix} \mathbf{I} & \mathbf{0} & \mathbf{0} \\ \mathbf{0} & \mathbf{0} & \mathbf{I} \\ \mathbf{0} & \mathbf{I} & \mathbf{0} \\ \mathbf{0} & \mathbf{0} & \mathbf{I} \end{bmatrix} \begin{bmatrix} \mathbf{p}_k^{(\alpha)} \\ \mathbf{p}_k^{(\beta)} \\ \mathbf{p}_c^{(\alpha)} \end{bmatrix} \tag{6.80}$$

The uncoupled system mass and stiffness matrices $\mathbf{M_q}$ and $\mathbf{K_q}$ can now be formed from $\mathbf{S}$ and the system $\boldsymbol{\mu}$ and $\boldsymbol{\kappa}$ (formed from the component $\boldsymbol{\mu}$ and $\boldsymbol{\kappa}$ as in equation (6.15)).

From $\mathbf{M_q} = \mathbf{S}^T \boldsymbol{\mu} \mathbf{S}$

$$\mathbf{M_q} = \begin{bmatrix} \mathbf{I} & \mathbf{0} & \mathbf{0} & \mathbf{0} \\ \mathbf{0} & \mathbf{0} & \mathbf{I} & \mathbf{0} \\ \mathbf{0} & \mathbf{I} & \mathbf{0} & \mathbf{I} \end{bmatrix} \begin{bmatrix} \boldsymbol{\mu}_{kk}^{(\alpha)} & \boldsymbol{\mu}_{kc}^{(\alpha)} & \mathbf{0} & \mathbf{0} \\ \boldsymbol{\mu}_{ck}^{(\alpha)} & \boldsymbol{\mu}_{cc}^{(\alpha)} & \mathbf{0} & \mathbf{0} \\ \mathbf{0} & \mathbf{0} & \boldsymbol{\mu}_{kk}^{(\beta)} & \boldsymbol{\mu}_{kc}^{(\beta)} \\ \mathbf{0} & \mathbf{0} & \boldsymbol{\mu}_{ck}^{(\beta)} & \boldsymbol{\mu}_{cc}^{(\beta)} \end{bmatrix} \begin{bmatrix} \mathbf{I} & \mathbf{0} & \mathbf{0} \\ \mathbf{0} & \mathbf{0} & \mathbf{I} \\ \mathbf{0} & \mathbf{I} & \mathbf{0} \\ \mathbf{0} & \mathbf{0} & \mathbf{I} \end{bmatrix} \tag{6.81}$$

This has a special format such that

$$\mathbf{M_q} = \begin{bmatrix} \mathbf{I}_{kk}^{(\alpha)} & \mathbf{0} & \boldsymbol{\mu}_{kc}^{(\alpha)} \\ \mathbf{0} & \mathbf{I}_{kk}^{(\beta)} & \boldsymbol{\mu}_{kc}^{(\beta)} \\ \boldsymbol{\mu}_{kc}^{(\alpha)T} & \boldsymbol{\mu}_{kc}^{(\beta)T} & \boldsymbol{\mu}_{cc}^{(\alpha)} + \boldsymbol{\mu}_{cc}^{(\beta)} \end{bmatrix} \tag{6.82}$$

Similarly $\mathbf{K_q}$ can be shown to be given by

$$\mathbf{K_q} = \begin{bmatrix} diag\left(\lambda_j^{(\alpha)}\right)_k & \mathbf{0} & \mathbf{0} \\ \mathbf{0} & diag\left(\lambda_j^{(\beta)}\right)_k & \mathbf{0} \\ \mathbf{0} & \mathbf{0} & \boldsymbol{\kappa}_{cc}^{(\alpha)} + \boldsymbol{\kappa}_{cc}^{(\beta)} \end{bmatrix} \tag{6.83}$$

As in the free interface method, the global eigenvalues and vectors are found from $\left[\mathbf{K_q} - \lambda_p \mathbf{M_q}\right] \boldsymbol{\varphi}_p = 0$ where $\boldsymbol{\varphi}_p$ is the p'th global modeshape and λ_p is the p'th global eigenvalue. The p'th global modeshape given by $\boldsymbol{\varphi}_p$, relates the component modal degrees of freedom to the global modal degrees of freedom. These modeshapes are related to the physical global eigenvectors $\boldsymbol{\psi}_p$ by the following transformation

$$\boldsymbol{\psi}_p = \mathbf{S} \boldsymbol{\varphi}_p \tag{6.84}$$

The fixed interface method is probably one of the most popular CMS methods. It produces very accurate results even with relatively few component modes [6.9]. The mass and stiffness matrices $\mathbf{M_q}$ and $\mathbf{K_q}$ are relatively easy to formulate and in addition they are sparse.

6.6 Damping

The techniques introduced so far have neglected damping. If the damping matrix is given by $\boldsymbol{\zeta}$, then the uncoupled damping matrix, $\mathbf{Z}$, can be formed in the same manner as the mass and stiffness matrices, thus

$$\mathbf{Z} = \mathbf{S}^T \boldsymbol{\zeta} \mathbf{S} \tag{6.85}$$

For example, if the damping is assumed to be proportional, for the fixed interface method with time harmonic excitation at ω, the uncoupled damping matrix is given by [6.10]

$$\mathbf{Z} = \frac{1}{\omega} \begin{bmatrix} \eta^{(\alpha)} diag\left(\lambda_j^{(\alpha)}\right) & \mathbf{0} & \mathbf{0} \\ \mathbf{0} & \eta^{(\beta)} diag\left(\lambda_j^{(\alpha)}\right) & \mathbf{0} \\ \mathbf{0} & \mathbf{0} & \eta^{(\alpha)} \boldsymbol{\kappa}_{cc}^{(\alpha)} + \eta^{(\beta)} \boldsymbol{\kappa}_{cc}^{(\beta)} \end{bmatrix} \tag{6.86}$$

The disadvantage of this expression is that the damping must be calculated for all the frequency points of interest.

6.7 Conclusions

In the first section of this chapter the concept of using component mode synthesis (CMS) techniques along with traditional approximations was introduced. The procedure was outlined in general and potential areas for data reduction were highlighted. The theory behind the CMS method was introduced; in particular two of the most popular CMS techniques have been presented in detail. The free interface method combines free interface substructure normal modes with residual flexibility modes. The free interface method is more complicated to implement than the fixed interface method, and the resultant uncoupled system mass and stiffness matrices are not sparse. Conversely the fixed interface method uses fixed interface normal modes combined with displacement constraint modes as assumed component modes. It is somewhat simpler than the free interface method, the appropriate terms are easily formed and the resulting uncoupled mass and stiffness matrices are comparatively sparse. It produces very accurate results even with relatively few component modes. For these reasons the fixed interface method will be applied in the following chapters to investigate the propagation of uncertainty

within a structure. In particular, the concept of only including uncertainty in the local component fixed interface modes, and assuming constant displacement constraint modes, will be investigated. In addition the potential use of free interface normal mode statistics in a fixed interface model will be investigated.

In chapter 7 the propagation of uncertainty from the component physical properties to the component modal properties will be examined. Expressions for the statistics of the component eigenvalues in terms of the statistics of the physical properties will be generated. In addition, the effect of this uncertainty on the uncoupled mass and stiffness matrices for the fixed interface CMS method will be explored. In chapter 8 the fixed interface CMS method will be used to propagate the uncertainty from a local component modal level to the global structural response. Expressions will be developed to express the statistics of the global modal response in terms of the statistics of the local component modes.

7. Uncertainty from component physical properties to component modal properties

In chapter 6 a process was outlined for performing a modal analysis of a structure with variable properties and potential areas for reducing the computational cost were highlighted. In this chapter the first stage of that process, i.e. the propagation of uncertainty from the component physical properties to the component modal properties will be examined. The process is outlined in Figure 6-4.

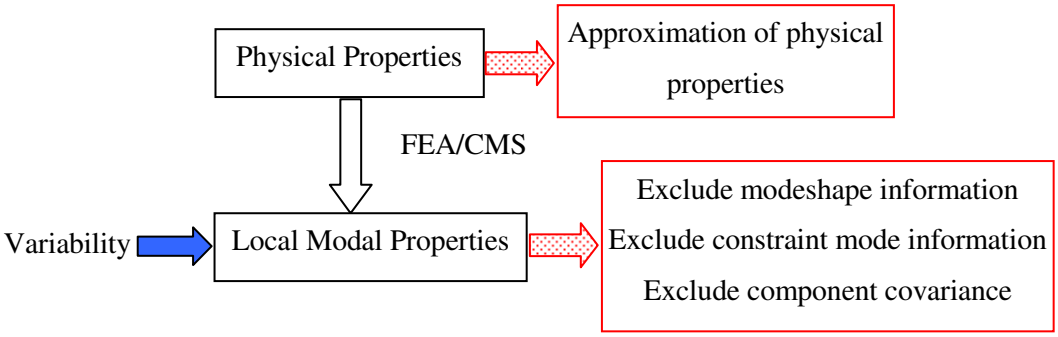

Figure 7-1 Potential areas for data reduction and approximation.

The aim is to relate the statistics of the variability in the physical properties to the variability in the local modal properties, to understand the potential areas for approximation and to quantify any information lost through use of these approximations. The following chapter is organised into three main sections. In the first section the mathematical expressions relating the statistics of the variability in the physical properties to the variability in the modal properties, are determined. In addition, the effect of physical property uncertainty on the uncoupled mass and stiffness matrices of a fixed interface CMS model is explored. As discussed in chapter 6, the fixed interface CMS method is somewhat simpler to implement than the free interface method. The uncoupled mass and stiffness matrices are easily formed and comparatively sparse, and it produces very accurate results with relatively few component modes. In the next section these expressions are reviewed and discussed in the context of the potential areas of data reduction listed in chapter 6. Finally, in the last section a numerical example is presented and, through the use of a Monte Carlo simulation, each potential area for data reduction is evaluated.

7.1 Relating physical property variability to local modal variability

In this section expressions relating the variability in local modal properties to the variability in the physical properties are obtained. Firstly the baseline system in introduced and nomenclature defined. Variability is introduced into the system's physical properties in section 7.1.2. The statistics of the uncertainty in the physical properties are assumed to be known and the levels of variability are assumed to be small such as those seen in the manufacturing production of nominally identical structures. The relationship between the physical property variability and the variability in the free interface local eigenvalues and eigenvectors is established in sections 7.1.3 and 7.1.4. A perturbational approach is used to relate their statistics, and comments are made on the possible distribution of the modal properties. The same method is applied to obtain the statistics of the fixed interface modal properties in terms of the statistics of the physical properties. Finally expressions are obtained for the constituent parts of the uncoupled mass and stiffness matrices for a fixed interface CMS format.

For simplicity, unless otherwise stated, all eigenvectors are assumed to be mass normalised.

7.1.1 The baseline system

As discussed in chapter 6, the undamped equation of motion for a component or substructure is given by

$$\mathbf{M}^{(i)}\ddot{\mathbf{x}}^{(i)} + \mathbf{K}^{(i)}\mathbf{x}^{(i)} = \mathbf{F}^{(i)} \tag{7.1}$$

where $\mathbf{x}^{(i)}$ is the vector of physical d.o.f., $\mathbf{M}^{(i)}$ and $\mathbf{K}^{(i)}$ are the component mass and stiffness matrices and $\mathbf{F}^{(i)}$ is the vector of external forces. For a component with n degrees of freedom, the mass and stiffness are of order $n \times n$, and the vectors of displacement and external forces are of order $1 \times n$. In this chapter the superscript i denoting the *i*'th component, will be dropped for convenience and all the matrices are assumed to be component matrices unless otherwise stated. An over-bar is used to represent the baseline or nominal unperturbed values; hence the equation of motion for the unperturbed component is given by

$$\bar{\mathbf{M}}\ddot{\mathbf{x}} + \bar{\mathbf{K}}\mathbf{x} = \bar{\mathbf{F}} \tag{7.2}$$

The eigenfrequencies and eigenvectors of the baseline system can be found from an eigensolution of this equation, with $\bar{\mathbf{F}} = \mathbf{0}$, thus

$$\left[\bar{\mathbf{K}} - \bar{\lambda}_j \bar{\mathbf{M}}\right]\bar{\boldsymbol{\varphi}}_j = \mathbf{0} \tag{7.3}$$

where $\bar{\lambda}_j$ is the *j*'th local eigenvalue and $\bar{\boldsymbol{\varphi}}_j$ is the *j*'th local eigenvector which is assumed to be mass normalised. The physical degrees of freedom $\mathbf{x}$ can be transposed to the modal degrees of freedom $\mathbf{y}$ by

$$\mathbf{x} = \bar{\boldsymbol{\varphi}}\mathbf{y} \tag{7.4}$$

Substituting equation (7.4) into equation (7.3) and pre-multiplying by $\bar{\boldsymbol{\varphi}}^T$ gives

$$\bar{\boldsymbol{\varphi}}^T \bar{\mathbf{M}} \bar{\boldsymbol{\varphi}} \ddot{\mathbf{y}} + \bar{\boldsymbol{\varphi}}^T \bar{\mathbf{K}} \bar{\boldsymbol{\varphi}} \mathbf{y} = \mathbf{0} \tag{7.5}$$

The mass and stiffness matrices are now uncoupled and contain no off diagonal elements.

$$\begin{aligned} \bar{\mathbf{M}}_j &= \bar{\boldsymbol{\varphi}}^T \bar{\mathbf{M}} \bar{\boldsymbol{\varphi}} \\ \bar{\mathbf{K}}_j &= \bar{\boldsymbol{\varphi}}_j{}^T \bar{\mathbf{K}} \bar{\boldsymbol{\varphi}} \end{aligned} \tag{7.6}$$

The eigenvectors were assumed to be mass normalised and hence

$$\begin{aligned} \bar{\mathbf{M}}_j &= \mathbf{I} \\ diag\left(\bar{\mathbf{K}}_j\right) &= \left\{\bar{\lambda}_j\right\} \end{aligned} \tag{7.7}$$

The modes are orthogonal such that if $i \neq j$

$$\begin{aligned} \bar{\boldsymbol{\varphi}}_i{}^T \bar{\mathbf{M}} \bar{\boldsymbol{\varphi}}_j &= 0 \\ \bar{\boldsymbol{\varphi}}_i{}^T \bar{\mathbf{K}} \bar{\boldsymbol{\varphi}}_j &= 0 \end{aligned} \tag{7.8}$$

7.1.2 Introducing variability into the physical properties

Let the mass and stiffness of the system be variable such that

$$\begin{aligned} \mathbf{M} &= \bar{\mathbf{M}} + \Delta\bar{\mathbf{M}} \\ \mathbf{K} &= \bar{\mathbf{K}} + \Delta\bar{\mathbf{K}} \end{aligned} \tag{7.9}$$

where $\Delta\bar{\mathbf{M}}$ and $\Delta\bar{\mathbf{K}}$ are of order $n \times n$ and given by,

$$\begin{aligned} \Delta\bar{\mathbf{M}} &= \bar{\mathbf{M}} \bullet \boldsymbol{\varepsilon}^{(m)} \\ \Delta\bar{\mathbf{K}} &= \bar{\mathbf{K}} \bullet \boldsymbol{\varepsilon}^{(k)} \end{aligned} \tag{7.10}$$

the dot product is defined as the Hadamard element-wise multiplication and, $\boldsymbol{\varepsilon}^{(m)}$ and $\boldsymbol{\varepsilon}^{(k)}$ are matrices of small random variables that possess some symmetry, such that

$$\begin{aligned} \mathbf{M} &= \bar{\mathbf{M}} \bullet \left(\mathbf{1} + \boldsymbol{\varepsilon}^{(m)} \right) \\ \mathbf{K} &= \bar{\mathbf{K}} \bullet \left(\mathbf{1} + \boldsymbol{\varepsilon}^{(k)} \right) \end{aligned} \tag{7.11}$$

No assumptions are made at this stage as to whether these variations are correlated or independent, and no assumptions are made about their distribution. They are assumed to have zero mean such that the mean or expected value of the component mass and stiffness are their baseline or unperturbed values. In practice correlations would normally exist between the variability in the mass and stiffness of a component. For example, if the cross-sectional area of a component varied, this would affect both its mass and stiffness properties. In addition spatial correlations may arise from manufacturing processes.

The general equation for the free vibration of the perturbed component is given by

$$\mathbf{M}\ddot{\mathbf{x}} + \mathbf{K}\mathbf{x} = \mathbf{0} \tag{7.12}$$

or

$$\left[\bar{\mathbf{M}} + \Delta\bar{\mathbf{M}} \right] \ddot{\mathbf{x}} + \left[\bar{\mathbf{K}} + \Delta\bar{\mathbf{K}} \right] \mathbf{x} = \mathbf{0} \tag{7.13}$$

The modes of the original component could be used to transform this to the baseline modal degrees of freedom. This can be done by substituting equation (7.4) into equation (7.13) and pre-multiplying by $\bar{\boldsymbol{\varphi}}^T$

$$\left[\bar{\boldsymbol{\varphi}}^T \bar{\mathbf{M}} \bar{\boldsymbol{\varphi}} + \bar{\boldsymbol{\varphi}}^T \Delta\bar{\mathbf{M}} \bar{\boldsymbol{\varphi}} \right] \ddot{\mathbf{y}} + \left[\bar{\boldsymbol{\varphi}}^T \bar{\mathbf{K}} \bar{\boldsymbol{\varphi}} + \bar{\boldsymbol{\varphi}}^T \Delta\bar{\mathbf{K}} \bar{\boldsymbol{\varphi}} \right] \mathbf{y} = \mathbf{0} \tag{7.14}$$

Using equation (7.7) this can be re-arranged as

$$\left[\mathbf{I}+\bar{\boldsymbol{\varphi}}^T\Delta\bar{\mathbf{M}}\bar{\boldsymbol{\varphi}}\right]\ddot{\mathbf{y}}+\left[diag\left\{\bar{\lambda}_j\right\}+\bar{\boldsymbol{\varphi}}^T\Delta\bar{\mathbf{K}}\bar{\boldsymbol{\varphi}}\right]\mathbf{y}=\mathbf{0} \tag{7.15}$$

This will relate the degrees of freedom to the modal degrees of freedom of the baseline system; this is not the same as the modal degrees of freedom of the variable system and therefore the equations are not uncoupled. Some data reduction can be achieved if a reduced set of baseline modes are used in the transformation, i.e. the number of modes used is less than the number of physical degrees of freedom.

7.1.3 Effect on free interface eigenvalues

A first order perturbation approximation can be used to relate the variations in the physical properties to the resultant variations in the free interface eigenvalues of the component. The free interface eigenvalues and eigenvectors are obtained from the solution to

$$\left(\mathbf{K}-\lambda_j\mathbf{M}\right)\boldsymbol{\varphi}_j=\mathbf{0},\ \ j=1,2,...,n \tag{7.16}$$

Applying a first order mean centred perturbation as introduced in chapter 4, an approximation of the eigenvalues is given by

$$\lambda_j\cong\bar{\lambda}_j+\left(\frac{\partial\lambda_j(\boldsymbol{\varepsilon})}{\partial\boldsymbol{\varepsilon}}\right)^T\Bigg|_{\boldsymbol{\varepsilon}=\boldsymbol{\mu}_\varepsilon}\boldsymbol{\varepsilon} \tag{7.17}$$

where

$$\frac{\partial\lambda_j(\boldsymbol{\varepsilon})}{\partial\boldsymbol{\varepsilon}}\Bigg|_{\boldsymbol{\varepsilon}=\boldsymbol{\mu}_\varepsilon}=\begin{bmatrix}\bar{\boldsymbol{\varphi}}_j^{\,T}\left[\dfrac{\partial\mathbf{K}}{\partial\varepsilon_1}-\bar{\lambda}_j\dfrac{\partial\mathbf{M}}{\partial\varepsilon_1}\right]\bar{\boldsymbol{\varphi}}_j\\ \bar{\boldsymbol{\varphi}}_j^{\,T}\left[\dfrac{\partial\mathbf{K}}{\partial\varepsilon_2}-\lambda_j\dfrac{\partial\mathbf{M}}{\partial\varepsilon_2}\right]\bar{\boldsymbol{\varphi}}_j\\ \vdots\\ \bar{\boldsymbol{\varphi}}_j^{\,T}\left[\dfrac{\partial\mathbf{K}}{\partial\varepsilon_i}-\lambda_j\dfrac{\partial\mathbf{M}}{\partial\varepsilon_i}\right]\bar{\boldsymbol{\varphi}}_j\end{bmatrix} \tag{7.18}$$

and where $\boldsymbol{\varepsilon}_i$ is the i'th element of the variability vector $\boldsymbol{\varepsilon}$ which contains all the variability elements from $\boldsymbol{\varepsilon}^{(m)}$ and $\boldsymbol{\varepsilon}^{(k)}$, and $\boldsymbol{\mu}_\varepsilon$ is the vector of mean values of $\boldsymbol{\varepsilon}$. By definition for an n d.o.f. component (if all the baseline modes are kept) the order of $\boldsymbol{\varepsilon}$ is $n(n+1)$. As in chapter 5 this can be expressed in a shortened format as

$$\lambda_j \cong \bar{\lambda}_j + \mathbf{A}_{j\lambda}{}^T \boldsymbol{\varepsilon} \tag{7.19}$$

where $\mathbf{A}_{j\lambda} = \left.\dfrac{\partial \lambda_j(\boldsymbol{\varepsilon})}{\partial \boldsymbol{\varepsilon}}\right|_{\boldsymbol{\varepsilon}=\boldsymbol{\mu}_\varepsilon}$. The subscript '$j\lambda$' is used here to distinguish this from a similar term used later for the eigenvectors. The partial derivative $\dfrac{\partial \mathbf{K}}{\partial \varepsilon_i}$ is given by

$$\frac{\partial \mathbf{K}}{\partial \varepsilon_i} = \frac{\partial\left(\bar{\mathbf{K}} + \bar{\mathbf{K}} \bullet \boldsymbol{\varepsilon}^{(k)}\right)}{\partial \varepsilon_i} \tag{7.20}$$

which as $\dfrac{\partial \bar{\mathbf{K}}}{\partial \varepsilon_i} = 0$ gives

$$\frac{\partial \mathbf{K}}{\partial \varepsilon_i} = \bar{\mathbf{K}} \bullet \frac{\partial \boldsymbol{\varepsilon}^{(k)}}{\partial \varepsilon_i} \tag{7.21}$$

Similarly the partial derivative $\dfrac{\partial \mathbf{M}}{\partial \varepsilon_i}$ is given by

$$\frac{\partial \mathbf{M}}{\partial \varepsilon_i} = \bar{\mathbf{M}} \bullet \frac{\partial \boldsymbol{\varepsilon}^{(m)}}{\partial \varepsilon_i} \tag{7.22}$$

Substituting these results into equation (7.19), the first order approximation of the component eigenvalues is given by

$$\lambda_j \cong \bar{\lambda}_j + \mathbf{A}_{j\lambda}{}^T \boldsymbol{\varepsilon} \tag{7.23}$$

where

$$\mathbf{A}_{j\lambda} = \begin{bmatrix} \bar{\boldsymbol{\varphi}}_j{}^T \left[\bar{\mathbf{K}} \bullet \dfrac{\partial \boldsymbol{\varepsilon}^{(k)}}{\partial \varepsilon_1} - \bar{\lambda}_j \bar{\mathbf{M}} \bullet \dfrac{\partial \boldsymbol{\varepsilon}^{(m)}}{\partial \varepsilon_1} \right] \bar{\boldsymbol{\varphi}}_j \\ \bar{\boldsymbol{\varphi}}_j{}^T \left[\bar{\mathbf{K}} \bullet \dfrac{\partial \boldsymbol{\varepsilon}^{(k)}}{\partial \varepsilon_2} - \bar{\lambda}_j \bar{\mathbf{M}} \bullet \dfrac{\partial \boldsymbol{\varepsilon}^{(m)}}{\partial \varepsilon_2} \right] \bar{\boldsymbol{\varphi}}_j \\ \vdots \\ \bar{\boldsymbol{\varphi}}_j{}^T \left[\bar{\mathbf{K}} \bullet \dfrac{\partial \boldsymbol{\varepsilon}^{(k)}}{\partial \varepsilon_i} - \bar{\lambda}_j \bar{\mathbf{M}} \bullet \dfrac{\partial \boldsymbol{\varepsilon}^{(m)}}{\partial \varepsilon_i} \right] \bar{\boldsymbol{\varphi}}_j \end{bmatrix} \tag{7.24}$$

As the terms in $\boldsymbol{\varepsilon}^{(m)}$ and $\boldsymbol{\varepsilon}^{(k)}$ were assumed to have zero mean, the mean or expected value of the perturbed component eigenvalues, is the baseline value $\mu_{\lambda_j} = E\left[\lambda_j\right] \cong \bar{\lambda}_j$.

Variance of the free interface eigenvalues

Of particular interest is the variance or spread of the variability in the eigenvalues and its relationship to the variance in the physical properties. Such an expression for the variance of the component eigenvalues, can be calculated from the expression in equation (7.23). In a similar manner to that used for the two DOF system in equation (5.32), if the variabilities are assumed to have zero mean $\boldsymbol{\mu}_{\boldsymbol{\varepsilon}} = \mathbf{0}$, then it can be shown that

$$\mathrm{var}\left(\delta_{\lambda_j}\right) \cong \mathbf{A}_{j\lambda}{}^{T}\, \mathrm{var}(\boldsymbol{\varepsilon})\, \mathbf{A}_{j\lambda} \tag{7.25}$$

where $\delta_{\lambda_j} = \left(\lambda_j - \bar{\lambda}_j\right)$ such that $\delta_{\lambda_j} \cong \mathbf{A}_{j\lambda}{}^{T}\boldsymbol{\varepsilon}$, and $\mathrm{var}(\boldsymbol{\varepsilon})$ is the variance/covariance matrix of the variability terms given by

$$\mathrm{var}(\boldsymbol{\varepsilon}) = \begin{bmatrix} \sigma_{\varepsilon_1}^2 & \sigma_{\varepsilon_1\varepsilon_2} & \cdots & \sigma_{\varepsilon_1\varepsilon_i} & \cdots \\ \sigma_{\varepsilon_1\varepsilon_2} & \sigma_{\varepsilon_2}^2 & \cdots & \sigma_{\varepsilon_2\varepsilon_i} & \cdots \\ \vdots & \vdots & \ddots & \cdots & \cdots \\ \sigma_{\varepsilon_1\varepsilon_i} & \sigma_{\varepsilon_2\varepsilon_i} & \sigma_{\varepsilon_3\varepsilon_i} & \sigma_{\varepsilon_i}^2 & \cdots \\ \vdots & \vdots & \vdots & \vdots & \ddots \end{bmatrix} \tag{7.26}$$

Similarly $\mathrm{var}\left(\delta_{\lambda_j}\right)$ is the variance of the change in the perturbed eigenvalues. This directly relates the variance of the perturbed component eigenvalues to the variance and covariance of the uncertain mass and stiffness matrices. One potential area for approximation or data reduction is to simplify the variability within the physical properties by discounting the covariance between the mass and stiffness terms.

Distribution of the free interface eigenvalues

The distribution of the component eigenvalues is of interest to the propagation of the uncertainty to the global eigenvalues, which will be discussed further in chapter 8. Of particular relevance is the extent to which the component eigenvalues are Gaussian or close to Gaussian distributed. The expression for the variability in the component eigenvalues in terms of the variability in the physical properties, equation (7.23), can be used to obtain an expression for the distribution of the component eigenvalues.

From equation (7.23)

$$\lambda_j \cong \overline{\lambda}_j + \mathbf{A}_{j\lambda}^T \boldsymbol{\varepsilon} \tag{7.27}$$

The multivariate expression for the change of variable method for a general function $\mathbf{y}_n = y_n(\mathbf{x}_n)$, where it is assumed that $\mathbf{y}_n$ is an n-valued function of $\mathbf{x}_n$ as discussed in chapter 4, is given by

$$p(\mathbf{y}) = \frac{np(\mathbf{x})}{\mathbf{J}} \tag{7.28}$$

where

$$p(y_1, y_2, ..., y_n) = \frac{np(x_1, x_2, .., x_n)}{\begin{vmatrix} \frac{\partial y_1}{\partial x_1} & \frac{\partial y_1}{\partial x_2} & \cdots & \frac{\partial y_1}{\partial x_n} \\ \frac{\partial y_2}{\partial x_1} & \frac{\partial y_2}{\partial x_2} & \cdots & \frac{\partial y_2}{\partial x_n} \\ \cdots & \cdots & \cdots & \cdots \\ \frac{\partial y_n}{\partial x_1} & \frac{\partial y_n}{\partial x_2} & \cdots & \frac{\partial y_n}{\partial x_n} \end{vmatrix}} \tag{7.29}$$

The order of the expression for the perturbed component eigenvalues from equation (7.23) is at most $2n^2$ for an n d.o.f. component (if all the baseline modes are kept). Assuming this to be the case then a number of 'dummy' output variables must be introduced which can be later removed from the resultant expression by integration. As we already have one required output variable, i.e. λ_j, then $2n^2 - 1$ 'dummy' output variables will be required. These can be selected to be equivalent to a subset of the input variables, e.g. $y_1 = \lambda_j$, $y_2 = \varepsilon_1$, $y_3 = \varepsilon_2$ etc. such that

$$p(\lambda_j, \varepsilon_1, \cdots, \varepsilon_{2n^2-1}) = \frac{2n^2 p(\varepsilon_1, \varepsilon_2, \cdots, \varepsilon_i, \cdots, \varepsilon_{2n^2})}{|\mathbf{J}|} \tag{7.30}$$

This relates the PDF of the free interface eigenvalues to the PDF of the uncertainty in the physical properties. Some broad comments can be made on the form of this relationship. If the uncertainty terms in $\boldsymbol{\varepsilon}$ that arise from the mass and stiffness variability are independent then the resultant distribution of the eigenvalues will tend towards a Gaussian distribution. This is by virtue of the fuzzy central limit theorem [7.6] whereby it is assumed that none of the variables exerts a much larger influence than the others. Thus, if the uncertainties in the physical

properties are small and unrelated, and many in number, then the *j*'th component eigenvalue will be approximately Gaussian distributed. However, it is reasonable to assume that the variations in the physical properties are related in some way due to manufacturing processes or material properties. Some further generalisations of the central limit theorems allow some 'weak' dependence of the random variables, such as the m-dependent central limit theorem, the martingale central limit theorem and the central limit theorem for mixing processes [7.2], [7.6].

In section 7.3 a numerical example will be considered and a Monte Carlo simulation used to compare the distribution of the free interface eigenvalues to those obtained from an eigensolution.

Second order perturbation

A more accurate approximation of the eigenvalues can be obtained by calculating the second order term in the perturbation expansion. It is proposed that this term could be used as an indication of the likely error in using a first order approximation. The equation for a mean centred second order perturbation approximation of the eigensolution is given in chapter 4 as

$$\lambda_j \cong \bar{\lambda}_j + \underbrace{\left(\frac{\partial \lambda_j}{\partial \boldsymbol{\varepsilon}}\right)^T\Bigg|_{\boldsymbol{\varepsilon}=\boldsymbol{\mu}_\varepsilon} \boldsymbol{\varepsilon}}_{\text{first order}} + \underbrace{\frac{1}{2}(\boldsymbol{\varepsilon})^T \mathbf{D}_{\lambda_j}\Big|_{\boldsymbol{\varepsilon}=\boldsymbol{\mu}_\varepsilon} \boldsymbol{\varepsilon}}_{\text{second order}} \tag{7.31}$$

where

$$\left\{\mathbf{D}_{\lambda_j}\right\}_{il} = \frac{\partial^2 \lambda_j}{\partial \varepsilon_i \partial \varepsilon_l}\Bigg|_{\boldsymbol{\varepsilon}=\boldsymbol{\mu}_\varepsilon} \tag{7.32}$$

$$\begin{aligned}\frac{\partial^2 \lambda_j}{\partial \varepsilon_i \partial \varepsilon_l} = & \bar{\boldsymbol{\varphi}}_j{}^T \left[\frac{\partial^2 \mathbf{K}}{\partial \varepsilon_i \partial \varepsilon_l} - \bar{\lambda}_j \frac{\partial^2 \mathbf{M}}{\partial \varepsilon_i \partial \varepsilon_l}\right] \bar{\boldsymbol{\varphi}}_j - \left(\bar{\boldsymbol{\varphi}}_j{}^T \frac{\partial \mathbf{M}}{\partial \varepsilon_i} \bar{\boldsymbol{\varphi}}_j\right)\left(\bar{\boldsymbol{\varphi}}_j{}^T G_{lj} \bar{\boldsymbol{\varphi}}_j\right) \\ & - \left(\bar{\boldsymbol{\varphi}}_j{}^T \frac{\partial \mathbf{M}}{\partial \varepsilon_l} \bar{\boldsymbol{\varphi}}_j\right)\left(\bar{\boldsymbol{\varphi}}_j{}^T G_{ij} \bar{\boldsymbol{\varphi}}_j\right) + 2 \sum_{\substack{r=1 \\ r \neq j}}^{n} \frac{\left(\bar{\boldsymbol{\varphi}}_j{}^T G_{ij} \bar{\boldsymbol{\varphi}}_j\right)\left(\bar{\boldsymbol{\varphi}}_j{}^T G_{lj} \bar{\boldsymbol{\varphi}}_j\right)}{\lambda_j - \lambda_r}\end{aligned} \tag{7.33}$$

In a similar manner to the two DOF system examined in chapter 5, it can be shown that the second order term equates to

$$\frac{1}{2}(\boldsymbol{\varepsilon})^T\left[2\sum_{\substack{r=1\\ r\neq j}}^{n}\frac{\mathbf{A}_{j\lambda}\mathbf{A}_{j\lambda}{}^T}{\bar{\lambda}_j-\bar{\lambda}_r}-\mathbf{B}_j\mathbf{A}_{j\lambda}{}^T-\mathbf{A}_{j\lambda}\mathbf{B}_j{}^T\right]\boldsymbol{\varepsilon} \tag{7.34}$$

where $\mathbf{A}_{j\lambda}$ is given in equation (7.24) and $\mathbf{B}_j$ is given by

$$\mathbf{B}_j=\begin{bmatrix}\bar{\boldsymbol{\varphi}}_j{}^T\dfrac{\partial\mathbf{M}}{\partial\varepsilon_1}\bar{\boldsymbol{\varphi}}_j\\ \bar{\boldsymbol{\varphi}}_j{}^T\dfrac{\partial\mathbf{M}}{\partial\varepsilon_2}\bar{\boldsymbol{\varphi}}_j\\ \vdots\\ \bar{\boldsymbol{\varphi}}_j{}^T\dfrac{\partial\mathbf{M}}{\partial\varepsilon_i}\bar{\boldsymbol{\varphi}}_j\end{bmatrix} \tag{7.35}$$

7.1.4 Effect on the free interface eigenvectors

A first order approximation for the eigenvectors of a perturbed system is given in chapter 4. It consists of a linear combination of the unperturbed eigenvectors. For the component, the *j*'th perturbed eigenvector is given by

$$\boldsymbol{\varphi}_j\cong\bar{\boldsymbol{\varphi}}_j+\sum_i\left(-\frac{1}{2}\bar{\boldsymbol{\varphi}}_j{}^T\frac{\partial\mathbf{M}}{\partial\varepsilon_i}\bar{\boldsymbol{\varphi}}_j\bar{\boldsymbol{\varphi}}_j\varepsilon_i+\sum_{\substack{p=1\\ p\neq j}}^{n}\frac{\bar{\boldsymbol{\varphi}}_p{}^T\left[\dfrac{\partial\mathbf{K}}{\partial\varepsilon_i}-\bar{\lambda}_j\dfrac{\partial\mathbf{M}}{\partial\varepsilon_i}\right]\bar{\boldsymbol{\varphi}}_j}{\bar{\lambda}_j-\bar{\lambda}_p}\bar{\boldsymbol{\varphi}}_p\varepsilon_i\right) \tag{7.36}$$

where the index p gives all the component modes and n is the d.o.f. of the component. In a similar manner to the two DOF, equation (7.36) can be written as

$$\boldsymbol{\varphi}_j\cong\bar{\boldsymbol{\varphi}}_j-\frac{1}{2}\mathbf{B}_j{}^T\boldsymbol{\varepsilon}\bar{\boldsymbol{\varphi}}_j+\sum_{\substack{p=1\\ p\neq j}}^{n}\frac{1}{\bar{\lambda}_j-\bar{\lambda}_p}\mathbf{A}_{j\boldsymbol{\varphi}}{}^T\boldsymbol{\varepsilon}\bar{\boldsymbol{\varphi}}_p \tag{7.37}$$

where $\mathbf{B}_j$ is given in equation (7.35) and $\mathbf{A}_{j\boldsymbol{\varphi}}$ is similar to $\mathbf{A}_{j\lambda}$ and given by

$$\mathbf{A}_{j\varphi} = \begin{bmatrix} \bar{\boldsymbol{\varphi}}_p{}^T \left[\bar{\mathbf{K}} \bullet \dfrac{\partial \boldsymbol{\varepsilon}^{(k)}}{\partial \varepsilon_1} - \bar{\lambda}_j \bar{\mathbf{M}} \bullet \dfrac{\partial \boldsymbol{\varepsilon}^{(m)}}{\partial \varepsilon_1} \right] \bar{\boldsymbol{\varphi}}_j \\ \bar{\boldsymbol{\varphi}}_p{}^T \left[\bar{\mathbf{K}} \bullet \dfrac{\partial \boldsymbol{\varepsilon}^{(k)}}{\partial \varepsilon_2} - \bar{\lambda}_j \bar{\mathbf{M}} \bullet \dfrac{\partial \boldsymbol{\varepsilon}^{(m)}}{\partial \varepsilon_2} \right] \bar{\boldsymbol{\varphi}}_j \\ \vdots \\ \bar{\boldsymbol{\varphi}}_p{}^T \left[\bar{\mathbf{K}} \bullet \dfrac{\partial \boldsymbol{\varepsilon}^{(k)}}{\partial \varepsilon_i} - \bar{\lambda}_j \bar{\mathbf{M}} \bullet \dfrac{\partial \boldsymbol{\varepsilon}^{(m)}}{\partial \varepsilon_i} \right] \bar{\boldsymbol{\varphi}}_j \end{bmatrix} \tag{7.38}$$

7.1.5 Effect on fixed interface modal properties

In the previous sections the effect of variations in the physical properties on the free interface eigenvalues and eigenvectors of the component have been investigated. However, the fixed interface eigenvalues and eigenvectors are also of interest as the fixed interface CMS method as presented in chapter 6, provides a convenient method for connecting several components together to form a structure. The free-interface relationships developed in the previous section can be applied to a subset of the mass and stiffness matrices.

In order to fix the coupling or interface d.o.f. the variable physical mass and stiffness matrices as defined in equation (7.11) are partitioned into interior and coupling d.o.f. thus

$$\mathbf{K} = \begin{bmatrix} \mathbf{k}_{ii} & \mathbf{k}_{ic} \\ \mathbf{k}_{ic}{}^T & \mathbf{k}_{cc} \end{bmatrix} = \begin{bmatrix} \bar{\mathbf{k}}_{ii} & \bar{\mathbf{k}}_{ic} \\ \bar{\mathbf{k}}_{ic}{}^T & \bar{\mathbf{k}}_{cc} \end{bmatrix} \bullet \left(\begin{bmatrix} \mathbf{1} & \mathbf{1} \\ \mathbf{1} & \mathbf{1} \end{bmatrix} + \begin{bmatrix} \boldsymbol{\varepsilon}_{ii}{}^{(k)} & \boldsymbol{\varepsilon}_{ic}{}^{(k)} \\ \boldsymbol{\varepsilon}_{ic}{}^{(k)T} & \boldsymbol{\varepsilon}_{cc}{}^{(k)} \end{bmatrix} \right) \tag{7.39}$$

$$\mathbf{M} = \begin{bmatrix} \mathbf{m}_{ii} & \mathbf{m}_{ic} \\ \mathbf{m}_{ci} & \mathbf{m}_{cc} \end{bmatrix} = \begin{bmatrix} \bar{\mathbf{m}}_{ii} & \bar{\mathbf{m}}_{ic} \\ \bar{\mathbf{m}}_{ic}{}^T & \bar{\mathbf{m}}_{cc} \end{bmatrix} \bullet \left(\begin{bmatrix} \mathbf{1} & \mathbf{1} \\ \mathbf{1} & \mathbf{1} \end{bmatrix} + \begin{bmatrix} \boldsymbol{\varepsilon}_{ii}{}^{(m)} & \boldsymbol{\varepsilon}_{ic}{}^{(m)} \\ \boldsymbol{\varepsilon}_{ic}{}^{(m)T} & \boldsymbol{\varepsilon}_{cc}{}^{(m)} \end{bmatrix} \right) \tag{7.40}$$

where the subscript i represents interior d.o.f. and c coupling d.o.f. The first order approximation of the free interface eigenvalues from equation (7.23) can be expressed in terms of these partitioned matrices. The fixed interface eigenvalues can be obtained from the eigensolution for a component whose interface d.o.f. are fixed or constrained,

$$\left(\mathbf{k}_{ii} - \left(\lambda_F \right)_j \mathbf{m}_{ii} \right) \left(\boldsymbol{\varphi}_F \right)_j = \mathbf{0}, \;\; j = 1, 2, ..., n \tag{7.41}$$

where $(\lambda_F)_j$ is the *j*'th fixed interface eigenvalue and $(\boldsymbol{\varphi}_F)_j$ is the *j*'th fixed interface eigenvector. The first order perturbation approximation for the fixed interface eigenvalues can be found from a reduced form of the free interface solution,

$$(\lambda_F)_j \cong (\bar{\lambda}_F)_j + \mathbf{A}_{j\lambda F}{}^{\mathrm{T}}\ \boldsymbol{\varepsilon} \tag{7.42}$$

where $\mathbf{A}_{j\lambda F}$ is given by

$$\mathbf{A}_{j\lambda F} = \begin{bmatrix} (\bar{\boldsymbol{\varphi}}_F)_j^T \left[\bar{\mathbf{k}}_{ii} \bullet \frac{\partial \boldsymbol{\varepsilon}_{ii}^{(k)}}{\partial \varepsilon_1} - (\bar{\lambda}_F)_j \bar{\mathbf{m}}_{ii} \bullet \frac{\partial \boldsymbol{\varepsilon}_{ii}^{(m)}}{\partial \varepsilon_1} \right] (\bar{\boldsymbol{\varphi}}_F)_j \\ (\bar{\boldsymbol{\varphi}}_F)_j^T \left[\bar{\mathbf{k}}_{ii} \bullet \frac{\partial \boldsymbol{\varepsilon}_{ii}^{(k)}}{\partial \varepsilon_2} - (\bar{\lambda}_F)_j \bar{\mathbf{m}}_{ii} \bullet \frac{\partial \boldsymbol{\varepsilon}_{ii}^{(m)}}{\partial \varepsilon_2} \right] (\bar{\boldsymbol{\varphi}}_F)_j \\ \vdots \\ (\bar{\boldsymbol{\varphi}}_F)_j^T \left[\bar{\mathbf{k}}_{ii} \bullet \frac{\partial \boldsymbol{\varepsilon}_{ii}^{(k)}}{\partial \varepsilon_i} - (\bar{\lambda}_F)_j \bar{\mathbf{m}}_{ii} \bullet \frac{\partial \boldsymbol{\varepsilon}_{ii}^{(m)}}{\partial \varepsilon_i} \right] (\bar{\boldsymbol{\varphi}}_F)_j \end{bmatrix} \tag{7.43}$$

and $(\bar{\boldsymbol{\varphi}}_F)_j$ are the unperturbed fixed interface eigenvectors.

Variance of the fixed interface eigenvalues

In a similar manner to the free interface eigenvalues, the variance of the fixed interface eigenvalues can be estimated as

$$\mathrm{var}\left(\delta_{(\lambda_F)_j}\right) \cong \mathbf{A}_{j\lambda F}{}^{T}\ \mathrm{var}(\boldsymbol{\varepsilon})\mathbf{A}_{j\lambda F} \tag{7.44}$$

where $\delta_{(\lambda_F)_j} = \left((\lambda_F)_j - (\bar{\lambda}_F)_j\right)$ such that $\delta_{(\lambda_F)_j} \cong \mathbf{A}_{j\lambda F}{}^{T}\boldsymbol{\varepsilon}$. This directly relates the variance of the fixed interface eigenvalues to the variance and covariance of the variations in the mass and stiffness.

Distribution of the fixed interface eigenvalues

The distribution of the fixed interface eigenvalues can be calculated in a similar manner to that used for the free interface values. However, without any specific knowledge of the component and the uncertainty, the same general conclusions will be drawn as for the free interface

eigenvalues. Namely that, if the uncertainty terms are independent, or weakly dependent, small, and many in number, then the eigenvalues will be approximately Gaussian distributed.

Fixed interface eigenvectors

In a similar manner to the free interface eigenvectors, a first order approximation for the fixed interface eigenvectors of the perturbed system can be generated from a linear combination of the unperturbed eigenvectors thus

$$\left(\boldsymbol{\varphi}_F\right)_j \cong \left(\bar{\boldsymbol{\varphi}}_F\right)_j - \frac{1}{2}\mathbf{B}_{jF}{}^T\boldsymbol{\varepsilon}\left(\bar{\boldsymbol{\varphi}}_F\right)_j + \sum_{\substack{p=1 \\ p\neq j}}^{n} \frac{1}{\left(\bar{\lambda}_F\right)_j - \left(\bar{\lambda}_F\right)_p}\mathbf{A}_{j\boldsymbol{\varphi}F}{}^T\boldsymbol{\varepsilon}\left(\bar{\boldsymbol{\varphi}}_F\right)_p \tag{7.45}$$

where $\mathbf{B}_{jF}$ and $\mathbf{A}_{j\boldsymbol{\varphi}F}$ are given by

$$\mathbf{B}_{jF} = \begin{bmatrix} \left(\bar{\boldsymbol{\varphi}}_F\right)_j^T \left(\bar{\mathbf{m}}_{ii} \bullet \frac{\partial \boldsymbol{\varepsilon}_{ii}^{(m)}}{\partial \varepsilon_1}\right)\left(\bar{\boldsymbol{\varphi}}_F\right)_j \\ \left(\bar{\boldsymbol{\varphi}}_F\right)_j^T \left(\bar{\mathbf{m}}_{ii} \bullet \frac{\partial \boldsymbol{\varepsilon}_{ii}^{(m)}}{\partial \varepsilon_2}\right)\left(\bar{\boldsymbol{\varphi}}_F\right)_j \\ \vdots \\ \left(\bar{\boldsymbol{\varphi}}_F\right)_j^T \left(\bar{\mathbf{m}}_{ii} \bullet \frac{\partial \boldsymbol{\varepsilon}_{ii}^{(m)}}{\partial \varepsilon_i}\right)\left(\bar{\boldsymbol{\varphi}}_F\right)_j \end{bmatrix} \tag{7.46}$$

$$\mathbf{A}_{j\boldsymbol{\varphi}F} = \begin{bmatrix} \left(\bar{\boldsymbol{\varphi}}_F\right)_p^T \left[\bar{\mathbf{k}}_{ii} \bullet \frac{\partial \boldsymbol{\varepsilon}_{ii}^{(k)}}{\partial \varepsilon_1} - \left(\bar{\lambda}_F\right)_j \left(\bar{\mathbf{m}}_{ii} \bullet \frac{\partial \boldsymbol{\varepsilon}_{ii}^{(m)}}{\partial \varepsilon_1}\right)\right]\left(\bar{\boldsymbol{\varphi}}_F\right)_j \\ \left(\bar{\boldsymbol{\varphi}}_F\right)_p^T \left[\bar{\mathbf{k}}_{ii} \bullet \frac{\partial \boldsymbol{\varepsilon}_{ii}^{(k)}}{\partial \varepsilon_2} - \left(\bar{\lambda}_F\right)_j \left(\bar{\mathbf{m}}_{ii} \bullet \frac{\partial \boldsymbol{\varepsilon}_{ii}^{(m)}}{\partial \varepsilon_2}\right)\right]\left(\bar{\boldsymbol{\varphi}}_F\right)_j \\ \vdots \\ \left(\bar{\boldsymbol{\varphi}}_F\right)_p^T \left[\bar{\mathbf{k}}_{ii} \bullet \frac{\partial \boldsymbol{\varepsilon}_{ii}^{(k)}}{\partial \varepsilon_i} - \left(\bar{\lambda}_F\right)_j \left(\bar{\mathbf{m}}_{ii} \bullet \frac{\partial \boldsymbol{\varepsilon}_{ii}^{(m)}}{\partial \varepsilon_i}\right)\right]\left(\bar{\boldsymbol{\varphi}}_F\right)_j \end{bmatrix} \tag{7.47}$$

7.1.6 Effect on the constituents of the fixed interface CMS matrices

Thus far the effects of variations in the physical properties on the modal properties of a component have been investigated. However, when investigating the response of a structure that consists of several substructures the Component Mode Synthesis techniques discussed in

chapter 6 may be applied as an efficient analysis method. It is therefore of interest to understand the effect of variations in the physical parameters on the constituent parts of the uncoupled CMS mass and stiffness matrices. The fixed interface method is one of the most popular of the CMS techniques, as it produces very accurate results with relatively few component modes and the mass and stiffness matrices are relatively straightforward to formulate.

As presented in chapter 6 the uncoupled component mass and stiffness matrices for the fixed interface method were shown to be given by,

$$\boldsymbol{\kappa} = \begin{bmatrix} \boldsymbol{\kappa}_{kk} & \boldsymbol{\kappa}_{kc} \\ \boldsymbol{\kappa}_{ck} & \boldsymbol{\kappa}_{cc} \end{bmatrix} = \begin{bmatrix} \boldsymbol{\varphi}_{Fk} & \mathbf{0} \\ \boldsymbol{\upsilon}_{ic} & \mathbf{I}_{cc} \end{bmatrix} \begin{bmatrix} \mathbf{k}_{ii} & \mathbf{k}_{ic} \\ \mathbf{k}_{ci} & \mathbf{k}_{cc} \end{bmatrix} \begin{bmatrix} \boldsymbol{\varphi}_{Fk} & \boldsymbol{\upsilon}_{ic} \\ \mathbf{0} & \mathbf{I}_{cc} \end{bmatrix} \tag{7.48}$$

$$\boldsymbol{\mu} = \begin{bmatrix} \boldsymbol{\mu}_{kk} & \boldsymbol{\mu}_{kc} \\ \boldsymbol{\mu}_{ck} & \boldsymbol{\mu}_{cc} \end{bmatrix} = \begin{bmatrix} \boldsymbol{\varphi}_{Fk} & \mathbf{0} \\ \boldsymbol{\upsilon}_{ic} & \mathbf{I}_{cc} \end{bmatrix} \begin{bmatrix} \mathbf{m}_{ii} & \mathbf{m}_{ic} \\ \mathbf{m}_{ci} & \mathbf{m}_{cc} \end{bmatrix} \begin{bmatrix} \boldsymbol{\varphi}_{Fk} & \boldsymbol{\upsilon}_{ic} \\ \mathbf{0} & \mathbf{I}_{cc} \end{bmatrix} \tag{7.49}$$

where $\boldsymbol{\varphi}_{Fk}$ are the 'kept' fixed interface normal modeshapes and $\boldsymbol{\upsilon}_{ic}$ are the coupling constraint modes (the subscript *i* representing interior d.o.f., *c* representing coupling d.o.f. and *k* representing kept modes). They have a special form as shown below

$$\begin{bmatrix} \boldsymbol{\kappa}_{kk} & \boldsymbol{\kappa}_{kc} \\ \boldsymbol{\kappa}_{ck} & \boldsymbol{\kappa}_{cc} \end{bmatrix} = \begin{bmatrix} diag\left(\lambda_F\right)_j & \mathbf{0} \\ \mathbf{0} & \mathbf{k}_{cc} - \mathbf{k}_{ci}\left(\mathbf{k}_{ii}\right)^{-1}\mathbf{k}_{ic} \end{bmatrix} \tag{7.50}$$

$$\begin{bmatrix} \boldsymbol{\mu}_{kk} & \boldsymbol{\mu}_{kc} \\ \boldsymbol{\mu}_{ck} & \boldsymbol{\mu}_{cc} \end{bmatrix} = \begin{bmatrix} \mathbf{I}_{kk} & \boldsymbol{\varphi}_{Fk}{}^{T}\left(\mathbf{m}_{ii}\boldsymbol{\upsilon}_{ic} + \mathbf{m}_{ic}\right) \\ \left[\boldsymbol{\varphi}_{Fk}{}^{T}\left(\mathbf{m}_{ii}\boldsymbol{\upsilon}_{ic} + \mathbf{m}_{ic}\right)\right]^{T} & \boldsymbol{\upsilon}_{ic}{}^{T}\left(\mathbf{m}_{ii}\boldsymbol{\upsilon}_{ic} + \mathbf{m}_{ic}\right) + \mathbf{m}_{ci}\boldsymbol{\upsilon}_{ic} + \mathbf{m}_{cc} \end{bmatrix} \tag{7.51}$$

These can then be used to form the global uncoupled mass and stiffness matrices, $\mathbf{K_q}$ and $\mathbf{M_q}$ as given in chapter 6. It is of interest to generate approximate expression for $\boldsymbol{\kappa}$ and $\boldsymbol{\mu}$ in terms of the baseline component eigenvalues and eigenvectors, and the variability. The proposed approximations are outlined below.

Uncoupled fixed interface stiffness matrix $\boldsymbol{\kappa}$

Consider first the term of the uncoupled stiffness matrix $\boldsymbol{\kappa}$, which is a diagonal matrix $\boldsymbol{\kappa}_{kk}$ with the terms being the fixed interface local eigenvalues of the component, for which a first order approximation was given by equation (7.42), namely,

$$\boldsymbol{\kappa}_{kk} = diag\left(\lambda_F\right)_j \cong diag\left(\left(\bar{\lambda}_F\right)_j + \mathbf{A}_{j\lambda F}{}^T\boldsymbol{\varepsilon}\right) \tag{7.52}$$

where $\mathbf{A}_{j\lambda F}$ is as given in equation (7.43). The second term in the uncoupled stiffness matrix is $\boldsymbol{\kappa}_{cc}$ which is given by

$$\boldsymbol{\kappa}_{cc} = \mathbf{k}_{cc} - \mathbf{k}_{ci}\left(\mathbf{k}_{ii}\right)^{-1}\mathbf{k}_{ic} \tag{7.53}$$

Substituting the expression for the variable stiffness terms from equation (7.39) into the above expression results in

$$\boldsymbol{\kappa}_{cc} = \bar{\mathbf{k}}_{cc}\bullet\left(\mathbf{1}+\boldsymbol{\varepsilon}_{cc}{}^{(k)}\right) - \left(\bar{\mathbf{k}}_{ic}\bullet\left(\mathbf{1}+\boldsymbol{\varepsilon}_{ic}{}^{(k)}\right)\right)^T\left(\bar{\mathbf{k}}_{ii}\bullet\left(\mathbf{1}+\boldsymbol{\varepsilon}_{ii}{}^{(k)}\right)\right)^{-1}\left(\bar{\mathbf{k}}_{ic}\bullet\left(\mathbf{1}+\boldsymbol{\varepsilon}_{ic}{}^{(k)}\right)\right) \tag{7.54}$$

The inverse of a matrix can be transformed using the Woodbury formula [7.1] which is given by

$$\left(\mathbf{W}+\mathbf{U}\mathbf{V}^T\right)^{-1} = \mathbf{W}^{-1} - \left[\mathbf{W}^{-1}\mathbf{U}\left(\mathbf{I}+\mathbf{V}^T\mathbf{W}^{-1}\mathbf{U}\right)^{-1}\mathbf{V}^T\mathbf{W}^{-1}\right] \tag{7.55}$$

where $\mathbf{W}$ is an $n\times n$ invertible matrix, $\mathbf{U}$ and $\mathbf{V}$ are $n\times m$ where $m\le n$. Applying this to the term $\left(\bar{\mathbf{k}}_{ii}\bullet\left(\mathbf{1}+\boldsymbol{\varepsilon}_{ii}{}^{(k)}\right)\right)^{-1}$ in equation (7.54) gives

$$\left(\bar{\mathbf{k}}_{ii}\bullet\left(\mathbf{1}+\boldsymbol{\varepsilon}_{ii}{}^{(k)}\right)\right)^{-1} = \left(\bar{\mathbf{k}}_{ii}+\left(\bar{\mathbf{k}}_{ii}\bullet\boldsymbol{\varepsilon}_{ii}{}^{(k)}\right)\right)^{-1} = \bar{\mathbf{k}}_{ii}^{-1} - \left[\bar{\mathbf{k}}_{ii}^{-1}\left(\mathbf{I}+\left(\bar{\mathbf{k}}_{ii}\bullet\boldsymbol{\varepsilon}_{ii}{}^{(k)}\right)\bar{\mathbf{k}}_{ii}^{-1}\right)^{-1}\left(\bar{\mathbf{k}}_{ii}\bullet\boldsymbol{\varepsilon}_{ii}{}^{(k)}\right)\bar{\mathbf{k}}_{ii}^{-1}\right] \tag{7.56}$$

Substituting this into equation (7.54) gives $\boldsymbol{\kappa}_{cc}$ as

$$\boldsymbol{\kappa}_{cc} = \bar{\mathbf{k}}_{cc}\bullet\left(\mathbf{1}+\boldsymbol{\varepsilon}_{cc}{}^{(k)}\right) - \left(\bar{\mathbf{k}}_{ic}\bullet\left(\mathbf{1}+\boldsymbol{\varepsilon}_{ic}{}^{(k)}\right)\right)^T\left(\bar{\mathbf{k}}_{ii}^{-1} - \left[\bar{\mathbf{k}}_{ii}^{-1}\left(\mathbf{I}+\left(\bar{\mathbf{k}}_{ii}\bullet\boldsymbol{\varepsilon}_{ii}{}^{(k)}\right)\bar{\mathbf{k}}_{ii}^{-1}\right)^{-1}\left(\bar{\mathbf{k}}_{ii}\bullet\boldsymbol{\varepsilon}_{ii}{}^{(k)}\right)\bar{\mathbf{k}}_{ii}^{-1}\right]\right)\left(\bar{\mathbf{k}}_{ic}\bullet\left(\mathbf{1}+\boldsymbol{\varepsilon}_{ic}{}^{(k)}\right)\right) \tag{7.57}$$

This expression is still an exact expression for $\boldsymbol{\kappa}_{cc}$ in terms of the variability matrix $\boldsymbol{\varepsilon}^{(k)}$. However, if the variability is assumed to be small, such that $\boldsymbol{\varepsilon}^{(k)} \ll 1$ then the inverse term still remaining in equation (7.57) can be approximated as $\left(\mathbf{I}+\left(\bar{\mathbf{k}}_{ii}\bullet\boldsymbol{\varepsilon}_{ii}{}^{(k)}\right)\bar{\mathbf{k}}_{ii}^{-1}\right)^{-1} \cong \mathbf{I}$, therefore

$$\boldsymbol{\kappa}_{cc} \cong \bar{\mathbf{k}}_{cc} \bullet \left(\mathbf{1} + \boldsymbol{\varepsilon}_{cc}^{(k)}\right) - \left(\bar{\mathbf{k}}_{ic} \bullet \left(\mathbf{1} + \boldsymbol{\varepsilon}_{ic}^{(k)}\right)\right)^T \left(\bar{\mathbf{k}}_{ii}^{-1} - \bar{\mathbf{k}}_{ii}^{-1}\left(\bar{\mathbf{k}}_{ii} \bullet \boldsymbol{\varepsilon}_{ii}^{(k)}\right)\bar{\mathbf{k}}_{ii}^{-1}\right)\left(\bar{\mathbf{k}}_{ic} \bullet \left(\mathbf{1} + \boldsymbol{\varepsilon}_{ic}^{(k)}\right)\right) \quad (7.58)$$

It can be seen that as the variability terms tend towards zero, then equation (7.58) tends towards the value of $\boldsymbol{\kappa}_{cc}$ for the baseline system, i.e. $\bar{\mathbf{k}}_{cc} - \left(\bar{\mathbf{k}}_{ic}\right)^T \left(\bar{\mathbf{k}}_{ii}^{-1}\right)\left(\bar{\mathbf{k}}_{ic}\right)$.

Combining the expressions for $\boldsymbol{\kappa}_{kk}$ and $\boldsymbol{\kappa}_{cc}$, the uncoupled stiffness matrix is approximated as

$$\boldsymbol{\kappa} \cong \begin{bmatrix} diag\left(\left(\bar{\lambda}_F\right)_j + \mathbf{A}_{j\lambda F}{}^T \boldsymbol{\varepsilon}\right) & \mathbf{0} \\ \mathbf{0} & \bar{\mathbf{k}}_{cc} \bullet \left(\mathbf{1} + \boldsymbol{\varepsilon}_{cc}^{(k)}\right) - \left(\bar{\mathbf{k}}_{ic} \bullet \left(\mathbf{1} + \boldsymbol{\varepsilon}_{ic}^{(k)}\right)\right)^T \left(\bar{\mathbf{k}}_{ii}^{-1} - \bar{\mathbf{k}}_{ii}^{-1}\left(\bar{\mathbf{k}}_{ii} \bullet \boldsymbol{\varepsilon}_{ii}^{(k)}\right)\bar{\mathbf{k}}_{ii}^{-1}\right)\left(\bar{\mathbf{k}}_{ic} \bullet \left(\mathbf{1} + \boldsymbol{\varepsilon}_{ic}^{(k)}\right)\right) \end{bmatrix} \quad (7.59)$$

Uncoupled fixed interface mass matrix $\boldsymbol{\mu}$

In a similar manner expressions for the terms of the mass matrix $\boldsymbol{\mu}$ are now sought, from equation (7.51)

$$\boldsymbol{\mu} = \begin{bmatrix} \boldsymbol{\mu}_{kk} & \boldsymbol{\mu}_{kc} \\ \boldsymbol{\mu}_{ck} & \boldsymbol{\mu}_{cc} \end{bmatrix} = \begin{bmatrix} \mathbf{I}_{kk} & \boldsymbol{\varphi}_{Fk}{}^T \left(\mathbf{m}_{ii}\boldsymbol{\upsilon}_{ic} + \mathbf{m}_{ic}\right) \\ \left[\boldsymbol{\varphi}_{Fk}{}^T \left(\mathbf{m}_{ii}\boldsymbol{\upsilon}_{ic} + \mathbf{m}_{ic}\right)\right]^T & \boldsymbol{\upsilon}_{ic}{}^T \left(\mathbf{m}_{ii}\boldsymbol{\upsilon}_{ic} + \mathbf{m}_{ic}\right) + \mathbf{m}_{ci}\boldsymbol{\upsilon}_{ic} + \mathbf{m}_{cc} \end{bmatrix} \quad (7.60)$$

The expressions for $\mathbf{m}_{ii}$, $\mathbf{m}_{ic}$ and $\mathbf{m}_{cc}$ from equation (7.40) can be substituted into the above to obtain

$$\boldsymbol{\mu}_{cc} = \boldsymbol{\upsilon}_{ic}{}^T \left(\left(\bar{\mathbf{m}}_{ii} + \bar{\mathbf{m}}_{ii} \bullet \boldsymbol{\varepsilon}_{ii}^{(m)}\right)\boldsymbol{\upsilon}_{ic} + \bar{\mathbf{m}}_{ic} + \bar{\mathbf{m}}_{ic} \bullet \boldsymbol{\varepsilon}_{ic}^{(m)}\right) + \left(\bar{\mathbf{m}}_{ic} + \bar{\mathbf{m}}_{ic} \bullet \boldsymbol{\varepsilon}_{ic}^{(m)}\right)^T \boldsymbol{\upsilon}_{ic} + \bar{\mathbf{m}}_{cc} + \bar{\mathbf{m}}_{cc} \bullet \boldsymbol{\varepsilon}_{cc}^{(m)} \quad (7.61)$$

and

$$\boldsymbol{\mu}_{kc} = \boldsymbol{\varphi}_{Fk}{}^T \left(\left(\bar{\mathbf{m}}_{ii} + \bar{\mathbf{m}}_{ii} \bullet \boldsymbol{\varepsilon}_{ii}^{(m)}\right)\boldsymbol{\upsilon}_{ic} + \bar{\mathbf{m}}_{ic} + \bar{\mathbf{m}}_{ic} \bullet \boldsymbol{\varepsilon}_{ic}^{(m)}\right) \quad (7.62)$$

where $\boldsymbol{\varphi}_{Fk}$ represent the 'kept' fixed interface normal modes, which in this case are either equal to or a subset of $\boldsymbol{\varphi}_F$. The coupling constraint modes are given by (see chapter 6)

$$\boldsymbol{\upsilon}_{ic} = -\left(\mathbf{k}_{ii}\right)^{-1}\mathbf{k}_{ic} \tag{7.63}$$

Substituting the expressions for $\mathbf{k}_{ii}$ and $\mathbf{k}_{ic}$ from equation (7.39) into the above gives

$$\boldsymbol{\upsilon}_{ic} = -\left(\bar{\mathbf{k}}_{ii} + \bar{\mathbf{k}}_{ii}\bullet\boldsymbol{\varepsilon}_{ii}^{(k)}\right)^{-1}\left(\bar{\mathbf{k}}_{ic} + \bar{\mathbf{k}}_{ic}\bullet\boldsymbol{\varepsilon}_{ic}^{(k)}\right) \tag{7.64}$$

Applying the Woodbury formula result from equation (7.56), it can be shown that the coupling constraint modes are given by

$$\boldsymbol{\upsilon}_{ic} = -\left(\bar{\mathbf{k}}_{ii}^{-1} - \left(\bar{\mathbf{k}}_{ii}^{-1}\left(\mathbf{I} + \left(\bar{\mathbf{k}}_{ii}\bullet\boldsymbol{\varepsilon}_{ii}^{(k)}\right)\bar{\mathbf{k}}_{ii}^{-1}\right)^{-1}\left(\bar{\mathbf{k}}_{ii}\bullet\boldsymbol{\varepsilon}_{ii}^{(k)}\right)\bar{\mathbf{k}}_{ii}^{-1}\right)\right)\left(\bar{\mathbf{k}}_{ic} + \bar{\mathbf{k}}_{ic}\bullet\boldsymbol{\varepsilon}_{ic}^{(k)}\right) \tag{7.65}$$

This expression is still exact but can be approximated if the variability is assumed to be small, such that $\boldsymbol{\varepsilon}^{(k)} \ll 1$, then $\left(\mathbf{I} + \left(\bar{\mathbf{k}}_{ii}\bullet\boldsymbol{\varepsilon}_{ii}^{(k)}\right)\bar{\mathbf{k}}_{ii}^{-1}\right)^{-1} \cong \mathbf{I}$, therefore

$$\boldsymbol{\upsilon}_{ic} \cong -\left(\bar{\mathbf{k}}_{ii}^{-1} - \left(\bar{\mathbf{k}}_{ii}^{-1}\left(\bar{\mathbf{k}}_{ii}\bullet\boldsymbol{\varepsilon}_{ii}^{(k)}\right)\bar{\mathbf{k}}_{ii}^{-1}\right)\right)\left(\bar{\mathbf{k}}_{ic} + \bar{\mathbf{k}}_{ic}\bullet\boldsymbol{\varepsilon}_{ic}^{(k)}\right) \tag{7.66}$$

The expressions for the coupling constraint modes $\boldsymbol{\upsilon}_{ic}$ and the 'kept' fixed interface normal modes $\boldsymbol{\varphi}_{ik}$ can be combined with the expressions for $\boldsymbol{\mu}_{kc}$ and $\boldsymbol{\mu}_{cc}$, to obtain an approximation for the mass matrix $\boldsymbol{\mu}$.

$$\boldsymbol{\mu} \cong \begin{bmatrix} \mathbf{I}_{kk} & \boldsymbol{\varphi}_{Fk}{}^{T}\left(\left(\bar{\mathbf{m}}_{ii} + \bar{\mathbf{m}}_{ii}\bullet\boldsymbol{\varepsilon}_{ii}^{(m)}\right)\boldsymbol{\upsilon}_{ic} + \bar{\mathbf{m}}_{ic} + \bar{\mathbf{m}}_{ic}\bullet\boldsymbol{\varepsilon}_{ic}^{(m)}\right) \\ \left(\left(\bar{\mathbf{m}}_{ii} + \bar{\mathbf{m}}_{ii}\bullet\boldsymbol{\varepsilon}_{ii}^{(m)}\right)\boldsymbol{\upsilon}_{ic} + \bar{\mathbf{m}}_{ic} + \bar{\mathbf{m}}_{ic}\bullet\boldsymbol{\varepsilon}_{ic}^{(m)}\right)^{T}\boldsymbol{\varphi}_{Fk} & \boldsymbol{\upsilon}_{ic}{}^{T}\left(\left(\bar{\mathbf{m}}_{ii} + \bar{\mathbf{m}}_{ii}\bullet\boldsymbol{\varepsilon}_{ii}^{(m)}\right)\boldsymbol{\upsilon}_{ic} + \bar{\mathbf{m}}_{ic} + \bar{\mathbf{m}}_{ic}\bullet\boldsymbol{\varepsilon}_{ic}^{(m)}\right) + \left(\bar{\mathbf{m}}_{ic} + \bar{\mathbf{m}}_{ic}\bullet\boldsymbol{\varepsilon}_{ic}^{(m)}\right)^{T}\boldsymbol{\upsilon}_{ic} + \bar{\mathbf{m}}_{cc}\bullet\left(1 + \boldsymbol{\varepsilon}_{cc}^{(m)}\right) \end{bmatrix} \tag{7.67}$$

where $\boldsymbol{\varphi}_{Fk}$ is a set of kept modes from the set $\boldsymbol{\varphi}_{F}$ given by a first order perturbation, see equation (7.45).

7.2 Potential areas of data reduction

In the previous section expressions relating the uncertainty in the physical properties to the uncertainty in the modal properties have been developed. In this section these expressions are reviewed and discussed in the context the potential areas of data reduction listed in chapter 6.

7.2.1 Approximation of the physical uncertainties

The uncertainty in the physical properties was assumed to be known and given by $\boldsymbol{\varepsilon}^{(m)}$ and $\boldsymbol{\varepsilon}^{(k)}$. No assumptions were made as to whether these variations are correlated or independent or on their distribution; they were assumed to have zero mean. In practice correlations would normally exist between the variability in the mass and stiffness of a component. For example, if the cross-sectional area of a component varied, this would affect both its mass and stiffness properties. In addition spatial correlations may arise from manufacturing processes, such as thickness variations in a sheet of rolled metal. In reality, the uncertainties in the physical properties are often difficult to quantify accurately and their simplification becomes a necessity rather than a means of data reduction. Indeed this is one of the significant benefits of the LMP method as it is often easier to measure the variability in the natural frequencies of a set of structures, than their physical properties or their normal modeshapes. Potential areas for simplification of the variability in the physical properties include assumptions on its distribution. For example, if the variability is assumed to be Gaussian distributed, then a significantly smaller number of test structures would be required to measure (within reasonable confidence limits) the mean and variance of the population. Another potential simplification is that the uncertainties are uniform throughout the structure, such as variations in material properties. The mass of a structure may be relatively easy to measure, and assuming the variations are uniform throughout the structure simplifies the creation of the mass variability matrix. The stiffness of a structure cannot be directly measured and instead would require the dimensions and material properties in order to calculate it.

7.2.2 Assuming constant local eigenvectors

A potential area of data reduction when analysing the component as part of a structure using a fixed interface CMS method, is to assume the local fixed interface modeshapes remain constant. This may be a reasonable assumption at low to mid frequencies and if the variability is small, such that small local changes in the physical properties do not overly affect the local modeshape. From equation (7.62) a partition of the uncoupled CMS mass matrix is given by

$$\boldsymbol{\mu}_{kc} = \boldsymbol{\mu}_{ck}{}^{T} = \boldsymbol{\varphi}_{Fk}{}^{T}\left(\left(\bar{\mathbf{m}}_{ii} + \bar{\mathbf{m}}_{ii}\bullet\boldsymbol{\varepsilon}_{ii}{}^{(m)}\right)\boldsymbol{\upsilon}_{ic} + \bar{\mathbf{m}}_{ic} + \bar{\mathbf{m}}_{ic}\bullet\boldsymbol{\varepsilon}_{ic}{}^{(m)}\right) \tag{7.68}$$

where $\boldsymbol{\varphi}_{Fk}$ are the 'kept' perturbed fixed interface normal modes. The use of a truncated set of fixed interface eigenvectors already offers some data reduction over using the full set $\boldsymbol{\varphi}_{F}$ and is commonly used in a standard CMS analyses. In addition to this the use of the unperturbed baseline fixed interface eigenvectors either as a full set, or truncated, could offer a further simplification, thus

$$\boldsymbol{\mu}_{kc} = \boldsymbol{\mu}_{ck}{}^{T} \cong \bar{\boldsymbol{\varphi}}_{Fk}{}^{T}\left(\left(\bar{\mathbf{m}}_{ii} + \bar{\mathbf{m}}_{ii}\bullet\boldsymbol{\varepsilon}_{ii}{}^{(m)}\right)\boldsymbol{\upsilon}_{ic} + \bar{\mathbf{m}}_{ic} + \bar{\mathbf{m}}_{ic}\bullet\boldsymbol{\varepsilon}_{ic}{}^{(m)}\right) \tag{7.69}$$

where $\bar{\boldsymbol{\varphi}}_{Fk}$ are the 'kept' baseline fixed interface eigenvectors.

7.2.3 Assuming constant component constraint modeshapes

In a similar manner to the component fixed interface normal eigenvectors, a potential simplification of the CMS matrices may be obtained from assuming the coupling constraint modes to be constant. In equation (7.66) an approximation for the constraint modes was proposed as

$$\boldsymbol{\upsilon}_{ic} \cong -\left(\bar{\mathbf{k}}_{ii}^{-1} - \left(\bar{\mathbf{k}}_{ii}^{-1}\left(\bar{\mathbf{k}}_{ii}\bullet\boldsymbol{\varepsilon}_{ii}{}^{(k)}\right)\bar{\mathbf{k}}_{ii}^{-1}\right)\right)\left(\bar{\mathbf{k}}_{ic} + \bar{\mathbf{k}}_{ic}\bullet\boldsymbol{\varepsilon}_{ic}{}^{(k)}\right) \tag{7.70}$$

This approximation was based on the variability being small. However, if in addition to being small, the variability does not have a strong spatial correlation, i.e. is fairly continuous throughout the component, then it may be reasonable to assume the constraint modeshapes to remain constant. Thus the coupling constraint modes could be approximated as

$$\boldsymbol{\upsilon}_{ic} \cong \bar{\boldsymbol{\upsilon}}_{ic} = -\left(\bar{\mathbf{k}}_{ii}\right)^{-1}\bar{\mathbf{k}}_{ic} \tag{7.71}$$

7.2.4 Truncation of the set of component modes

The component baseline modes $\bar{\boldsymbol{\varphi}}$ are used in the perturbation approximation of the component eigenvalues and vectors. A commonly used method for data reduction is to use a truncated set of baseline modes. Often the higher modes do not contribute significantly and may be disregarded.

This potential data reduction can be used in the formation of CMS matrices if the component is being analysed as part of a built-up structure using a CMS method. From equation (7.52) the uncoupled component stiffness matrix is approximated by

$$\boldsymbol{\kappa}_{kk} \cong diag\left(\left(\overline{\lambda}_F\right)_j + \mathbf{A}_{j\lambda F}{}^T \boldsymbol{\varepsilon}\right) \tag{7.72}$$

where in the formation of $\mathbf{A}_{j\lambda F}$, a reduced set of 'kept' baseline component modes $\overline{\lambda}_{Fk}$, $\overline{\boldsymbol{\varphi}}_{Fk}$ may be used in place of $\overline{\lambda}_F$, $\overline{\boldsymbol{\varphi}}_F$.

7.2.5 Free interface component statistics

The potential to use the free interface component statistics to approximate the fixed interface component statistics provides an interesting and elegant simplification. The fixed interface method is one of the most popular CMS methods as it produces very accurate results even with relatively few component modes, and the mass and stiffness matrices are sparse and relatively easy to formulate. However, the component free interface modes are typically easier to measure than the fixed interface ones. The ability to use the statistics, in particular the variance of the free interface modes as representative of the variance of the fixed interface modes would offer a significant advantage. It is expected that the component fixed and free modes are likely to be similar away from the boundaries, particularly in the higher mode orders.

From equations (7.25) and (7.44) the variance of the free interface and fixed interface eigenvalues is related to the variance of the variability thus,

$$\begin{aligned} \operatorname{var}\left(\delta_{\lambda_j}\right) &\cong \mathbf{A}_{j\lambda}{}^T \operatorname{var}(\boldsymbol{\varepsilon}) \mathbf{A}_{j\lambda} \\ \operatorname{var}\left(\delta_{(\lambda_F)_j}\right) &\cong \mathbf{A}_{j\lambda F}{}^T \operatorname{var}(\boldsymbol{\varepsilon}) \mathbf{A}_{j\lambda F} \end{aligned} \tag{7.73}$$

Rearranging each of these equations it can be shown that

$$\begin{aligned} \operatorname{var}(\boldsymbol{\varepsilon}) &\cong \left(\mathbf{A}_{j\lambda}{}^T\right)^{-1} \operatorname{var}\left(\delta_{\lambda_j}\right)\left(\mathbf{A}_{j\lambda}\right)^{-1} \\ \operatorname{var}(\boldsymbol{\varepsilon}) &\cong \left(\mathbf{A}_{j\lambda F}{}^T\right)^{-1} \operatorname{var}\left(\delta_{(\lambda_F)_j}\right)\left(\mathbf{A}_{j\lambda F}\right)^{-1} \end{aligned} \tag{7.74}$$

The rigid body modes of the free interface component have a natural frequency of zero, and a variance of zero. If these rigid body modes are removed from the free interface expression, and

sufficient modes in each model retained such that the order of $\mathbf{A}_{j\lambda}$ is compatible with $\mathbf{A}_{j\lambda F}$, then these expressions can be combined to approximate the variance of the fixed interface eigenvalues by the variance of the free interface eigenvalues as

$$\mathrm{var}\left(\delta_{(\lambda_F)_j}\right) \cong \left(\mathbf{A}_{j\lambda F}{}^T\right)\left(\mathbf{A}_{j\lambda}{}^T\right)^{-1} \mathrm{var}\left(\delta_{\lambda_j}\right)\left(\mathbf{A}_{j\lambda}\right)^{-1}\left(\mathbf{A}_{j\lambda F}\right) \tag{7.75}$$

$$\mathrm{var}\left(\delta_{\lambda_j}\right) \approx \mathrm{var}\left(\delta_{(\lambda_F)_j}\right) \tag{7.76}$$

where $(\lambda_F)_j$ is the *j*'th fixed interface component mode and λ_j is the *j*'th free interface component mode after the rigid body modes have been removed. It should be noted that these modes do not necessarily correspond to each other in terms of similarity of modeshape, but simply in terms of increasing mode number.

7.2.6 Use of eigensolution approximations

The main eigensolution approximation investigated here is the mean centred perturbation approach. Other potential eigensolution approximations were presented and discussed in chapter 4 and both the perturbational method and in the interpolated mode method were applied to a two DOF system in chapter 5. An advantage of the perturbational approach is the potential for relating the statistics of the physical property variability to the statistics of the modal properties. If the variability is assumed to be small then a first order perturbation is likely to be sufficient, although the second order term has been evaluated; see equation (5.63).

7.3 Numerical example

Consider a simple example of a rod as given in Figure 7-2.

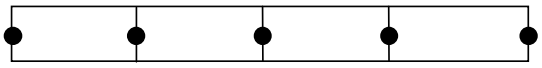

Figure 7-2 Rod component.

The rod is discretised into individual elements modelled as a lumped-mass formulation; it has four elements and five degrees of freedom. At each end there is an interface which may have

fixed or free boundary conditions. The baseline mass and stiffness matrices for the rod are given by

$$\bar{\mathbf{M}} = \begin{bmatrix} \bar{m}_1 & 0 & 0 & 0 & 0 \\ 0 & \bar{m}_2 & 0 & 0 & 0 \\ 0 & 0 & \bar{m}_3 & 0 & 0 \\ 0 & 0 & 0 & \bar{m}_4 & 0 \\ 0 & 0 & 0 & 0 & \bar{m}_5 \end{bmatrix} \tag{7.77}$$

$$\bar{\mathbf{K}} = \begin{bmatrix} \bar{k}_1 + \bar{k}_2 & -\bar{k}_2 & 0 & 0 & 0 \\ -\bar{k}_2 & \bar{k}_2 + \bar{k}_3 & -\bar{k}_3 & 0 & 0 \\ 0 & -\bar{k}_3 & \bar{k}_3 + \bar{k}_4 & -\bar{k}_4 & 0 \\ 0 & 0 & -\bar{k}_4 & \bar{k}_4 + \bar{k}_5 & -\bar{k}_5 \\ 0 & 0 & 0 & -\bar{k}_5 & \bar{k}_5 + \bar{k}_6 \end{bmatrix} \tag{7.78}$$

A specific scenario of correlated and uncorrelated uncertainty will be examined. Consider the case where the density of the rod material varies along the length such that there is a correlated variation with a sinusoidal form in the uncertainty of the mass elements. This mass uncertainty will be represented by ε_m. In addition there are some uncorrelated variations in the stiffness elements $\bar{k}_1$ and $\bar{k}_4$ from variations in the Young's Modulus, represented by $\varepsilon_{\bar{k}_1}$ and $\varepsilon_{\bar{k}_4}$ respectively. The variability matrices for the mass and stiffness are given by

$$\boldsymbol{\varepsilon}^{(m)} = \begin{bmatrix} 0 & 0 & 0 & 0 & 0 \\ 0 & \frac{\sqrt{2}}{2}\varepsilon_m & 0 & 0 & 0 \\ 0 & 0 & \varepsilon_m & 0 & 0 \\ 0 & 0 & 0 & \frac{\sqrt{2}}{2}\varepsilon_m & 0 \\ 0 & 0 & 0 & 0 & 0 \end{bmatrix} \tag{7.79}$$

$$\boldsymbol{\varepsilon}^{(k)} = \begin{bmatrix} \frac{\bar{k}_1 \varepsilon_{\bar{k}_1}}{\bar{k}_1 + \bar{k}_2} & 0 & 0 & 0 & 0 \\ 0 & 0 & 0 & 0 & 0 \\ 0 & 0 & \frac{\bar{k}_4 \varepsilon_{\bar{k}_4}}{\bar{k}_3 + \bar{k}_4} & \varepsilon_{\bar{k}_4} & 0 \\ 0 & 0 & \varepsilon_{\bar{k}_4} & \frac{\bar{k}_4 \varepsilon_{\bar{k}_4}}{\bar{k}_4 + \bar{k}_5} & 0 \\ 0 & 0 & 0 & 0 & 0 \end{bmatrix} \tag{7.80}$$

Therefore, from equation (7.11) the perturbed mass and stiffness matrices are given by

$$\mathbf{M}=\begin{bmatrix} \bar{m}_1 & 0 & 0 & 0 & 0 \\ 0 & \bar{m}_2\left(1+\frac{\sqrt{2}}{2}\varepsilon_m\right) & 0 & 0 & 0 \\ 0 & 0 & \bar{m}_3\left(1+\varepsilon_m\right) & 0 & 0 \\ 0 & 0 & 0 & \bar{m}_4\left(1+\frac{\sqrt{2}}{2}\varepsilon_m\right) & 0 \\ 0 & 0 & 0 & 0 & \bar{m}_5 \end{bmatrix} \tag{7.81}$$

$$\mathbf{K}=\begin{bmatrix} \left(\bar{k}_1+\bar{k}_2\right)\left(1+\frac{\bar{k}_1\varepsilon_{\bar{k}_1}}{\bar{k}_1+\bar{k}_2}\right) & -\bar{k}_2 & 0 & 0 & 0 \\ -\bar{k}_2 & \bar{k}_2+\bar{k}_3 & -\bar{k}_3 & 0 & 0 \\ 0 & -\bar{k}_3 & \left(\bar{k}_3+\bar{k}_4\right)\left(1+\frac{\bar{k}_4\varepsilon_{\bar{k}_4}}{\bar{k}_3+\bar{k}_4}\right) & -\bar{k}_4\left(1+\varepsilon_{\bar{k}_4}\right) & 0 \\ 0 & 0 & -\bar{k}_4\left(1+\varepsilon_{\bar{k}_4}\right) & \left(\bar{k}_4+\bar{k}_5\right)\left(1+\frac{\bar{k}_4\varepsilon_{\bar{k}_4}}{\bar{k}_4+\bar{k}_5}\right) & -\bar{k}_5 \\ 0 & 0 & 0 & -\bar{k}_5 & \bar{k}_5+\bar{k}_6 \end{bmatrix} \tag{7.82}$$

The variability matrix $\boldsymbol{\varepsilon}$ consists of

$$\boldsymbol{\varepsilon}=\begin{bmatrix} \varepsilon_m & \varepsilon_{\bar{k}_1} & \varepsilon_{\bar{k}_4} \end{bmatrix}^T \tag{7.83}$$

The partial derivatives in equation (7.17) are given by (all other partial derivatives result in null matrices)

$$\frac{\partial \mathbf{M}}{\partial \varepsilon_m}=\begin{bmatrix} 0 & 0 & 0 & 0 & 0 \\ 0 & \bar{m}_2\frac{\sqrt{2}}{2} & 0 & 0 & 0 \\ 0 & 0 & \bar{m}_3 & 0 & 0 \\ 0 & 0 & 0 & \bar{m}_4\frac{\sqrt{2}}{2} & 0 \\ 0 & 0 & 0 & 0 & 0 \end{bmatrix} \tag{7.84}$$

$$\frac{\partial \mathbf{K}}{\partial \varepsilon_{\bar{k}_1}} = \begin{bmatrix} \bar{k}_1 & 0 & 0 & 0 & 0 \\ 0 & 0 & 0 & 0 & 0 \\ 0 & 0 & 0 & 0 & 0 \\ 0 & 0 & 0 & 0 & 0 \\ 0 & 0 & 0 & 0 & 0 \end{bmatrix}, \quad \frac{\partial \mathbf{K}}{\partial \varepsilon_{\bar{k}_4}} = \begin{bmatrix} 0 & 0 & 0 & 0 & 0 \\ 0 & 0 & 0 & 0 & 0 \\ 0 & 0 & \bar{k}_4 & -\bar{k}_4 & 0 \\ 0 & 0 & -\bar{k}_4 & \bar{k}_4 & 0 \\ 0 & 0 & 0 & 0 & 0 \end{bmatrix} \tag{7.85}$$

Applying these to equation (7.23) the approximate perturbed eigenvalues for the rod are given by

$$\lambda_j \cong \bar{\lambda}_j + \mathbf{A}_{j\lambda}^T \boldsymbol{\varepsilon} \tag{7.86}$$

where

$$\mathbf{A}_{j\lambda} = \begin{bmatrix} -\bar{\lambda}_j \left(\bar{\phi}_{j,2}{}^2 \bar{m}_2 \frac{\sqrt{2}}{2} + \bar{\phi}_{j,3}{}^2 \bar{m}_3 + \bar{\phi}_{j,4}{}^2 \bar{m}_4 \frac{\sqrt{2}}{2} \right) \\ \bar{\phi}_{j,1}{}^2 \bar{k}_1 \\ \left(\bar{\phi}_{j,3}{}^2 + \bar{\phi}_{j,4}{}^2 - 2\bar{\phi}_{j,3}\bar{\phi}_{j,4} \right) \bar{k}_4 \end{bmatrix} \tag{7.87}$$

The variance of the perturbed eigenvalues can be estimated from equation (7.25) as

$$\mathrm{var}\left(\delta_{\lambda_j} \right) \cong \mathbf{A}_{j\lambda}{}^T \, \mathrm{var}(\boldsymbol{\varepsilon}) \mathbf{A}_{j\lambda} \tag{7.88}$$

where $\mathrm{var}(\boldsymbol{\varepsilon})$ is given by

$$\mathrm{var}(\boldsymbol{\varepsilon}) = \begin{bmatrix} \sigma_{\varepsilon_m}^2 & 0 & 0 \\ 0 & \sigma_{\varepsilon_{\bar{k}_1}}^2 & 0 \\ 0 & 0 & \sigma_{\varepsilon_{\bar{k}_4}}^2 \end{bmatrix} \tag{7.89}$$

and $\sigma_{\varepsilon_m}^2$, $\sigma_{\varepsilon_{\bar{k}_1}}^2$, $\sigma_{\varepsilon_{\bar{k}_4}}^2$ are the variances of the variabilities ε_m , $\varepsilon_{\bar{k}_1}$ and $\varepsilon_{\bar{k}_4}$ respectively.

The second order term in the mean centred perturbation of the free interface eigenvalues is given in equation (5.63) as

$$\frac{1}{2}(\boldsymbol{\varepsilon})^T\left[2\sum_{\substack{r=1\\ r\neq j}}^{n}\frac{\mathbf{A}_{j\lambda}\mathbf{A}_{j\lambda}{}^T}{\bar{\lambda}_j-\bar{\lambda}_r}-\mathbf{B}_j\mathbf{A}_{j\lambda}{}^T-\mathbf{A}_{j\lambda}\mathbf{B}_j{}^T\right]\boldsymbol{\varepsilon} \tag{7.90}$$

where $\mathbf{A}_{j\lambda}$ is as above, and

$$\mathbf{B}_j=\begin{bmatrix}\bar{\phi}_{j,2}{}^2\bar{m}_2\dfrac{\sqrt{2}}{2}+\bar{\phi}_{j,3}{}^2\bar{m}_3+\bar{\phi}_{j,4}{}^2\bar{m}_4\dfrac{\sqrt{2}}{2}\\ 0\\ 0\end{bmatrix} \tag{7.91}$$

The first order perturbation estimation of the eigenvectors is given by (7.37) namely,

$$\boldsymbol{\varphi}_j\cong\bar{\boldsymbol{\varphi}}_j-\frac{1}{2}\mathbf{B}_j{}^T\boldsymbol{\varepsilon}\bar{\boldsymbol{\varphi}}_j+\sum_{\substack{p=1\\ \mathrm{p}\neq j}}^{n}\frac{1}{\bar{\lambda}_j-\bar{\lambda}_p}\mathbf{A}_{j\boldsymbol{\varphi}}{}^T\boldsymbol{\varepsilon}\bar{\boldsymbol{\varphi}}_p \tag{7.92}$$

where $\mathbf{A}_{j\boldsymbol{\varphi}}$ is given by

$$\mathbf{A}_{j\boldsymbol{\varphi}}=\begin{bmatrix}-\bar{\lambda}_j\left(\bar{\phi}_{j,2}\bar{\phi}_{p,2}\bar{m}_2\dfrac{\sqrt{2}}{2}+\bar{\phi}_{j,3}\bar{\phi}_{p,3}\bar{m}_3+\bar{\phi}_{j,4}\bar{\phi}_{p,4}\bar{m}_4\dfrac{\sqrt{2}}{2}\right)\\ \bar{\phi}_{j,1}\bar{\phi}_{p,1}\bar{k}_1\\ \left(\bar{\phi}_{j,3}\bar{\phi}_{p,3}+\bar{\phi}_{j,4}\bar{\phi}_{p,4}-\bar{\phi}_{j,3}\bar{\phi}_{p,4}-\bar{\phi}_{p,3}\bar{\phi}_{j,4}\right)\bar{k}_4\end{bmatrix} \tag{7.93}$$

In a similar manner, the fixed interface eigenvalues and eigenvectors can be estimated from equations (7.42) and (7.45), where

$$\mathbf{A}_{j\lambda F}=\begin{bmatrix}-\left(\bar{\lambda}_f\right)_j\left(\left(\bar{\phi}_f\right)_{j,1}{}^2\bar{m}_2\dfrac{\sqrt{2}}{2}+\left(\bar{\phi}_f\right)_{j,2}{}^2\bar{m}_3+\left(\bar{\phi}_f\right)_{j,3}{}^2\bar{m}_4\dfrac{\sqrt{2}}{2}\right)\\ 0\\ \left(\left(\bar{\phi}_f\right)_{j,2}{}^2+\left(\bar{\phi}_f\right)_{j,3}{}^2-2\left(\bar{\phi}_f\right)_{j,2}\left(\bar{\phi}_f\right)_{j,3}\right)\bar{k}_4\end{bmatrix} \tag{7.94}$$

$$\mathbf{A}_{j\varphi F} = \begin{bmatrix} -\left(\bar{\lambda}_f\right)_j \left(\left(\bar{\phi}_f\right)_{j,1} \left(\bar{\phi}_f\right)_{p,1} \bar{m}_2 \frac{\sqrt{2}}{2} + \left(\bar{\phi}_f\right)_{j,2} \left(\bar{\phi}_f\right)_{p,2} \bar{m}_3 + \left(\bar{\phi}_f\right)_{j,3} \left(\bar{\phi}_f\right)_{p,3} \bar{m}_4 \frac{\sqrt{2}}{2} \right) \\ 0 \\ \left(\left(\bar{\phi}_f\right)_{j,2} \left(\bar{\phi}_f\right)_{p,2} + \left(\bar{\phi}_f\right)_{j,3} \left(\bar{\phi}_f\right)_{p,3} - \left(\bar{\phi}_f\right)_{j,2} \left(\bar{\phi}_f\right)_{p,3} - \left(\bar{\phi}_f\right)_{p,2} \left(\bar{\phi}_f\right)_{j,3} \right) \bar{k}_4 \end{bmatrix} \tag{7.95}$$

$$\mathbf{B}_{jF} = \begin{bmatrix} \left(\bar{\phi}_f\right)_{j,1}{}^2 \bar{m}_2 \frac{\sqrt{2}}{2} + \left(\bar{\phi}_f\right)_{j,2}{}^2 \bar{m}_3 + \left(\bar{\phi}_f\right)_{j,3}{}^2 \bar{m}_4 \frac{\sqrt{2}}{2} \\ 0 \\ 0 \end{bmatrix} \tag{7.96}$$

A Monte Carlo simulation of a numerical example was conducted in Matlab [7.3]. The baseline, unperturbed, mass and stiffness matrices for the component are given by

$$\bar{\mathbf{M}} = \begin{bmatrix} 9.5013 & 0 & 0 & 0 & 0 \\ 0 & 2.3114 & 0 & 0 & 0 \\ 0 & 0 & 6.0684 & 0 & 0 \\ 0 & 0 & 0 & 4.8598 & 0 \\ 0 & 0 & 0 & 0 & 8.9130 \end{bmatrix}, \ kg \tag{7.97}$$

$$\bar{\mathbf{K}} = \begin{bmatrix} 12.1856 & -4.5647 & 0 & 0 & 0 \\ -4.5647 & 4.7497 & -0.1850 & 0 & 0 \\ 0 & -0.1850 & 8.3991 & -8.2141 & 0 \\ 0 & 0 & -8.2141 & 12.6611 & -4.4470 \\ 0 & 0 & 0 & -4.4470 & 10.6014 \end{bmatrix}, \ N/m \tag{7.98}$$

The values of the individual masses and stiffnesses were chosen randomly from a uniform distribution between $(0,10)$. The variability terms in $\boldsymbol{\varepsilon}$ were randomly generated from a Gaussian distribution with zero mean and a standard deviation of 0.03; this was based on the typical levels of standard deviation seen in manufactured components as discussed in chapter 2. In Table 7-1 the results from a MC simulation compare the eigenvalues of the baseline system to the average eigenvalues obtained from a MC simulation with 1000 realisations and the first order estimation of the eigenvalues. Also shown is the percentage error between the MC simulation result and the first order approximation. The second order perturbation term was calculated as an estimate of the percentage error incurred in only using a first order approximation.

j 'th component mode	Baseline eigenvalue $(rad/s)^2$	Average eigenvalue MC simulation $(rad/s)^2$	1st order approximation $(rad/s)^2$	% error of 1st order approx. w.r.t. MC simulation	Estimated % error based on 2nd order perturbation term
1	0.20243	0.20260	0.20250	0.05	0.01
2	0.62156	0.62180	0.62190	-0.02	0.00
3	1.22470	1.22480	1.22490	-0.01	0.01
4	2.71670	2.71830	2.71740	0.03	0.05
5	3.75090	3.75590	3.75370	0.06	0.76

Table 7-1 Component first order perturbation approximation of free interface eigenvalue, 1000 MC realisations.

As it can be seen from the results, the first order approximation of the eigenvalues provides a good estimation of the eigenvalue with errors of below 0.1%. In general the second order term provides a useful estimation of the likely error in the first order approximation. The size of the actual second order term increases significantly with increase frequency. This is due to the modal summation term, $\sum_{\substack{r=1 \\ r\neq j}}^{n} \frac{1}{\bar{\lambda}_j - \bar{\lambda}_r}$, in the second order expression which will increase in size as the modal spacing reduces, which is the case at higher frequencies.

In Table 7-2 the first order estimate of the variance of the *j*'th component eigenvalue, from equation (7.88), is compared to that obtained from the MC simulation of the above ensemble for 1000 realisations of the component. As can be seen from the results, the approximation of the variance is reasonably accurate with an error of up to 5%. Increasing the number of realisations improves the percentage difference between the first order approximation and the MC simulations, with a percentage difference of -1.1% to 0.6% for a set of 10,000 realisations.

j 'th component mode	1st order approximation of variance	MC simulation 1000 realisations	% error
1	2.113E-05	2.034E-05	-3.85
2	2.873E-04	2.889E-04	0.53
3	9.087E-05	8.699E-05	-4.46
4	1.613E-03	1.546E-03	-4.33
5	1.440E-02	1.369E-02	-5.13

Table 7-2 Component free interface eigenvalue variance.

One potential area of approximation identified in chapter 6 was the use of free interface component statistics to approximate fixed interface component statistics. The variance of the

fixed interface eigenvalues is summarised in Table 7-3; both the first order perturbation approximation and the MC simulation result are shown along with the percentage error.

j'th fixed interface component mode	1st order approximation of variance	MC simulation 1000 realisations	% error
1	1.005E-04	9.635E-05	-4.26
2	1.901E-03	1.842E-03	-3.22
3	1.558E-02	1.484E-02	-5.00

Table 7-3 Component fixed interface eigenvalue variance.

The levels of fixed interface eigenvalue variance can be compared to those obtained from the free interface analysis in Table 7-2. It can be seen that the fixed interface variance for the first to third modes are similar to the free interface levels for the third to fifth modes. It is likely that this is due to the first two free interface modes having significant response at the boundaries. This would suggest that at higher modes, the free interface eigenvalue statistics may be representative of the levels of fixed interface eigenvalue variability.

The distribution of the natural frequencies can also be examined. In section 7.1.3 the distribution of the eigenvalues was considered along with the possibility of the central limit theorem applying. In Figure 7-3 to Figure 7-7, the distribution of the free interface natural frequencies $\sqrt{\lambda_j}$ are shown. Those obtained from the MC simulation in the upper graphs and those from the first order perturbation in the lower graphs. Also shown in the figures are Gaussian distributions with the same mean and variance as each set of natural frequencies.

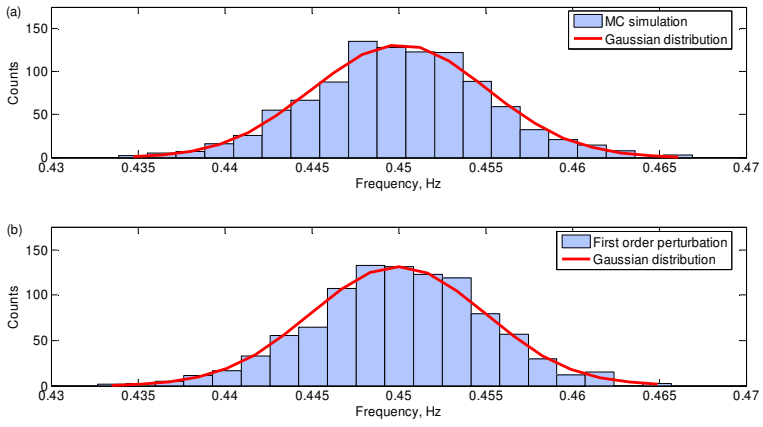

Figure 7-3 Distribution of the first natural frequency, (a) 1000 MC realisations, (b) first order perturbation.

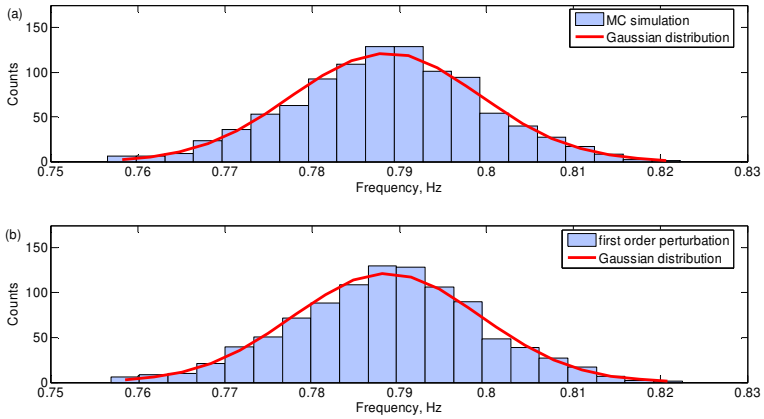

Figure 7-4 Distribution of the second natural frequency, (a) 1000 MC realisations, (b) first order perturbation.

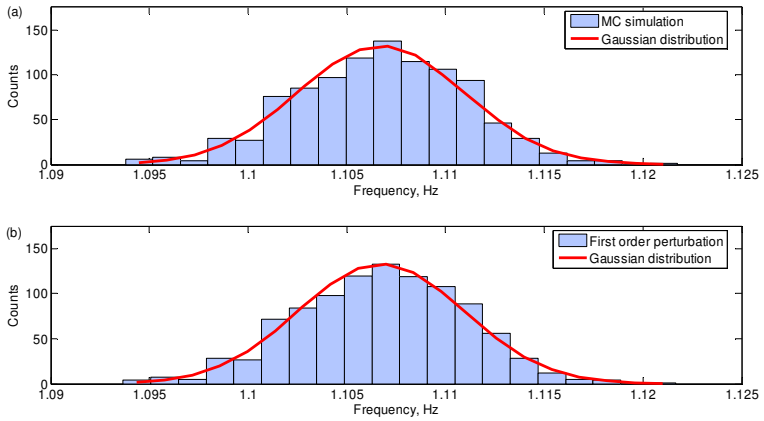

Figure 7-5 Distribution of the third natural frequency, (a) 1000 MC realisations, (b) first order perturbation.

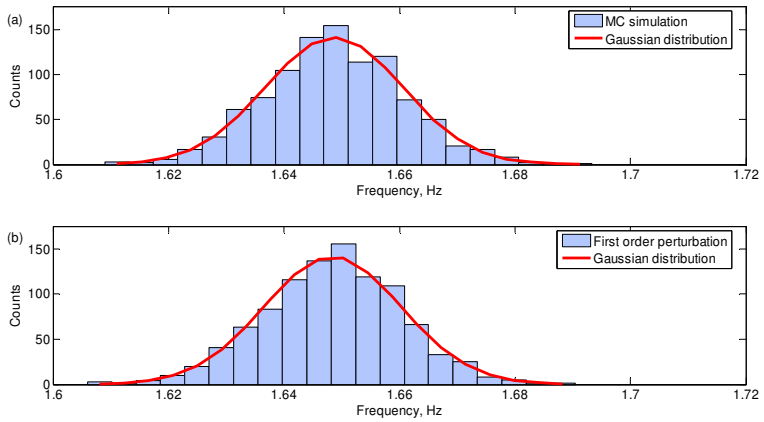

Figure 7-6 Distribution of the fourth natural frequency, (a) 1000 MC realisations, (b) first order perturbation.

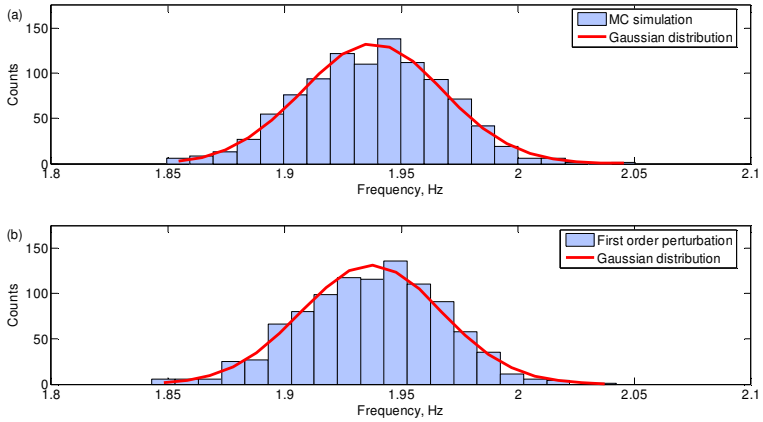

Figure 7-7 Distribution of the fifth natural frequency, (a) 1000 MC realisations, (b) first order perturbation.

It can be seen that the distribution of the first order perturbation approximations is representative of the distribution of the results from a MC simulation. In addition a Gaussian distribution appears to be a good fit to the distributions of the component eigenvalues. To test this goodness-of-fit a χ^2 test has been conducted; the cumulative χ^2 probabilities are listed in Table 7-4. A value below 95% represents a 95% confidence that the sample set cannot be rejected as having come from the distribution being tested against, see [2.10] for further information. The χ^2 test is conducted on classified (binned) data and outlying bins are summed to ensure at least five counts in each; this reduces the skewing effect of out-lying results.

***j*'th component mode**	**Chi-squared fit of MC simulation to Gaussian distribution**	**Chi-squared fit of first order perturbation approximation to Gaussian distribution**
1	27.0%	68.7%
2	24.7%	46.8%
3	99.7%	94.1%
4	48.4%	18.8%
5	48.5%	93.9%

Table 7-4 Goodness of fit of the free interface component eigenvalues to a Gaussian distribution; summary of χ^2 cumulative probabilities.

It can be seen from Table 7-4 that for the MC simulation, the distribution of four of the five modes are well described by a Gaussian distribution. For the first order perturbation, the distribution of all five modes are well described by a Gaussian distribution. These results are not surprising as the variability in the physical properties was Gaussian distributed. In chapter 9, a

more complex numerical example is considered and the effect of different variability distributions is examined.

In section 7.1.6 the effect of variations in the physical properties on the constituents of the fixed interface CMS matrices was examined. In particular approximate expressions for the CMS matrices were generated using first order perturbations for both the appropriate eigenvalues and eigenvectors. The approximate CMS matrices defined in equations (7.59) and (7.67) have been calculated for the numerical example being considered. In this case the rod is considered to be clamped at one end in order for a realistic CMS analysis to be carried out. The results for the component eigenvalues from the approximate CMS matrices are compared to those obtained from CMS matrices generated from the MC simulation, see Table 7-5. Also listed are the eigenvalues obtained from CMS matrices with only the variability of the fixed interface eigenvalues, and all other elements of the matrices fixed at their baseline values, as shown in equations (7.99) and (7.100). This type of approximation is used in the LMP method and is considered in chapter 8 to propagate the component level uncertainty to the variability in global response of a built-up structure.

$$\boldsymbol{\kappa} \cong \begin{bmatrix} diag\left(\left(\bar{\lambda}_F\right)_j + \mathbf{A}_{j\lambda F}\boldsymbol{\varepsilon}\right) & \mathbf{0} \\ \mathbf{0} & \bar{\mathbf{k}}_{cc} - \bar{\mathbf{k}}_{ci}\left(\bar{\mathbf{k}}_{ii}\right)^{-1}\bar{\mathbf{k}}_{ic} \end{bmatrix} \tag{7.99}$$

$$\boldsymbol{\mu} \cong \begin{bmatrix} \mathbf{I}_{kk} & \bar{\boldsymbol{\varphi}}_{Fk}{}^T\left(\bar{\mathbf{m}}_{ii}\bar{\boldsymbol{\upsilon}}_{ic} + \bar{\mathbf{m}}_{ic}\right) \\ \left[\bar{\boldsymbol{\varphi}}_{Fk}{}^T\left(\bar{\mathbf{m}}_{ii}\bar{\boldsymbol{\upsilon}}_{ic} + \bar{\mathbf{m}}_{ic}\right)\right]^T & \bar{\boldsymbol{\upsilon}}_{ic}{}^T\left(\bar{\mathbf{m}}_{ii}\bar{\boldsymbol{\upsilon}}_{ic} + \bar{\mathbf{m}}_{ic}\right) + \bar{\mathbf{m}}_{ci}\bar{\boldsymbol{\upsilon}}_{ic} + \bar{\mathbf{m}}_{cc} \end{bmatrix} \tag{7.100}$$

		MC simulation eigenvalue from CMS matrices	Eigenvalue from approximated CMS matrices	% error	Eigenvalue from CMS matrices variability only in local eigenvalues	% error
	μ and κ as defined in equations:	(7.50) and (7.51)	(7.59) and (7.67)		(7.99) and (7.100)	
***j* 'th component mode:**	**1**	2.03E-01	2.03E-01	0.00%	2.03E-01	0.05%
	2	1.22E+00	1.22E+00	0.02%	1.22E+00	-0.02%
	3	2.06E+00	2.06E+00	0.04%	2.06E+00	0.04%
	4	3.76E+00	3.75E+00	0.05%	3.75E+00	0.05%

Table 7-5 MC Simulation of rod clamped at one end: component eigenvalues obtained from CMS matrices.

As it can be seen from the results in Table 7-5 the component eigenvalues obtained from the approximate CMS matrices compare well with those obtained from the MC simulation. In addition, the CMS matrices with variability in only the local eigenvalues also provide a very good approximation of the eigenvalues. Although this numerical example considers a simple component, it would suggest that the variability in the other elements of the CMS matrices do not significantly contribute to the variability in the response. This principle is used in the LMP method and is further examined in chapter 8.

A first order approximation for the component eigenvectors was obtained in equation (7.92). This can be compared to the results from the MC simulation using a Modal Assurance Criterion (MAC) comparison [7.4]. A MAC comparison is often used to compare experimentally obtained modeshapes to those obtained from an FE model. The MAC number for a comparison of two eigenvectors ϕ_A and ϕ_B, is given by

$$MAC(A,B) = \frac{\left|\phi_A^H \phi_B\right|^2}{\left(\phi_A^H \phi_A\right)\left(\phi_B^H \phi_B\right)} \tag{7.101}$$

where ϕ_A^H is the complex conjugate transpose. In this case the eigenvectors are undamped and so contain only real parts. A MAC value always ranges from zero to one, with zero being no correlation between the vectors and one being identical vectors. When comparing two sets of eigenvectors containing several modes, a matrix of MAC values is usually generated. If the two sets of eigenvectors are identical, then the MAC comparison matrix would contain ones on the leading diagonal and zeros elsewhere. A MAC value of over 0.9 is usually considered to indicate a consistent result.

The results from a MAC comparison of the first order perturbation of the component eigenvectors and those obtained from the MC simulation are shown in Figure 7-8. Averaging the eigenvectors themselves would be a nonsensical result. Therefore the MAC values are averaged and the average MAC result for the comparison of each corresponding eigenvector pair is shown. The average MAC value for each eigenvector comparison is labelled on the plot. As it can be seen from the results, the first order perturbation of the component eigenvectors provides a very good estimate of the exact result.

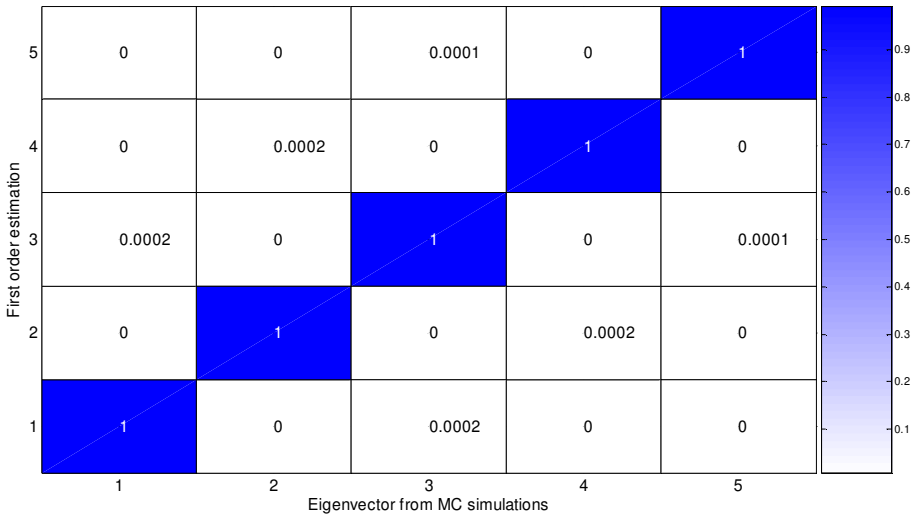

Figure 7-8 MAC comparison of first order perturbation of eigenvector to MC simulation.

7.4 Conclusions

In this chapter the propagation of uncertainty from the variations in physical properties to local modal properties has been examined in detail. The aim was to relate the statistics of the variability in the physical properties to the variability in the local modal properties, to understand the potential areas for data reduction and to generate expressions for such approximations. A perturbational approach was used to generate expressions relating the mean and variance of the free and fixed interface local modes, to the statistics of the physical parameter uncertainty. A first order perturbation was used to approximate the perturbed eigenvalues of the free and fixed interface component. The second order perturbation term was also generated and it was suggested that this could be used as a measure of the error in using only a first order term. It was proposed that the variance of the free interface eigenvalues could be used as an indication of the variance of the fixed interface eigenvalues. This potential simplification is particularly relevant to the LMP method and will be applied to a more complex numerical example in chapter 9. A general method for relating the PDF of the eigenvalue distribution to the PDF of the physical variability was suggested, and the possibility of the central limit theorem applying was reviewed. In addition, a first order expression was generated for the fixed and free interface component eigenvectors. Expressions were also generated for the fixed interface component CMS matrices in terms of the physical parameter uncertainties. This gives an intermediate approximation between the perturbed CMS matrices and the LMP method and will be further examined in a numerical example in chapter 9. Finally, the numerical example of a rod was considered and the expressions for the various approximations discussed above compared to the results of a Monte Carlo simulation.

8. Uncertainty from component modal to global modal models

In this chapter the propagation of statistics from the local modal properties to the global modal properties is considered. The local modal/perturbational method (LMP) method first proposed by Mace and Shorter [6.3] is extended to obtain expressions for the statistics of the global modal properties of an ensemble of nominally identical structures. This is based on the statistics of the components or substructures. Thereby giving a simplification of the problem compared to current methods of Monte Carlo simulations of FE models with variable physical properties. As this allows the baseline substructures to be modelled separately, the properties of individual substructures can be changed, or assumptions about their statistics changed, independently of the other substructures. This significantly increases the flexibility of the model to design changes. It also provides the opportunity to investigate the effect of reducing (or increasing) the variability in an individual component and subsequently its effect on the variability of the response of the whole structure. This could be used to optimise the tolerances within the components to provide a cost effective solution, targeting the components with the largest effect on the global response variability.

A first order perturbation expansion is used to obtain a general expression for the global eigenvalues in terms of the variable local component eigenvalues. This leads to an estimation for the mean of the p'th global eigenvalue. However, it is often convenient to assume that the nominal or design values of a structures properties, in this case the component eigenvalues, are their mean value. Thus the baseline unperturbed values of the local component natural frequencies, lead to the baseline unperturbed global natural frequencies, which is in turn the mean response. In this case it is the variance of the uncertain properties that is of particular interest. Hence the relationship between the variance and covariance, of the local component eigenvalues to the variance of the global eigenvalues is developed. The importance of cross-correlations between component variations is determined. The expression for the variance of the global eigenvalues is used to estimate a limiting 'statistical overlap' ratio, beyond which deterministic analysis is of little use. In addition, an estimation of the error in approximating the perturbed global eigenvalues is proposed and calculated. Not only are the mean and variance of the global eigenvalues of interest, but also their distribution. A method for obtaining this distribution, if the properties of the component uncertainties and their dependence are known, is given. The implications of several general cases of the component uncertainties on the distribution of the global eigenvalues are considered. A first order perturbation estimate is also developed for the global eigenvectors, directly relating them to the uncertainties in the local component natural frequencies. This is then used in conjunction with the expression for the

perturbed global eigenvalues, to obtain a first order approximation of the global frequency response function (FRF).

An example structure of two coupled rods is considered. The structure is modelled using CMS and a combination of correlated and uncorrelated uncertainty is introduced into the local eigenvalues of each rod. Expressions for the statistics of the global eigenvalues in terms of the statistics of the local eigenvalues are developed. A numerical example is presented and results from a Monte Carlo (MC) simulation compared to first order estimates of the FRF and variance of the global eigenvalues. The error in approximating the global eigenvalues is estimated and compared to the error found in the simulations. The distribution of the global eigenvalues from the MC simulation is examined, compared to a Gaussian distribution and a chi-squared goodness-of-fit test is applied. The accuracy of the first order approximation of the global eigenvectors is examined using a Modal Assurance Criteria (MAC) comparison.

8.1 Component mode synthesis matrices

As presented in chapter 6, the global system response can be calculated using the fixed interface CMS method in which the CMS mass and stiffness matrices are given by

$$\mathbf{K_q} = \begin{bmatrix} diag\left(\boldsymbol{\lambda}_\mathbf{F}\right)_\mathbf{j} & \mathbf{0} \\ \mathbf{0} & \boldsymbol{\kappa}_{cc} \end{bmatrix} \tag{8.1}$$

$$\mathbf{M_q} = \begin{bmatrix} \mathbf{I} & \boldsymbol{\mu}_{kc} \\ \boldsymbol{\mu}_{kc}{}^{T} & \boldsymbol{\mu}_{cc} \end{bmatrix} \tag{8.2}$$

the suffix *q* representing modal matrices as opposed to physical mass and stiffness matrices. The elements are defined in section 6.5. In particular

$$diag\left(\boldsymbol{\lambda}_\mathbf{F}\right)_\mathbf{j} = \begin{bmatrix} diag\left(\lambda_F^{(1)}\right)_j & 0 & 0 & 0 \\ 0 & \ddots & 0 & 0 \\ 0 & 0 & diag\left(\lambda_F^{(n)}\right)_j & 0 \\ 0 & 0 & 0 & \ddots \end{bmatrix} \tag{8.3}$$

has as its diagonal elements the component fixed interface natural frequencies where $diag\left(\lambda_F^{(n)}\right)_j$ is the *j*'th component natural frequency of the *n*'th component. Uncertainty in the

component modal properties thus gives uncertainty in $diag(\boldsymbol{\lambda}_j)$ and also in the matrices $\boldsymbol{\mu}_{kc}$, $\boldsymbol{\mu}_{cc}$ and $\boldsymbol{\kappa}_{cc}$ which include uncertainty in the component mode shapes.

To avoid confusion, the symbols $\boldsymbol{\Lambda}/\boldsymbol{\Phi}$ will be used to represent global eigenvalues/vectors as opposed to local component eigenvalues/vectors given by $\boldsymbol{\lambda}/\boldsymbol{\varphi}$. Thus, the global eigenvalues and vectors are found from $\left[\mathbf{K_q} - \Lambda_p \mathbf{M_q}\right]\boldsymbol{\Phi}_p = 0$ where $\boldsymbol{\Phi}_p$ is the p'th global modeshape and Λ_p is the p'th global eigenvalue. The CMS mass and stiffness matrices $\mathbf{K_q}$ and $\mathbf{M_q}$ can also be generated from the following transformation

$$\begin{aligned} \mathbf{M_q} &= \mathbf{S}^T\mathbf{M}\mathbf{S} \\ \mathbf{K_q} &= \mathbf{S}^T\mathbf{K}\mathbf{S} \end{aligned} \tag{8.4}$$

where $\mathbf{M}$ and $\mathbf{K}$ are the physical global mass and stiffness matrices for the structure, and $\mathbf{S}$ is given by

$$\mathbf{S} = \left[\begin{array}{cccc|c} \mathbf{B}_{f1} & 0 & 0 & 0 & \mathbf{C}_1 \\ 0 & \mathbf{B}_{f2} & 0 & 0 & \mathbf{C}_2 \\ 0 & 0 & \ddots & 0 & \vdots \\ 0 & 0 & 0 & \mathbf{B}_{fn} & \mathbf{C}_n \end{array}\right] \tag{8.5}$$

where $\mathbf{B}_{fn}$ are the fixed interface normal modes for the n'th component and $\mathbf{C}_n$ are the constraint modes for the n'th component.

The p'th global modeshape given by $\boldsymbol{\Phi}_p$, is defined in terms of the component modal degrees of freedom. Thus it expresses the global modeshape in terms of the subsystem component modes. These modeshapes are assumed to be mass normalised and can be related to the global eigenvectors $\boldsymbol{\psi}_p$ in physical d.o.f. by the transformation

$$\boldsymbol{\psi}_p = \mathbf{S}\boldsymbol{\Phi}_p \tag{8.6}$$

8.2 Introducing variability into the system

Uncertainty in the physical properties introduces uncertainties in the global mass and stiffness $\mathbf{M}$ and $\mathbf{K}$, and consequently uncertainties in $\mathbf{K_q}$ and $\mathbf{M_q}$ as discussed in chapter 7. Consider the case where variability is introduced into the *j*'th component natural frequency of the *i*'th component, $\left(\lambda_F^{(i)}\right)_j$, such that

$$\left(\lambda_F^{(i)}\right)_j = \left(\bar{\lambda}_F^{(i)}\right)_j \left(1 + x_j^{(i)}\right) \tag{8.7}$$

where $\left(\bar{\lambda}_F^{(i)}\right)_j$ is the baseline or unperturbed value, and $x_j^{(i)}$ is a random variable. No assumptions, at this stage, are made as to whether these variations are correlated in some way or fully independent, or on their distributions. If the variations are assumed to have zero mean, then the expected value of the perturbed component natural frequencies is the baseline or unperturbed value. The variance of the perturbed component natural frequencies is then given by

$$\sigma^2_{\left(\lambda_F^{(i)}\right)_j} = E\left[\left(\left(\lambda_F^{(i)}\right)_j\right)^2\right] = \left(\bar{\lambda}_F^{(i)}\right)_j^{\,2} \sigma^2_{x_j^{(i)}} \tag{8.8}$$

where $\sigma^2_{x_j^{(i)}}$ is the variance of the random variable $x_j^{(i)}$. These variations in the local modal eigenvalues $x_j^{(i)}$ form a variability vector $\mathbf{x}$, where x_i is the *i*'th element and $\boldsymbol{\mu}_\mathbf{x}$ is a vector of the mean values.

8.3 Effect on global eigenvalues

Using a mean centred first order perturbation as discussed in chapter 4, the global eigenvalues are given by

$$\Lambda_p \cong \bar{\Lambda}_p + \left(\frac{\partial \Lambda_p(\mathbf{x})}{\partial \mathbf{x}}\right)^T \Bigg|_{\mathbf{x}=\boldsymbol{\mu}} \mathbf{x} \tag{8.9}$$

where

$$\frac{\partial \Lambda_p(\mathbf{x})}{\partial \mathbf{x}} = \begin{bmatrix} \bar{\boldsymbol{\Phi}}_p{}^T \left[\dfrac{\partial \mathbf{K_q}}{\partial x_1} - \bar{\Lambda}_p \dfrac{\partial \mathbf{M_q}}{\partial x_1} \right] \bar{\boldsymbol{\Phi}}_p \\ \bar{\boldsymbol{\Phi}}_p{}^T \left[\dfrac{\partial \mathbf{K_q}}{\partial x_2} - \bar{\Lambda}_p \dfrac{\partial \mathbf{M_q}}{\partial x_2} \right] \bar{\boldsymbol{\Phi}}_p \\ \vdots \\ \bar{\boldsymbol{\Phi}}_p{}^T \left[\dfrac{\partial \mathbf{K_q}}{\partial x_i} - \bar{\Lambda}_p \dfrac{\partial \mathbf{M_q}}{\partial x_i} \right] \bar{\boldsymbol{\Phi}}_p \end{bmatrix} \tag{8.10}$$

and where the over-bar signifies baseline unperturbed values and $\mathbf{K_q}$ and $\mathbf{M_q}$ are the variable global CMS stiffness and mass matrices which are hence functions of $\mathbf{x}$. The suffix *p* is used to refer to global eigenvalues, and the suffix *j* is used to refer to local component eigenvalues.

From equation (8.1) and (8.7), $\mathbf{K_q}$ is given by

$$\mathbf{K_q} = \begin{bmatrix} diag\left(\left(\bar{\lambda}_F^{(i)} \right)_j \left(1 + x_j^{(i)} \right) \right) & \mathbf{0} \\ \mathbf{0} & \mathbf{k}_{cc} \end{bmatrix} \tag{8.11}$$

Each partial derivative $\dfrac{\partial \mathbf{K_q}}{\partial x_i}$ is given by

$$\frac{\partial \mathbf{K_q}}{\partial x_i} = \begin{bmatrix} diag\left(\left(\bar{\lambda}_F^{(i)} \right)_j \dfrac{\partial \mathbf{x}}{\partial x_i} \right) & \mathbf{0} \\ \mathbf{0} & \mathbf{0} \end{bmatrix} \tag{8.12}$$

By virtue of its definition, $\mathbf{M_q}$ is independent of variations in the component natural frequencies, and hence $\dfrac{\partial \mathbf{M_q}}{\partial \mathbf{x}} = \mathbf{0}$.

Combining the above results and equation (8.9), the first order perturbation of the *p*'th global eigenvalue is given by

$$\Lambda_p \cong \bar{\Lambda}_p + \mathbf{A}_{p\Lambda}^T \mathbf{x} \tag{8.13}$$

where

$$\mathbf{A}_{p\Lambda} = \left[\begin{array}{c} \bar{\mathbf{\Phi}}_p{}^T \begin{bmatrix} diag\left(\left(\bar{\lambda}_F^{(i)} \right)_j \dfrac{\partial \mathbf{x}}{\partial x_1} \right) & \mathbf{0} \\ \mathbf{0} & \mathbf{0} \end{bmatrix} \bar{\mathbf{\Phi}}_p \\ \bar{\mathbf{\Phi}}_p{}^T \begin{bmatrix} diag\left(\left(\bar{\lambda}_F^{(i)} \right)_j \dfrac{\partial \mathbf{x}}{\partial x_2} \right) & \mathbf{0} \\ \mathbf{0} & \mathbf{0} \end{bmatrix} \bar{\mathbf{\Phi}}_p \\ \vdots \\ \bar{\mathbf{\Phi}}_p{}^T \begin{bmatrix} diag\left(\left(\bar{\lambda}_F^{(i)} \right)_j \dfrac{\partial \mathbf{x}}{\partial x_i} \right) & \mathbf{0} \\ \mathbf{0} & \mathbf{0} \end{bmatrix} \bar{\mathbf{\Phi}}_p \end{array} \right]^T \Bigg|_{\mathbf{x}=\boldsymbol{\mu}_\mathbf{x}} \tag{8.14}$$

Therefore a perturbation in a component eigenvalue will lead to a large or small variation in the global eigenvalue, if the corresponding component of the eigenvector $\bar{\mathbf{\Phi}}_p$ is large or small. If there are m elements in the variability vector $\mathbf{x}$ and p global modes such that $\bar{\mathbf{\Phi}}_p$ has dimensions (p x 1), then the dimensions of $\mathbf{A}_{p\Lambda}$ are (p x m).

From chapter 4, if the mean value of the variability is zero $E[\mathbf{x}] = 0$ then the expected value of the perturbed global eigenvalues is $\Lambda_p \cong \bar{\Lambda}_p$, thus if there are no variations in the local component eigenvalues, there are no variations in the global eigenvalues.

8.3.1 Variance of the global eigenvalues

The relationship between the perturbed global eigenvalues and the perturbed local component eigenvalues in equation (8.13) can be used to relate their statistics. Of particular interest is the variance of the global eigenvalues as this is a good measure of the level of variability. Using the matrix format above the change in the variable global eigenvalues can be written as

$$\delta_{\Lambda_p} \cong \mathbf{A}_{p\Lambda}^T \mathbf{x} \tag{8.15}$$

The variance of δ_{Λ_p} is then given by

$$\mathrm{var}\left(\delta_{\Lambda_p} \right) \cong \mathbf{A}_{p\Lambda}{}^T \, \mathrm{var}(\mathbf{x}) \, \mathbf{A}_{p\Lambda} \tag{8.16}$$

where $\mathrm{var}\left(\delta_{\Lambda_p}\right)$ is the variance/covariance matrix of δ_{Λ_p} and similarly for $\mathbf{x}$. This directly relates the variance of the perturbed global eigenvalues to the variance and covariance of the local eigenvalues. Importantly, the diagonal terms of the matrix $\mathrm{var}(\mathbf{x})$ contain the variance of the change in the local eigenvalues, and the off-diagonal terms contain the covariance of the changes between local eigenvalues. Thus

$$\mathrm{var}(\mathbf{x}) = \begin{bmatrix} \sigma_{x_1}^2 & \sigma_{x_1x_2} & \cdots & \sigma_{x_1x_m} \\ \sigma_{x_1x_2} & \sigma_{x_2}^2 & \cdots & \sigma_{x_2x_m} \\ \vdots & \vdots & \ddots & \vdots \\ \sigma_{x_1x_m} & \sigma_{x_2x_m} & \cdots & \sigma_{x_m}^2 \end{bmatrix} \tag{8.17}$$

Similarly the matrix $\mathrm{var}\left(\delta_{\Lambda_p}\right)$ contains variance terms on the leading diagonal.

As can be seen from equation (8.16) and from $\mathbf{A}_{p\Lambda}$ as given in equation (7.24), the variance of a perturbation in a component eigenvalue will lead to a large or small variance in the variation in the global eigenvalue, if the corresponding component of the eigenvector $\bar{\mathbf{\Phi}}_p$ is large or small. It can also be noted that the variance of the *p*'th global eigenvalue is independent of the mean of the uncertainties.

If the correlations between the uncertainty in the component eigenvalues is assumed to be weak or non-existent, i.e. the covariance is zero, then the off-diagonal terms in $\mathrm{var}(\mathbf{x})$ are zero, and equation (8.16) becomes

$$\mathrm{var}\left(\delta_{\Lambda_p}\right) \cong \mathbf{A}_{p\Lambda}{}^T \, diag\left(\mathrm{var}(\mathbf{x})\right) \mathbf{A}_{p\Lambda} \tag{8.18}$$

Neglecting the covariance of the component eigenvalue variability is a potential area for data truncation or reduction, although it will of course lead to an approximation of the results, the significance of which will depend on the level of covariance, i.e. how strongly related the variabilites between component eigenvalues are, and the magnitude of the associated elements of the unperturbed global modal eigenvector.

8.3.1.1 Modal spacing and variability

Not only is the variance of the global eigenvalues of interest for examining the variability, but its relationship to the modal spacing is the limiting factor on the usefulness of a deterministic analysis. If the uncertainty in a specific global eigenvalue is taken to be approximately plus or minus one standard deviation $\pm\sigma_{\Lambda_p}$. Then the ratio of this to the average modal spacing can be thought of as the 'statistical overlap'. When examining the response from an ensemble of nominally identical structures, the uncertainties within the structures, give rise to the variance in the response. As the statistical overlap approaches one, the response of a given mode from one sample structure, may fall with the uncertainty range of a neighbouring mode on a different sample structure. Thus if the modal spacing is defined as $\bar{\Delta}_{\Lambda_p} = \bar{\Lambda}_{p+1} - \bar{\Lambda}_p$, then an approximate limiting factor is given by

$$\bar{\Delta}_{\Lambda_p} \cong 2\sqrt{\mathbf{A}_{p\Lambda}{}^T \operatorname{var}(\mathbf{x}) \mathbf{A}_{p\Lambda}} \tag{8.19}$$

8.3.2 Distribution of the global eigenvalues

Existing published work has considered the distribution of random global eigenvalue problems, but not considered them in terms of the statistics of the component eigenvalues. In addition to relating the statistics of the local eigenvalues to those of the global eigenvalues, the expression in equation (8.13) can, if the uncertainties in $\mathbf{x}$ are known, be used to estimate the distribution of the global eigenvalues. A method for this is presented below. From equation (8.13)

$$\Lambda_p \cong \bar{\Lambda}_p + \mathbf{A}_{p\Lambda}^T \mathbf{x} \tag{8.20}$$

The multivariate expression for the change of variable method for a general function $\mathbf{y}_n = y_n(\mathbf{x}_n)$, where it is assumed that $\mathbf{y}_n$ is an N-valued function of $\mathbf{x}_n$ as discussed in chapter 4, is given by

$$p(\mathbf{y}) = \frac{Np(\mathbf{x})}{\mathbf{J}} \tag{8.21}$$

where

$$p(y_1, y_2, ..., y_n) = \frac{Np(x_1, x_2, .., x_n)}{\begin{vmatrix} \frac{\partial y_1}{\partial x_1} & \frac{\partial y_1}{\partial x_2} & \cdots & \frac{\partial y_1}{\partial x_n} \\ \frac{\partial y_2}{\partial x_1} & \frac{\partial y_2}{\partial x_2} & \cdots & \frac{\partial y_2}{\partial x_n} \\ \cdots & \cdots & \cdots & \cdots \\ \frac{\partial y_n}{\partial x_1} & \frac{\partial y_n}{\partial x_2} & \cdots & \frac{\partial y_n}{\partial x_n} \end{vmatrix}} \tag{8.22}$$

Changes in the local component eigenvalues, do not lead to unique perturbed global eigenvalues. By definition from equation (8.7) the order of $\mathbf{x}$ depends on the number of components (i) and the number of kept local modes for each component $\left(\lambda_F^{(i)}\right)_j$ used. If the order of $\mathbf{x}$ is P (upper case is simply used here to avoid confusion with $p(x)$), then in equation (8.22) $N = P$ and $\mathbf{y}_n$ is a P valued function of $\mathbf{x}_n$.

In addition, as there are P input variables, a number of 'dummy' output variables must be introduced which can be later removed from resultant expression by integration. As we already have one required output variable, i.e. Λ_p, then $(P-1)$ 'dummy' output variables will be required. These can be selected to be equivalent to a subset of the input variables, e.g. $y_1 = \Lambda_p$, $y_2 = x_1$, $y_3 = x_2$ etc. such that

$$p(\Lambda_p, y_2 ..., y_{n-1}) = \frac{\mathrm{P}\, p(\mathbf{x})}{|\mathbf{J}|} \tag{8.23}$$

where $p(\mathbf{x}) = p(x_1, x_2, \cdots, x_m)$. This directly relates the PDF of the global eigenvalues to the PDF of the uncertainty in the local eigenvalues. Even without specific knowledge of the uncertainty terms $\mathbf{x}$, some broad comments can still be made on the distribution of the global perturbed eigenvalues based on examination of their general relationship to the uncertainties.

If the uncertainty terms in $\mathbf{x}$ are independent (i.e. uncorrelated) and all Gaussian distributed, but not necessarily from the same distribution (i.e. with the same mean and variance), then the distribution of the global perturbed eigenvalues will be Gaussian. This arises from the properties of the summation of independent Gaussian random variables see [8.8]. In this case the *p*'th global eigenvalue is a summation of independent Gaussian distributed variables, and hence is Gaussian distributed. The resultant Gaussian distribution will be centred around $\bar{\Lambda}_p$ and have a

variance given by equation (8.16). There is some evidence from the industrial results examined in chapters 2 and 3, to suggest that a Gaussian distribution is a reasonable assumption for the distribution of the local eigenvalues. In which case, only the variance and covariance's of the local component eigenvalues, are required to fully estimate the statistics of the global eigenvalues.

Alternatively, if the uncertainty terms are independent identically-distributed random variables, (i.e. have the same mean and variance), then as the number of terms increases The Central Limit Theorem [8.4] will apply and the distribution of the global perturbed eigenvalues will tend towards Gaussian. This is the classical interpretation of the more general set of central limit theorems, as all the input variables are required to have come from the same distribution, even though the type of distribution may be arbitrary. In this case the rate of convergence, i.e. the number of input variables required for the distribution of the *p*'th global eigenvalue to tend towards Gaussian, is estimated by the Berry-Esséen theorem [8.5] as at least on the order of $n^{-1/2}$, where n is the number of input variables. In this case there are P input variables, and hence the rate of convergence will be at least on the order of $(P)^{-1/2}$. In addition the theorem states that the convergence will be uniform. One caveat of the Berry-Esséen theorem is that the third central moment of the input distribution must exist and be finite.

Further more general applications of the central limit theorem do not require the input variables to have identical distributions but incorporate some condition which guarantees that none of the variables exert a much larger influence than the others. Two such conditions are the Lindeberg condition [8.5] and the Lyapunov condition [8.5]. These types of conditions are sometimes referred to as 'fuzzy' central limit theorems. Applying this to the distribution of the *p*'th global eigenvalue means that if the uncertainties in the local component eigenvalues are small and unrelated (and many in number), then the *p*'th global eigenvalue will be approximately Gaussian distributed.

Other generalisations of the central limit theorems allow some 'weak' dependence of the random variables (see [8.5] and [7.6]), such as the m-dependent central limit theorem, the martingale central limit theorem and the central limit theorem for mixing processes.

8.3.3 Estimation of the error

An estimation of the error in applying approximating the global eigenvalues by means of a first order perturbation can be obtained by calculating the second order term. From chapter 4, if the

eigenvalues are distinct then the general second order term of a mean centred perturbation is given by

$$\frac{1}{2}(\mathbf{x})^T \mathbf{D}_{\Lambda_p}\Big|_{\mathbf{x}=\boldsymbol{\mu}} (\mathbf{x}) \tag{8.24}$$

where

$$\left\{\mathbf{D}_{\Lambda_p}\right\}_{mn} = \frac{\partial^2 \Lambda_p}{\partial x_m \partial x_n}\Bigg|_{\mathbf{x}=\boldsymbol{\mu}} \tag{8.25}$$

$$\begin{aligned}\frac{\partial^2 \Lambda_p}{\partial x_m \partial x_n}\Bigg|_{\mathbf{x}=\boldsymbol{\mu}} = & \bar{\boldsymbol{\Phi}}_p{}^T \left[\frac{\partial^2 \mathbf{K_q}}{\partial x_m \partial x_n} - \bar{\Lambda}_p \frac{\partial \mathbf{M_q}^2}{\partial x_m \partial x_n}\right]\bar{\boldsymbol{\Phi}}_p - \left(\bar{\boldsymbol{\Phi}}_p{}^T \frac{\partial \mathbf{M_q}}{\partial x_m}\bar{\boldsymbol{\Phi}}_p\right)\left(\bar{\boldsymbol{\Phi}}_p{}^T \mathbf{G}_{pn}\bar{\boldsymbol{\Phi}}_p\right) \\ & - \left(\bar{\boldsymbol{\Phi}}_p{}^T \frac{\partial \mathbf{M_q}}{\partial x_n}\bar{\boldsymbol{\Phi}}_p\right)\left(\bar{\boldsymbol{\Phi}}_p{}^T \mathbf{G}_{pm}\bar{\boldsymbol{\Phi}}_p\right) + 2\sum_{\substack{r=1 \\ r\neq p}}^{N} \frac{\left(\bar{\boldsymbol{\Phi}}_p{}^T \mathbf{G}_{pm}\bar{\boldsymbol{\Phi}}_p\right)\left(\bar{\boldsymbol{\Phi}}_p{}^T \mathbf{G}_{pn}\bar{\boldsymbol{\Phi}}_p\right)}{\bar{\Lambda}_p - \bar{\Lambda}_r}\end{aligned} \tag{8.26}$$

$$\mathbf{G}_{pm} = \left[\frac{\partial \mathbf{K_q}}{\partial x_m} - \bar{\Lambda}_p \frac{\partial \mathbf{M_q}}{\partial x_m}\right] \tag{8.27}$$

and x_n is the n'th value of the variability vector $\mathbf{x}$. If variability is introduced into component eigenvalues of the general form as in equation (8.7)

$$\left(\lambda_F^{(i)}\right)_j = \left(\bar{\lambda}_F^{(i)}\right)_j \left(1 + x_j^{(i)}\right) \tag{8.28}$$

then the partial derivatives w.r.t. the mass matrix are zero, and the second derivative w.r.t. to the stiffness is also zero. Thus the second order term for the variability in the p'th global eigenvalue is given by

$$\frac{1}{2}(\mathbf{x})^T \frac{\partial^2 \Lambda_p}{\partial \mathbf{x}_m \partial \mathbf{x}_n}\Bigg|_{\mathbf{x}=\boldsymbol{\mu}} (\mathbf{x}) = (\mathbf{x})^T \left(\sum_{\substack{r=1 \\ r\neq p}}^{N} \frac{\mathbf{A}_{p\Lambda}\mathbf{A}_{p\Lambda}^T}{\bar{\Lambda}_p - \bar{\Lambda}_r}\right)(\mathbf{x}), \quad \forall m,n \tag{8.29}$$

where $\mathbf{A}_{p\Lambda}$ is as defined in equation (7.24). It can be noted that although the global eigenvalues are required to be distinct such that $\bar{\Lambda}_p \neq \bar{\Lambda}_r$, as they approach each other the contribution from

the second order term will increases significantly. It is proposed that the second order term be used as an estimation of the error in a first order estimation. This will be used later to examine the error in the estimation of the response of simple structure of two coupled rods.

8.4 Effect on global eigenvectors

A mean centred perturbation can also be used to obtain an estimation for the perturbed global eigenvectors. From chapter 4, a first order approximation can be obtained from a linear combination of the unperturbed eigenvectors

$$\frac{\partial \boldsymbol{\psi}_p}{\partial x_m} \cong \sum_{v=1}^{n} a_{pmv} \bar{\boldsymbol{\psi}}_v \tag{8.30}$$

where the index v gives all the global modes, and

$$a_{pmv} = \frac{\bar{\boldsymbol{\psi}}_v{}^T \left[\dfrac{\partial \mathbf{K_q}}{\partial x_m} - \bar{\Lambda}_p \dfrac{\partial \mathbf{M_q}}{\partial x_m} \right] \bar{\boldsymbol{\psi}}_p}{\bar{\Lambda}_p - \bar{\Lambda}_v}, \qquad v \neq p \tag{8.31}$$

$$a_{pmp} = -\frac{1}{2} \bar{\boldsymbol{\psi}}_p{}^T \frac{\partial \mathbf{M_q}}{\partial x_m} \bar{\boldsymbol{\psi}}_p \tag{8.32}$$

The perturbation is performed on the p'th physical global eigenvector $\boldsymbol{\psi}_p$, as opposed to the modal eigenvector $\boldsymbol{\Phi}_p$; the two are related as in equation (6.84). The total first order variation in the global eigenvectors is obtained from summing the contributions from the perturbations in each component mode. Consider the case, as before, where variability is introduced into component natural frequencies $\left(\lambda_F^{(i)}\right)_j$ such that $\left(\lambda_F^{(i)}\right)_j = \left(\bar{\lambda}_F^{(i)}\right)_j \left(1 + x_j^{(i)}\right)$, then using equations (4.32) to (8.32) and writing in general matrix format as used in chapters 5 and 7, the first order perturbation of the eigenvectors can be written as

$$\boldsymbol{\psi}_p \cong \bar{\boldsymbol{\psi}}_p + \sum_{v=1}^{n} \frac{\mathbf{A}_{p\boldsymbol{\psi}}{}^T \mathbf{x}}{\bar{\Lambda}_p - \bar{\Lambda}_v} \bar{\boldsymbol{\psi}}_v, \qquad v \neq p \tag{8.33}$$

where

$$\mathbf{A}_{p\boldsymbol{\psi}} = \begin{bmatrix} \bar{\boldsymbol{\psi}}_v^{\,T} \begin{bmatrix} diag\left(\left(\bar{\lambda}_F^{(i)}\right)_j \dfrac{\partial \mathbf{x}}{\partial x_1}\right) & \mathbf{0} \\ \mathbf{0} & 0 \end{bmatrix} \bar{\boldsymbol{\psi}}_p \\ \bar{\boldsymbol{\psi}}_v^{\,T} \begin{bmatrix} diag\left(\left(\bar{\lambda}_F^{(i)}\right)_j \dfrac{\partial \mathbf{x}}{\partial x_2}\right) & \mathbf{0} \\ \mathbf{0} & 0 \end{bmatrix} \bar{\boldsymbol{\psi}}_p \\ \vdots \\ \bar{\boldsymbol{\psi}}_v^{\,T} \begin{bmatrix} diag\left(\left(\bar{\lambda}_F^{(i)}\right)_j \dfrac{\partial \mathbf{x}}{\partial x_m}\right) & \mathbf{0} \\ \mathbf{0} & 0 \end{bmatrix} \bar{\boldsymbol{\psi}}_p \end{bmatrix} \tag{8.34}$$

Thus the change in eigenvectors can be expressed as

$$\boldsymbol{\delta\psi}_p \cong \sum_{v=1}^{n} \frac{\mathbf{A}_{p\boldsymbol{\psi}}{}^{T}\mathbf{x}}{\bar{\Lambda}_p - \bar{\Lambda}_v} \bar{\boldsymbol{\psi}}_v, \qquad v \neq p \tag{8.35}$$

This takes the original method for the first order perturbation of the eigenvectors from Fox and Kapoor [4.5] and extends it to relate them directly to the uncertainty in the local component eigenvalues. This result can now be used in conjunction with the estimated global eigenvalues, to obtain a first order estimate of the global FRF.

8.5 Frequency response function

The undamped FRF measured at the response at point X_r due to a harmonic force $Fe^{i\omega t}$ applied at X_e, is given by

$$\frac{W(X_r)}{F} = \sum_p \frac{\boldsymbol{\psi}_p(X_r)\boldsymbol{\psi}_p(X_e)}{\left(\Lambda_p - \Lambda\right)} \tag{8.36}$$

where the eigenvectors are assumed to be mass normalised. Combining the first order perturbation approximations for the global perturbed eigenvalues and eigenvectors, the undamped FRF function can be approximated as

$$\frac{W(X_r)}{F} = \sum_p \frac{\left(\bar{\boldsymbol{\psi}}_p(X_r) + \sum_{v=1}^{n} \frac{\mathbf{A}_{p\boldsymbol{\psi}}(X_r)\mathbf{x}}{\bar{\Lambda}_p - \bar{\Lambda}_v}\bar{\boldsymbol{\psi}}_v\right)\left(\bar{\boldsymbol{\psi}}_p(X_e) + \sum_{v=1}^{n} \frac{\mathbf{A}_{p\boldsymbol{\psi}}(X_e)\mathbf{x}}{\bar{\Lambda}_p - \bar{\Lambda}_v}\bar{\boldsymbol{\psi}}_v\right)}{\left(\bar{\Lambda}_p + \mathbf{A}_{p\Lambda}^T\mathbf{x} - \Lambda\right)}, \qquad v \neq p$$

(8.37)

where from equations (7.24) and (8.34),

$$\mathbf{A}_{p\Lambda} = \left[\begin{array}{c} \bar{\boldsymbol{\Phi}}_p{}^T \begin{bmatrix} diag\left(\left(\bar{\lambda}_F^{(i)}\right)_j \frac{\partial \mathbf{x}}{\partial x_1}\right) & \mathbf{0} \\ \mathbf{0} & \mathbf{0} \end{bmatrix} \bar{\boldsymbol{\Phi}}_p \\ \bar{\boldsymbol{\Phi}}_p{}^T \begin{bmatrix} diag\left(\left(\bar{\lambda}_F^{(i)}\right)_j \frac{\partial \mathbf{x}}{\partial x_2}\right) & \mathbf{0} \\ \mathbf{0} & \mathbf{0} \end{bmatrix} \bar{\boldsymbol{\Phi}}_p \\ \vdots \\ \bar{\boldsymbol{\Phi}}_p{}^T \begin{bmatrix} diag\left(\left(\bar{\lambda}_F^{(i)}\right)_j \frac{\partial \mathbf{x}}{\partial x_i}\right) & \mathbf{0} \\ \mathbf{0} & \mathbf{0} \end{bmatrix} \bar{\boldsymbol{\Phi}}_p \end{array}\right]_{\mathbf{x}=\boldsymbol{\mu}_\mathbf{x}} \tag{8.38}$$

$$\mathbf{A}_{p\boldsymbol{\psi}}(X_r) = \left[\begin{array}{c} \bar{\boldsymbol{\psi}}_v(X_r)^T \begin{bmatrix} diag\left(\left(\bar{\lambda}_F^{(i)}\right)_j \frac{\partial \mathbf{x}}{\partial x_1}\right) & \mathbf{0} \\ \mathbf{0} & 0 \end{bmatrix} \bar{\boldsymbol{\psi}}_p(X_r) \\ \bar{\boldsymbol{\psi}}_v(X_r)^T \begin{bmatrix} diag\left(\left(\bar{\lambda}_F^{(i)}\right)_j \frac{\partial \mathbf{x}}{\partial x_2}\right) & \mathbf{0} \\ \mathbf{0} & 0 \end{bmatrix} \bar{\boldsymbol{\psi}}_p(X_r) \\ \vdots \\ \bar{\boldsymbol{\psi}}_v(X_r)^T \begin{bmatrix} diag\left(\left(\bar{\lambda}_F^{(i)}\right)_j \frac{\partial \mathbf{x}}{\partial x_m}\right) & \mathbf{0} \\ \mathbf{0} & 0 \end{bmatrix} \bar{\boldsymbol{\psi}}_p(X_r) \end{array}\right] \tag{8.39}$$

similarly for $\mathbf{A}_{p\boldsymbol{\psi}}(X_e)$. In section 8.7 this expression for the first order estimation of the FRF of the structure will be compared to a Monte Carlo simulation for the example of two coupled rods.

8.6 Correlated and uncorrelated constituents of the substructure uncertainty

The general form of the uncertainty in the substructure natural frequencies was defined in equation (8.7) as

$$\left(\lambda_F^{(i)}\right)_j = \left(\bar{\lambda}_F^{(i)}\right)_j \left(1 + x_j^{(i)}\right) \tag{8.40}$$

No assumptions were made on the possible correlations between terms. However, it can be helpful to consider separating this general form into several types of uncertainty. The various sources of variability in a structure can be divided into four categories (β symbols have generally been used to signify correlated uncertainties and ε to represent uncorrelated), consider these to be given by:

1) Full correlated variations in a particular component that affect all the eigenvalues in that particular component. An example might be variations in the Young's modulus or similar material properties that affect the whole component. These variations are assumed to be uncorrelated across different components and hence are represented by $\varepsilon^{(i)}$ for subsystem i.
2) As (1) except there is assumed to be some correlation in the variations across components. An example might be two components which whilst modelled separately are manufactured from the same base material and hence changes in the material properties have a correlated effect on both components. Another possible example might be a tensioned joint condition between two components which puts some global stress into both components. They are given by $\beta^{(i)}$ for subsystem i.
3) Correlated variations in the individual eigenvalues within a particular component. These might arise, for example, from geometric deformities within a component that leads to some spatially correlated variation in the local eigenvalues. They are given by $\beta_j^{(i)}$ for the j'th eigenvalue in subsystem i.
4) Uncorrelated random variations in the individual eigenvalues. These are the random variations in each component eigenvalue which are uncorrelated to each other and uncorrelated across components. They are given by $\varepsilon_j^{(i)}$ for the j'th eigenvalue in subsystem i.

Splitting the variability into these four source types can be useful when considering an example. The total variability in a component eigenvalue is a sum of these different types of variability such that

$$x_j^{(i)} = \varepsilon^{(i)} + \beta^{(i)} + \varepsilon_j^{(i)} + \beta_j^{(i)} \tag{8.41}$$

No assumptions are made on the distributions of any of these terms, however they are all assumed to be independent from each other and to have zero mean. The uncertainty in the component eigenvalues is now of the form

$$\left(\lambda_F^{(i)}\right)_j = \left(\overline{\lambda}_F^{(i)}\right)_j \left(1 + \varepsilon^{(i)} + \beta^{(i)} + \varepsilon_j^{(i)} + \beta_j^{(i)}\right) \tag{8.42}$$

Expanding the representation of the uncertainty in this way allows for the separation of the correlated and uncorrelated sources of uncertainty. An example structure will now be considered, with uncertainty in the component eigenvalues in this form.

8.7 Numerical example

Consider the example of two coupled rods, see Figure 8-1.

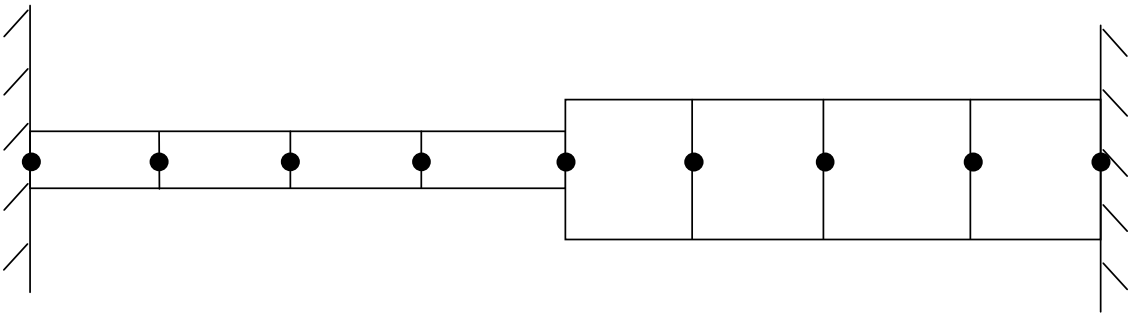

Figure 8-1 Two coupled rods.

The rods are modelled as a mass spring chain. Each rod has four elements and there are seven global degrees of freedom (DOF). For fixed interface CMS analysis of the structure, it divides into two obvious components; component one being the first rod and component two being the second rod. Each component has three internal DOF and three fixed interface modes.

The elements of the global CMS mass and stiffness matrices $\mathbf{K_q}$ and $\mathbf{M_q}$ are given by

$$diag\left(\left(\lambda_F\right)_j\right)=\begin{bmatrix} \left(\overline{\lambda}_F^{(1)}\right)_1 & 0 & 0 & 0 & 0 & 0 \\ 0 & \left(\overline{\lambda}_F^{(1)}\right)_2 & 0 & 0 & 0 & 0 \\ 0 & 0 & \left(\overline{\lambda}_F^{(1)}\right)_3 & 0 & 0 & 0 \\ 0 & 0 & 0 & \left(\overline{\lambda}_F^{(2)}\right)_1 & 0 & 0 \\ 0 & 0 & 0 & 0 & \left(\overline{\lambda}_F^{(2)}\right)_2 & 0 \\ 0 & 0 & 0 & 0 & 0 & \left(\overline{\lambda}_F^{(2)}\right)_3 \end{bmatrix} \tag{8.43}$$

$$\kappa_{cc}=\kappa_{cc}^{(1)}+\kappa_{cc}^{(2)} \tag{8.44}$$

$$\mu_{kc}=\begin{Bmatrix}\mu_{kc}^{(1)}\\ \mu_{kc}^{(2)}\end{Bmatrix} \tag{8.45}$$

$$\mu_{cc}=\mu_{cc}^{(1)}+\mu_{cc}^{(2)} \tag{8.46}$$

A specific scenario of correlated and uncorrelated uncertainty is considered. In order to best demonstrate the contributions from both correlated and uncorrelated uncertainty, the example shown here will include each of the four types of uncertainty $\varepsilon^{(i)}$, $\varepsilon_j^{(i)}$, $\beta^{(i)}$ and $\beta_j^{(i)}$.

Assume that component one has some fully correlated variations in its fixed interface eigenvalues due to material property uncertainties, this will be given by $\varepsilon^{(1)}$. Component two is assumed to have no such uncertainties, such that $\varepsilon^{(2)}=0$. There exists a joint between the two components, which exerts some stress into both rods and gives rise to some correlated variations in all the fixed interface eigenvalues for both components

$$\beta^{(2)}=2\beta^{(1)} \tag{8.47}$$

In addition component one due to manufacturing processes has a spatially correlated term, $\beta_j^{(1)}$ term given by

$$\beta_j^{(1)} = \beta \sin\left(\frac{(j-1)\pi}{4}\right), \quad \beta_j^{(2)} = 0 \tag{8.48}$$

Finally, there are some uncorrelated random variations in the local eigenvalues in component two. From equation (8.13) and the assumptions above, an approximation of the p'th global eigenvalues is given by

$$\Lambda_p \cong \bar{\Lambda}_p + \mathbf{A}_{p\Lambda}^T \mathbf{x} \tag{8.49}$$

where

$$\mathbf{x}^T = \left[\varepsilon^{(1)} \quad \beta^{(1)} \quad \beta \quad \varepsilon_1^{(2)} \quad \varepsilon_2^{(2)} \quad \varepsilon_3^{(2)} \right] \tag{8.50}$$

and the p'th row of $\mathbf{A}_{p\Lambda}^T$ is given by (the fixed interface subscript for the component modes has been dropped for brevity)

$$\mathbf{A}_{p\Lambda}^T = \left[\bar{\Phi}_p{}^T diag \begin{pmatrix} \bar{\lambda}_1^{(1)} \\ \bar{\lambda}_2^{(1)} \\ \bar{\lambda}_3^{(1)} \\ 0 \\ 0 \\ 0 \\ 0 \end{pmatrix} \bar{\Phi}_p \quad \bar{\Phi}_p{}^T diag \begin{pmatrix} \bar{\lambda}_1^{(1)} \\ \bar{\lambda}_2^{(1)} \\ \bar{\lambda}_3^{(1)} \\ 2\bar{\lambda}_1^{(2)} \\ 2\bar{\lambda}_2^{(2)} \\ 2\bar{\lambda}_3^{(2)} \\ 0 \end{pmatrix} \bar{\Phi}_p \quad \bar{\Phi}_p{}^T diag \begin{pmatrix} 0 \\ \sin\left(\frac{\pi}{4}\right)\bar{\lambda}_2^{(1)} \\ \sin\left(\frac{\pi}{2}\right)\bar{\lambda}_3^{(1)} \\ 0 \\ 0 \\ 0 \\ 0 \end{pmatrix} \bar{\Phi}_p \quad \bar{\Phi}_p{}^T diag \begin{pmatrix} 0 \\ 0 \\ 0 \\ \bar{\lambda}_1^{(2)} \\ 0 \\ 0 \\ 0 \end{pmatrix} \bar{\Phi}_p \quad \bar{\Phi}_p{}^T diag \begin{pmatrix} 0 \\ 0 \\ 0 \\ 0 \\ \bar{\lambda}_2^{(2)} \\ 0 \\ 0 \end{pmatrix} \bar{\Phi}_p \quad \bar{\Phi}_p{}^T diag \begin{pmatrix} 0 \\ 0 \\ 0 \\ 0 \\ 0 \\ \bar{\lambda}_3^{(2)} \\ 0 \end{pmatrix} \bar{\Phi}_p \right] \tag{8.51}$$

Similarly, from equation (8.35) the perturbed p'th global physical eigenvector can be shown to be given by

$$\boldsymbol{\delta\psi}_p \cong \sum_{v=1}^{n} \frac{\mathbf{A}_{p\psi}{}^T \mathbf{x}}{\bar{\Lambda}_p - \bar{\Lambda}_v} \bar{\boldsymbol{\psi}}_v, \qquad v \neq p \tag{8.52}$$

where (again the fixed interface subscript has been dropped)

$$\mathbf{A}_{p\psi} = \left[\bar{\psi}_v{}^T diag\begin{pmatrix} \bar{\lambda}_1^{(1)} \\ \bar{\lambda}_2^{(1)} \\ \bar{\lambda}_3^{(1)} \\ 0 \\ 0 \\ 0 \end{pmatrix} \bar{\psi}_p \quad \bar{\psi}_v{}^T diag\begin{pmatrix} \bar{\lambda}_1^{(1)} \\ \bar{\lambda}_2^{(1)} \\ \bar{\lambda}_3^{(1)} \\ 2\bar{\lambda}_1^{(2)} \\ 2\bar{\lambda}_2^{(2)} \\ 2\bar{\lambda}_3^{(2)} \\ 0 \end{pmatrix} \bar{\psi}_p \quad \bar{\psi}_v{}^T diag\begin{pmatrix} 0 \\ \sin\left(\frac{\pi}{4}\right)\bar{\lambda}_2^{(1)} \\ \sin\left(\frac{\pi}{2}\right)\bar{\lambda}_3^{(1)} \\ 0 \\ 0 \\ 0 \\ 0 \end{pmatrix} \bar{\psi}_p \quad \bar{\psi}_v{}^T diag\begin{pmatrix} 0 \\ 0 \\ 0 \\ \bar{\lambda}_1^{(2)} \\ 0 \\ 0 \\ 0 \end{pmatrix} \bar{\psi}_p \quad \bar{\psi}_v{}^T diag\begin{pmatrix} 0 \\ 0 \\ 0 \\ 0 \\ \bar{\lambda}_2^{(2)} \\ 0 \\ 0 \end{pmatrix} \bar{\psi}_p \quad \bar{\psi}_v{}^T diag\begin{pmatrix} 0 \\ 0 \\ 0 \\ 0 \\ 0 \\ \bar{\lambda}_3^{(2)} \\ 0 \end{pmatrix} \bar{\psi}_p \right] \tag{8.53}$$

The variance of the p'th global eigenvalue can be estimated from equation (8.16) as,

$$\mathrm{var}\left(\delta_{\Lambda_p}\right) \cong \mathbf{A}_{p\Lambda}{}^T \,\mathrm{var}(\mathbf{x})\,\mathbf{A}_{p\Lambda} \tag{8.54}$$

where the p'th row of $\mathbf{A}_{p\Lambda}$ is given by equation (8.51) and $\mathrm{var}(\mathbf{x})$ is given by

$$\mathrm{var}(\mathbf{x}) = \begin{bmatrix} \sigma^2_{\varepsilon^{(1)}} & \sigma_{\varepsilon^{(1)}\beta^{(1)}} & \sigma_{\varepsilon^{(1)}\beta} & \sigma_{\varepsilon^{(1)}\varepsilon_1^{(2)}} & \sigma_{\varepsilon^{(1)}\varepsilon_2^{(2)}} & \sigma_{\varepsilon^{(1)}\varepsilon_3^{(2)}} \\ \sigma_{\varepsilon^{(1)}\beta^{(1)}} & \sigma^2_{\beta^{(1)}} & \sigma_{\beta^{(1)}\beta} & \sigma_{\beta^{(1)}\varepsilon_1^{(2)}} & \sigma_{\beta^{(1)}\varepsilon_2^{(2)}} & \sigma_{\beta^{(1)}\varepsilon_3^{(2)}} \\ \sigma_{\varepsilon^{(1)}\beta} & \sigma_{\beta^{(1)}\beta} & \sigma^2_{\beta} & \sigma_{\beta\varepsilon_1^{(2)}} & \sigma_{\beta\varepsilon_2^{(2)}} & \sigma_{\beta\varepsilon_3^{(2)}} \\ \sigma_{\varepsilon^{(1)}\varepsilon_1^{(2)}} & \sigma_{\beta^{(1)}\varepsilon_1^{(2)}} & \sigma_{\beta\varepsilon_1^{(2)}} & \sigma^2_{\varepsilon_1^{(2)}} & \sigma_{\varepsilon_1^{(2)}\varepsilon_2^{(2)}} & \sigma_{\varepsilon_1^{(2)}\varepsilon_3^{(2)}} \\ \sigma_{\varepsilon^{(1)}\varepsilon_2^{(2)}} & \sigma_{\beta^{(1)}\varepsilon_2^{(2)}} & \sigma_{\beta\varepsilon_2^{(2)}} & \sigma_{\varepsilon_1^{(2)}\varepsilon_2^{(2)}} & \sigma^2_{\varepsilon_2^{(2)}} & \sigma_{\varepsilon_2^{(2)}\varepsilon_3^{(2)}} \\ \sigma_{\varepsilon^{(1)}\varepsilon_3^{(2)}} & \sigma_{\beta^{(1)}\varepsilon_3^{(2)}} & \sigma_{\beta\varepsilon_3^{(2)}} & \sigma_{\varepsilon_1^{(2)}\varepsilon_3^{(2)}} & \sigma_{\varepsilon_2^{(2)}\varepsilon_3^{(2)}} & \sigma^2_{\varepsilon_3^{(2)}} \end{bmatrix} \tag{8.55}$$

From this the statistical overlap, which limits the usefulness of a deterministic analysis, can also be estimated

$$\bar{\Delta}_{\Lambda_p} \cong 2\sqrt{\sigma_{\Lambda_p}{}^2} \tag{8.56}$$

A Monte Carlo simulation of a numerical example was conducted in Matlab [7.3]. The baseline, unperturbed, mass and stiffness matrices for the two components are given by

$$M^{(1)} = \begin{bmatrix} 0.35 & 0 & 0 & 0 & 0 \\ 0 & 0.7 & 0 & 0 & 0 \\ 0 & 0 & 0.7 & 0 & 0 \\ 0 & 0 & 0 & 0.7 & 0 \\ 0 & 0 & 0 & 0 & 0.35 \end{bmatrix}, K^{(1)} = \begin{bmatrix} 1.4 & -1 & 0 & 0 & 0 \\ -1 & 2 & -1 & 0 & 0 \\ 0 & -1 & 2.3 & -1.3 & 0 \\ 0 & 0 & -1.3 & 2.3 & -1 \\ 0 & 0 & 0 & -1 & 1 \end{bmatrix} \tag{8.57}$$

$$M^{(2)} = \begin{bmatrix} 1 & 0 & 0 & 0 & 0 \\ 0 & 2 & 0 & 0 & 0 \\ 0 & 0 & 2 & 0 & 0 \\ 0 & 0 & 0 & 2 & 0 \\ 0 & 0 & 0 & 0 & 1 \end{bmatrix}, K^{(2)} = \begin{bmatrix} 2.3 & -2.3 & 0 & 0 & 0 \\ -2.3 & 5.2 & -2.9 & 0 & 0 \\ 0 & -2.9 & 5.2 & -2.3 & 0 \\ 0 & 0 & -2.3 & 4.6 & -2.3 \\ 0 & 0 & 0 & -2.3 & 2.3 \end{bmatrix} \tag{8.58}$$

The values of the component mass and stiffnesses were chosen such that the ratios of the free-free eigenvalues of the components are irrational.

In order to provide a realistic FRF light proportional damping was added to the structure, where $\zeta = 0.01$ is the modal damping ratio. This was assumed to be constant in each mode such that the FRF is given by

$$\frac{W(X_r)}{F} = \sum_p \frac{\boldsymbol{\psi}_p(X_r)\boldsymbol{\psi}_p(X_e)}{\left(\Lambda_p - \Lambda + 2i\zeta\sqrt{\Lambda_p\Lambda}\right)} \tag{8.59}$$

The uncertainty terms in $\mathbf{x}$ have a standard deviation of $\sigma = 0.012$ and are taken from a Gaussian distribution with zero mean. This results in combined normalised standard deviations for each local component natural frequency as given in Table 8-1. This level of uncertainty was chosen to demonstrate typical levels of uncertainty seen in the manufactured components.

Component mode	σ
$\left(\bar{\lambda}_F^{(1)}\right)_1$	0.017
$\left(\bar{\lambda}_F^{(1)}\right)_2$	0.019
$\left(\bar{\lambda}_F^{(1)}\right)_3$	0.021
$\left(\bar{\lambda}_F^{(2)}\right)_1$	0.027
$\left(\bar{\lambda}_F^{(2)}\right)_2$	0.027
$\left(\bar{\lambda}_F^{(2)}\right)_3$	0.027

Table 8-1 Normalised standard deviation of the local component modes.

Figure 8-2 shows an example FRF for the baseline unperturbed system. Figure 8-3 shows the FRFs for a sample 20 realisations of the structure. From this the variability in the response due to the uncertainty in the local component natural frequencies can be seen.

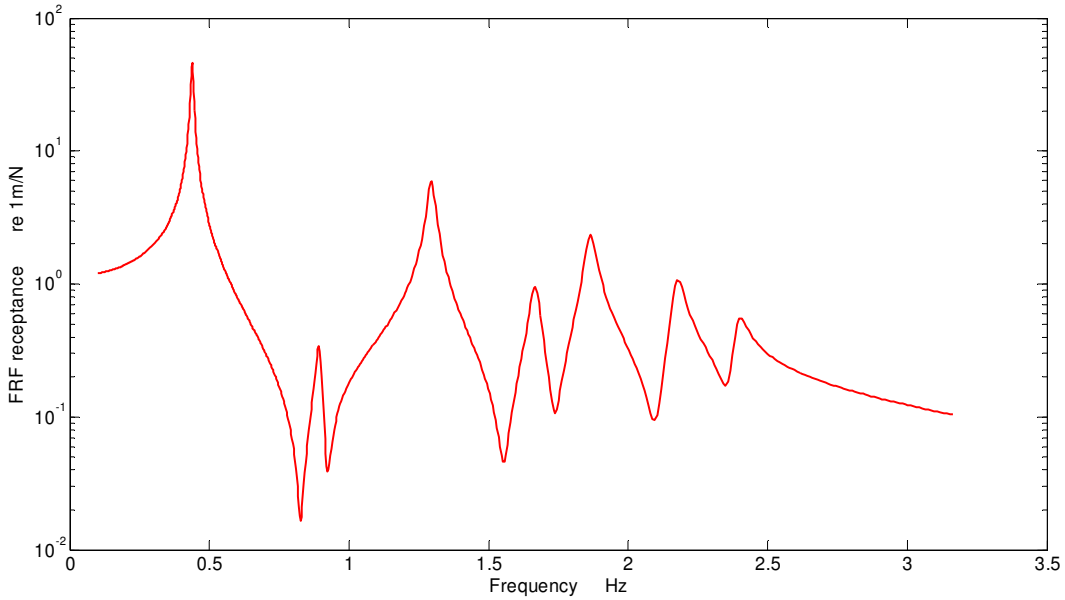

Figure 8-2 FRF (point receptance) of baseline structure (excitation applied at joint).

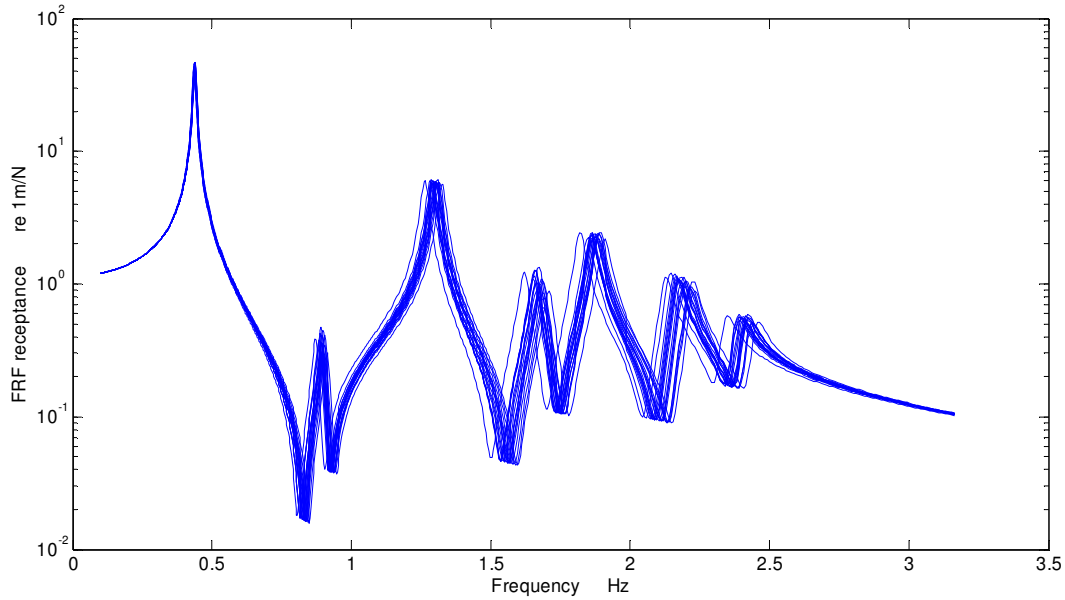

Figure 8-3 FRF (point receptance) of 20 realisations of the structure (excitation applied at joint).

Figure 8-4 shows the maximum/minimum envelope of the response for an ensemble of 1000 structures. In particular it compares the envelope of an 'exact' eigensolution of the ensemble, compared to the envelope of their estimated FRFs from a first order estimation of both the global eigenvalues and eigenvectors.

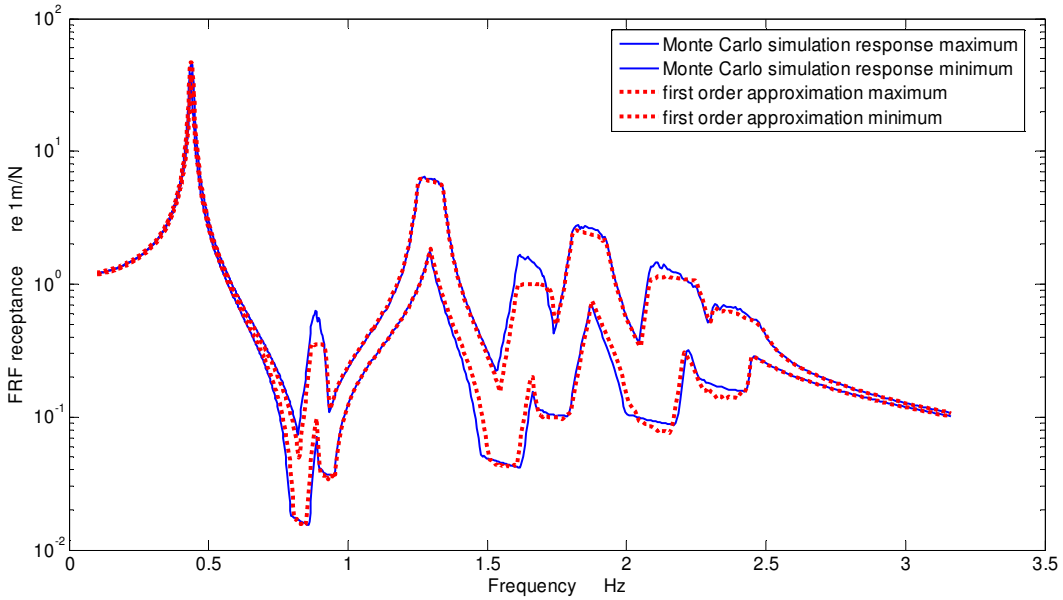

Figure 8-4 FRF (point receptance) comparison of exact and first order approximation, 1000 realisations.

As it can be seen from the results, the first order estimation provides a very good approximation to the FRF.

In Table 8-2 the first order estimate of the variance of the p'th global eigenvalue, from equation (8.16), is compared to that obtained from the Monte Carlo simulation of the above ensemble of 1000 realisations of the structure.

p 'th global mode	1st order approximation of variance	MC simulation 1000 realisations	% difference
1	7.572E-07	7.668E-07	1.2
2	2.123E-04	2.135E-04	0.6
3	1.055E-03	1.078E-03	2.1
4	3.109E-03	3.191E-03	2.6
5	4.166E-03	4.257E-03	2.2
6	1.342E-02	1.399E-02	4.1
7	1.341E-02	1.342E-02	0.1

Table 8-2 Variance of the p'th global eigenvalue.

The first order estimation of the variance is reasonably accurate with the percentage difference between the two of up to 4.1%. It can be noticed that the first order estimation is always less than that from the MC simulation.

As the variance increases with increasing global eigenvalues, so the limit for statistical overlap will be approached. It can be seen in Figure 8-4 that the spread of results for the sixth and seventh mode are starting to merge. The statistical overlap as given by equation (8.56) can estimated as an indication of the spread of the global modes in comparison to their spacing. The spacing between the sixth and seventh global mode of the baseline unperturbed system results in a statistical overlap of 1.07. Table 8-3 shows the statistical overlap for the first six modes of the structure

Modes	Statistical overlap
1-2	0.004
2-3	0.072
3-4	0.175
4-5	0.565
5-6	0.414
6-7	1.071

Table 8-3 Statistical overlap for the first six modes.

The second order term can be calculated as an estimate of the error in the approximation of the *p*'th global eigenvalue. Table 8-4 shows the average results for 1000 MC simulations. The exact eigensolution result and the first order perturbation approximation are listed for comparison. From these an 'actual percentage error' is calculated. This can be compared to the estimated percentage error generated from the second order term. For this numerical example the error in the first order approximation is very small. The second order term provides a good general indication of the likely error.

p 'th global mode	Eigenvalue	1st order approximation	2nd order term	Actual % error	Estimated % error
1	0.1919	0.1919	-0.0002	-0.0104	-0.0894
2	0.7970	0.7971	-0.0003	-0.0113	-0.0384
3	1.6759	1.6760	-0.0005	-0.0060	-0.0291
4	2.7759	2.7770	-0.0010	-0.0396	-0.0353
5	3.4733	3.4725	0.0001	0.0230	0.0025
6	4.7288	4.7290	-0.0008	-0.0042	-0.0159
7	5.7196	5.7189	0.0004	0.0122	0.0073

Table 8-4 Estimation of the error in a first order approximation of the global eigenvalues.

The distribution of the global eigenvalues from the MC simulation can be examined. Two typical examples of the results are shown in Figure 8-5 and Figure 8-6. Also shown in the figures are Gaussian distributions with the same mean and variance as each set of eigenvalues. It can be seen that a Gaussian distribution appears to be a good fit to the distribution of the global eigenvalues. To test this, a χ^2 goodness-of-fit test has been conducted. The results are given as cumulative χ^2 results such that a probability of below 95% represents a 95% confidence that the sample set cannot be rejected as having come from the distribution being tested against, see [8.8] for further information. The χ^2 test is conducted on classified (binned) data and outlying bins are summed to ensure at least five counts in each; this reduces the skewing effect of outlying results. A summary of the subsequent results can be found in Table 8-5. Also shown are the results for a MC simulation of increased size (an additional 1000 runs).

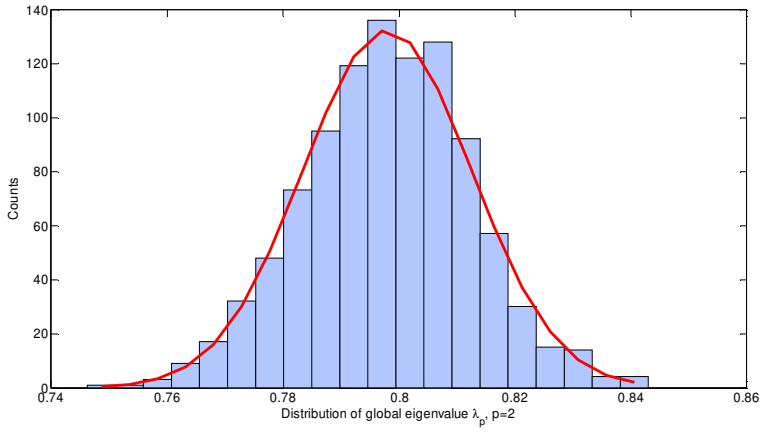

Figure 8-5 Distribution of the 2nd global eigenvalue $p = 2$, 1000 MC runs.

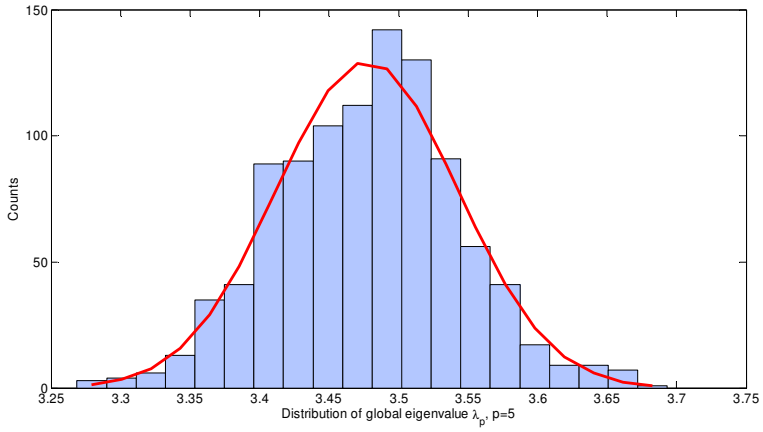

Figure 8-6 Distribution of the 5th global eigenvalue $p = 5$, 1000 MC runs.

Global eigenvalue	Number of MC summulation runs = 1000	Number of MC summulation runs = 2000
1	0.95	0.11
2	0.25	0.49
3	0.88	0.55
4	0.76	0.35
5	0.98	0.64
6	0.16	0.48
7	0.77	0.01

Table 8-5 Cumulative χ^2 results for the goodness-of-fit of the global eigenvalues to a Gaussian distribution.

From the χ^2 results in Table 8-5 it can be seen that for a simulation size of 1000 runs, five of the seven global eigenvalues cannot be rejected as having come from a Gaussian distribution. For an increased sample size of 2000 MC runs, the distribution of all the global modes cannot be rejected as having come from a Gaussian distribution. As for this example, the uncertainty terms in $\mathbf{x}$ were specified to be Gaussian distributed, then from equation (8.13) it can be seen that the component eigenvalues will be Gaussian distributed. This is by virtue of the premise that the sum of independent, Gaussian distributed variables is itself Gaussian distributed. As the *p*'th global eigenvalue is a summation of the variations in the component eigenvalues, it will also tend towards a Gaussian distribution.

The first order estimation of the *p*'th global eigenvector can be compared to an exact eigenvector from an eigensolution with a Modal Assurance Criterion (MAC) comparison as used in chapter 7. As a reminder the MAC number for the comparison of two eigenvectors ϕ_A and ϕ_B, is given by

$$MAC(A,B) = \frac{\left|\phi_A^H \phi_B\right|^2}{\left(\phi_A^H \phi_A\right)\left(\phi_B^H \phi_B\right)} \tag{8.60}$$

where ϕ_A^H is the complex conjugate transpose. In this example a MAC comparison has been used to compare the first order estimation of the global eigenvectors to those obtained from a MC simulation. The MAC values are averaged and the average MAC result for the comparison of each eigenvector pair is shown in Figure 8-7. The average MAC value for each eigenvector comparison is labelled on the plot. As it can be seen from the results, the first order perturbation of the global eigenvectors provides a very good estimate of the exact result.

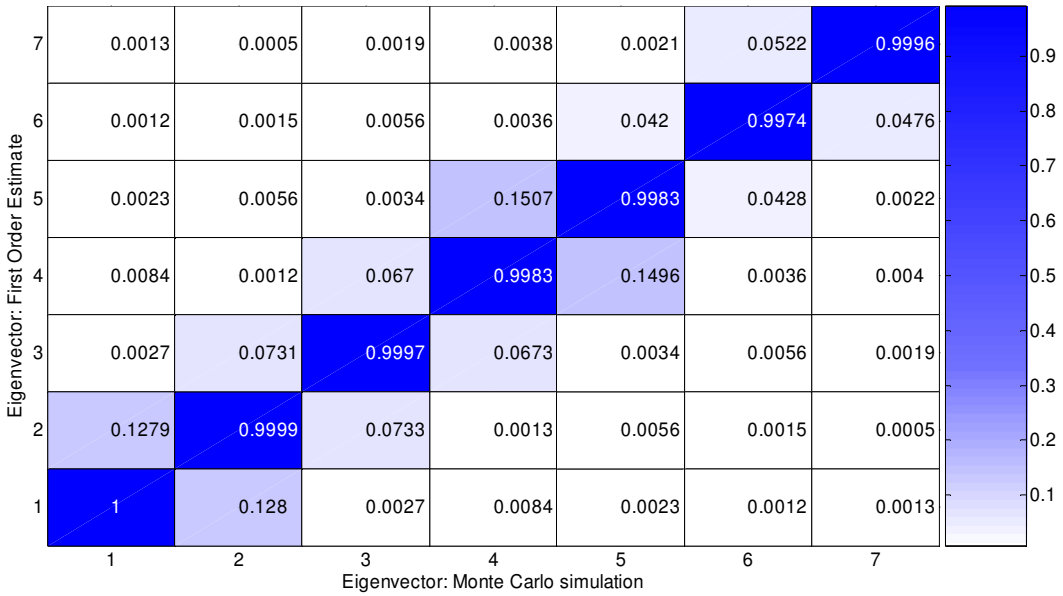

Figure 8-7 MAC eigenvector comparison of first order estimate.

8.8 Conclusions

In this chapter the LMP method was extended to obtain estimates for the statistics of the global eigenvalues for any general perturbations, correlated or uncorrelated, in the local eigenvalues of a structure. An expression for the variance of the global eigenvalues was developed, and this was shown to depend on the variance and covariance of the substructure local eigenvalues and the global modal eigenvectors of the unperturbed structure. From this the spread of the response of the global eigenvalues can be estimated from a single eigensolution of the baseline system, and the statistics of the substructure eigenvalues. In practice, the substructure eigenvalue statistics are usually more convenient to measure or predict than the statistics of the physical properties. Furthermore there is some evidence from industrial results which suggests that the distribution of component eigenvalues is typically Gaussian or close to Gaussian. If this is assumed to be the case, then a smaller sample set of measured component natural frequencies would be required to estimate the statistics of the ensemble accurately. Indeed for a structure which is in the early design stages, it may be sufficient to use the typical variance of a similar component as a reasonable first estimate.

It was suggested that the second order perturbation term can be used as an estimation of the error in approximating the perturbed global eigenvalues, and a general expression for this generated. A method for obtaining the distribution of the global perturbed eigenvalues was presented. Several possible applications of central limit theorems were suggested as approximations to this distribution. Alternatively, if the distribution of the substructure local

eigenvalues was assumed to be Gaussian, then it was shown that the distribution of the global perturbed eigenvalues will also be Gaussian, with expressions for the mean and variance generated. An expression for the perturbed global eigenvectors is generated using a first order perturbation and this is used to obtain an expression for a first order estimate of the structure's FRF.

A numerical example of two coupled rods was considered and a combination of correlated and uncorrelated uncertainty was introduced into the local eigenvalues of each rod. Comparisons are made for the estimated statistics of the response compared to those obtained from a MC simulation. The first order estimation of the statistics of the global eigenvalues was found to be very accurate, as was the first order estimate of the perturbed global eigenvectors which were used to generate an estimated FRF function. The second order perturbation term was calculated and compared to the actual error in estimating the global eigenvalues.

The ability to combine the substructure uncertainties whilst modelling them separately allows for the design of a component to be altered without the need to remodel the whole structure, which makes the method very flexible. It also allows for the possibility of conducting studies to rank the substructure variabilities for their contribution to the global eigenvalue variations, thus allowing cost effective targeting of tolerance reduction methods.

In chapter 9 a numerical example is considered, the methods developed in chapters 7 and 8 are applied and compared to results obtained from a MC simulation.

9. Numerical Example

In the previous chapters the relationship between the variability in the structure's physical properties to the variability in the modal properties has been investigated. Expressions relating the variability statistics to the response statistics have been generated. In this chapter a more complex numerical example than those presented in the previous two chapters will be used to demonstrate the application of the methods presented earlier. The example consists of a three-dimensional frame intended to represent an idealised automotive vehicle chassis frame. The frame is formed from two sub-components and variability is introduced into both the physical properties and local modal properties. The results are compared to those obtained from a Monte Carlo simulation.

Further details of the example structure and the FE model are outlined in the following introduction. The results obtained from the model are divided into two main sections, which generally correspond to the methods developed in chapters 7 and 8. The first of these considers the propagation of uncertainty from the physical properties to the local modal properties of the components. The second section is concerned with the propagation of uncertainty from the local modal properties to the global modal properties and ultimately the frequency response function (FRF).

9.1 Introduction

The numerical example considered is of a 3-dimensional frame shown in Figure 9-1. The frame is 1.2m long and 0.9m wide. Each beam is assumed to have a circular cross-section with a radius of 0.02m. It is considered to be constructed from two separate components which possess independent variability in their physical properties. The two components are shown in the figure. The frame represents an idealised vehicle chassis frame and the material properties have been selected to approximate steel. The baseline material properties are summarised in Appendix C.

An FE model [9.1] has been constructed of the frame using space frame elements. A space frame element is a straight bar of uniform cross-section which is capable of resisting axial forces, bending moments about the two principal axes in the plane of its cross section and twisting moment about its centroid axis [9.2]. Each element has twelve degrees of freedom (DOF) arising from the three translational and three rotational axes, from a node at each end. Therefore the mass and stiffness matrices for each element are 12x12 matrices. These are given

in Appendix C. The FE model consists of 17 elements and 16 nodes, which are shown in Figure 9-2. The frame is considered to be fixed to ground at node 1 to eliminate rigid-body modes. For details on Finite Element methods refer to [9.1]. A fixed interface component mode synthesis model was then created using the local modal results for each of the two components from the baseline FE model. The division of the frame into components attempted to avoid creating structures with symmetrical geometries, as this typically results in a large number of pairs of modes. There are some difficulties in predicting the response statistics of modes where the modal overlap is high. In practice FE analysis of symmetrical structures are typically conducted on a portion of the model with appropriate boundary conditions applied at the axis of symmetry. Rather than further sub-divide the component FE models, their geometries were chosen to avoid symmetry.

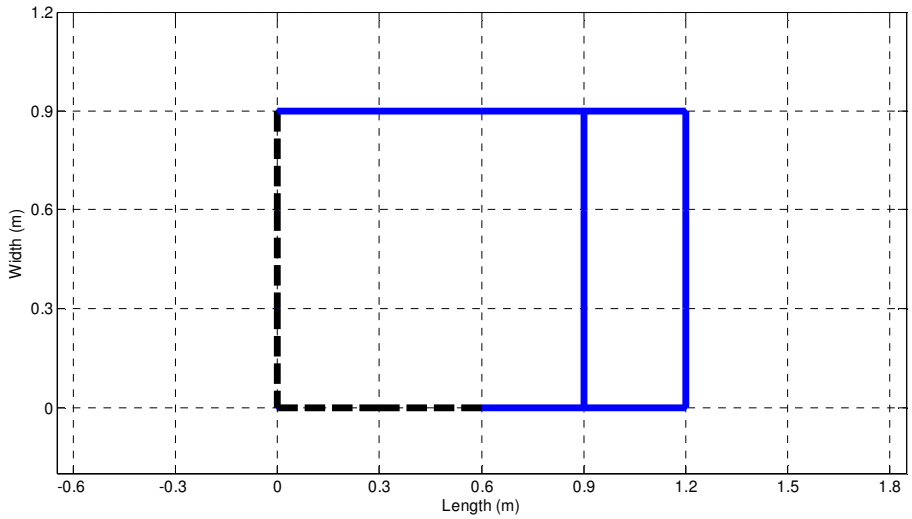

Figure 9-1 Frame: component 1, component 2.

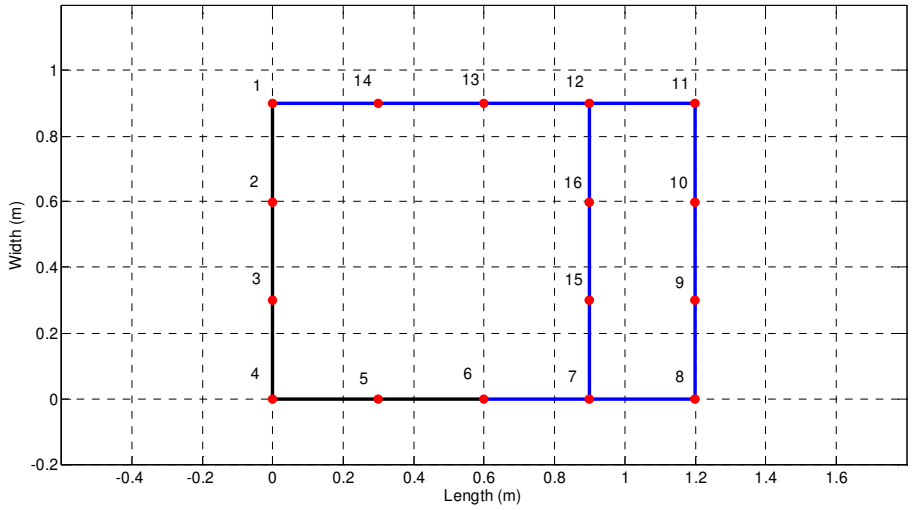

Figure 9-2 Finite element model node locations.

9.2 Variability from physical properties to component modal properties

In a similar manner to the example presented in chapter 7, variability is introduced into the physical properties of the two components of the frame. It is assumed, for ease of modelling, that the variabilities introduced into the mass and stiffnesses of each component are independent of each other. Hence any changes in the mass arise from density variations and do not affect the stiffness and any stiffness changes arise from the Young's modulus and do not affect the mass. However, correlations do exist between the stiffness of elements within the same component, and similarly for the mass.

The specific scenario considered is as follows:

- The stiffness of each element in component 1 varies by the same correlated amount represented by $\varepsilon_k^{(1)}$.
- The mass of each element within component 1 varies independently such that the q'th element varies by an amount $\varepsilon_{m,q}^{(1)}$.
- The stiffness of each element within component 2 varies independently such that the r'th element varies by an amount $\varepsilon_{k,r}^{(2)}$.
- The mass of each element in component 2 varies with a sinusoidal correlation around the frame by an amount $\varepsilon_m^{(2)}$.

The sinusoidal correlation in the mass of component two is of the same form as that applied to the mass of a beam in chapter 7.

These uncertainties form a variability vector $\boldsymbol{\varepsilon}_{\mathbf{P}}$ of physical property variations. There are five elements in component 1 and twelve elements in component 2, hence $\boldsymbol{\varepsilon}_{\mathbf{P}}$ is of size (19×1), and is given by

$$\boldsymbol{\varepsilon}_{\mathbf{P}} = \begin{bmatrix} \varepsilon_k^{(1)} & \varepsilon_{m,q}^{(1)} & \cdots & \varepsilon_{m,5}^{(1)} & \varepsilon_{k,r}^{(2)} & \cdots & \varepsilon_{k,12}^{(2)} & \varepsilon_m^{(2)} \end{bmatrix}^T \tag{9.1}$$

The variability terms within $\boldsymbol{\varepsilon_P}$ were randomly generated from a Gaussian distribution with zero mean and a standard deviation of 0.03; this was based on the typical levels of standard deviation seen in manufactured components as discussed in chapter 2.

In Table 9-1 the first ten fixed interface eigenvalues for each component are summarised. Listed for comparison are the baseline values from the components with unperturbed properties, the average results from a MC simulation (1000 realisations) with variable physical properties, and the first order approximations. Also shown is the percentage error between the MC simulation and the first order approximation. The second order perturbation term was also calculated as an estimation of the percentage error incurred in only using a first order approximation.

***j*'th component mode**	**Baseline eigenvalue $(rad/s)^2$**	**Average eigenvalue MC simulation $(rad/s)^2$**	**1st order approximation $(rad/s)^2$**	**% error of 1st order approx. w.r.t. MC simulation**	**Estimated % error based on 2nd order perturbation term**
Component 1					
1	6.830E+06	6.821E+06	6.820E+06	0.02	-0.30
2	1.359E+07	1.357E+07	1.356E+07	0.03	-0.70
3	1.604E+07	1.602E+07	1.602E+07	0.02	0.64
4	2.858E+07	2.853E+07	2.852E+07	0.03	0.13
5	4.598E+07	4.592E+07	4.590E+07	0.03	-0.34
6	5.427E+07	5.419E+07	5.417E+07	0.04	0.66
7	6.710E+07	6.699E+07	6.697E+07	0.03	1.03
8	9.355E+07	9.342E+07	9.337E+07	0.05	0.82
9	1.150E+08	1.149E+08	1.148E+08	0.05	1.59
10	1.808E+08	1.805E+08	1.804E+08	0.04	1.44
Component 2					
1	1.770E+06	1.769E+06	1.770E+06	-0.06	-0.24
2	1.988E+06	1.988E+06	1.989E+06	-0.04	0.28
3	5.663E+06	5.659E+06	5.664E+06	-0.08	-0.05
4	9.357E+06	9.345E+06	9.354E+06	-0.09	-0.09
5	1.283E+07	1.283E+07	1.283E+07	-0.01	-0.51
6	1.374E+07	1.372E+07	1.374E+07	-0.09	0.17
7	1.664E+07	1.663E+07	1.664E+07	-0.05	0.18
8	2.168E+07	2.160E+07	2.168E+07	-0.36	-2.31
9	2.186E+07	2.194E+07	2.187E+07	0.34	2.01
10	2.314E+07	2.315E+07	2.314E+07	0.04	0.64

Table 9-1 Component first order perturbation approximation of fixed interface eigenvalue, 1000 MC realisations.

In general the second order term over estimates the error in the first order approximation, but still provides a useful indication of the likely discrepancy. The size of the second order term increases with frequency, due to the modal summation term in the second order expansion. This has the effect of increasing the size of the second order term as the modal spacing reduces,

which is the case at higher frequencies. At higher frequencies the modal spacing decreases and the response of a given mode from one sample component may fall within the uncertainty range of a neighbouring mode on a different sample of the component. The statistical overlap is defined as the ratio of the uncertainty in a specific eigenvalue (taken to be approximately plus or minus one standard deviation), to the average modal spacing. This indicates the useful limits of a deterministic analysis. The statistical overlap may also be a concern at lower frequencies when two modes of a component are particularly close together or equal. The statistical overlap of the first ten modes for each component is shown in Table 9-2.

	Statistical overlap	
Modes	**Component 1**	**Component 2**
1-2	0.1	0.3
2-3	0.4	0.0
3-4	0.1	0.0
4-5	0.1	0.1
5-6	0.4	0.5
6-7	0.3	0.1
7-8	0.2	0.2
8-9	0.3	2.8
9-10	0.1	0.4

Table 9-2 Statistical overlap of the first ten modes for each component.

The first ten fixed interface modes of component 1 are well spaced, however, the eighth mode of component 2 is very close to the ninth mode and the statistical overlap is greater than 1. This will compromise the estimation of the variance of the eighth and ninth modes of component two as the variability within the modes is greater than the spacing between them.

Table 7-2 shows a comparison of the first order estimation of the variance of the fixed interface component eigenvalues to results obtained from the MC simulation of 1000 realisations. The first order estimation of the variance in component 1 is quite good with a maximum error of 3.74%. For component 2 the variance of the eighth and ninth modes can be seen to be quite inaccurate. This is due to the model spacing issue identified above. Otherwise, the maximum error in the first order estimation of the variance for component 2 is −10.51%. In general the first order estimations of the variance for component 1 are more accurate than those for component 2. This is due to component 2 consisting of many more elements than component 1, and with variability being introduced into each element hence the variability in the component as whole is greater. As the number of realisations in the MC simulation is increased the percentage error between the MC simulation and the first order approximation reduces. For a MC simulation of 5000 realisations the maximum percentage error for the first order

approximation of the variance in the first ten fixed interface eigenvalues of component 1 is 1.79% and in component 2 is −5.04% (eighth and ninth mode estimations not included).

j 'th component mode	MC simulation 1000 realisations $(rad/s)^4$	1st order approximation of variance $(rad/s)^4$	% error
Component 1			
1	5.506E+10	5.380E+10	2.29
2	2.282E+11	2.212E+11	3.08
3	3.032E+11	2.964E+11	2.24
4	9.427E+11	9.077E+11	3.71
5	2.440E+12	2.363E+12	3.14
6	3.492E+12	3.368E+12	3.56
7	5.048E+12	4.864E+12	3.64
8	1.019E+13	9.824E+12	3.58
9	1.523E+13	1.478E+13	2.91
10	3.790E+13	3.648E+13	3.74
Component 2			
1	7.823E+08	8.089E+08	-3.40
2	1.516E+09	1.573E+09	-3.75
3	5.890E+09	5.904E+09	-0.24
4	1.479E+10	1.552E+10	-4.91
5	5.087E+10	5.494E+10	-8.00
6	3.419E+10	3.639E+10	-6.41
7	1.516E+11	1.675E+11	-10.51
8	6.656E+10	9.621E+10	-44.56
9	7.048E+10	9.225E+10	-30.89
10	8.723E+10	9.199E+10	-5.47

Table 9-3 Component fixed interface eigenvalue variance.

One potential area of approximation identified in chapter 6 was the use of free interface component statistics to approximate fixed interface component statistics. The normalised standard deviation of the fixed interface eigenvalues is compared to that of the free interface eigenvalues in Table 9-4. It can be seen from the results that they are similar in level. This supports the use of the free interface variance in place of the fixed interface values.

	MC simulation 1000 realisations	
***j*'th component mode**	**Normalised standard deviation of the *j*'th free interface mode**	**Normalised standard deviation of the *j*'th fixed interface mode**
Component 1		
1	0.035	0.034
2	0.034	0.035
3	0.036	0.034
4	0.034	0.034
5	0.035	0.034
6	0.034	0.034
7	0.034	0.034
8	0.035	0.034
9	0.034	0.034
10	0.037	0.034
Component 2		
1	0.019	0.016
2	0.019	0.020
3	0.019	0.014
4	0.011	0.013
5	0.020	0.018
6	0.011	0.013
7	0.016	0.023
8	0.023	0.012
9	0.013	0.012
10	0.014	0.013

Table 9-4 Comparison of component fixed and free interface normalised standard deviation of eigenvalues.

The distribution of the natural frequencies $\left(\sqrt{\lambda_j}\right)$ has been examined. In Figure 9-3 to Figure 9-7, the results obtained for the MC simulation of the fixed interface modes for component 2 (upper graphs), are compared to those from the first order perturbation (lower graphs). Also shown are Gaussian distributions with the same mean and variance as each set of natural frequencies.

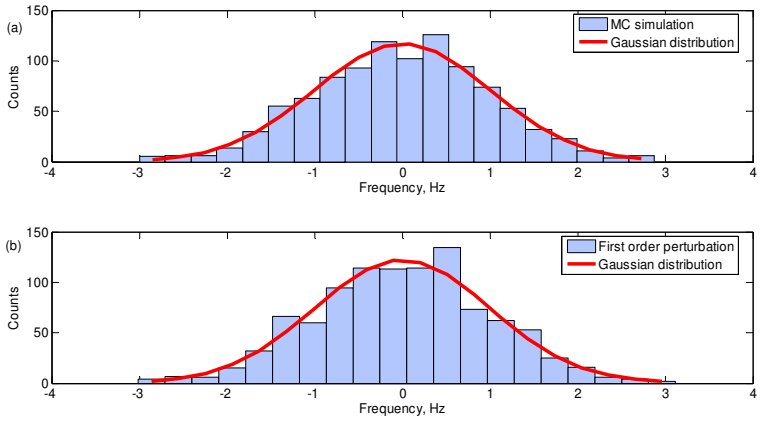

Figure 9-3 Distribution of the first natural frequency of component 2 with fixed boundary conditions, (a) 1000 MC simulations, (b) first order perturbation.

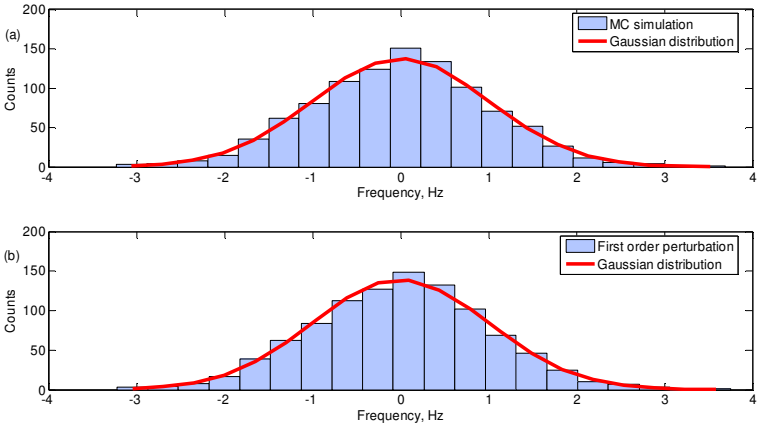

Figure 9-4 Distribution of the second natural frequency of component 2 with fixed boundary conditions, (a) 1000 MC simulations, (b) first order perturbation.

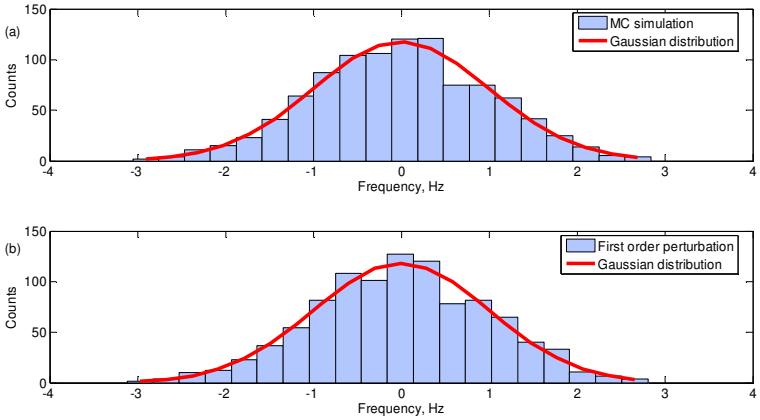

Figure 9-5 Distribution of the third natural frequency of component 2 with fixed boundary conditions, (a) 1000 MC simulations, (b) first order perturbation.

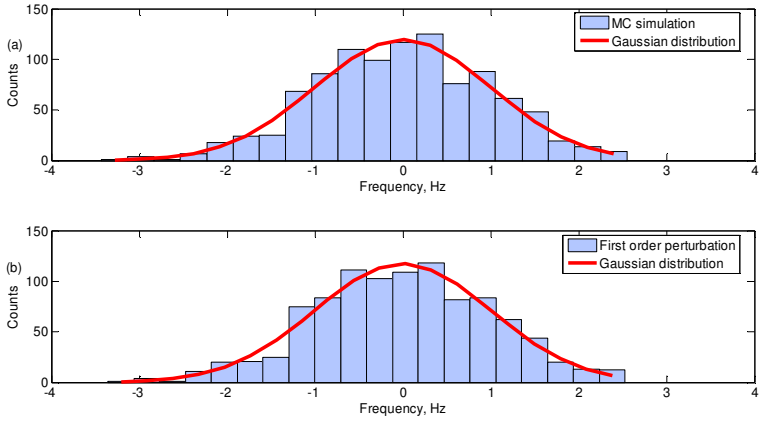

Figure 9-6 Distribution of the fourth natural frequency of component 2 with fixed boundary conditions, (a) 1000 MC simulations, (b) first order perturbation.

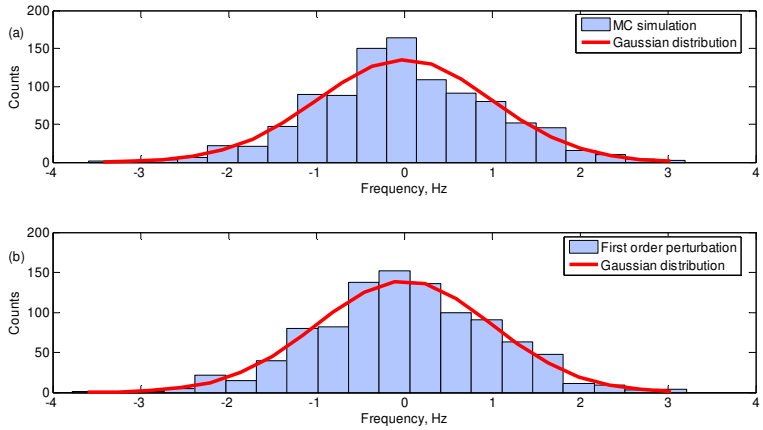

Figure 9-7 Distribution of the fifth natural frequency of component 2 with fixed boundary conditions, (a) 1000 MC simulations, (b) first order perturbation.

The results for component 1 are similar but are not shown here for brevity. In section 7.1.3 the possibility of the central limit theorem applying was discussed. It can be seen that a Gaussian distribution appears to be a good fit to the distributions of the component natural frequencies. To test the goodness-of-fit, a χ^2 test has been conducted; the cumulative χ^2 probabilities are listed in Table 9-5 (a value below 95% represents a 95% confidence that the sample set cannot be rejected as having come from the distribution being tested against). For further information on the χ^2 test see [2.10].

j 'th component mode	MC simulation	First order perturbation	MC simulation	First order perturbation
	Component 1		Component 2	
1	96.6%	92.1%	42.0%	94.2%
2	75.3%	69.2%	4.8%	1.2%
3	99.4%	98.7%	17.5%	56.5%
4	61.6%	50.4%	92.6%	95.7%
5	79.2%	95.8%	99.8%	99.4%
6	74.2%	72.8%	78.5%	37.0%
7	71.9%	74.0%	35.4%	27.0%
8	90.1%	87.6%	76.7%	54.6%
9	84.8%	99.7%	91.9%	66.3%
10	96.9%	98.5%	24.2%	81.0%

Table 9-5 χ^2 **goodness of fit of the fixed interface component natural frequencies to a Gaussian distribution; summary of cumulative probabilities.**

It can be seen from Table 9-5 that for component 1, seven of the first ten modes from the MC simulation cannot be rejected as having come from a Gaussian distribution (six for the first order perturbation). For component 2, nine of the modes from the MC simulation cannot be rejected as having come from a Gaussian distribution (eight for the first order perturbation). These results confirm the conclusions in chapter 7 that for Gaussian distributed variability in the physical properties the eigenvalues can be expected to tend towards a Gaussian distribution. It is likely that the higher number of modes from component 2 with a probability of less than 95% (compared to component 1), is due to the larger number of elements in component 2 increasing the variability and increasing the tendency towards a Gaussian distributed response.

For comparison the MC simulations were repeated with Rayleigh distributed variability in the physical properties. This was done to investigate if the component natural frequencies still tend towards a Gaussian distribution even if the variabilities in the physical properties are not Gaussian distributed. The Rayleigh distribution was selected as it can, under some circumstances, approach a Gaussian distribution, and the results from chapters 2 and 3 found some evidence for variability in components being Gaussian or near to Gaussian distributed. The variability terms were randomly generated from a Rayleigh distribution with a standard deviation of 0.03. The Rayleigh distribution is a positive distribution, and so the resultant values were normalised around zero by subtracting the mean; these then formed the elements of $\boldsymbol{\varepsilon_P}$. The resultant distribution in the component natural frequencies was again tested against a Gaussian distribution and the results are shown in Table 9-6.

j 'th component mode	MC simulation	First order perturbation	MC simulation	First order perturbation
	Component 1		Component 2	
1	100.0%	100.0%	69.3%	90.5%
2	100.0%	100.0%	99.8%	99.9%
3	100.0%	100.0%	60.0%	37.6%
4	100.0%	100.0%	15.9%	60.0%
5	100.0%	100.0%	57.8%	99.0%
6	100.0%	100.0%	94.6%	96.5%
7	100.0%	100.0%	99.6%	100.0%
8	100.0%	100.0%	7.6%	2.9%
9	100.0%	100.0%	98.3%	98.7%
10	100.0%	100.0%	42.7%	23.9%

Table 9-6 χ^2 goodness of fit of the fixed interface component natural frequencies to a Gaussian distribution with Rayleigh distributed physical properties; summary of cumulative probabilities.

The distribution of the eigenvalues of component 1 can all be rejected as having come from a Gaussian distribution. However, for component 2 seven of the first ten modes from the MC simulation cannot be rejected as being Gaussian distributed (five of the ten modes for the first order perturbation). These results would support the hypothesis that the higher number of elements in component 2 increases the tendency towards the central limit theorem applying and the distribution of the eigenvalues approaching a Gaussian distribution.

A first order approximation for the component eigenvectors has been calculated for a Gaussian distributed variability. The results are compared to those obtained from the MC simulation using an orthogonality comparison. This is equivalent to a mass scaled MAC. Figure 9-8 shows an orthogonality comparison for the first fourteen fixed interface modes of component 2. As with the MAC values used in chapters 7 and 8, the orthogonality values are averaged and the mean value represented by the z-axis of the colour-map and for ease of viewing labelled on the figure. The first order perturbation of the component eigenvectors provides a very good estimation at low frequencies. At higher frequencies the variability in the response increases and the first order approximation is less accurate. Figure 9-9 shows an orthogonality comparison for the twelve fixed interface modes of component 1. The first order perturbation for component 1 provides an excellent estimation of the eigenvectors. As with the eigenvalues discussed earlier, component 1 consists of less elements than component 2, and with variability introduced into the physical properties of each element, the response of component 1 generally displays less variability than that of component 2.

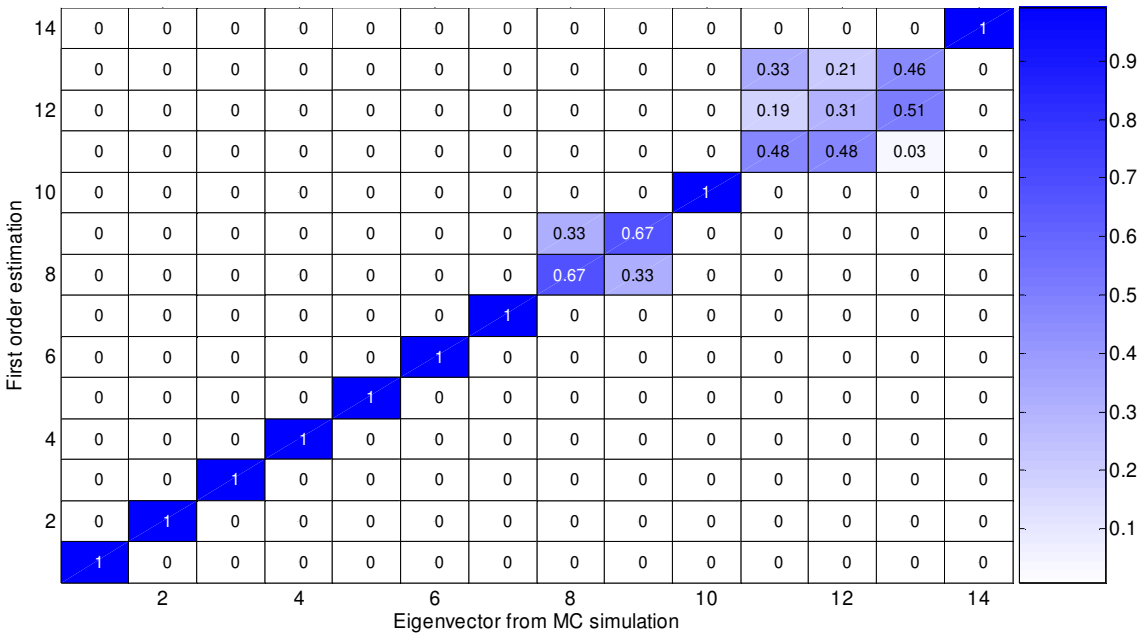

Figure 9-8 Orthogonality comparison of the first order perturbation of eigenvector to MC simulation: component 2 fixed interface modes, 1000 realisations.

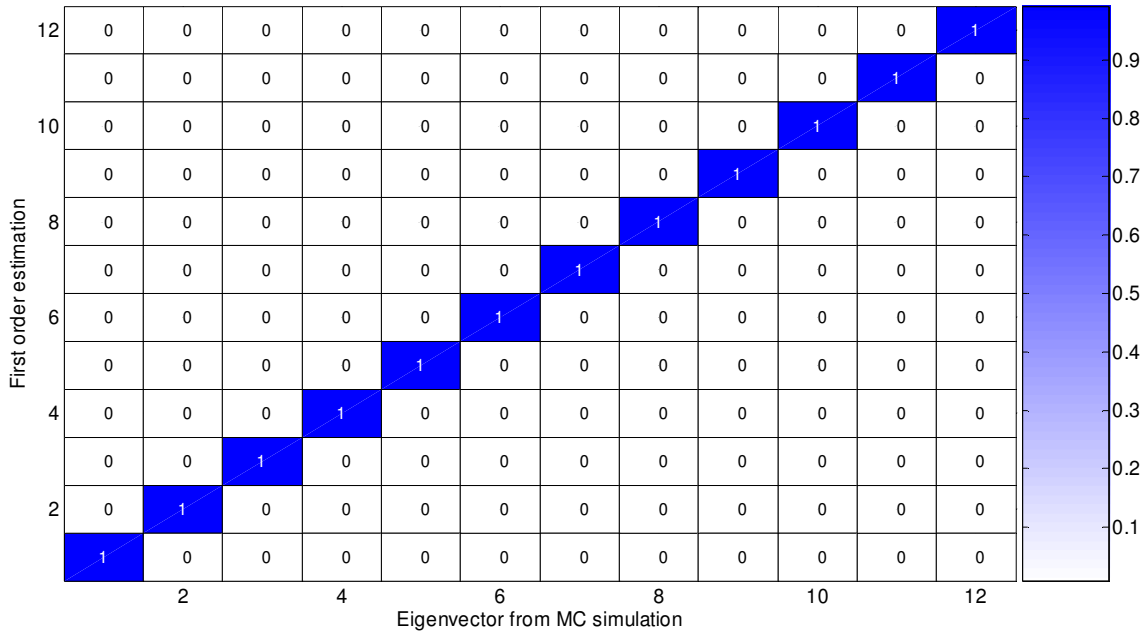

Figure 9-9 Orthogonality comparison of the first order perturbation of eigenvector to MC simulation: component 1 fixed interface modes, 1000 realisations.

For reference the modeshapes for the first ten modes of the frame are shown in Appendix C.

9.3 Variability from component modal properties to global modal response

In the previous section the propagation of variability from the physical properties of the frame to the component modal properties was examined. In this section the variability in the global modes of the built-up frame will be examined. In chapter 8 the local mode perturbational (LMP) method was introduced. Through the use of this, the statistics of the global response can be approximated by introducing variability into the fixed interface component modes and using a CMS model combined with a perturbational expansion. Using this method assumes that the constraint modes and component modeshapes are constant. This procedure involves two main areas of approximation; the assumption that introducing the variability into only the local component modes is valid, and the perturbational approximation. To investigate these two areas of approximation, the following scenarios will be compared:-

(a). Variability is introduced into the physical properties of the frame and the global modal response obtained from an eigensolution.
(b). Variability is introduced into the local modal properties (fixed interface component eigenvalues) and the global modal response obtained through the use of a fixed interface CMS model and an eigensolution.
(c). Variability is introduced into the local modal properties (fixed interface component eigenvalues) and the global modal response obtained through the use of a fixed interface CMS model and a first order perturbation.

Figure 9-10 shows an example of the variability within the FRF for the frame with uncertain physical properties. In order to provide a realistic FRF, light proportional damping was added to the structure where $\zeta = 0.01$ was the modal damping ratio. As for the example in chapter 8, this was assumed to be constant in each mode.

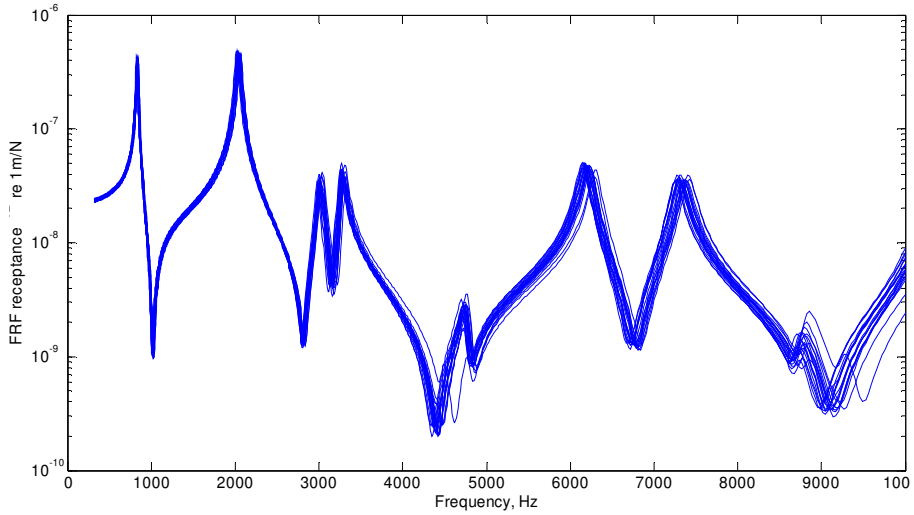

Figure 9-10 Magnitude of FRF (point receptance node 9) of 20 realisations of the frame with uncertain physical properties.

Figure 9-11 shows a comparison of the maximum/minimum envelope of the response for an ensemble of 1000 realisations. It compares the results for the three scenarios listed above (a)-(c). In the first of these (a), variability is introduced in the physical properties of the frame as used in section 9.2, i.e. Gaussian distributed uncertainty with a normalised standard deviation of 0.03. It includes a combination of correlated and uncorrelated terms within the mass and stiffness. In the second scenario (b), uncorrelated variability is introduced directly into the component fixed interface eigenvalues. The variability is Gaussian distributed with normalised standard deviations equal to those arising in the fixed interface component eigenvalues from the MC simulation used in (a). The third scenario (c), is identical to (b) except that the global response is obtained from a first order perturbation rather than an eigensolution. Also shown in Figure 9-12 are the 10^{th} and 90^{th} percentiles.

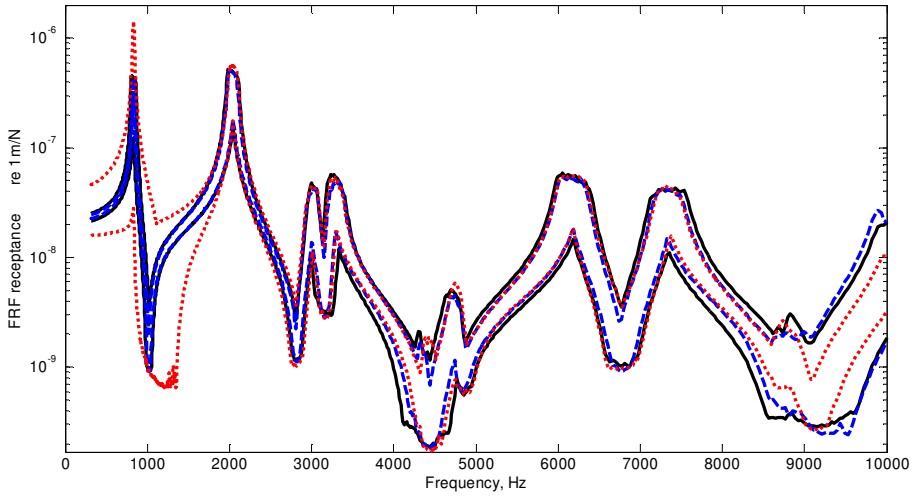

Figure 9-11 Effect of approximations on the FRF envelope (point receptance node 9) 1000 MC realisations; ——— scenario (a) max/min, — — — scenario (b) max/min, ▪▪▪▪▪▪▪ scenario (c) max/min.

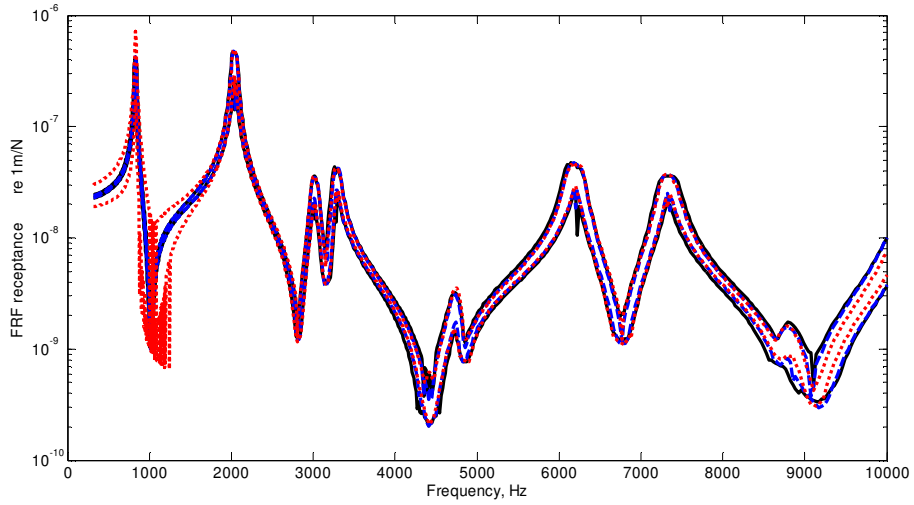

Figure 9-12 Effect of approximations on the FRF percentiles (point receptance node 9) 1000 MC realisations; ——— scenario (a) 90th/10th, — — — scenario (b) 90th/10th, ▪▪▪▪▪▪▪ scenario (c) 90th/10th.

It can be seen from the FRF comparison that approximating the uncertainty in the physical properties of the frame by including uncertainty in the local modal properties (b), gives a good estimation of the uncertainty in the global modal response. In addition, the use of a first order approximation (c) in place of an eigensolution, does not significantly affect the response.

In Table 9-7 the first ten global eigenvalues of the frame are summarised. Listed for comparison are the values obtained from the MC simulation each of the three scenarios (a)-(c). Also shown is the percentage error of each approximation compared to (a).

p 'th global frame mode	Baseline eigenvalue $(rad/s)^2$	Scenario (a) average eigenvalue MC simulation $(rad/s)^2$	Scenario (b) average eigenvalue MC simulation $(rad/s)^2$	Scenario (c) first order approximation $(rad/s)^2$	% error of scenario (b) w.r.t. (a)	% error of scenario (c) w.r.t. (a)
1	6.927E+05	6.919E+05	6.927E+05	6.927E+05	-0.11	-0.11
2	9.351E+05	9.342E+05	9.352E+05	9.353E+05	-0.11	-0.13
3	1.490E+06	1.488E+06	1.490E+06	1.490E+06	-0.11	-0.12
4	4.167E+06	4.162E+06	4.163E+06	4.165E+06	-0.02	-0.07
5	8.070E+06	8.061E+06	8.072E+06	8.075E+06	-0.13	-0.16
6	9.105E+06	9.090E+06	9.101E+06	9.106E+06	-0.12	-0.17
7	9.590E+06	9.576E+06	9.590E+06	9.595E+06	-0.15	-0.20
8	1.077E+07	1.076E+07	1.077E+07	1.077E+07	-0.09	-0.08
9	1.381E+07	1.379E+07	1.380E+07	1.380E+07	-0.09	-0.10
10	1.642E+07	1.632E+07	1.634E+07	1.643E+07	-0.10	-0.64

Table 9-7 First ten global frame eigenvalues, 1000 MC realisations.

Approximating the variability in the physical properties by introducing variability in the local component modal properties (b) has no significant effect on the resultant global eigenvalues. This is of considerable benefit as it is very difficult to quantify the variability in the physical properties of a structure, whereas in comparison measuring the variability in the local modes is relatively easy. In addition, the use of first order expansion to approximate an eigensolution (c) provides a good estimation of the global eigenvalues. The second order perturbation term has also been calculated for scenario (c) as an estimate the percentage error incurred in only using a first order term. This is listed below in Table 9-8.

p 'th global frame mode	Baseline eigenvalue $(rad/s)^2$	Scenario (a) average eigenvalue MC simulation $(rad/s)^2$	Scenario (c) first order approximation $(rad/s)^2$	% error of scenario (c) w.r.t. (a)	Estimated % error based on 2nd order term
1	6.927E+05	6.919E+05	6.927E+05	-0.11	-0.01
2	9.351E+05	9.342E+05	9.353E+05	-0.13	0.01
3	1.490E+06	1.488E+06	1.490E+06	-0.12	0.00
4	4.167E+06	4.162E+06	4.165E+06	-0.07	-0.06
5	8.070E+06	8.061E+06	8.075E+06	-0.16	-0.25
6	9.105E+06	9.090E+06	9.106E+06	-0.17	-0.28
7	9.590E+06	9.576E+06	9.595E+06	-0.20	0.24
8	1.077E+07	1.076E+07	1.077E+07	-0.08	0.16
9	1.381E+07	1.379E+07	1.380E+07	-0.10	-0.07
10	1.642E+07	1.632E+07	1.643E+07	-0.64	-0.82

Table 9-8 Estimation of the error for a first order approximation of the first ten global frame eigenvalues, 1000 MC realisations.

In general the second order term provides a reasonable estimation of the likely error in using a first order perturbation, with a better estimation above the first few modes.

It was further proposed that the variance of the component free interface eigenvalues could be used as an approximation of the variance of the component fixed interface eigenvalues. There are practical advantages in doing this as the free interface component modes are typically much easier to measure than the fixed ones. To examine the effect of this approximation, the variance of the global eigenvalues obtained from a first order perturbation using the normalised standard deviation of the fixed interface component modes (c), is compared to those obtained from a first order perturbation using the normalised standard deviation of the free interface component modes. The results are summarised in Table 9-9 and are compared to the variance of the global eigenvalues obtained from the MC simulation (b). As can be seen from the results, the first order approximation of the global eigenvalue variance, using the variance of the fixed interface component eigenvalues (c), is very good. However, the first order approximation of the global eigenvalue variance, using the free interface values, is quite poor. This may be in part due to the frequency shift of similar modes within the results for the fixed and free interface component modes. For example, the motion of the frame in a particular free interface mode may have a close equivalent fixed interface mode, for which the variance of the two is quite closely related. But, using the variance of the free interface modes in nominal order, may not match the free interface mode to its closest fixed interface equivalent. The use of the free interface modes to estimate the global eigenvalue variance could most likely be improved if the free interface modes were matched to their closest fixed interface equivalent. But this would negate the advantage of being able to measure, and use, only free interface modes. Therefore, it is further suggested that the average free interface variance is used. This may reduce the effect of mode mismatching. The results for the first order approximation of the global eigenvalues using the average free interface component variance are listed in Table 9-9.

p 'th global frame mode	Global eigenvalue variance MC simulation (b) $(rad/s)^4$	First order approximation of global eigenvalue variance (c) $(rad/s)^4$	% error	First order approximation using free interface component eigenvalue variance $(rad/s)^4$	% error	First order approximation using average free interface component eigenvalue variance $(rad/s)^4$	% error
1	1.13E+07	1.14E+07	-1.13	1.61E+07	-42.43	1.17E+07	-3.57
2	6.10E+07	6.22E+07	-2.00	6.05E+07	0.75	4.15E+07	31.92
3	7.07E+06	7.12E+06	-0.73	1.27E+07	-80.15	9.55E+06	-35.05
4	3.64E+09	3.68E+09	-1.35	4.12E+09	-13.34	3.80E+09	-4.62
5	8.53E+09	8.68E+09	-1.80	1.43E+10	-68.00	1.11E+10	-30.53
6	1.10E+10	1.11E+10	-0.63	8.73E+09	20.65	1.60E+10	-45.07
7	1.91E+10	1.78E+10	6.77	1.94E+10	-1.32	1.68E+10	11.85
8	1.90E+10	1.81E+10	4.58	2.06E+10	-8.52	1.69E+10	11.40
9	3.17E+10	3.25E+10	-2.68	2.34E+10	26.13	4.58E+10	-44.52
10	9.02E+10	8.02E+10	10.99	4.94E+10	45.18	4.95E+10	45.11

Table 9-9 Comparison of fixed/free interface component variance in a first order perturbation to approximate global eigenvalue variance.

The error for estimating the global eigenvalue variance using the average free interface variance whilst still quite poor is an improvement over using the individual values. The average magnitude of the percentage error when using the individual values is 30.6%, when using the averaged values it is 26.4%.

There were no issues with the statistical overlap of the first ten modes. The modal spacing verses the variability was sufficiently high so as not to compromise the variance calculations up to the eighteenth mode (6.7kHz).

The distribution of global natural frequencies has been investigated and a χ^2 test used to examine the null hypothesis of a fit to a Gaussian distribution. The distributions of the global natural frequencies obtained from the earlier listed scenarios (a)-(c) were tested. The results for χ^2 cumulative probabilities are shown in Table 9-10; a value of less than 95% indicates a 95% confidence that the sample set cannot be rejected as having come from a Gaussian distribution.

p 'th global mode	Variability introduced into physical properties (a)	Variability introduced into component eigenvalues (b)	First order perturbation (c)
1	67.2%	75.9%	31.7%
2	87.5%	75.9%	55.0%
3	95.7%	98.1%	67.7%
4	11.4%	57.5%	42.3%
5	95.6%	91.5%	20.7%
6	69.4%	51.1%	85.5%
7	34.8%	26.3%	51.9%
8	50.7%	73.9%	48.0%
9	67.2%	59.7%	81.4%
10	24.5%	87.6%	59.6%

Table 9-10 χ^2 goodness of fit of the distribution global natural frequencies to a Gaussian distribution; summary of cumulative probabilities.

In general the distribution of the first ten natural frequencies of the frame cannot be rejected as having come from a Gaussian distribution. The χ^2 results for scenario (a) show the distribution arising from a MC simulation with variability introduced into the physical properties of the frame and only two of the first ten modes are rejected as being Gaussian. The estimated global eigenvalues from scenario (b) with variability introduced directly into the component fixed interface eigenvalues, are also a good fit to a Gaussian distribution. As are the results from (c) with a first order perturbation used to approximate the eigensolution of scenario (b). These results suggest that for Gaussian distributed variability in the physical properties of a structure, the resultant distribution of the global eigenvalues will also be Gaussian. Moreover, approximating the response by introducing uncertainty directly into the component eigenvalues and using a first order perturbation, accurately results in a Gaussian distributed response.

A first order approximation of the global eigenvectors was calculated and used in the estimation of a first order FRF. As for the component eigenvectors an orthogonality comparison has been used to evaluate the accuracy of the approximation. In Figure 9-13 the results from the first order approximation are compared to those obtained from the MC simulation, with uncertainty introduced in the local modal properties. It can be seen that the eigenvectors from the first order approximation provide a very good estimation.

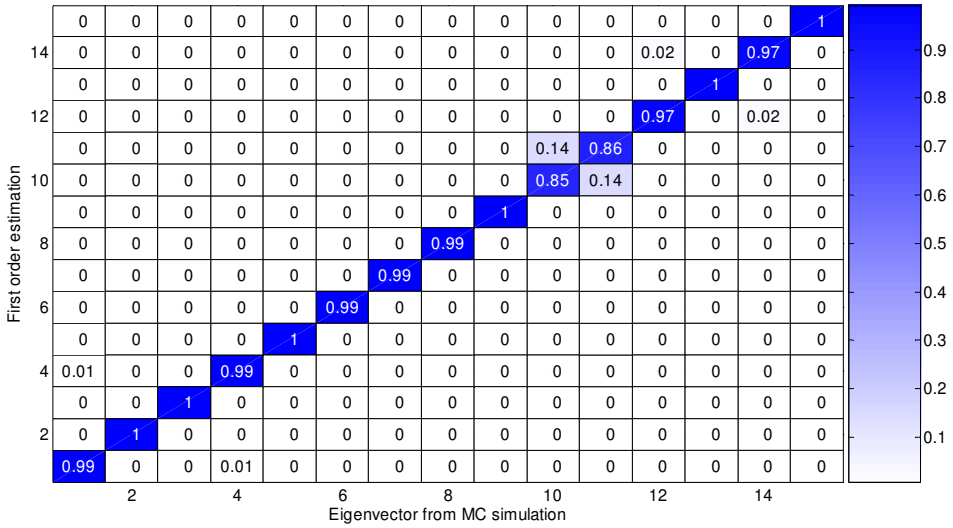

Figure 9-13 Orthogonality comparison, first order perturbation of the global eigenvector to MC simulation: 1000 realisations.

9.4 Conclusions

In this chapter a numerical example of a 3-dimensional frame has been considered and the methods investigated in chapters 7 and 8 have been applied. Variability was introduced into the physical properties of the frame and the effect on the local component and global response examined. A first order perturbation was shown to provide a good estimate of the statistics of both the component eigenvalues and eigenvectors. The distribution of the component eigenvalues was examined for both Gaussian and Rayleigh distributed physical property variations. It was shown that for Gaussian distributed uncertainty the component eigenvalues are also Gaussian distributed. For the case of Rayleigh distributed uncertainty, the majority of the component eigenvalues of component 2 could not be rejected as having come from a Gaussian distribution. Although all the eigenvalues from component 1 could be rejected as having come from a Gaussian distribution. It is suggested that as component 2 consists of twelve elements, compared to five for component 1, that the distribution is more likely to tend towards Gaussian due to the central limit theorem. The variance of the component free interface eigenvalues was shown to be similar to that of the fixed interface values.

In investigating the propagation of uncertainty from the component modal level to the global modal level, a first order perturbation was shown to provide a good estimation of both the global eigenvalues and eigenvectors. The variance of the free interface component eigenvalues was used to approximate the fixed interface values. Although this was shown to be fairly inaccurate, the error involved in using this approximation would probably be less than the error

in trying to estimate the variability in the physical properties of a structure. It is therefore suggested that the free interface component eigenvalues still represent a reasonable alternative to the expensive and complicated task of quantifying the uncertainty within the physical properties of a structure. The average free interface eigenvalue variance would probably be improved if the free interface modes were matched to their closet fixed interface equivalent, but that this would negate the benefit of being able to measure only free interface values. Thus it was suggested that the average variance of the free interface eigenvalues might provide a better approximation, as this would reduce the effect of modal mismatching, and this was shown to be the case. The distribution of the global eigenvalues arising from uncertain physical properties was tested against a Gaussian distribution and found to be a good fit. In addition, the approximation of introducing variability at the component modal level, and using a first order perturbation, also resulted in a Gaussian distributed response.

10. Conclusions

This thesis has investigated methods for studying how uncertainty propagates within built-up structures. In particular it has examined the use of Component Mode Synthesis (CMS) along with reduced data sets to approximate the statistics of the variable response.

In order to establish typical levels of variability within manufactured structures a literature review was conducted. This was to determine whether the levels of variability were low enough to apply modelling techniques that include series expansions, and reasonably be able to ignore higher order terms. Typical levels of normalised standard deviation within nominally identical components were found to be around 0.03. In general, the distributions of the measured responses were found to be close to Gaussian in form.

One of the disadvantages with the published literature was the small sample size of the studies. For this reason the statistical analysis of an extensive vehicle variability study was conducted. The data presented here contributes greatly to the available information on typical variability found between nominally identical manufactured structures. The raw data supplied by the manufacturer was collected during a monitoring programme, which selected a cross-section of production vehicles prior to despatch from two product lines. The tests included engine noise, airborne body transfer functions and roller induced road noise. A full statistical analysis of the data has been presented. The results suggest that the typical levels of averaged normalised standard deviation range from 0.09 to 0.32. However, the higher levels were seen in the road noise results where vehicles fitted with a selection of different wheel rim materials and tyres, have contributed greatly to the variations. A more realistic range based on the variability of nominally identical wheels and tyres is 0.09 to 0.2. The frequency distributions of the linear results were, in general, best described by a lognormal distribution and therefore the corresponding decibel values will be best described by a Gaussian distribution. The environmental conditions were monitored for each test and it was shown that the variation in the ambient temperature did not contribute to the variability in the measured response.

Having established the general levels of variability within manufactured structures and its likely distribution, various techniques for studying uncertainty propagation were examined. These included Monte Carlo simulations, perturbational methods and assumed modeshape methods including the interpolated mode method. A two-degree of freedom model was used to evaluate some of these techniques as regards their suitability for the propagation of uncertainty. Variability was introduced into the physical properties of the model to represent inconsistencies

arising from the mass production of nominally identical systems. This was then related to the resultant statistics of the variable response. The perturbation expansion approach was shown to provide a possible route for propagating uncertainty in a structure, from the physical properties to the modal response. However, one of the main drawbacks was the rapidly increasing complexity of the calculations when applied to a system with more than a few degrees of freedom.

A procedure was introduced combining perturbational expansions with the CMS method. Potential areas for data reduction and model simplification were highlighted. Two of the most popular CMS methods were introduced; in particular the fixed interface method which uses fixed interface normal modes combined with displacement constraint modes as assumed component modes. The method is relatively straightforward, the appropriate terms are easily formed and the resulting uncoupled mass and stiffness matrices are comparatively sparse. For these reasons the fixed interface method was applied to the propagation of uncertainty within structures. In particular, the concept of only including uncertainty in the local component fixed interface eigenvalues, and assuming constant eigenvectors and displacement constraint modes.

In investigating the propagation of uncertainty from the physical properties to the global modal properties, the process was examined in two stages. The first of these examined in detail the propagation of variations in physical properties to component modal properties. The relationships between the statistics of the variability in the physical properties to the statistics of the variability in the component modal properties were determined. This was done using a perturbational approach. Expressions were generated for the fixed interface component CMS matrices in terms of the physical parameter uncertainties. It was proposed that the variance of the free interface eigenvalues could be indicative of the variance of the fixed interface eigenvalues and this relationship was established. A general method for relating the probability density function (PDF) of the eigenvalue distribution to the PDF of the physical variability was suggested, and the possibility of the central limit theorem applying was reviewed.

Following this, the propagation of uncertainty from the component modal level to the global modal properties was examined. The general case of variations, correlated or uncorrelated, in the local eigenvalues of a structure was considered and expressions were generated for the statistics of the global eigenvalues and eigenvectors. An expression for the variance of the global eigenvalues was developed, and this was shown to depend on the variance and covariance of the substructure local eigenvalues and the global modal eigenvectors of the unperturbed structure. From this the spread of the response of the global eigenvalues can be estimated from a single eigensolution of the baseline system, and the statistics of the component

eigenvalues. This is a significant benefit as it is often difficult to quantify the variability in a structure's physical properties. The component eigenvalue statistics are generally much easier to measure, especially for the free interface modes. Furthermore, the evidence from the industrial results suggests that the distribution of component eigenvalues is typically Gaussian or close to Gaussian. If this is assumed to be the case, then a smaller sample set of measured component natural frequencies would be required to estimate the statistics of the ensemble accurately. Indeed for a structure which is in the early design stages, it may be sufficient to use the typical variance of a similar component as a reasonable first estimate.

A numerical example of a 3-dimensional frame was considered and the methods investigated in this thesis were applied. Variability was introduced into the physical properties of the frame and the effect on the local component and global modal properties examined. The first order approximations of the statistics of both the component and global modal properties were shown to provide very good estimates. The distribution of the component modal properties was examined for both Gaussian and Rayleigh distributed uncertainty. The distribution of the response was found to tend towards a Gaussian distribution, particularly for the larger component consisting of more elements. The component modes were therefore assumed to be Gaussian distributed and given this, the global response was also Gaussian. The variance of the free interface component eigenvalues was used to approximate the fixed interface eigenvalue variance. Although this was shown to be fairly inaccurate, the error involved in using this approximation would probably be less than the error in trying to estimate the variability in the physical properties of a structure. It was suggested that the average variance of the free interface eigenvalues might provide a better approximation, as this would reduce the effect of modal mismatching, and this was shown to be the case.

Recommendations for further research include the following:

- Extending the methods to consider damping effects.
- Further investigation of the potential use of the free interface component variance as an approximation for the fixed interface variance.
- Further development of the method to include joint uncertainties.

Appendix A: Statistical and Mathematical Concepts

A.1. Definition of a random variable

A random variable X is defined as a real function whose domain is the probability space S and that:

1) The set $X \leq x$ is an event for any real number x.
2) The probability of the events $X = +\infty$ and $X = -\infty$ equals zero.

Reference: [A.1.]

A.2. Distribution function

The distribution function is the probability that a variable X takes on a value less than or equal to a number x. The distribution function is sometimes also denoted as $F(x)$.

Reference: [A.2.]

A.3. Independence

Two variables a and b are statistically independent if the conditional probability $P(a|b)$ of a given b satisfies $P(a|b) = P(a)$.

Reference: [A.4.]

A.4. Probability density function

The probability density function $P(x)$ of a continuous distribution is defined as the derivative of the distribution function $D(x)$, which is often written as $D(x) \equiv \int_{-\infty}^{x} P(x)dx$.

Reference: [A.1.]

A.5. Expectation

The expected value of a continuous function is given by $E\left[f(x)\right]=\int f(x)P(x)dx$. Similarly for a single discrete variable, $E\left[f(x)\right]=\sum_{x} f(x)P(x)$.

Reference: [A.4.]

A.6. Moments

The *n*'th moment of a probability function $P(x)$ taken about zero may be obtained from $\mu_n^{'}=E\left[x^n\right]=\int x^n P(x)dx$. The first moment of a function is given by its mean. The central moments are those taken about the mean and are given by $\mu_n=E\left[(x-\mu)^n\right]=\int(x-\mu)^n P(x)dx$. The most common moments used are the variance (second moment), skew (third moment) and kurtosis (fourth moment).

Reference: [A.4.]

A.7. Variance and standard deviation

The variance of a random variable is a measure of its spread or dispersion and is given by the second central moment. It is represented as $\mathrm{var}(x)$ or σ_x^2, and given by $\sigma_x^2=E\left[(x-\mu_x)^2\right]=\int(x-\mu)^2 P(x)dx$.

Reference: [A.4.]

A.8. Covariance

The covariance between two real random variables *x* and *y* is given by $\mathrm{cov}(x,y)\equiv E\left[(x-\mu_x)(y-\mu_y)\right]=E[xy]-\mu_x\mu_y$. It is a measure of how much the two variables vary together, i.e. a measure of their dependence. The covariance of independent variables is zero. It can be shown that the variance of the sum of the two variables *x* and *y* is given by

$\mathrm{var}(x+y) = \mathrm{var}(x) + \mathrm{var}(y) + 2\mathrm{cov}(x,y)$, and so if the two variables are independent, then the variance of their sum is equal to the sum of their variances.

Reference: [A.4.]

A.9. Statistical correlation

The correlation between two random variables x and y is given by $cor(x,y) \equiv \dfrac{\mathrm{cov}(x,y)}{\sigma_x \sigma_y}$. It indicates the strength and direction of a linear relationship between the variables.

Reference: [A.4.]

A.10. Elementary matrix

The elementary matrix $\mathbf{E}_{ij}$ is defined as the matrix of order $(m \times n)$ which has a unity in the (i,j)'th position, and all other elements are zero. For example,

$$\mathbf{E}_{23} = \begin{bmatrix} 0 & 0 & 0 & \cdots & 0 \\ 0 & 0 & 1 & \cdots & 0 \\ 0 & 0 & 0 & \cdots & 0 \\ \vdots & \vdots & \vdots & \vdots & \vdots \\ 0 & 0 & 0 & \cdots & 0 \end{bmatrix}$$

The elementary vector is similarly

$$e_1 = \begin{bmatrix} 1 \\ 0 \\ \vdots \\ 0 \end{bmatrix}, \quad e_2 = \begin{bmatrix} 0 \\ 1 \\ \vdots \\ 0 \end{bmatrix}, \quad e_n = \begin{bmatrix} 0 \\ 0 \\ \vdots \\ 1 \end{bmatrix}$$

Reference: [A.3.]

A.11. Kronecker product

The Kronecker product is the tensor product of two matrices. Consider a matrix $\mathbf{A} = \left[a_{ij} \right]$ or order $(m \times n)$ and a matrix $\mathbf{B} = \left[b_{ij} \right]$ or order $(r \times s)$. The Kronecker product of the two matrices, denoted by $\mathbf{A} \otimes \mathbf{B}$ is defined as the partitioned matrix,

$$\mathbf{A} \otimes \mathbf{B} = \begin{bmatrix} a_{11}\mathbf{B} & a_{12}\mathbf{B} & \cdots & a_{1n}\mathbf{B} \\ a_{21}\mathbf{B} & a_{22}\mathbf{B} & \cdots & a_{21}\mathbf{B} \\ \vdots & \vdots & \vdots & \vdots \\ a_{m1}\mathbf{B} & a_{m2}\mathbf{B} & \cdots & a_{mn}\mathbf{B} \end{bmatrix}$$

The resultant matrix is of the order $(mr \times ns)$.

Reference: [A.3.]

A.12. Derivative of a matrix with respect to a matrix

Let $\mathbf{Y} = \left[y_{ij} \right]$ be a matrix of order $(p \times q)$ and $\mathbf{X} = \left[x_{rs} \right]$ be a matrix of order $(m \times n)$, then the derivative of $\mathbf{Y}$ with respect to $\mathbf{X}$ is given by

$$\frac{\partial \mathbf{Y}}{\partial \mathbf{X}} = \begin{bmatrix} \dfrac{\partial \mathbf{Y}}{\partial x_{11}} & \dfrac{\partial \mathbf{Y}}{\partial x_{12}} & \cdots & \dfrac{\partial \mathbf{Y}}{\partial x_{1n}} \\ \dfrac{\partial \mathbf{Y}}{\partial x_{21}} & \dfrac{\partial \mathbf{Y}}{\partial x_{22}} & \cdots & \dfrac{\partial \mathbf{Y}}{\partial x_{2n}} \\ \vdots & \vdots & \vdots & \vdots \\ \dfrac{\partial \mathbf{Y}}{\partial x_{m1}} & \dfrac{\partial \mathbf{Y}}{\partial x_{m2}} & \cdots & \dfrac{\partial \mathbf{Y}}{\partial x_{mn}} \end{bmatrix} = \sum_{r,s} E_{rs} \otimes \frac{\partial \mathbf{Y}}{\partial x_{rs}}$$

where $\otimes$ is the Kronecker product and E_{rs} is the elementary matrix.

Reference: [A.3.]

Appendix B: List of all documented vehicle specifications.

Air conditioning (Yes/No)
Alternator code
Battery code
Body colour
Chamber temperature
Chamber humidity
Emissions specification
Engine rated power
Engine type
Engine volume
Final drive ratio
Fuel type (Petrol/Diesel)
Hand of drive
Heated windscreen (Yes/No)
Name of Ford test plant
Number of engine cylinders
Outside weather conditions
Radio specification code
Sunroof (Yes/No)
Test Date
Transmission type
Tyre manufacturer
Tyre size
Vehicle body style
Vehicle country specification
Vehicle model year
Vehicle programme number
Vehicle trim level
Vehicle under tray material
Vehicle version
Vin number
Wheel rim material
Wheel rim style

Appendix C: Numerical Example

C.1. Element baseline material properties

Radius (m)	Length (m)	Density (kg/m^3)	Young's Modulus (N/m^2)	Possion's Ratio
0.02	0.30	7800	2.00E+11	0.30

Table C.11: Baseline material properties common to all elements.

C.2. Element Stiffness Matrix

The element stiffness matrix is given by

$$K_e = \begin{bmatrix} k_{11} & k_{12} \\ k_{12}^T & k_{22} \end{bmatrix}$$

where

$$K_{11} = \frac{AE}{8l^3}\begin{bmatrix} 4l^2 & 0 & 0 & 0 & 0 & 0 \\ 0 & 12r_z^2 & 0 & 0 & 0 & 12lr_z^2 \\ 0 & 0 & 12r_y^2 & 0 & -12lr_y^2 & 0 \\ 0 & 0 & 0 & \dfrac{2l^2r_J^2}{(1+\nu)} & 0 & 0 \\ 0 & 0 & -12lr_y^2 & 0 & 16l^2r_y^2 & 0 \\ 0 & 12lr_z^2 & 0 & 0 & 0 & 16l^2r_z^2 \end{bmatrix}$$

$$K_{12} = \frac{AE}{8l^3}\begin{bmatrix} -4l^2 & 0 & 0 & 0 & 0 & 0 \\ 0 & -12r_z^2 & 0 & 0 & 0 & 12lr_z^2 \\ 0 & 0 & -12r_y^2 & 0 & -12lr_y^2 & 0 \\ 0 & 0 & 0 & \dfrac{-2l^2r_J^2}{(1+\nu)} & 0 & 0 \\ 0 & 0 & 12lr_y^2 & 0 & 8l^2r_y^2 & 0 \\ 0 & -12lr_z^2 & 0 & 0 & 0 & 8l^2r_z^2 \end{bmatrix}$$

$$K_{22} = \frac{AE}{8l^3}\begin{bmatrix} 4l^2 & 0 & 0 & 0 & 0 & 0 \\ 0 & 12r_z^2 & 0 & 0 & 0 & -12lr_z^2 \\ 0 & 0 & 12r_y^2 & 0 & 12lr_y^2 & 0 \\ 0 & 0 & 0 & \dfrac{2l^2 r_J^2}{(1+\nu)} & 0 & 0 \\ 0 & 0 & 12lr_y^2 & 0 & 16l^2 r_y^2 & 0 \\ 0 & -12lr_z^2 & 0 & 0 & 0 & 16l^2 r_z^2 \end{bmatrix}$$

and E is Young's Modulus, A is the cross-sectional area, l is the length, ν is Poisson's ratio, r_y is the radius of gyration about the y-axis, r_z is the radius of gyration about the z-axis and r_J is given by $r_J^2 = J/A$ where J is the torsion constant of the cross section (which for a circular shaft is given by the polar moment of area of the cross-section). The radius of gyration is given by $r_y^2 = I_y/A$, where I_y is the polar moment of the cross-section about the y-axis, similarly for r_z. Source reference [9.1].

C.3. Element Mass Matrix

The element mass matrix is given by

$$M_e = \begin{bmatrix} m_{11} & m_{12} \\ m_{12}^T & m_{22} \end{bmatrix}$$

where

$$m_{11} = \frac{\rho Al}{105}\begin{bmatrix} 70 & 0 & 0 & 0 & 0 & 0 \\ 0 & 78 & 0 & 0 & 0 & 22l \\ 0 & 0 & 78 & 0 & -22l & 0 \\ 0 & 0 & 0 & 70r_x^2 & 0 & 0 \\ 0 & 0 & -22l & 0 & 8l^2 & 0 \\ 0 & 22l & 0 & 0 & 0 & 8l^2 \end{bmatrix}$$

$$m_{12} = \frac{\rho Al}{105}\begin{bmatrix} 35 & 0 & 0 & 0 & 0 & 0 \\ 0 & 27 & 0 & 0 & 0 & -13l \\ 0 & 0 & 27 & 0 & 13l & 0 \\ 0 & 0 & 0 & 35r_x^2 & 0 & 0 \\ 0 & 0 & -13l & 0 & -6l^2 & 0 \\ 0 & 13l & 0 & 0 & 0 & -6l^2 \end{bmatrix}$$

$$m_{22} = \frac{\rho A l}{105}\begin{bmatrix} 70 & 0 & 0 & 0 & 0 & 0 \\ 0 & 78 & 0 & 0 & 0 & -22l \\ 0 & 0 & 78 & 0 & 22l & 0 \\ 0 & 0 & 0 & 70r_x^2 & 0 & 0 \\ 0 & 0 & 22l & 0 & 8l^2 & 0 \\ 0 & -22l & 0 & 0 & 0 & 8l^2 \end{bmatrix}$$

where A is the cross-sectional area, l is the length, ρ is the density and r_x is the radius of gyration about the x-axis and given by $r_x^2 = I_x / A$ where I_x is the polar moment of area of the cross-section. Source reference [9.1].

C.4. Frame modeshapes

The first ten modeshapes of the frame are shown below. The eigenvectors were normalised to a maximum size of 0.2.

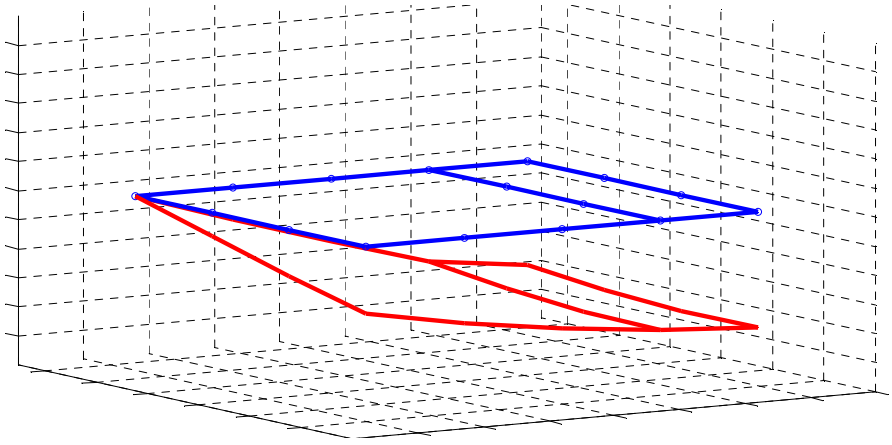

Figure C. 1 Frame modeshape: first mode.

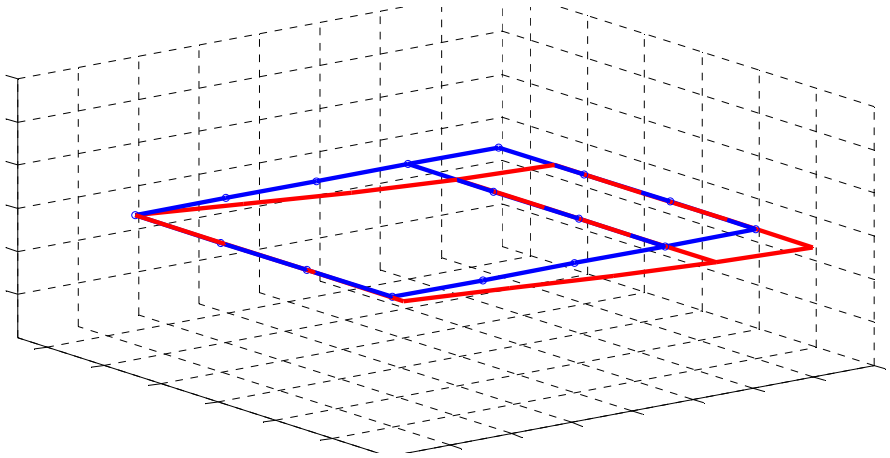

Figure C. 2 Frame modeshape: second mode.

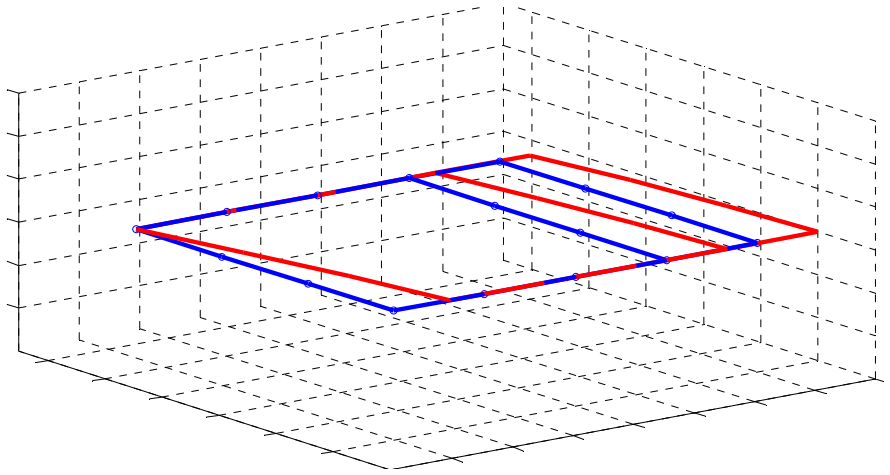

Figure C. 3 Frame modeshape: third mode.

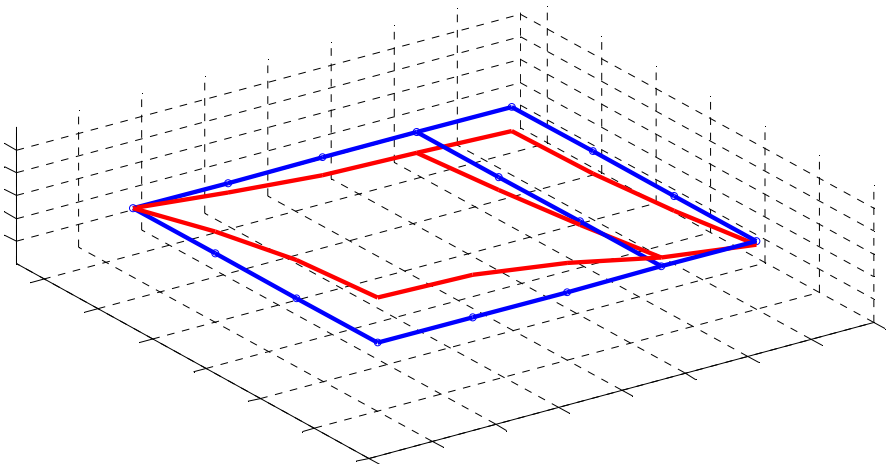

Figure C. 4 Frame modeshape: fourth mode.

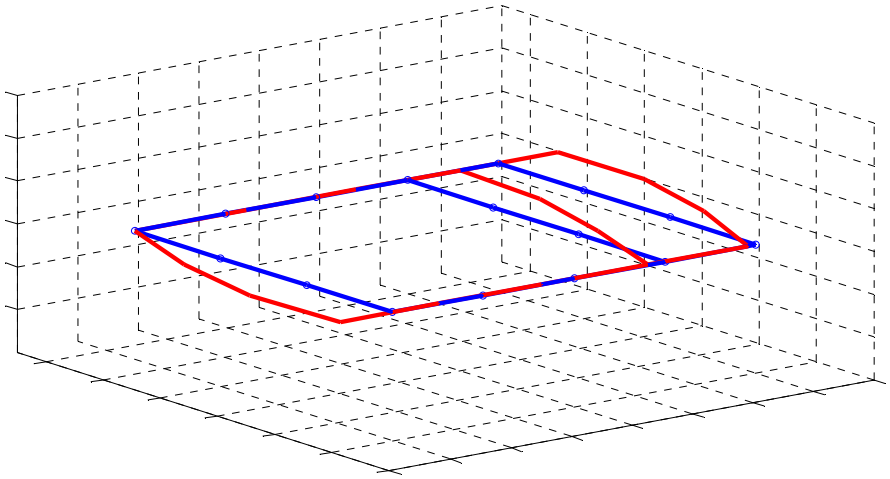

Figure C. 5 Frame modeshape: fifth mode.

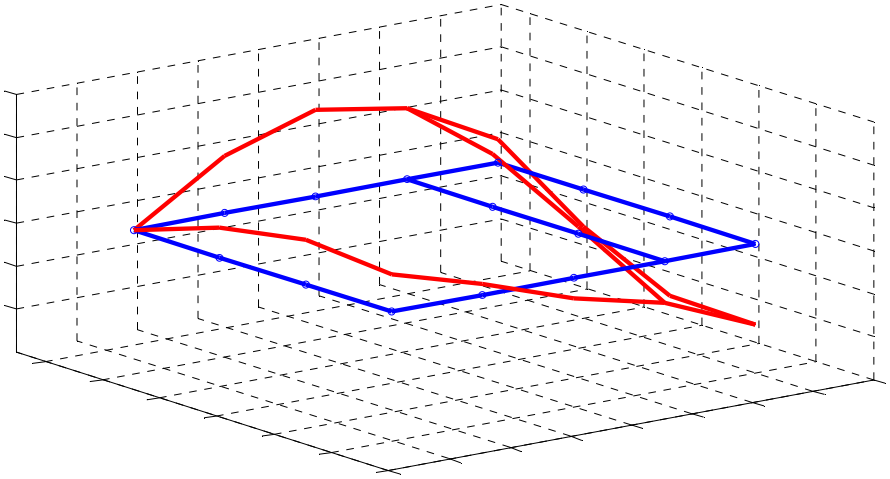

Figure C. 6 Frame modeshape: sixth mode.

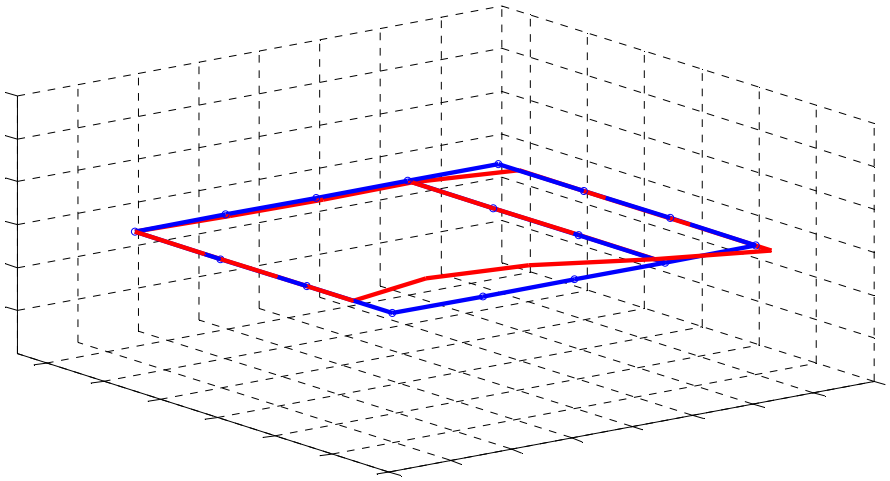

Figure C. 7 Frame modeshape: seventh mode.

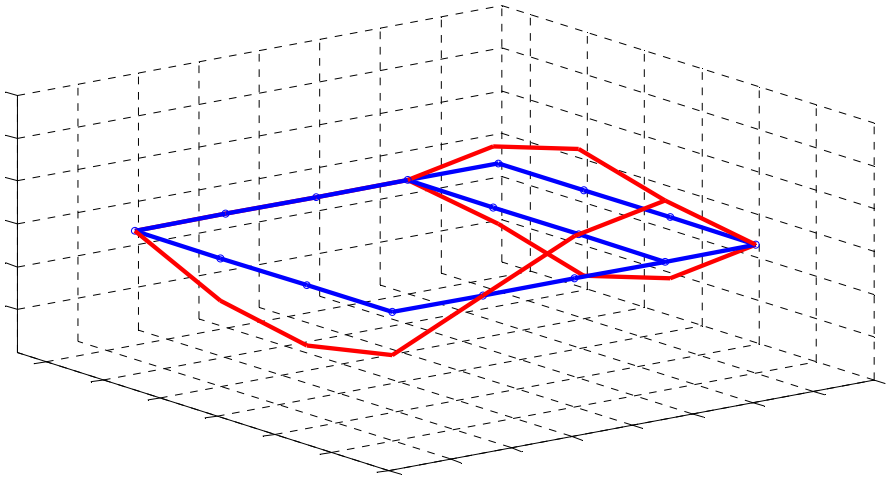

Figure C. 8 Frame modeshape: eighth mode.

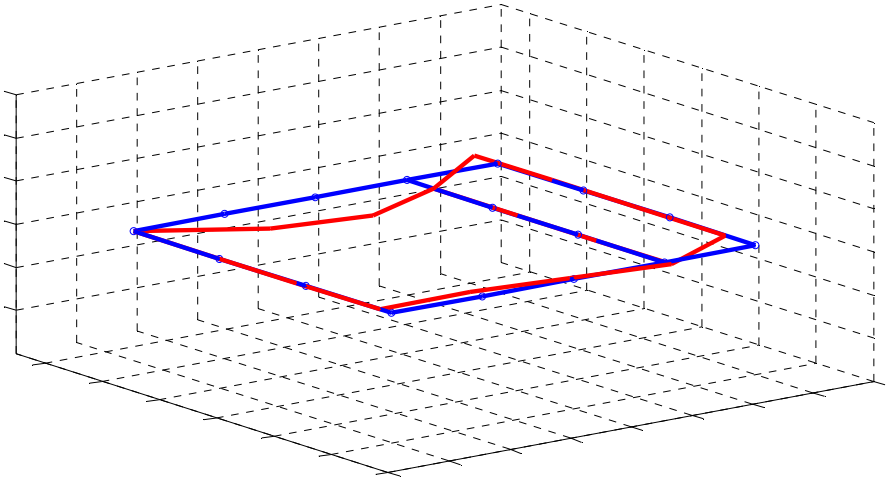

Figure C. 9 Frame modeshape: ninth mode.

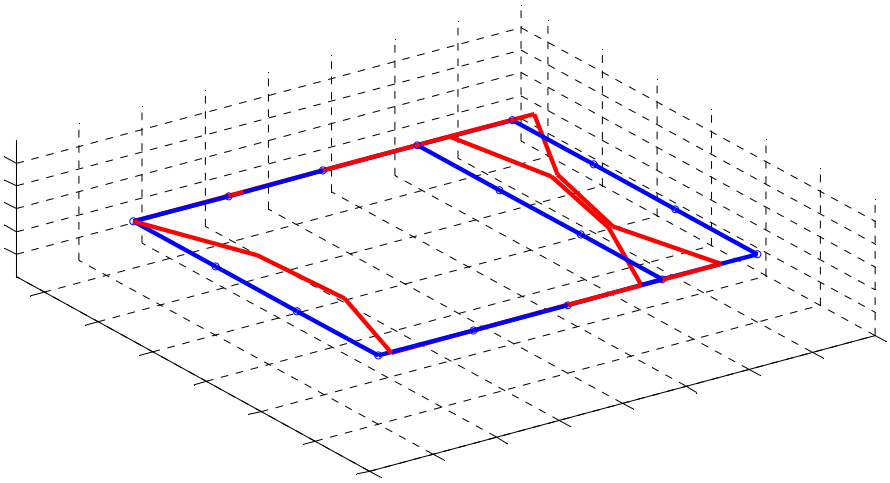

Figure C. 10 Frame modeshape: tenth mode.

11. References

[2.1] R. Brown and J. Gear, Dynamic Variations within Nominally Identical Product Lines, 4th year project University of Auckland, September 1999.

[2.2] M. W. Zehn and A. Saitov, Determination of Spatially Distributed Probability Density Functions for Parameter Estimation in model Updating Procedures, ISMA 25, Leuven, 2000.

[2.3] P. Cornwell, C. R. Farrar, S. W. Doebling and H. Sohn, Environmental Variability of Modal Properties, Experimental Techniques, November/December 1999, pp 45-48.

[2.4] P. Lardeur, E. Lacouture and E Blain, Spot weld modelling techniques and performances of finite element models for the vibrational behaviour of automotive structures, ISMA 25, 2000 Leuven.

[2.5] E. Balmès, Predicted Variability and Differences between Tests of a Single Structure, IMAC 1998, Santa Barbara 1998.

[2.6] D. J. Ewins and M. Imregun, On the Reliability of Computational Dynamic Response Prediction Capabilities (DYNAS), Journal of the society of environmental engineers, March 1988, pp3-13.

[2.7] J. R. Maguire, A Correlation Benchmark for Dynamic Analysis, NAFEMS 2nd International Conference: Structural Dynamics Modelling, Test, Analysis and Correlation, Cumbria, 3-5 July, 1996, pp1-12.

[2.8] B.W. Lindgren, Statistical Theory, 3rd Ed Macmillan Publishing, 1976.

[2.9] Feller, W., An introduction to probability theory and its applications, Vol. I & II, John Wiley & Sons, New York, 1966.

[2.10] Kreyszig, E., Advanced Engineering Mathematics, 6th Ed. John Wiley & Sons, 1988.

[2.11] M.S. Kompella and R.J. Bernhard, Measurement of the Statistical Variation of Structural-Acoustic Characteristics of Automotive Vehicles, SAE 931272.

[2.12] M.S. Kompella and R.J. Bernhard, Variation of Structural-Acoustic Characteristics of Automotive Vehicles, Noise Control Engineering Journal, 1996 44(2) Mar-Apr pp 93-99.

[2.13] R.J. Bernhard, Observations of the Structural Acoustics of Automobiles, InterNoise 2000 Nice, 27-30th August, Keynote Lecture pp 93-106.

[2.14] M.S. Kompella and R.J. Bernhard, Techniques for Prediction of the Statistical Variation of Multiple-Input-Multiple-Output System Response, Journal of Noise Control Engineering, 1997 45(3) 133-142.

[2.15] D. A. Bies and C. H. Hansen, Engineering Noise Control, Unwin Hyman, pp 6.

[2.16] O. Cramer, The variation of the specific heat ratio and the speed of sound in air with temperature, pressure, humidity, and CO2 concentration, The Journal of the Acoustical Society of America Volume 93, Issue 5, pp 2510-2516.

[2.17] L. E. Kinsler, A. R. Frey, A. B Coppens and J. V Sanders, Fundamentals of Acoustics, 3rd Ed, John Wiley & Sons, 1982, pp 156-157.

[3.1] Feller, W., An introduction to probability theory and its applications, Vol. I & II, John Wiley & Sons, New York, 1966.

[4.1] Rao, S. S., Mechanical Vibrations, 3rd edition, 1995, Addison-Wesley Publishing

[4.2] Bhaskar, A., Gross modifications in structural dynamic via interpolated modes, Proceedings 7th International Conference On Recent Advances in Structural Dynamics, Southampton, July 2000, vol. I, pp. 61-73.

[4.3] Sadu, S. S., Bhaskar, A and Nagra, B. C., Interpolation approach for gross dynamic modifications of structures, 2000.

[4.4] Adhikari, S. and Friswell, M. I., 'Random eigenvalue problems in structural dynamics', AIAA journal, AIAA-2004-1747, 45th AIAA/ASME/ASCE/AHS/ASC Structures, Structural Dynamics and Materials Conference, Palm Springs, California, Apr. 2004, pp. 19-22.

[4.5] Fox, R. L. and Kapoor, M. P., 'Rates of change of eigenvalues and eigenvectors', AIAA Journal, Vol. 6, No. 12, December 1968, pp. 2426-2429.

[4.6] Collins, J. D. and Thomson, W. T., "The eigenvalue problem for structural systems with statistical properties", AIAA Journal, Vol. 17, No. 4, April 1969, pp. 642-648.

[4.7] Ramu, S. A. and Ganesan, R., "Stability analysis of a stochastic column subjected to stochastically distributed loadings using the finite element methods", Finite Elements in Analysis and Design, Vol. 11, 1992, pp. 105-115.

[4.8] Ramu, S. A. and Ganesan, R., "Stability of stochastic Leipholz column with stochastic loading", Archive of Applied Mechanics, Vol. 62, 1992a, pp. 363-375.

[4.9] Ramu, S. A. and Ganesan, R., "A Galerkin finite element technique for stochastic field problems", Computer Methods in Applied Mechanics and Engineering, Vol. 105, 1993a, pp. 315-331.

[4.10] Ramu, S. A. and Ganesan, R., "Parametric instability of stochastic columns", International Journal of Solids and Structures, vol. 30, No. 10, 1993b, pp. 1339-1354.

[4.11] Sankar, T. S., Ramu, S. A. and Ganesan, R., "Stochastic finite element analysis for high speed rotors", Journal of Vibration and Acoustic, ASME, Vol. 115, 1993, pp. 59-64.

[4.12] Adhikari, S., "Complex modes in linear stochastic systems", Proceedings of the First International Conference on Vibration Engineering and Technology of Machinery (VETOMAC-I), edited by K. Venkatraman and C. S. Manohar, Indian Institute of Science, Bangalore, India, October 2000.

[4.13] Adhikari, S., “Complex modes in stochastic systems”, Advances in Vibration Engineering, Vol. 3, No. 1, 2004, pp. 1-11.

[4.14] Plaut, R. H. and Huseyin, K., ‘Derivative of eigenvalues and eigenvectors in non-self adjoint systems’, AIAA Journal, Vol. 11, No. 2, February 1973, pp. 250-251.

[4.15] Johnson, N. L. and Kotz, S., “Distributions in statistics: Continuous univariate distributions – 2, chapter 29, The Houghton Mifflin Series in Statistics, Houghton Mifflin company, Boston, USA, 1970.

[4.16] Mathai, A. M., and Provost, S. B., Quadratic forms in random variable: Theory and applications, Marcel Dekker, Inc., 270 Madison Avenue, New York, NY 10016, USA, 1992.

[4.17] Adhikari, S. and Langley, R. S., ‘Distribution of eigenvalues of linear stochastic systems’, Proceedings of the ninth international conference on applications of statistics and probability in civil engineering (ICASP 9), San Francisco, California, USA, Vol. 1 of Applications of statistics and probability in civil engineering, Millpress, Rotterdam Netherlands, July, 2003, pp. 201-207.

[4.18] S. S. Shapiro and A. J. Gross, Statistical Modelling Techniques, Marcel Dekker, New York, 1981.

[4.19] J. S Bendat, Principles and Applications of Random Noise Theory, John Wiley & Sons. Sons. New York 1958.

[4.20] McKay, M. D., Conover, W. J., and Beckman, R. J., A comparison of three methods for selecting values of input variables in the analysis of output from a computer code, Technometrics, (1979) 21(2) pp239–245.

[4.21] Olsson, A., Sandberg, G. and Dahlblom, O., On Latin Hypercube Sampling for Structural Reliability Analysis. (2003), Structural Safety, 25(1), pp47-68.

[4.22] Press, W. H.; Flannery, B. P.; Teukolsky, S. A.; and Vetterling, W. T. "Cholesky Decomposition." in Numerical Recipes in FORTRAN: The Art of Scientific Computing, 2nd ed. Cambridge, England: Cambridge University Press, pp. 89-91, 1992.

[5.1] Hills E., Mace B.R., Ferguson N.S. ‘Response Statistics of Uncertain Structures’, Institute of Acoustics Spring Conference 2004, Vol. 26 Pt 2, pp 474-486.

[5.2] Hills E., Mace B.R., Ferguson N.S., ‘Response statistics of stochastic built-up structures’, *Proceedings of ISMA 2004, International Conference on Noise and Vibration Engineering, Katholieke Universiteit Leuven, Belgium,* 20-22 September 2004, 3273-85.

[6.1] Hurty, W. C. Dynamic analysis of structural systems using component modes, AIAA Journal, 1965,Vol. 3, No. 4, pp678-685.

[6.2] Craig, R. R., Jr., and Bampton, M. C. C., Coupling of Substructures for Dynamic Analysis, AIAA Journal, Vol. 6 No. 7, July 1968, pp1313-1319.

[6.3] Mace, B. R. and Shorter, P. J., A local modal/perturbational method for estimating frequency response statistics of built-up structures with uncertain properties, Journal of Sound and Vibration, 2001, 242(5), pp 793-811.

[6.4] Craig, R. R., Jr., Structural Dynamics: An introduction to computer methods, John Wiley & Sons, New York, 1981.

[6.5] Noor, A. K. and Peters, J. M., Reduced Basis Technique for Nonlinear Analysis of Structures, AIAA Journal, Vol. 18, No. 4, 1980, pp.455-462.

[6.6] Craig, R. R., Jr., A Brief Tutorial on Substructure Analysis and Testing, 18th International Modal Analysis Conference, San Antonio, February 9, 2000.

[6.7] Rubin, S., Improved Component-Mode Representation for Structural Dynamic Analysis, AIAA Journal, Vol. 13, No. 8, Aug. 1975, pp. 995-1006.

[6.8] MacNeal, R. H., A Hybrid Method of Component Mode Synthesis, Journal of Computers & Structures, Vol. 1, No. 4, Dec. 1971, pp. 581-601.

[6.9] Craig, R. R., Jr., Coupling of substructures for dynamic analyses: An overview, AIAA Dynamics Specialists Conference, Paper No. 2000-1573, Atlanta, April 5, 2000.

[6.10] Shorter, P., Combining Finite Elements and Statistical Energy Analysis, Ph.D. Thesis, University of Auckland, July 1998.

[6.11] Craig, R. R. Jr., and Hale, A. L., Block-Krylov Component Mode Synthesis Method for Structural Model Reduction, AIAA J. Guidance, Control, and Dynamics, Vol 11, No. 6, 1988, pp. 562-570.

[7.1] Woodbury, M. A., Inverting modified matrices, Statistical Research Group Memorandum Report No. 42, Princeton University, Princeton, N. J., 1950.

[7.2] Feller, W., An introduction to probability theory and its applications, John Wiley & Sons, New York, 1966.

[7.3] Matlab v7.0.1.24704, service pack 1, Copyright 1984-2004, The MathWorks, Inc..

[7.4] Ewins, D. J., Model validation: Correlation for updating, Sadhana, Vol 25, Part 3, June 2000, pp. 221-234.

[7.5] Kreyszig, E., Advanced Engineering Mathematics, 6th Ed. John Wiley & Sons, 1988.

[7.6] Adams, W. J., The life and times of the central limit theorem, Kaedmon Publishing, New York, 1974

[8.1] Mace, B. R. and Shorter, P. J., A local modal/perturbational method for estimating frequency response statistics of built-up structures with uncertain properties, Journal of Sound and Vibration, 2001, 242(5), pp 793-811.

[8.2] Alexander, G., Kronecker products and matrix calculus: with applications, Horwood, Chichester, 1981.

[8.3] Matlab v7.0.1.24704, service pack 1, Copyright 1984-2004, The MathWorks, Inc..

[8.4] B.W. Lindgren, Statistical Theory, 3rd Ed Macmillan Publishing, 1976.

[8.5] Feller, W., An introduction to probability theory and its applications, John Wiley & Sons, New York, 1966.

[8.6] Adams, W. J., The life and times of the central limit theorem, Kaedmon Publishing, New York, 1974.

[8.7] Ewins, D. J., Model validation: Correlation for updating, Sadhana, Vol 25, Part 3, June 2000, pp. 221-234.

[8.8] Kreyszig, E., Advanced engineering mathematics, 6th edition, 1988, John Wiley & Sons, pp1253.

[9.1] Petyt M., Introduction to finite element vibration analysis, Cambridge University Press, 1990.

[9.2] Rao S., S., The finite element method in engineering, Butterworth-Heinemann, 3 ed., 1998.

[9.3] Kreyszig, E., Advanced Engineering Mathematics, 6th Ed. John Wiley & Sons, 1988.

[A.1.] Papoulis, A., The Concept of a Random Variable, Ch. 4 in Probability, Random Variables, and Stochastic Processes, 2nd ed. New York: McGraw-Hill, pp. 83-115, 1984.

[A.2.] Evans, M., Hastings, N., and Peacock, B., Statistical Distributions, 3rd ed. New York, Wiley, pp. 6-8, 2000.

[A.3.] Graham, A., Kronecker products and calculus: with applications, Ellis Horwood Ltd, John Wiley & Sons, 1981.

[A.4.] Feller, W., An introduction to probability theory and its applications, John Wiley & Sons, New York, 2nd ed. 1964.

[C.1.] Petyt M., Introduction to finite element vibration analysis, Cambridge University Press, 1990.

12. Bibliography

Olsson, A. and Sandberg, G., Latin Hypercube Sampling for Stochastic Finite Element Analysis. (2002), Journal of Engineering Mechanics, 128(1), pp121-125.

McKay, M., Latin hypercube sampling as a tool in uncertainty analysis of computer models, Proceedings of the 24th conference on Winter simulation, p.557-564, December 13-16, 1992, Arlington, Virginia, United States.

Craig, R. R., Jr. and Chang, C. J., Free Interface methods for substructure coupling for dynamic analysis, AIAA Journal, Vol. 14, No. 11, pp1633-1635.

Ferris, J. B., Bernitsas, M. M. and Stein, J. L., Redesigning the dynamics of structural systems, AIAA Journal Vol. 38, No. 1, January 2000, pp147-154.

Craig, R. R., Jr., Substructure methods in vibration, Transactions of the ASME, June 1995, Vol. 117, pp207-213.

Morgan, J. A., Pierre, C., Hulbert, G. M., Calculation of component mode synthesis matrices from measured frequency response functions, part 1: theory, Journal of vibration and acoustics, April 1998, Vol. 120 pp503-508.

Castanier, M. P., Tan, Y. C., Pierre, C., Characteristic constraint modes for component mode synthesis, AIAA Journal, Col. 39, No. 6, June 2001, pp1182-1187.

Biondi, B., and Muscolino, G., Component mode synthesis method for coupled continuous and FE discretized substructures, Engineering Structures, 25 (2003), pp419-433.

Morgan, J. A., Pierre, C., Hulbert, G. M., Forced response of coupled substructures using experimentally based component mode synthesis, AIAA Journal, Vol. 35, No. 2, February 1997, pp334-339.

Kronecker products and calculus: with applications., Graham, A., Ellis Horwood Ltd, John Wiley & Sons, 1981